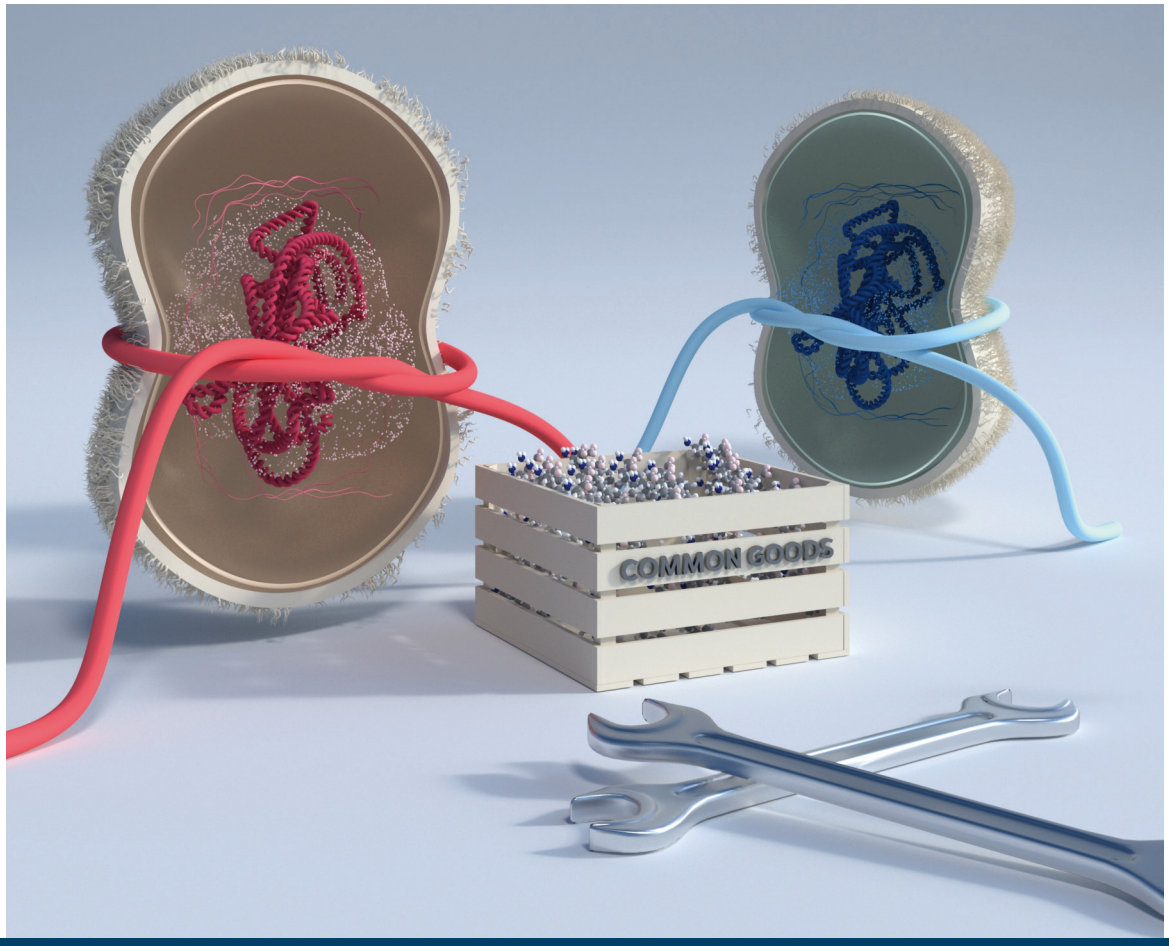

Communities of Niche-optimized Strains (CoNoS) – a novel concept for improving biotechnological production

Rico Zuchowski

Schlüsseltechnologien / Key Technologies
Band / Volume 280
ISBN 978-3-95806-743-1

Mitglied der Helmholtz-Gemeinschaft

JÜLICH
Forschungszentrum

Schriften des Forschungszentrums Jülich
Reihe Schlüsseltechnologien / Key Technologies Band / Volume 280

Forschungszentrum Jülich GmbH
Institut für Bio- und Geowissenschaften (IBG)
Biotechnologie (IBG-1)

Communities of Niche-optimized Strains (CoNoS) – a novel concept for improving biotechnological production

Rico Zuchowski

Schriften des Forschungszentrums Jülich
Reihe Schlüsseltechnologien / Key Technologies Band / Volume 280

ISSN 1866-1807 ISBN 978-3-95806-743-1

Bibliografische Information der Deutschen Nationalbibliothek.
Die Deutsche Nationalbibliothek verzeichnet diese Publikation in der
Deutschen Nationalbibliografie; detaillierte Bibliografische Daten
sind im Internet über http://dnb.d-nb.de abrufbar.

Herausgeber und Vertrieb:	Forschungszentrum Jülich GmbH Zentralbibliothek, Verlag 52425 Jülich Tel.: +49 2461 61-5368 Fax: +49 2461 61-6103 zb-publikation@fz-juelich.de www.fz-juelich.de/zb
Umschlaggestaltung:	Grafische Medien, Forschungszentrum Jülich GmbH
Druck:	Grafische Medien, Forschungszentrum Jülich GmbH
Copyright:	Forschungszentrum Jülich 2024

Schriften des Forschungszentrums Jülich
Reihe Schlüsseltechnologien / Key Technologies, Band / Volume 280

D 61 (Diss. Düsseldorf, Univ., 2023)

ISSN 1866-1807
ISBN 978-3-95806-743-1

Vollständig frei verfügbar über das Publikationsportal des Forschungszentrums Jülich (JuSER)
unter www.fz-juelich.de/zb/openaccess.

Das heißt, viele Experten vermuten, dass es so war.
Ebenso viele sind völlig entgegengesetzter Meinung.
Wer hätte das gedacht.

– Frank Schätzing, 2006. Nachrichten aus einem unbekannten Universum

The results described in this dissertation have been published in the following original publications:

Schito, S.*, Zuchowski, R.*, Bergen, D., Strohmeier, D., Wollenhaupt, B., Menke, P., Seiffarth, J., Nöh, K., Kohlheyer, D., Bott, M., Wiechert, W., Baumgart, M., Noack, S. (2022). Communities of Niche-optimized Strains (CoNoS) - Design and creation of stable, genome-reduced co-cultures. *Metabolic engineering*, 73, 91-103.

Zuchowski, R.*, Schito, S.*, Neuheuser, F., Menke, P., Berger, D., Hollmann, N., Gujar, S., Sundermeyer, L., Mack, C., Wirtz, A., Weiergräber, O., Polen, T., Bott, M., Wiechert, W., Noack, S., Baumgart, M. (2023). Discovery of novel amino acid production traits by evolution of synthetic co-cultures. *Microbial Cell Factories*, 22:71.

* These authors contributed equally to this work.

Content

Summary

Global challenges such as climate change and resource depletion require a transformation of the fossil-based economy toward a modern, sustainable bioeconomy. In this context, the establishment of efficient microbial production processes based on renewable carbon sources is of major importance. In natural environments, bacteria usually grow in complex communities and often evolve auxotrophies, which are relieved by cross-feeding interactions with other community members. This division of labor can lead to a more efficient use of the available resources, because of which it was proposed to be a viable strategy for increasing the efficiency of microbial production processes. In this thesis, we describe the design and setup of synthetic, genome-reduced microbial communities according to the concept of Communities of Niche-optimized Strains (CoNoS), which are comprised of a pair of mutually dependent amino acid-auxotrophic strains of *Corynebacterium glutamicum*, an industrially important microbial cell factory. The aim was to analyze the production capabilities of such communities in comparison with those of monocultures. This was exemplarily tested with respect to L-arginine production with a CoNoS composed of an L-leucine- and an L-arginine-auxotrophic strain.

We initially started from ten communities with different pairs of mutual amino acid auxotrophic strains. The auxotrophic strains were rationally engineered to overproduce the amino acid required by the partner strain, and then the community was subjected to adaptive laboratory evolution (ALE) to improve growth. This resulted in stable communities with growth properties close to wild type monocultures. Genome analysis of the communities obtained by ALE enabled the identification of the ABC transporter ArgTUV as the first and presumably only L-arginine importer of *C. glutamicum*. Deletion of the *argTUV* genes in an L-arginine production strain improved L-arginine production in the monoculture by 24 %. This result demonstrated that the CoNoS approach is a valuable concept for identifying novel production traits, with metabolite transport and exchange being a major target. Also, further target genes improving amino acid overproduction were identified in other auxotrophic strains. Evolution of a monoculture with a poorly performing L-tryptophan-auxotrophic strain revealed a link between a protein named TrpP and the expression level of the *suf* gene cluster, which is responsible for assembly and repair of iron-sulfur clusters in proteins. It turned out that the deletion of *trpP* improved L-tryptophan production, but the molecular basis of this effect is still unclear.

For a CoNoS production process, it seems beneficial for product yield to limit growth of the community member that does not produce the desired final product. For this purpose, different metabolic switches were tested regarding their capability of community control in our CoNoS consisting of an L-arginine and an L-leucine auxotrophic strain. Here, a mechanism based on repression of the essential *pfkA* gene in the L-arginine auxotrophic strain using a gluconate-regulatable expression system was most promising. The L-arginine titer of a bioprocess with this CoNoS outcompeted a fermentation based on a prototrophic monoculture with identical mutations for improved L-arginine synthesis by more than 70 %. This increase was presumably due to carbon and energy savings from the auxotrophy, as an L-leucine-auxotrophic monoculture supplemented with L-leucine also produced more than 2-fold higher L-arginine titers than the prototrophic monoculture. In summary, CoNoS turned out to be a valuable tool to identify novel production traits and might also be used in the future to develop new co-culture production processes contributing to a sustainable bioeconomy.

Zusammenfassung

Globale Herausforderungen wie der Klimawandel und die Verknappung der natürlichen Ressourcen erfordern eine Transformation der auf der Nutzung fossiler Rohstoffe basierenden Wirtschaft hin zu einer modernen, nachhaltigen Bioökonomie. In diesem Zusammenhang ist die Etablierung hocheffizienter mikrobieller Produktionsprozesse auf der Grundlage erneuerbarer Kohlenstoffquellen von großer Bedeutung. In ihrer natürlichen Umgebung wachsen Bakterien in der Regel in komplexen Gemeinschaften und haben häufig Auxotrophien entwickelt, die durch *cross-feeding*-Interaktionen mit anderen Mitgliedern der Gemeinschaft ausgeglichen werden. Diese Arbeitsteilung kann zu einer effizienteren Nutzung der verfügbaren Ressourcen führen, weshalb sie eine potenzielle Strategie zur Steigerung der Effizienz mikrobieller Produktionsprozesse darstellt. In dieser Arbeit beschreiben wir das Design und den Aufbau von synthetischen, genomreduzierten mikrobiellen Gemeinschaften nach dem Konzept der *Communities of Niche-optimized Strains* (CoNoS), die aus einem Paar wechselseitig Aminosäure-auxotropher Stämme von *Corynebacterium glutamicum*, einer industriell wichtigen mikrobiellen Zellfabrik, bestehen. Ziel war es, die Produktionsmöglichkeiten solcher Gemeinschaften im Vergleich zu Monokulturen zu analysieren. Dies wurde exemplarisch für die L-Arginin-Produktion mit einem CoNoS getestet, das aus einem L-Leucin- und einem L-Arginin-auxotrophen Stamm bestand.

Zunächst wurden zehn Gemeinschaften mit verschiedenen Paaren von wechselseitig Aminosäure-auxotrophen Stämmen konstruiert. Die Stämme wurden zunächst auf rationale Weise genetisch so verändert, dass sie die vom Partnerstamm benötigte Aminosäure überproduzieren. Anschließend wurde die Gemeinschaft einer adaptiven Laborevolution (ALE) unterzogen, um ein schnelleres Wachstum zu erzielen. Dies führte zu stabilen Gemeinschaften mit Wachstumseigenschaften, die denen von Wildtyp-Monokulturen nahekommen. Die Genomanalyse der durch ALE erhaltenen Gemeinschaften ermöglichte die Identifizierung des ABC-Transporters ArgTUV als ersten und vermutlich einzigen L-Arginin-Importer von *C. glutamicum*. Die Deletion der *argTUV*-Gene in einem L-Arginin produzierenden Stamm verbesserte die L-Arginin-Produktion in der Monokultur um 24 %. Dieses Ergebnis zeigt, dass der CoNoS-Ansatz ein wertvolles Konzept zur Identifizierung neuartiger Produktionsmerkmale ist, wobei vor allem Gene des Transports und Austausches von Metaboliten ein zentrales Ziel der Mutationen darstellen. Auch weitere Zielgene zur Verbesserung der Aminosäureproduktion

wurden in anderen auxotrophen Stämmen identifiziert. Bei der Evolution einer Monokultur mit einem langsam wachsenden L-Tryptophan-auxotrophen Stamm wurde eine Verbindung zwischen dem Protein TrpP und dem Expressionslevel des *suf*-Genclusters festgestellt, welches für den Aufbau und die Reparatur von Eisen-Schwefel-Clustern in Proteinen verantwortlich ist. Die Deletion von *trpP* verbesserte die L-Tryptophan-Produktion, wobei die molekularen Grundlagen dieser Wirkung noch unbekannt sind.

Bei einem CoNoS-Produktionsprozess scheint es für die Produktausbeute von Vorteil zu sein, das Wachstum eines Gemeinschaftsmitglieds zu begrenzen. Zu diesem Zweck wurden in unserem CoNoS, bestehend aus einem L-Arginin- und einem L-Leucin-auxotrophen Stamm, verschiedene metabolische Schalter auf ihre Fähigkeit zur Kontrolle der Gemeinschaft getestet. Dabei erwies sich ein Mechanismus, der auf der Repression des essentiellen *pfkA*-Gens im L-Arginin auxotrophen Stamm unter Verwendung eines Gluconat-regulierbaren Expressionssystems beruht, als besonders vielversprechend. Mit diesem CoNoS konnte der L-Arginin-Titer in einer Fermentation gegenüber einer prototrophen Monokultur mit identischen Mutationen für eine verbesserte L-Arginin-Synthese um mehr als 70 % gesteigert werden. Dieser Anstieg war vermutlich auf die Kohlenstoff- und Energieeinsparungen durch die Auxotrophie zurückzuführen, da eine mit L-Leucin supplementierte L-Leucin-auxotrophe Monokultur ebenfalls einen mehr als zwei Mal so hohen L-Arginin-Titer als die prototrophe Monokultur erreichte. Insgesamt hat sich das CoNoS-Konzept als wertvolles Instrument zur Identifizierung neuartiger Produktionsmerkmale erwiesen, und könnte in Zukunft auch für die Entwicklung neuer Co-Kultur-basierter Produktionsverfahren genutzt werden, die zu einer nachhaltigen Bioökonomie beitragen.

Abbreviations

AC-COA	Acetyl coenzyme A
ACGLU	Acetylglutamate
ACGLU-P	Acetylglutamyl-phosphate
ACG5SA	Acetylglutamate-5-semialdehyde
ACORN	Acetylornithine
ALE	Adaptive laboratory evolution
ArgB	Acetylglutamate kinase (Cg1582)
ArgC	*N*-Acetyl-γ-glutamyl-phosphate reductase (Cg1580)
ArgD	Acetylornithine aminotransferase (Cg1583)
ArgF	Ornithine carbamoyltransferase (Cg1584)
ArgG	Argininosuccinate synthase (Cg1586)
ArgH	Argininosuccinate lyase (Cg1587)
ArgJ	*N*-Acetylglutamate synthase (Cg1581)
ArgR	Transcriptional repressor of arginine biosynthesis (Cg1585)
ARGSUC	Arginosuccinate
ACT	Acetate
BCAA	Branched-chain amino acids
BrnFE	Branched-chain amino acid exporter (Cg0314-0315)
BrnQ	Branched-chain amino acid uptake carrier (Cg2537)
CDW	Cell dry weight
CgmA	Cadaverine export permease (Cg2895)
CoNoS	Communities of Niche-optimized strains
Def1	Peptide deformylase 1 (Cg3034)
DHAP	Dihydroxyacetone phosphate
DO	Dissolved oxygen concentration
FarR	Transcriptional regulator involved in amino acid biosynthesis (Cg3202)
FUM	Fumarate
Gdh	Glutamate dehydrogenase (Cg2280)
Glk	Glucokinase (Cg2399)
GLU-L	L-glutamate
GntK	Gluconate kinase (Cg2732)
GntP	Gluconate permease (Cg3216)
GntR1	Gluconate-responsive repressor 1 (Cg2783)
GntR2	Gluconate-responsive repressor 2 (Cg1935)
IlvE	Branched-chain amino acid aminotransferase (Cg2418)
IolT1	*myo*-Inositol transporter 1 (Cg0223)
IolT2	*myo*-Inositol transporter 2 (Cg3387)
2-IPPM	2-isopropylmalate
3-IPPM	3-isopropylmalate
IPTG	Isopropyl-β-D-thiogalactopyranoside
LeuA	2-isopropylmalate synthase (Cg0303)
LeuB	3-isopropylmalate dehydrogenase (Cg1453)
LeuCD	Isopropylmalate isomerase (Cg1487-1488)
LtbR	Leucine and tryptophan biosynthesis regulator (Cg1486)

LysE	Lysine efflux permease (Cg1424)
MACS	Magnetic-activated cell sorting
MAGE	Multiplex automated genome engineering
MALDI-ToF-MS	Matrix-assisted Laser Desorption/Ionization
MFA	Metabolic flux analysis
MOPS	*N*-(Morpholino)propanesulfonic acid
MS	Mass Spectrometry
NagS	*N*-Acetylglutamate synthase (Cg3035)
PEP	2-Phosphoenolpyruvate
PfkA	6-Phosphofructokinase (Cg1409)
Pgi	Glucose-6-phosphate isomerase (Cg0973)
PHB	Poly-(3-hydroxybutyrate)
PpgK	Polyphosphate glucokinase (Cg2091)
PPP	Pentose phosphate pathway
PtsG	Glucose phosphotransferase system (Cg1537)
RipA	Transcriptional regulator of iron proteins and repressor of aconitase (Cg1120)
SU	Subunit
TCA	Tricarboxylic acid cycle
ToF	Time of flight
TrpP	Put. L-tryptophan permease (Cg3357)
wt/vol	Weight per volume
αKG	α-Ketoglutarate
Δ	Deletion

Further abbreviations not included in this section are according to international standards, as, for example, listed in the author guidelines of the Journal of Biological Chemistry (JBC).

1. Introduction

1.1 Utilization of bacteria in industrial biotechnology

1.1.1 Toward a sustainable bioeconomy

As early as 7000 BC, microorganisms were employed for bioproduction, presumably starting with the fermentation of sugars to produce alcohol (Demain, 2010). For a very long time, only food and beverages were produced via fermentation. The first microbial processes for acetone-butanol-fermentation in defined medium and penicillin production were developed during the first decades of the 20th century (Demain, 2010, Fleming, 1929, Weizmann and Rosenfeld, 1937). From there on, the spectrum of compounds produced from renewable resources using microorganisms broadened drastically. These compounds find nowadays applications as biopharmaceuticals, in food and agriculture, in the cosmetics and textile industries, as well as in chemical manufacturing (Demain, 2010). Newly developed products such as biodegradable plastics and biofuels potentially play an essential role in replacing petro-based processes in times of over-consumption of resources, environmental pressures, and global warming (Tang and Zhao, 2009).

This overall development culminated more recently into the emerging paradigm of "bioeconomy" in industry and politics, the "production of renewable biological resources and the conversion of these resources and waste streams into value-added products, such as food, feed, bio-based products as well as bio-energy" (European-Commission, 2012). Currently, despite the number of biotechnologically produced chemicals having substantially increased, including many novel products that could not be produced via petrochemical processes such as proteins and specific pharmaceuticals with complex stereochemistry, many bio-based processes still are not competitive (Lee *et al.*, 2019). This especially accounts for important bulk chemicals, e.g., acrylic acid and monomers for polyethylene terephthalate (PET) and polytrimethylene terephthalate (PTT), as well as, for example, replacement products like gasoline-range alkanes and bioplastics (Lee *et al.*, 2019). Thus, the development of a sustainable bioeconomy is highly dependent on progress in this field (Aguilar *et al.*, 2019). In this context, the bioprocess efficiency with which the compounds of interest are produced is of high importance. For example, the efficiency of the microbial fermentation for penicillin production increased more than 10.000 times over the years (Thykaer and Nielsen, 2003), drastically reducing the resources needed and the CO_2 produced. Establishing and improving new microbial production strains and bioprocesses for compounds

with all sorts of the described uses is, therefore, one decisive way of moving toward a sustainable bioeconomy.

1.1.2 Microbial strain development

A plethora of microbial strains producing hundreds of natural and non-natural chemicals have been constructed so far, with many unexplored reactions left in the biochemical space (Lee *et al.*, 2019). Comparing this with the magnitude of over 100,000 interesting antimicrobial compounds predicted to be produced by the genus *Streptomyces* alone (Watve *et al.*, 2001), this represents only a marginal fraction of the potential offered by nature.

When the first bioprocesses were set up in the first half of the 20th century, as in the case of penicillin, establishing and improving microbial production meant first the screening of different isolates for production, followed by random mutagenesis, e.g., via X-ray treatment, and afterward the screening or selection of better-producing strains (Demain, 2010). Since then, bioproduction has made an enormous leap forward with the development of recombinant DNA methods (Jackson *et al.*, 1972, Mertz and Davis, 1972). This technology quickly enabled breakthroughs such as human insulin produced in *Escherichia coli*, opening up a whole new industry (Johnson, 1983, Chance *et al.*, 1981). The recombinant DNA technology enabled far more precise genetic changes than previously imaginable, which allowed for the newly structured way of strain construction, later termed metabolic engineering (Bailey, 1991): Iterative cycles of genetic modifications followed by the analysis of the resulting metabolic changes and hence the choice of the next modification. With further progress in genome editing techniques such as CRISPR (Jinek *et al.*, 2012) as well as in systems biology and metabolic modeling, even more precise Design-Build-Test-Learn cycles are now possible (Nielsen and Keasling, 2016).

There are many targets for metabolic engineering, but the two most fundamental ways are the redirection of the metabolite flow and the expression of heterologous genes, mostly enzymes or transporters (Bailey, 1991). Especially the alteration in protein levels – e.g., by genomic changes altering codon usage, promoter strength, regulatory elements, mRNA or protein stability (Makrides, 1996) or simply through the addition of several further gene copies (Tyo *et al.*, 2009) – can allow for revised regulation, reduced competition between enzymes for precursors or improved directing of metabolites toward the desired branch (Bailey, 1991).

The complementary, "classical" way of dealing with metabolic complexity in strain construction via untargeted mutagenesis is still relevant. This approach can accelerate strain development, and many different physical agents, such as UV and ionizing radiation, or chemical agents, e.g., nucleobase analogs and DNA intercalating agents, are used for this (Sanghavi *et al.*, 2020). However, random mutagenesis yields a high number of mutagenized cells that need to be screened for better performance, even in the more refined site-directed mutagenesis process (Flavell *et al.*, 1975, Müller *et al.*, 1978). Strategies that enable high-throughput screening of a large library of strains are, for example, multiplex automated techniques such as MAGE (Wang *et al.*, 2009) or transcription factor-based approaches (Binder *et al.*, 2013, Binder *et al.*, 2012). The usage of physical and chemical agents can also be combined, for example, to create a huge diversity in one population of bacteria through radiation followed by screening with the chemical agent. This entails cultivation cycles with increasing concentrations of the desired product or its analog. During this cultivation, cells better adapted, e.g., through an increased strain tolerance or due to circumvention of negative regulatory cycles, are enriched and can easily be identified (Lee and Kim, 2015). Long-term selection in adaptive laboratory evolution (ALE) experiments, both with and more commonly without previous mutagenesis, is one important strategy for identifying strains with adaptive changes and relevant mutations, yielding insights into, e.g., nutrient or stress metabolism by accumulating beneficial mutations (recently reviewed in (Dragosits and Mattanovich, 2013)). This approach of evolution-guided metabolic engineering (as opposed to "rational" metabolic engineering) progressed recently due to advances in the implementation of cheap next-generation sequencing possibilities coupled with technological progress, e.g., allowing for automated phenotyping approaches involving a liquid handling robotic system (Unthan *et al.*, 2015), vastly increasing the pace of strain optimization (Dragosits and Mattanovich, 2013, Stella *et al.*, 2019). The combination of rational and evolution-guided metabolic engineering is, therefore, highly relevant for the construction of optimal strains. However, despite all progress, the process of constructing new strains from scratch for industrial-scale production usually still requires 6-8 years with costs of over 50,000,000 US$ (Nielsen and Keasling, 2016).

Usually, several modifications are necessary for optimizing production due to the number of complex regulatory layers in the central carbon metabolism with its "bowtie" structure, i.e., its funneling of all different carbon and energy sources into only twelve precursor metabolites, that afterward get converted to the high diversity of all relevant metabolites (Nielsen and Keasling,

2016). Bacteria acquired these tight regulatory systems during evolution to coordinate their complex metabolism, amongst others to avoid waste of energy and carbon in dispensable proteins, which require more polymerization energy and more than 100-fold more ATP per 1g cell dry weight than DNA and RNA (Noack and Baumgart, 2019). What is more, these costs are further extended several-fold through the actual cost of the proteins that take transcription and translation machinery into account (Stoebel *et al.*, 2008). For example, half of the proteome mass of *E. coli* is unused depending on the environmental conditions, and the growth rates in the different environments were inversely proportional to the unused proteome mass (O'Brien *et al.*, 2016). Reducing the metabolic and regulatory complexity evolved for the rapidly changing environmental conditions therefore is a relevant part of metabolic engineering to improve bioproduction. In addition to the deletion of only individual genes, e.g., for transcriptional regulators, the large-scale deletion of genes, e.g., for complete biosynthetic pathways, can reduce the overall complexity, which is pursued in several genome-reduction projects. Attempts have been made to construct minimal cells in a "bottom-up" approach, however, currently without biotechnological relevance (Hutchison *et al.*, 2016, Choe *et al.*, 2016). "Top-down" approaches, on the other hand, encompass the deletion of genes with functions assumed to be dispensable under biotechnological production conditions. Examples of successfully engineered strains yielding higher production were constructed by deleting genes for flagella movement in *Pseudomonas putida* (Martinez-Garcia *et al.*, 2014), for biofilm formation in *Pseudomonas taiwanensis* (Wynands *et al.*, 2019), or secondary metabolites synthesis in *Bacillus amyloliquefaciens* (Zhang *et al.*, 2020). However, the overall success rate in constructing genome-reduced biotechnological strains with improved product yield is low (Noack and Baumgart, 2019).

Further reduction of the genome by deleting highly expressed, essential genes, such as for amino acid biosynthesis, was also shown to be beneficial for microbial strain growth, even though this is accompanied by the risk of extinction in absence of an external metabolite source (D'Souza *et al.*, 2014). Those deletions were suggested to increase the metabolic efficiency, as uptake of metabolites is usually cheaper than their synthesis (D'Souza *et al.*, 2014). In nature, amino acid or vitamin synthesis genes like these were often found to be missing in the various strains of one species, which is predicted to result in cross-feeding interactions between and fitness increases for bacteria growing in communities in their specific ecological niches (Goyal, 2018, Morris, 2015). Therefore, bacterial interactions in their native communities differ drastically from a bacterial

monoculture in bioreactors (Figure 1.1). In such native communities, for example in bacterial consortia in the nutrient-poor pelagic zone of freshwater lakes (Neuenschwander *et al.*, 2018), strains often adapt to the selective pressure of limited nutrients with smaller genomes and highly efficient growth (Noack and Baumgart, 2019). Reducing the metabolic complexity and burden, which is complemented via interaction in a bacterial community, therefore offers a new field for strain engineering. Despite this potential, the usage of communities for production was almost completely neglected by the field of microbial biotechnology and only starts to get more attention (McCarty and Ledesma-Amaro, 2019).

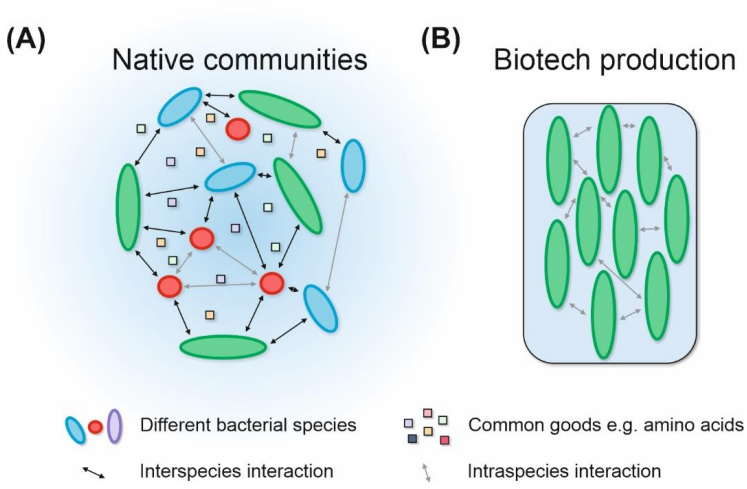

Figure 1.1: Comparison of microbial growth characteristics in different environments. (A) Bacteria growing in native communities consisting of several different species or different strains of the same species. In such communities, the bacteria face interspecies (black arrows) and intraspecies (grey arrows) interactions, e.g., the exchange of common goods such as amino acids or vitamins. (B) Biotechnological production cultures are mostly cultivated as monoculture in a bioreactor. Under these conditions, only intraspecies interactions are present. Adapted from (Noack and Baumgart, 2019).

1.2 Microbial communities

Microbial communities in nature can be very diverse, easily comprising tens of thousands of species (Torsvik *et al.*, 1996). Each species inhabits a specific ecological niche, with the latter describing – independent of the many different concepts of this term – the relationship between the organism and its environment, the biotic and abiotic factors, in which the other species play a

key role (Pocheville, 2015). All sorts of biotic interactions between microorganisms can be found, from antagonistic relationships (primary consumption, predation, and scavenging) (Guerrero *et al.*, 1986, Jurkevitch and Davidov, 2006) to competition (both inter- and intraspecific) (Hibbing *et al.*, 2010) and cooperation, with all of them having arisen and changed during evolution innumerable times.

Cooperation occurs within and between different species and ranges from rather commensal interactions such as H_2O_2 detoxification (Morris *et al.*, 2011) to mutualisms with examples such as metabolite cross-feeding interactions and interspecies electron transfer (Biebl and Pfennig, 1978). Synthetic approaches, such as with two amino acid auxotrophic *E. coli* strains that relied on cross-feeding interactions, have underlined how both partners can benefit from these interactions, increasing the overall community fitness and stabilizing the community (Pande *et al.*, 2014). In native cooperating communities, one common type of adaptation is physical aggregation and filament or periplasmic tubule formation (Ishii *et al.*, 2005, Wanner *et al.*, 2008), which was also observable for synthetic *E. coli* communities (Preussger *et al.*, 2020) and for *P. putida* growing in a microbial consortium (Hansen *et al.*, 2007). Another relevant adaptation is gene loss, which was suggested in the Black Queen hypothesis to be a primary driver of the development of cooperation due to fitness increases, at least between bacteria with leaky functions (Morris, 2015, Morris *et al.*, 2012). According to this hypothesis, leaky common goods, such as extracellular catalase activity, are dispensable for individuals as long as other community members still produce this good, selectively favoring loss of the corresponding genes until the production level drops too low (Morris *et al.*, 2011, Morris *et al.*, 2012). Notably, gene loss in bacterial strains was found to be omnipresent, represented by the differentiation between the “core-genome” and “pan-genome” of bacteria. The core-genome comprises genes that are shared by all sequenced strains of one species, encoding mainly proteins with housekeeping functions or functions related to cell envelope and regulation. The pan-genome is composed of the core-genome as well as the remaining genes only present in some of the strains (Tettelin *et al.*, 2005, Tettelin *et al.*, 2008). About 250 genes per genome were previously estimated to belong to the core-genome in the bacterial domain based on the frequency of their occurrences among analyzed genomes (Lapierre and Gogarten, 2009), with the most considerable fraction of the remaining pan-genome genes being found to be related to metabolic functions (McNally *et al.*, 2016). Intra-species metabolic exchange (either mutualistic or commensal) was predicted to reduce those strain-specific

metabolic auxotrophies, especially for amino acids and organic acids as well as vitamins and carbohydrates (Goyal, 2018). The evolution of two-species microbial communities in a multi-species genome-scale metabolic model simulation also supports the hypothesis of cross-feeding interactions arising over time (McNally and Borenstein, 2018).

Experimental evidence for the emergence of cooperation is rare. One example is the evolution of a commensal cross-feeding interaction from a single *E. coli* precursor strain, resulting in a stable coexistence between a strain specialized in D-glucose metabolization and further specialists consuming its excreted metabolites (Helling *et al.*, 1987). These genetically and phenotypically differentiated strains were later shown to grow more efficiently in co-culture, reaching higher biomass productivity than their parental strain in monoculture (Yang *et al.*, 2020). With synthetic biology tools, establishing cross-feeding interactions yielding higher biomass productivity compared to the appropriate monoculture controls was possible both with the overflow metabolite acetate as well as with amino acids (Bernstein *et al.*, 2012, Pande *et al.*, 2014). In one study with 1035 pairs of auxotrophic *E. coli* strains, 17% formed a cross-feeding interaction enabling community growth (Wintermute and Silver, 2010). Also, the emergence of cooperation and the shift from commensalism to mutualism under specific conditions in a synthetic *Salmonella enterica* ser. *Typhimurium* – *E. coli* community was shown (Harcombe, 2010). Over time, *S. enterica* – feeding on metabolic waste (likely acetate) of its partner *E. coli* strain – evolved to excrete costly L-methionine, for which the *E. coli* strain was auxotrophic (Harcombe, 2010). In addition to this, further examples of coevolution in synthetic consortia were observed. In laboratory evolution experiments with various synthetic communities, an increase in the ability to survive population density reduction (Shou *et al.*, 2007), increased maximum OD_{600} (Henriksen *et al.*, 2022), and an increase in production of the cross-fed product were found for both co-cultures of the same as well as of different species (Konstantinidis *et al.*, 2021, Preussger *et al.*, 2020). These examples of coevolution resulting in increased growth efficiency occurring in a relatively short timeframe suggest that coevolution plays a significant role in native communities, resulting in stronger cooperative interactions benefitting both partner strains.

The benefits regarding productivity and efficiency of an evolved community possess a substantial potential for improving biotechnological production. Moreover, engineered consortia, in general, are of interest since they could allow for better controllability, robustness (Brenner *et al.*, 2008, Mee and Wang, 2012), and especially metabolic division of labor and modularity to

reduce cross-reactivity through compartmentalization (Tsoi *et al.*, 2018, McCarty and Ledesma-Amaro, 2019). Synthetic consortia have been applied to perform tasks one strain alone could not, amongst them improved microbial degradation and the utilization of carbon and energy sources impossible to be metabolized in a monoculture (Hays *et al.*, 2015). A few examples of co-cultures could indeed outcompete the existing monocultures regarding product yield (Guo *et al.*, 2020, Li *et al.*, 2018a, Mohanakrishnan *et al.*, 2020). This, however, can often be attributed to other factors, such as improved carbon source utilization of a community. Examples for this are the degradation of complex substrates like cellulosic biomass during isobutanol production (Minty *et al.*, 2013) and crude oil for biosurfactant production (Antoniou *et al.*, 2015), but also D-glucose utilization in a *Cupriavidus necator*, *P. putida* and *Azotobacter vinelandii* co-culture for poly-(3-hydroxy-butyrate) (PHB) production (Mohanakrishnan *et al.*, 2020). Another factor are benefits from splitting the biosynthetic pathway to circumvent the accumulation of toxic metabolites, feedback inhibition, or otherwise product degradation, such as in caffeoylmalic acid production in two separate *E. coli* strains (Li *et al.*, 2018a). Proof for improved bioproduction efficiency employing synthetic communities in comparison to a comparable reference monoculture – for a production process that can be performed by a monoculture of one of the strains alone – is still missing. To utilize the potential of communities in microbial production, a novel concept is required.

1.3 Communities of Niche-optimized Strains

1.3.1 Concept and challenges

The concept of Communities of Niche-optimized strains (CoNoS, see Figure 1.2) is a novel approach to provide proof-of-principle that communities can produce a certain metabolite more efficiently than a production strain in monoculture (Noack and Baumgart, 2019). The comparative analysis of manmade genome reduction projects and natural genome reduction suggested that the deletion of long and essential metabolic pathways, such as for amino acids, is ideal for saving energy and carbon, which could then be redirected toward production in a “producer strain” (Noack and Baumgart, 2019). The resulting auxotrophies are relieved by a second strain – defined as the “helper strain” – of the same species that produces the missing metabolite. This helper strain carries a different auxotrophy and depends on the first strain for a different metabolite, thereby establishing a synthetic community depending on cross-feeding interactions between the two

strains. It was proposed that resource utilization and overall production can be optimized with this concept compared to production processes with monocultures (Noack and Baumgart, 2019).

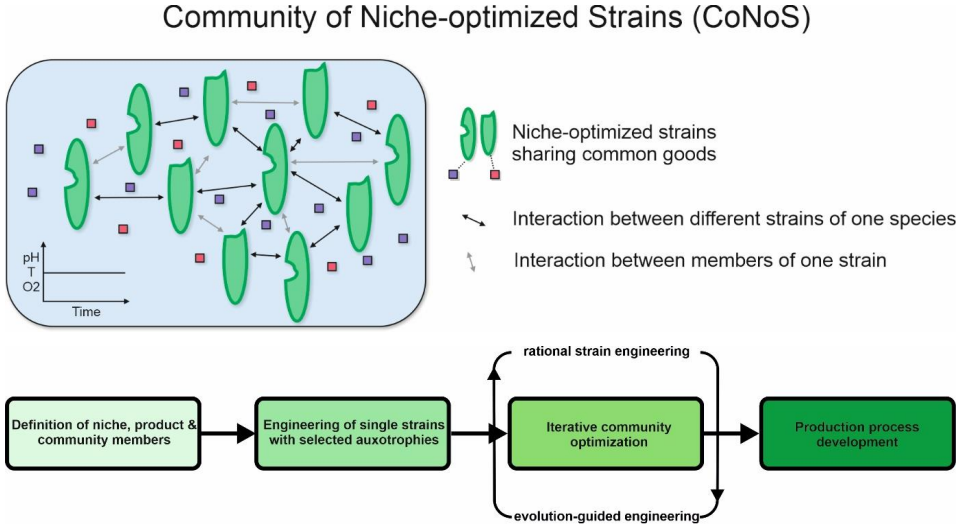

Figure 1.2: Community of Niche-optimized Strains (CoNoS). Two strains of one species, each harboring a different metabolic auxotrophy (indicated by different kinds of holes in the strains' cell shape), are used to set up a synthetic community. Growth is only possible by cross-feeding of common goods that relieve the specific auxotrophies. In comparison to natural environments, the synthetic community will grow in a bioreactor, enabling tight control of the environmental conditions, e.g., regarding pH, temperature, and O_2 availability necessary for community stability. To establish such a CoNoS, a precise workflow is required. Adapted from (Noack and Baumgart, 2019).

To set up a CoNoS, several steps are required, beginning with the precise definition of the niche, the product, and the organism used for the process. Here, the (ecological) niche describes all abiotic and biotic factors, including the cross-feeding interaction and the product accumulation, that affect the survival of the strains (Noack and Baumgart, 2019). These choices are linked very closely together since the upscaling process in the future has to be taken into account. Upscaling is generally a challenge that harbors many potential difficulties, especially when comparable examples of communities in the bioreactor are missing (Takors, 2012). Production organisms such as *E. coli* react very sensitively to changes in reaction conditions and to heterogeneities in the bioreactor, e.g., in D-glucose availability, by changing their transcriptome (Löffler *et al.*, 2016), which is an unwanted ATP sink. Some heterogeneities cannot be completely avoided, making it

essential to define the niche – which includes temperature, pH, growth medium, macro- and micronutrients, stresses, products – as close as possible beforehand to the later production environment and to choose fitting production strains and products (Noack and Baumgart, 2019). Addressing heterogeneities already during strain design as well as the selection of organisms that are more tolerant to those heterogeneities can then result in better production processes (Limberg *et al.*, 2016). This relates to the definition of evaluation criteria, which is another important point. Since an improved bioprocess is the main aim of the CoNoS approach, product titer, yield per mol D-glucose, and productivity (titer g/ $L_{reactor}$·h) are the primary evaluation criteria (Noack and Baumgart, 2019). Under consideration of the desired product and the possible conditions in the specific niche, the community members are selected. Here, the production capacities, specific tolerances, and efforts to construct viable strains for industrial-scale use, have to be considered (Noack and Baumgart, 2019). Same species co-cultures as well as mixed co-cultures are possible and have been successfully used before, e.g., an *E. coli* strains co-culture for resveratrol production (Camacho-Zaragoza *et al.*, 2016) or an *E. coli* – *C. glutamicum* co-culture for L-lysine production from starch and sucrose (Sgobba *et al.*, 2018). The selection of possible pathways for deletion should be made after consideration of the strains' niche. Deleting genes for highly expressed proteins involved in key metabolic pathways, such as amino acid biosynthesis, is an attractive option since amino acid auxotrophies are common and highly relevant regarding their energy demand, in case of L-arginine formation 2 mol ATP and 3 mol NADPH per mol L-arginine (Goyal, 2018, Noack and Baumgart, 2019). In a cycle of iterative optimization steps, additional strain engineering can be used to improve the CoNoS regarding growth behavior and product titer. Here, a combination of rational and evolution-guided steps is advisable, as the untargeted coevolution of the strains leading to a precise adaptation to the specific niche is of high importance (Noack and Baumgart, 2019). Extensive characterization of both single strains in supplemented monocultures and of the community is necessary to avoid the buildup of side effects such as strongly reduced growth or toxic intermediate accumulation in the community, which would later impair the process (Noack and Baumgart, 2019).

The CoNoS concept represents one potential strategy to harness the benefits of genome reduction and microbial co-cultures for a more efficient bioproduction. Experimentally, this hypothesis is backed up by growth benefits of auxotrophic strains and communities without performance losses

that have almost exclusively been shown for *E. coli* (D'Souza *et al.*, 2014, Pande *et al.*, 2014). However, several challenges and uncertainties have to be solved to reach this ambitious aim. As these benefits have almost exclusively been shown for *E. coli*, it is unclear if these increases in efficiency are applicable to other organisms. Experiments with co-cultures of, e.g., two *C. glutamicum* strains suggest that, at least in this example, the L-lysine-auxotrophic strain cross-fed by its partner strain cannot keep up with the growth rate of the comparable monoculture (Burmeister *et al.*, 2019). Especially gram-positive bacteria such as *C. glutamicum* possess a more complex cell envelope, including an outer mycolic acid layer already known for impeding amino acid efflux, making, for example, the addition of detergents or penicillin necessary for high-efflux of L-glutamate (Eggeling and Sahm, 2001). This makes amino acid cross-feeding regarding both uptake and export potentially costlier than for *E. coli*. Although this costly export is not limited to microbial consortia, since an "extended" overflow metabolism was determined for several biotechnologically relevant production organisms, the concentrations are – besides a few exceptions such as acetate for *E. coli* (Helling *et al.*, 1987) – likely not high enough to sustain an auxotrophic partner strain (Paczia *et al.*, 2012).

It might also be a fallacy to assume that the savings in carbon and energy result in improved production titers: Even if a single strain in a supplemented monoculture is more efficient and the synergy between the two strains in co-culture is optimal, the efficiency benefits might be topped by the energy and carbon costs to sustain the helper strain. A targeted shut-off of the helper strain to reduce its resource consumption after the transition to the production phase was suggested for growth-decoupled processes (Noack and Baumgart, 2019). Examples, e.g., optogenetic control to regulate the population ratio and productivity of mixed consortia, are known (Lalwani *et al.*, 2021). However, they do not include a reference process in a comparable monoculture. Additional modifications, such as switch-based strain shut-off, could result in yet-to-be-discovered problems with community dynamics regarding production. Lastly, even if this approach were to be more efficient on a small scale, results from comparable large-scale production processes are missing, therefore yet unknown problems might loom in the upscaling (Takors, 2012).

Overall, many challenges and pitfalls must be overcome to set up a successful production process with a CoNoS. In the following three subchapters, the specific design of a CoNoS bioprocess to be established in this work will be described.

1.3.2 Defining niche, product, and community members

Among the key products of industrial biotechnology are amino acids, making up the largest fraction of the global amino acid market volume in 2022 of 28.3 billion US$, estimated to rise by 2050 to 49.67 billion US$ (GrandViewResearch, 2023, Wendisch, 2020). Especially for bulk chemicals like several of the amino acids, only a few percent increase in process efficiency are easily worth millions, making research in this direction worthwhile. Microbial production of amino acids is mostly done with *C. glutamicum* since, in the 1950s, a low-cost glutamate production process with this organism was developed, causing researchers to pursue establishing and improving further amino acid production processes (Hashimoto, 2017, Kinoshita *et al.*, 1957).

C. glutamicum is a gram-positive, non-pathogenic, non-sporulating, non-motile, facultative anaerobic, biotin-auxotrophic soil bacterium with a high GC-content, with single cells forming short rods to ellipsoidal spheres (Abe *et al.*, 1967). The genome sequence of *C. glutamicum* has been available for twenty years now (Kalinowski *et al.*, 2003, Ikeda and Nakagawa, 2003), and the bacterium has, in contrast to its relatives *Mycobacterium tuberculosis* and *Corynebacterium diphtheriae* from the same phylum *Actinomycetota*, GRAS ("generally regarded as safe") status. *C. glutamicum* is genetically well accessible. Many tools are available for stable genomic mutations and integrations (Schäfer *et al.*, 1994), plasmid-based gene expression (Kirchner and Tauch, 2003), CRISPR-Cpf1 (Jiang *et al.*, 2017) and CRISPRi (Cleto *et al.*, 2016). A genome-scale network model was already established, enabling future in-depth metabolic modeling studies (Zelle *et al.*, 2015). A characteristic feature of *C. glutamicum* and most other members of the CMN group (*Corynebacterium*, *Mycobacterium*, *Nocardia*) of *Actinomycetota* is its unusual structural cell envelope organization, which comprises a thick arabinogalactan-peptidoglycan layer linked to an outer membrane-like lipid layer consisting mainly of mycolic acids (Bayan *et al.*, 2003). Together with its high tolerance to stresses and its phage resistance, *C. glutamicum* has become a favorite host for biotechnological production processes (Eggeling and Bott, 2005).

During the last decades, *C. glutamicum* was engineered to produce about 70 natural and non-natural compounds, including food, feed, and a variety of products for medical, pharmaceutical, and nutraceutical applications as well as for the chemical industry, including bulk biofuels (Becker *et al.*, 2018, Wolf *et al.*, 2021). Among those, industrially relevant production strains – mainly for amino acids – were usually constructed based on either mutagenesis and

selection or, more recently, by rational metabolic engineering (Lee and Wendisch, 2017). Almost all amino acids can be produced via fermentation with *C. glutamicum*. The annual production in 2019 was, for example, 500 metric tons of L-leucine, 1,200 metric tons of L-arginine, 41,000 tons of L-tryptophan, 2,600,000 tons of L-lysine, and 3,210,000 tons of L-glutamic acid, with a minor contribution of extraction and enzymatic processing for some of them (Wendisch, 2020). *C. glutamicum* could also harbor potential for higher production efficiency through genome reduction. Quantitative proteomics studies identified parts of their relevant enzymatic machinery as unnecessary. Many central metabolic enzymes are present in much higher amounts than required for maintaining optimal growth in a bioreactor (Voges *et al.*, 2015). Moreover, it was shown for some carbon sources such as D-glucose that the cells maintain stable enzyme concentrations independent of the availability of the substrate (Noack *et al.*, 2017), basically freezing high amounts of carbon and energy in presumably unused proteins (Noack and Baumgart, 2019). This all makes up for *C. glutamicum* as an ideal host organism to set up an amino acid production process applying the CoNoS concept. Notably, in one approach, the 13.4 % genome-reduced *C. glutamicum* C1* strain was constructed, for which, however, no increased growth rate or production capacity was yet found (Baumgart *et al.*, 2017).

In this thesis, the production of L-arginine with the CoNoS approach will be pursued. This semi-essential amino acid has a variety of uses as food and health supplement as well as in the pharmaceutical and cosmetics industry, with functions as an ergogenic aid and potential effects against hypertension and coronary heart diseases (Siani *et al.*, 2000, Alvares *et al.*, 2011, Park *et al.*, 2014). High titer reference processes for L-arginine production were established based on rational engineering and mutagenesis cycles, yielding for example 92.5 g L^{-1} of L-arginine with a yield of 0.40 g L-arginine per gram carbon source (D-glucose plus sucrose), and several targets for strain engineering are known (Park *et al.*, 2014, Zhan *et al.*, 2019). Such reference processes are required to compare yield, productivity, and titer of the CoNoS-based production process later. For *C. glutamicum* grown on D-glucose as energy and carbon source, the synthesis of 1 mol L-arginine is highly demanding. It requires 2 mol ATP and 3 mol NADPH, suggesting that savings in parallel energy-demanding processes could improve its production.

As a medium, growth of *C. glutamicum* in complex medium or with molasses as a C-source is possible (Eggeling and Bott, 2005). The use of defined CGXII medium (Keilhauer *et al.*, 1993), which has become the standard medium for *C. glutamicum* cultivation for metabolic engineering

and systems biology, allows for very high growth rates and high reproducibility (Unthan *et al.*, 2014). Defined minimal medium prevents unwanted side reactions and changing media qualities, simplifies product analysis, and renders downstream processing more cost-efficient (Hermann, 2003). To study cross-feeding interactions, a medium without the exchanged metabolites is also essential, making CGXII the medium of choice.

1.3.3 Deletion targets: Amino acid synthesis pathways

Having decided on the production of L-arginine with a co-culture of two *C. glutamicum* strains in CGXII medium, the following step is to decide on the targets for genome reduction that yield the two auxotrophic strains. We formulated several criteria an auxotrophy has to meet to be considered suitable in the CoNoS setup:

1) Cross-fed compounds must be primary metabolites for their synthesis to be coupled to biomass formation. This ensures that growth without cross-feeding is not possible and that cross-feeding is required right from the start of the cultivation (Noack and Baumgart, 2019).

2) Complementation of the auxotrophy must be possible by external supply of the missing metabolite, allowing for the phenotyping of monocultures of each strain (Schito *et al.*, 2022).

3) A decrease in carbon and energy demand must accompany the introduced auxotrophies. This decrease must be higher than the costs for metabolite uptake and carbon flux changes in each strain (Schito *et al.*, 2022).

4) Introducing auxotrophies by deleting genes or operons should not affect the transcription of other genes unrelated to the respective biosynthesis pathway (Schito *et al.*, 2022).

As described in previous chapters, amino acid biosynthesis pathways perfectly match these criteria and are typical auxotrophies of native microorganisms, allowing for high energy savings (D'Souza *et al.*, 2014, Goyal, 2018, Noack and Baumgart, 2019). Additionally, as an amino acid was chosen as the desired product, this would reduce the number of modifications in the producer strain, as it is not required to produce one metabolite for cross-feeding as well as a second metabolite for the desired bioprocess. During this work, the potential of all amino acids for the CoNoS setup was evaluated, identifying that not all amino acids are equally suitable for cross-feeding interactions, and several different auxotrophies were tested (Schito *et al.*, 2022). Based on those results, the final choice fell on a CoNoS based on an L-arginine and an L-leucine auxotrophic strain. The biosynthesis of L-arginine and L-leucine branching from the primary carbon

metabolism in *C. glutamicum* and the genomic organization of the biosynthetic genes are shown in Figure 1.3.

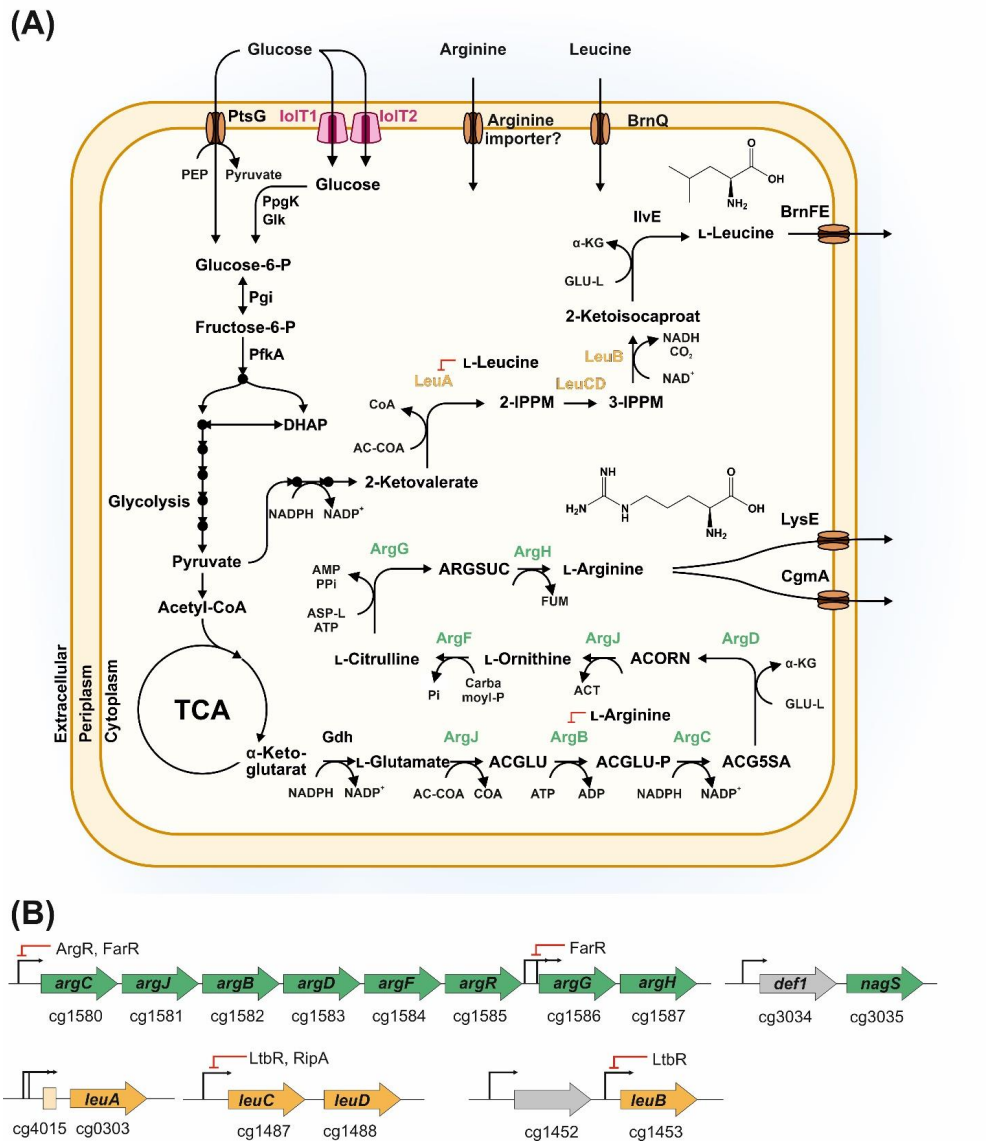

Figure 1.3: L-Arginine and L-leucine biosynthesis and transport during the primary carbon metabolism of *C. glutamicum*. (A) Primary carbon metabolism of *C. glutamicum* with D-glucose

as carbon source. L-Arginine and L-leucine biosynthesis, their respective structure as well as their feedback inhibition on protein level are shown. Adapted from (Park *et al.*, 2014, Vogt *et al.*, 2014, Zelle *et al.*, 2015, Ramp, 2022). **(B)** Genomic organization with promoters (black arrows) and transcription-based regulation (red arrows) of L-leucine and L-arginine biosynthetic genes. Adapted from (Schito *et al.*, 2022). Abbreviations: αKG (α-ketoglutarate), AC-COA (acetyl coenzyme A), ACGLU (acetylglutamate), ACGLU-P (acetylglutamyl-phosphate), ACG5SA (acetylglutamate-5-semialdehyde), ACORN (acetylornithine), ArgB (acetylglutamate kinase), ArgC (*N*-acetyl-γ-glutamyl-phosphate reductase), ArgD (acetylornithine aminotransferase), ArgF (ornithine carbamoyltransferase), ArgG (argininosuccinate synthase), ArgH (argininosuccinate lyase), ArgJ (*N*-acetylglutamate synthase), ArgR (transcriptional repressor of arginine biosynthesis), ARGSUC (argininosuccinate), ACT (acetate), BrnFE (branched-chain amino acid exporter), BrnQ (branched-chain amino acid uptake carrier), CgmA (cadaverine export permease), Defl (peptide deformylase 1), DHAP (dihydroxyacetone phosphate), FarR (transcriptional regulator involved in amino acid biosynthesis), FUM (fumarate), Gdh (glutamate dehydrogenase), Glk (glucokinase), GLU-L (L-glutamic acid), IlvE (branched-chain amino acid aminotransferase), IolT1 (*myo*-Inositol transporter 1), IolT2 (*myo*-Inositol transporter 2), 2-IPPM (2-isopropylmalate), 3-IPPM (3-isopropylmalate), LeuA (2-isopropylmalate synthase), LeuB (3-isopropylmalate dehydrogenase), LeuCD (isopropylmalate isomerase), LtbR (leucine and tryptophan biosynthesis regulator), LysE (lysine efflux permease), NagS (*N*-acetylglutamate synthase), PEP (2-phosphoenolpyruvate), PfkA (6-phosphofructokinase), Pgi (glucose-6-phosphate isomerase), PpgK (polyphosphate glucokinase), PtsG (glucose phosphotransferase system), RipA (transcriptional regulator of iron proteins and repressor of aconitase), TCA (tricarboxylic acid cycle).

1.3.4 Iterative strain engineering and production process development

To establish an efficient production process with a CoNoS, the co-culture has to grow to a high cell density within an acceptable amount of time. The production of the cross-fed amino acids has to be increased, as previous analyses of *C. glutamicum* wild type culture supernatant suggested only 35 µM of L-arginine accumulation and no detectable L-leucine (Paczia *et al.*, 2012). Especially in larger volumes in which these metabolites are further diluted, this could impede CoNoS growth. To change this, several rational metabolic engineering targets for optimization of their synthesis are already known.

Biosynthesis of L-arginine starts from L-glutamic acid derived from the TCA cycle. The enzymatic machinery is encoded by the ARG-operon *argCJBDFGH* (Sakanyan *et al.*, 1996) and *nagS* (encoding *N*-acetylglutamate synthase) (Petri *et al.*, 2013). Two transcriptional start sites were found, one in front of *argC* (encoding *N*-acetyl-γ-glutamyl-phosphate reductase) and the other in front of *argG* (encoding argininosuccinate synthase) (Pfeifer-Sancar *et al.*, 2013). The key enzyme for L-arginine production is the *N*-acetylglutamate kinase (ArgB), which is feedback inhibited by L-arginine (see Figure 1.3A). This regulation can be circumvented via the point

mutations A26V and M31V in ArgB (Ikeda *et al.*, 2009). Furthermore, the two transcriptional regulators ArgR and FarR are known to regulate the L-arginine biosynthesis gene cluster. ArgR binds at the promoters of *argC* and *argG*, regulating the expression level of *argCJBDF* – but not of *argGH* – in dependence on the intracellular arginine concentration (Yim *et al.*, 2011). The other regulator, FarR, controls not only the transcript level of the ARG cluster (see Figure 1.3B) but also of the *gdh* gene (encoding glutamate dehydrogenase) (Hänßler *et al.*, 2007). The deletion of both regulators was beneficial for L-arginine production (Ikeda *et al.*, 2009, Park *et al.*, 2014). Another target for metabolic engineering is the L-arginine export. Two exporters of L-arginine are known: lysine efflux permease (LysE) and cadaverine export permease (CgmA). Plasmid-based expression of the gene encoding the major L-arginine exporter LysE results in an increased L-arginine titer (Xu *et al.*, 2013). CgmA, on the other hand, is the export system for putrescine and cadaverine with some activity for L-arginine, therefore deletion of its repressor CgmR improves the final L-arginine titer as well (Lubitz *et al.*, 2016). The availability of the precursor molecule for L-arginine production, L-glutamate, depends, amongst others, on L-glutamate export via the mechanosensitive exporter YggB (Nakamura *et al.*, 2007). YggB deletion is beneficial for L-arginine production (Park *et al.*, 2014). General carbon flux optimization and increases in the NADPH level via a cofactor manipulating strategy, including increased flux into the PPP or expression of *pntAB* encoding the membrane-bound transhydrogenase from *E. coli*, are also promising ways of improving the L-arginine titer (Park *et al.*, 2014, Zhan *et al.*, 2019).

L-Leucine biosynthesis starts from central metabolism at the level of pyruvate, and four genes, *leuA* (Patek *et al.*, 1994), *leuB* (Patek *et al.*, 1998), and *leuCD* (Patek *et al.*, 1994), encode the enzymatic machinery. Metabolic engineering for improving L-leucine production is challenging since its biosynthesis is linked to the other branched-chain amino acids (BCAA) by parallel and debranching reactions, partly of identical enzymes (Leyval *et al.*, 2003). The key enzyme 2-isopropylmalate synthase (LeuA), catalyzing the first reaction specific for L-leucine biosynthesis, i.e., the conversion of 2-ketoisovalerate and acetyl-CoA to 2-isopropylmalate and CoA, is feedback inhibited by L-leucine (Patek *et al.*, 1994) (see Figure 1.3A&B). Expression of *leuA* on transcription level is also regulated via an upstream attenuator sequence (Patek *et al.*, 1994). LeuA can be deregulated via a promoter exchange to a stronger promoter in front of *leuA*, which can be even more effective when combined with further gene copies (Vogt *et al.*, 2014). Using the *leuA* sequence of the L-leucine-producing strain B018 created via random mutagenesis

by Amino GmbH (Frellstedt, Germany), containing mutations resulting in the amino acid exchanges R529H and G532D, is also a viable strategy (Vogt *et al.*, 2014). The protein leucine and tryptophan biosynthesis regulator (LtbR) regulates the transcription of *leuB* (encoding 3-isopropylmalate dehydrogenase) and *leuCD* (encoding isopropylmalate isomerase) (Brune *et al.*, 2007), and its deletion improves L-leucine production significantly (Vogt *et al.*, 2014). Increasing D-glucose uptake and cofactor supply is also beneficial, while plasmid-based expression of the L-leucine exporter BrnFE (Kennerknecht *et al.*, 2002) did not improve production (Vogt *et al.*, 2014). One problem of BCAA production is the formation of other BCAA as byproducts, as the final aminotransferase step via branched-chain amino acid aminotransferase (IlvE) is unspecific (Radmacher *et al.*, 2002) and general metabolic engineering steps toward increased L-leucine production such as relieving feedback-inhibition of acetohydroxy acid synthase (AHAS) (Keilhauer *et al.*, 1993, Elisakova *et al.*, 2005) also increase formation of the other BCAA. This could ideally be improved to increase the overall L-leucine titer as well. Testing other, more specific aminotransferases, however, did not result in improved titer yet (Feng *et al.*, 2018).

For reaching sufficient CoNoS growth, as few rational changes in the helper-strain as possible are desirable. Especially large-scale carbon flux and cofactor supply changes might hinder the CoNoS process later. Therefore, relieving feedback inhibition will be the starting point. In Figure 1.3A, metabolic engineering strategies to relieve feedback inhibition in L-leucine and L-arginine production are marked.

As soon as sufficient growth of the CoNoS is established, ALE can be conducted to generate strains better adapted to the generated niche. However, further, neutral or non-beneficial mutations can accumulate in addition to the desired mutations during evolution experiments, especially when production-decreasing mutations would enable faster growth of subpopulations (Stella *et al.*, 2021, Zuchowski *et al.*, 2023). Since only verified, stable genomic changes are sought, sequencing and rational reengineering of only the beneficial mutations are necessary to establish a reproducible production process later. Co-culture evolution experiments resulting in improved growth were successfully applied before (Zhang and Reed, 2014, Preussger *et al.*, 2020), which led to improved production of the cross-fed metabolite. This suggests that cross-feeding is often the growth rate-limiting factor for the communities. Therefore, co-culture-based ALE is an interesting concept for metabolic engineering to identify traits that improve cross-feeding of *C. glutamicum* (Stella *et al.*, 2019). Compared to established procedures with monocultures, this

ideally results in finding novel production traits in amino acid biosynthesis or transport. This could extend the benefits of the CoNoS approach also to current best-producing monocultures.

1.4 Aims of this thesis

In this thesis, the establishment of a novel L-arginine production process based on synthetic communities of niche-optimized strains (Noack and Baumgart, 2019) with a moderate L-arginine producer strain as a proof-of-principle is pursued. Due to a reduction of the metabolic burden of one amino acid synthesis pathway of *C. glutamicum* enabled by growing in a highly efficient community of obligate cross-feeders, the final production process is hypothesized to be more efficient in producing this relevant bulk chemical. This is the first step toward the overall aim of the project "CoNoS" this thesis is contributing to, the generation of a CoNoS that produces a selected amino acid more efficiently than pure cultures of current best producers.

As a first step, several different communities harboring different metabolic auxotrophies need to be set up and characterized in detail. These first-generation CoNoS, stably but compared to the WT slowly growing, should then be employed in ALE experiments to enable better adaptation of the synthetic community to the provided niche. The resulting strains should be sequenced, and selected mutations could be reintroduced afterward into the unevolved strain. The identified mutations could then provide new knowledge about the evolution of communities in general, as they will point to the main hindrances in the way of community stabilization. Moreover, novel targets and knowledge for improving current amino acid-producing strains could be generated by evolving either monocultures or co-cultures.

Based on the evolved and reengineered communities, further rational metabolic engineering could be applied to improve both mono- and co-culture production titer. Further adaptations to the production process, for example, by regulating the strain ratio, should then be tested. The final second-generation CoNoS must then be characterized regarding the efficiency of its L-arginine production in comparison to a monoculture harboring the same mutations for improved arginine in larger-scale fermentation systems. Higher L-arginine titers in the co-culture would then be a proof of concept regarding the CoNoS principle for biotechnological production.

2. Results

2.1 Communities of Niche-optimized Strains (CoNoS) – Design and creation of stable, genome-reduced co-cultures

Schito, S.*, Zuchowski, R.*, Bergen, D., Strohmeier, D., Wollenhaupt, B., Menke, P., Seiffarth, J., Nöh, K., Kohlheyer, D., Bott, M., Wiechert, W., Baumgart, M., Noack, S. (2022). Communities of Niche-optimized Strains (CoNoS) - Design and creation of stable, genome-reduced co-cultures. *Metabolic engineering*, 73, 91-103.

* These authors contributed equally to this work.

Author contributions

SS: Conceptualization, Methodology, Investigation, Data analysis, Writing – Initial Draft, Visualization, Revision & Writing – final manuscript

RZ: Conceptualization, Methodology, Investigation, Data analysis, Writing – Initial Draft, Visualization, Revision & Writing – final manuscript

DS: Investigation, Methodology, Data analysis

BW: Investigation, Data analysis, Writing – Initial Draft

PM: Investigation, Data analysis

JS: Investigation, Data analysis

KN: Supervision, Data analysis, Writing – Initial Draft

DK: Supervision, Data analysis, Writing – Initial Draft, Funding acquisition

MBo: Revision & Writing – final manuscript, Funding acquisition

WW: Revision & Writing – final manuscript, Funding acquisition

MBa: Conceptualization, Supervision, Revision & Writing – final manuscript, Funding acquisition

SN: Conceptualization, Supervision, Revision & Writing – final manuscript, Funding acquisition

Overall contribution: 30%

Metabolic Engineering 73 (2022) 91–103

Contents lists available at ScienceDirect

Metabolic Engineering

journal homepage: www.elsevier.com/locate/meteng

Communities of Niche-optimized Strains (CoNoS) – Design and creation of stable, genome-reduced co-cultures

Simone Schito [a,1], Rico Zuchowski [a,1], Daniel Bergen [a], Daniel Strohmeier [a], Bastian Wollenhaupt [a], Philipp Menke [a], Johannes Seiffarth [a], Katharina Nöh [a], Dietrich Kohlheyer [a], Michael Bott [a], Wolfgang Wiechert [a,b], Meike Baumgart [a], Stephan Noack [a,*]

[a] Institut für Bio- und Geowissenschaften, IBG-1: Biotechnologie, Forschungszentrum Jülich, Jülich, Germany
[b] Computational Systems Biotechnology (AVT.CSB), RWTH Aachen University, D-52074, Aachen, Germany

ARTICLE INFO

Keywords:
Microbial communities
Synthetic cocultures
C. glutamicum
Genome reduction

ABSTRACT

Current bioprocesses for production of value-added compounds are mainly based on pure cultures that are composed of rationally engineered strains of model organisms with versatile metabolic capacities. However, in the comparably well-defined environment of a bioreactor, metabolic flexibility provided by various highly abundant biosynthetic enzymes is much less required and results in suboptimal use of carbon and energy sources for compound production. In nature, non-model organisms have frequently evolved in communities where genome-reduced, auxotrophic strains cross-feed each other, suggesting that there must be a significant advantage compared to growth without cooperation. To prove this, we started to create and study synthetic communities of niche-optimized strains (CoNoS) that consists of two strains of the same species *Corynebacterium glutamicum* that are mutually dependent on one amino acid. We used both the wild-type and the genome-reduced C1* chassis for introducing selected amino acid auxotrophies, each based on complete deletion of all required biosynthetic genes. The best candidate strains were used to establish several stably growing CoNoS that were further characterized and optimized by metabolic modelling, microfluidic experiments and rational metabolic engineering to improve amino acid production and exchange. Finally, the engineered CoNoS consisting of an L-leucine and L-arginine auxotroph showed a specific growth rate equivalent to 83% of the wild type in monoculture, making it the fastest co-culture of two auxotrophic *C. glutamicum* strains to date. Overall, our results are a first promising step towards establishing improved biobased production of value-added compounds using the CoNoS approach.

1. Introduction

Current bioprocesses for the production of value-added compounds are mainly based on pure cultures that are composed of rationally engineered strains of platform organisms with versatile metabolic capacities. These strains often possess vast overcapacities of specific central metabolic proteins, a natural mechanism to cope with rapidly changing environmental conditions. On the one hand, a complex genome confers robustness to a cell, but on the other hand, it affects the predictability for biotechnological applications (Wynands et al., 2019).

In support of this, O'Brien and co-workers recently performed a genome-scale analysis of absolute protein data originating from *Escherichia coli* experiments across 16 different environments (O'Brien et al., 2016). They argue that almost half of the proteome mass is unused in certain environments and, most importantly, reduction in unused protein expression is shown to be a common mechanism to increase cellular growth rates in adaptive evolution experiments.

For another industrially important organism, *Corynebacterium glutamicum*, two quantitative proteomics studies showed that: *i)* the cellular amount of various central metabolic enzymes is much higher than necessary for maintaining optimal growth in bioreactor environments (Voges et al., 2015), and *ii)* cells maintain stable enzyme concentrations when grown on a specific primary carbon source, independent of its availability (Noack et al., 2017). This means that even under substrate

* Corresponding author. Institute of Bio- and Geosciences, IBG-1: Biotechnology, Forschungszentrum Jülich GmbH, Jülich, D-52425, Germany.
E-mail address: s.noack@fz-juelich.de (S. Noack).
[1] These authors contributed equally to this work.

https://doi.org/10.1016/j.ymben.2022.06.004
Received 1 March 2022; Received in revised form 20 May 2022; Accepted 17 June 2022
Available online 21 June 2022

limiting conditions, *e.g.*, in a fed-batch scenario without overfeeding, a significant amount of carbon and energy is captured in unused proteins. In other words, in the comparably well-defined environment of a bioreactor, metabolic flexibility provided by overexpression of biosynthetic genes is much less required and results in suboptimal production processes due to the waste of carbon and energy sources that could be re-directed toward a more efficient bio-production.

Synthetic genome reduction is one promising strategy to reduce these undesired protein overcapacities. Recently, we constructed a genome-reduced chassis of *C. glutamicum* by following comprehensive gene deletions including those for the three prophages, IS elements and several other genes not relevant for growth under defined D-glucose conditions (Baumgart et al., 2013, 2018; Unthan et al., 2015). The resulting strain, denoted as C1*, possesses a genome reduced by 13.4%. However, no significant increase in specific growth rate was observed compared to the wild type under various conditions.

To find an explanation for this surprising finding, we performed a comparative analysis of natural and synthetic reduced genomes and their corresponding ecological niches (Noack and Baumgart, 2019). This analysis revealed that: *i)* only deleting expressed genes can lead to noticeable carbon and energy savings that are useable for improving biomass or product synthesis; *ii)* such streamlined strains cannot exist as pure cultures but depend on the environment, *e.g.*, another community member, to complement deleted functions, and *iii)* bacterial cross-feeding interactions have evolved quite frequently in nature and, thus, there must be significant advantages for such communities.

We therefore introduced the term "Communities of Niche-optimized Strains" (CoNoS). More specifically, a CoNoS consists of at least two strains of the same species, each carrying one or more auxotrophy (Fig. 1). The strains are supposed to cross-feed each other and thereby save carbon and energy by sharing the available enzymatic capacity for the required amino acids. In this way, the strains involved in a CoNoS create a synthetic niche that mimics the naturally occurring community interactions.

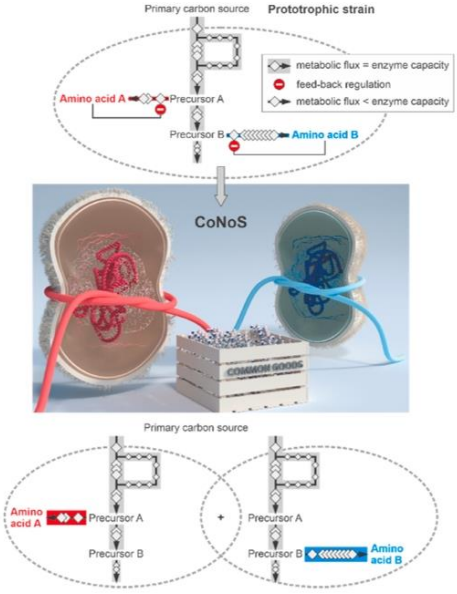

Fig. 1. CoNoS-framework for the design and creation of stable, genome-reduced co-cultures for improved amino acid production utilizing synthetic bacterial communities. As an example, the creation of a CoNoS is depicted that consists of two streamlined strains that are additionally made auxotrophic for amino acids A and B, respectively, to introduce cross-feeding interactions for these common goods.

Moreover, as McCarty and Ledesma-Amaro have pointed out, switching bioproduction from monocultures to synthetic microbial communities of auxotrophs offers many other potential advantages (McCarty and Ledesma-Amaro, 2019). One of these relates to modularity and the ability to partition engineered biosynthetic pathways among specialized strains, which could facilitate the process of metabolic engineering and reduce cross-reactivities through compartmentalization.

In this study, we successfully designed and engineered CoNoS that consists of two strains of the model organism *C. glutamicum*. We have succeeded in establishing stable, genome-reduced and fast-growing CoNoS based on greatly increased amino acid exchange rates. Based on a comprehensive characterization of engineered CoNoS, the challenges in strain and process development are discussed to establish such synthetic communities for efficient bioproduction in the near future.

2. Results

2.1. Model-based design of C. glutamicum CoNoS

For the design and stable operation of a CoNoS, the strain engineering and target product selection underlies two major criteria:

1) Introduced auxotrophies should result in a significant release of carbon and energy due to the lack of expressed genes.
2) External supply of the essential metabolite should allow full complementation of the introduced auxotrophy. This is of particular importance for the independent phenotyping of engineered strains under different environmental conditions.

Following these criteria, we decided to focus on the creation of CoNoS for the overproduction of selected proteinogenic amino acids.

We started with an *in silico* feasibility analysis for introducing single amino acid auxotrophies in *C. glutamicum*. Briefly, by taking all 20 proteinogenic amino acids into account, we performed constraint-based flux balance analysis (cFBA) using an extended genome-scale model and a newly created focused network model of *C. glutamicum*. Auxotrophies were modeled by blocking at least one essential reaction step in the corresponding amino acid biosynthetic pathway at a time. Optimal cell growth was simulated with D-glucose as primary carbon and energy source and by allowing unrestricted uptake of the essential amino acid (for details see Material and Methods section).

As a result, most amino acid auxotrophic strains under supplemented conditions are theoretically feasible and the simulated growth phenotypes are consistent with our CoNoS approach (Fig. 2A). As expected, the predicted optimal growth rates were always higher than for the wild type, because more carbon is supplied via the corresponding essential amino acid in addition to a fixed amount of D-glucose (Fig. 2B). Depending on the individual demand of the amino acid for biomass generation and its position in the metabolic network, this growth rate effect might be comparably low (<1% for L-tryptophan, L-histidine and L-cysteine) or high (>10% for L-aspartate and L-asparagine). It is important to note that due to a lack of empirical data, both models do not account for a potential growth advantage of auxotrophic strains in terms of lower gene expression and lower protein production costs (see criterion 1), and the predicted increases in growth rate should not be misinterpreted in this regard.

Exceptions were found for L-glutamate and L-glutamine, whose simulated auxotrophies led to unreasonably high growth rates. Both

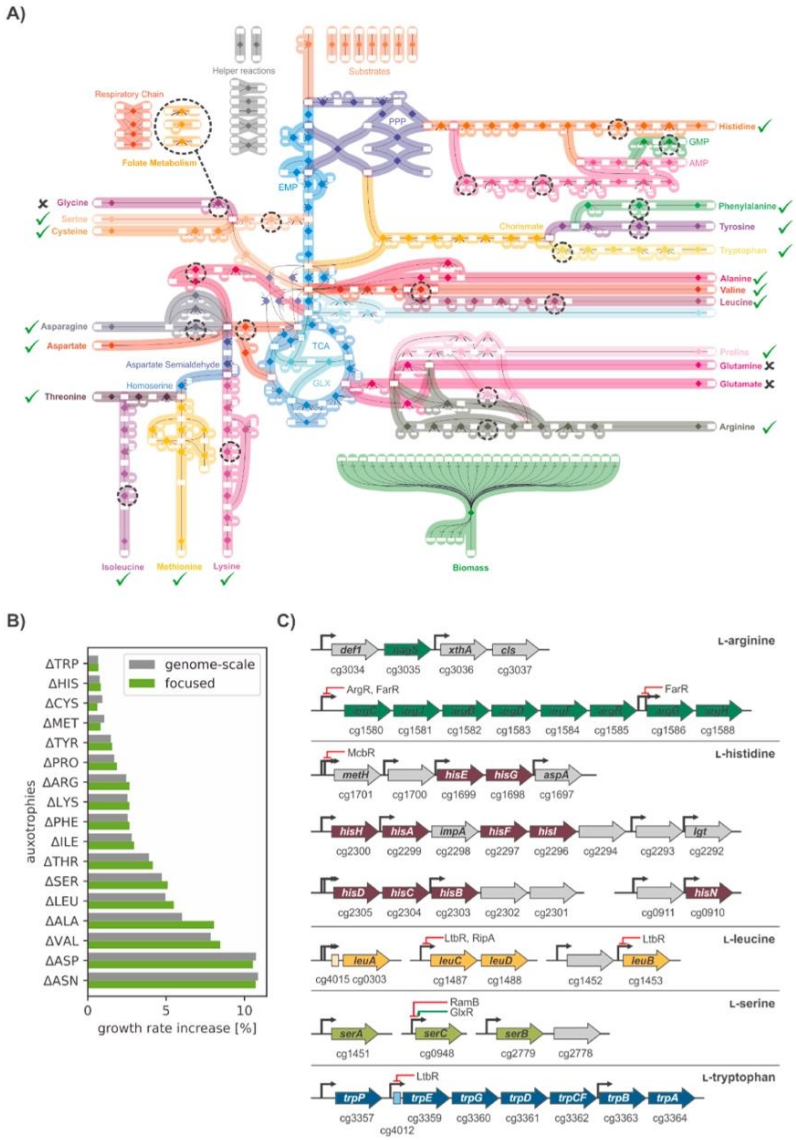

Fig. 2. Model-based design of *C. glutamicum* CoNoS. A) Focused metabolic network model of *C. glutamicum*. Feasible amino acid auxotrophies are check-marked in green. Non-feasible auxotrophies are cross-marked in black and corresponding linkages to the C1 metabolism (L-glycine) as well as transaminase reactions (L-glutamate and L-glutamine) are additionally highlighted. B) Predicted increases in growth rate when single amino acid auxotrophic strains are cultured under supplemented conditions. C) Structural genes encoding the enzymes for synthesis of those amino acids selected for introducing auxotrophies.

amino acids play essential roles in the transamination of different metabolic compounds such as the 2-oxo precursors of most proteinogenic L-amino acids in *C. glutamicum* (Eggeling and Bott, 2005). These transaminations lead either to the formation of additional L-glutamate (in the case of L-glutamine as amine source) or directly to α-ketoglutarate, which can be recycled in the tricarboxylic acid cycle (cf. Fig. 2A). Conclusively, strain designs carrying single amino acid auxotrophies for L-glutamate and L-glutamine are not sufficiently defined for our modelling-assisted CoNoS approach (see criterion 2).

Furthermore, simulation of an L-glycine-auxotrophic strain is not feasible because the required inactivation of the L-serine hydroxyl methyltransferase step (encoded by *glyA*) then also prevents recycling of tetrahydrofolate into 5,10-methylene-tetrahydrofolate. The latter is the major source of C1 units in the cell, making GlyA a key enzyme in the biosynthesis of purines, thymidine, methionine, choline and lipids. In fact, the gene *glyA* is essential in *C. glutamicum* (Peters-Wendisch et al., 2005), but it can be deleted in *E. coli* (Mundhada et al., 2016; Vidal et al., 2008).

Following the *in silico* analysis, we thoroughly studied the transcriptional and metabolic organization of all encoding genes and catalytic enzymes for the synthesis of the 17 proteinogenic amino acids in *C. glutamicum*. We utilized our revised genome annotation list (Baumgart et al., 2018) and the following criteria:

1) Target genes should be organized in one or only a few transcriptional units to allow easy and full deletion of the pathway.
2) Deletion of target genes does not affect transcription of neighboring genes.
3) Associated operons do not contain any relevant genes not related to the amino acid synthesis pathway.

The data obtained were compared with the known demand of each amino acid for biomass synthesis in order to evaluate the potential of a corresponding auxotrophic strain in a CoNoS setting. Finally, our evaluation resulted in the selection of the five amino acids L-arginine, L-histidine, L-leucine, L-serine, and L-tryptophan for establishing CoNoS for amino acid overproduction (Fig. 2C).

2.2. Construction and phenotyping of selected auxotrophic strains

Amino acid auxotrophic strains were constructed by deleting the whole biosynthetic machinery for the respective amino acids L-arginine, L-histidine, L-leucine, L-serine or L-tryptophan (Fig. 2C). Both *C. glutamicum* ATCC 13032 (WT) and the derived genome-reduced *C. glutamicum* C1* (Baumgart et al., 2018) were used as precursor strain. The deletion of the L-histidine biosynthetic machinery is not possible in the C1* background because of the missing L-histidine importer PheP (cg1305) as shown previously (Kulis-Horn et al., 2014). In total, nine auxotrophic strains were constructed that are listed in Table 1. The auxotrophy of each newly constructed strain will be indicated with the Δ symbol followed by the amino acid abbreviation, *e.g.*, ΔARG has the whole L-arginine biosynthetic machinery deleted.

Subsequently, the growth performance of all engineered strains was tested by running small-scale cultures in a BioLector system. Defined CGXII medium with D-glucose as primary carbon and energy source was applied and the corresponding amino acid was supplemented at different concentrations (Fig. 3A). All auxotrophic strains were not able to grow under non-supplemented conditions, confirming the success of the prior genome reduction step. Furthermore, the minimal amount of amino acid supplementation to reach growth at wild-type levels was identified for the L-arginine, L-leucine, and L-serine auxotrophic strains. Interestingly, none of these strains showed a higher growth rate as was predicted by the *in silico* analyses (cf. Fig. 2B). In particular, for the L-leucine and L-serine strains, a 5% increase from 0.59 ± 0.01 h^{-1} (measured control) to 0.62 h^{-1} (simulated auxotrophy) could have been detected, taking into account the measurement accuracy. This is

Table 1
Bacterial strains used in this study.

Strain	Characteristics	Reference
E. coli		
DH5α	F-Φ80*dlac*Δ(*lacZ*)M15 Δ(*lacZYA-argF*) U169 *endA1 recA1 hsdR17* (rK- mK+) *deoR thi-1 phoA supE44 λ- gyrA96 relA1*; strain used for cloning procedures	Hanahan (1983)
C. glutamicum		
ATCC 13032 (WT)	Biotin-auxotrophic wild type	Kinoshita et al. (1957)
C1*	Derivative of ATCC 13032 with a genome reduced by 13.4%	Baumgart et al. (2018)
C1* ΔTRP	C1* with an in-frame deletion of Δ*trpP* (cg3357) Δ*trpE* (cg3359) Δ*trpG* (cg3360) Δ*trpD* (cg3361) Δ*trpCF* (cg3362) Δ*trpB* (cg3363) Δ*trpA* (cg3364)	This study
WT* ΔTRP	WT with an in-frame deletion of Δ*trpP* (cg3357) Δ*trpE* (cg3359) Δ*trpG* (cg3360) Δ*trpD* (cg3361) Δ*trpCF* (cg3362) Δ*trpB* (cg3363) Δ*trpA* (cg3364)	This study
C1* ΔSerA	C1* with an in-frame deletion of Δ*serA* (cg1451)	This study
C1* ΔSerAC	C1* ΔSerA with an in-frame deletion of Δ*serC* (cg0948)	This study
C1* ΔSER	C1* ΔSerAC with an in-frame deletion of Δ*serB* (cg2779)	This study
WT ΔSerA	WT with an in-frame deletion of Δ*serA* (cg1451)	This study
WT ΔSerAC	WT ΔSerA with an in-frame deletion of Δ*serC* (cg0948)	This study
WT ΔSER	WT ΔSerAC with an in-frame deletion of Δ*serB* (cg2779)	This study
C1* ΔLeuA	C1* with an in-frame deletion of Δ*leuA* (cg0303)	This study
C1* ΔLeuACD	C1* ΔLeuA with an in-frame deletion of Δ*leuC* (cg1487) Δ*leuD* (cg1488)	This study
C1* ΔLEU	C1* ΔLeuACD with an in-frame deletion of Δ*leuB* (cg1453)	This study
WT ΔLeuA	WT with an in-frame deletion of Δ*leuA* (cg0303)	This study
WT ΔLeuACD	WT ΔLeuA with an in-frame deletion of Δ*leuC* (cg1487) Δ*leuD* (cg1488)	This study
WT ΔLEU	WT ΔLeuACD with an in-frame deletion of Δ*leuB* (cg1453)	This study
C1* ΔNagS	C1* with an in-frame deletion of Δ*nagS* (cg3035)	This study
C1* ΔARG	C1* ΔNagS with an in-frame deletion of Δ*argC* (cg1580) Δ*argJ* (cg1581) Δ*argB* (cg1582) Δ*argD* (cg1583) Δ*argF* (cg1584) Δ*argR* (cg1585) Δ*argG* (cg1586) Δ*argH* (cg1588)	This study
WT ΔNagS	WT with an in-frame deletion of Δ*nagS* (cg3035)	This study
WT ΔARG	WT ΔNagS with an in-frame deletion of Δ*argC* (cg1580) Δ*argJ* (cg1581) Δ*argB* (cg1582) Δ*argD* (cg1583) Δ*argF* (cg1584) Δ*argR* (cg1585) Δ*argG* (cg1586) Δ*argH* (cg1588)	This study
WT ΔHisEG	WT with an in-frame deletion of Δ*hisE* (cg1699) Δ*hisG* (cg1698)	This study
WT ΔHisEGHAF	WT ΔHisEG with an in-frame deletion of Δ*hisH* (cg2300) Δ*hisA* (cg2299) Δ*impA* (cg2298) Δ*hisF* (cg2297) Δ*hisI* (cg2296)	This study
WT ΔHisEGHAFDCB	WT ΔHisEGHAF with an in-frame deletion of Δ*hisD* (cg2305) Δ*hisC* (cg2304) Δ*hisB* (cg2303)	This study
WT ΔHIS	WT ΔHisEGHAFDCB with an in-frame deletion of Δ*hisN* (cg0910)	This study
C1* ΔARG LEU$^+$	C1* ΔARG with an exchange of *leuA* (cg0303) 180 bp upstream region including the leader peptide and native promoter with *tuf* promoter	This study
C1* ΔLEU ARG$^+$	C1* ΔLEU with in frame-deletion of Δ*argR* (cg1585)	This study
C1* ΔTRP LEU$^+$	C1* ΔTRP with an exchange of *leuA* (cg0303) 180 bp upstream region	This study

(*continued on next page*)

Table 1 (*continued*)

Strain	Characteristics	Reference
	including the leader peptide and native promoter with *tuf* promoter	
C1* ΔLEU TRP^{+}	C1* ΔLEU with point mutations $trpL_{fbr}$ $TrpE_{S38R}$ (Cg3359)	This study
WT ΔHIS TRP^{+}	WT ΔHIS with point mutations $trpL_{fbr}$ $TrpE_{S38R}$ (Cg3359)	This study
WT ΔTRP HIS^{+}	WT ΔTRP with point mutation $HisG_{A270D}$ (Cg1698)	This study
WT ΔARG LEU^{++}	WT ΔARG with exchange of *leuA* (cg0303) and 180 bp upstream region to *leuA*_B018 (B018: L-leucine producing *C. glutamicum* strain created by random mutagenesis) under control of the *tuf* promoter	This study
C1* ΔLEU ARG^{++}	C1* ΔLEU ARG^{+} with point mutations $ArgB_{A26V\ M31V}$ (Cg1582)	This study
C1* ΔLEU ARG^{+}:: P_{tac}-eYFP	C1* ΔLEU ARG^{+} with eYFP fluorescent protein under control of tac promoter integrated in the IGR between cg1121 and cg1122	This study
WT ΔLEU ARG^{++}:: P_{tac}-eYFP	WT ΔLEU ARG^{+} with eYFP fluorescent protein under control of tac promoter integrated in the IGR between cg1121 and cg1122	This study
WT ΔARG LEU^{++}:: P_{tac}-crimson	WT ΔARG LEU^{++} with crimson fluorescent protein under control of tac promoter integrated in the IGR between cg1121 and cg1122	This study

surprising since we also expected an additional growth advantage of these auxotrophs through the deletion of the strongly expressed amino acid biosynthetic genes.

In case of the L-histidine and L-tryptophan auxotrophs, the specific growth rate was strongly reduced compared to the wild type (Fig. 3A). This effect could be due to several reasons and one can speculate about a general limitation of the uptake of the corresponding amino acid, a down-regulation of the D-glucose uptake or an accumulation of growth-inhibitory intermediates as a consequence of enzyme inactivation and the lack of complete biosynthetic pathways. Clearly, a slow-growing auxotrophic strain is less suitable for a CoNoS because it would affect the performance of the entire co-culture due to the mutual exchange of amino acids required for growth. Except for the L-tryptophan auxotrophic strain, no difference in growth rates were detected between the strains based on the C1* and wild type, respectively (data not shown).

2.3. Setup and engineering of stable CoNoS

With the strains auxotrophic for 5 different amino acid at hand, we could potentially establish 10 different CoNoS. To pre-select pairs of interest, we performed *in silico* co-culture simulations using a similar model-based design as for the single cFBA, but now applying the SteadyCom approach (for details see Material and Methods section).

In general, the predicted relative abundances in the simulated co-cultures are consistent with the results of the cFBA approach. Auxotrophic strains exhibiting a higher increased growth rate under supplemented conditions also occurred in lower fractions in the corresponding CoNoS setting (cmp. Figs. 2B and 3B). These uneven distributions are

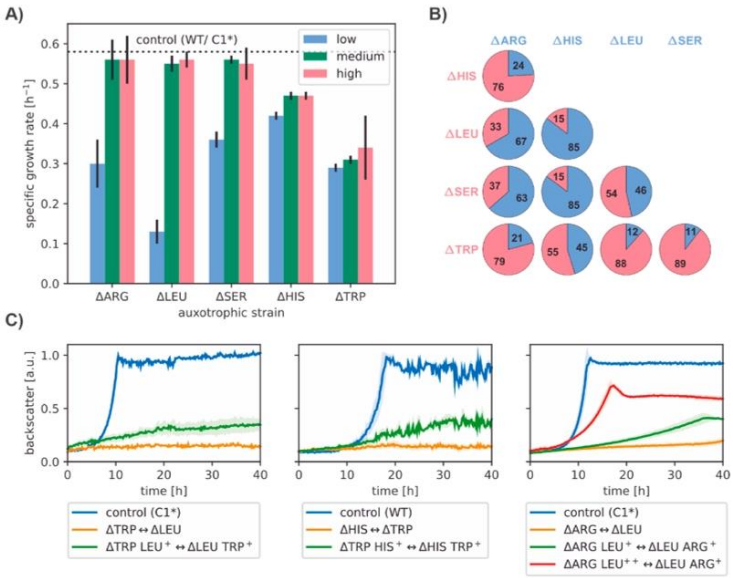

Fig. 3. Setup of stable CoNoS. A) Growth performance of engineered auxotrophic strains. Cultures were performed in triplicate in defined CGXII medium containing 111 mM D-glucose and different additions of the corresponding amino acid. B) *In silico* prediction of relative abundances of selected auxotrophic strains in different co-culture combinations. C) Growth performance of selected CoNoS. Cultures were performed in triplicate in non-supplemented CGXII medium with 111 mM D-glucose. Further engineered strains are marked with a plus sign. The predecessor used for the correspondent strain construction (*C. glutamicum* C1* or WT) was cultivated as a positive control. Backscatter data were normalized by the maximum value recorded for each positive control culture. Mean values and standard deviations are shown as lines and shaded areas, respectively.

due to different demands of the amino acids for the cellular composition of *C. glutamicum*. For example, the demand of L-histidine for protein synthesis (0.066 mmol g^{-1}) is nearly two thirds lower as compared to L-arginine (0.188 mmol g^{-1}), which explains the predicted ratio of 76:24.

From these results we selected three pairs of auxotrophs whose predicted distributions span a certain range and whose introduced auxotrophies partially overlap, namely ΔTRP ↔ ΔLEU, ΔHIS ↔ ΔTRP and ΔARG ↔ ΔLEU. All three CoNoS were cultivated under non-supplemented D-glucose conditions in a BioLector. Low cell population growth was observed only for the CoNoS consisting of the L-arginine and L-leucine-auxotrophic strains (Fig. 3C). The two strains, although highly inefficient, were able to mutually exchange the required amount of amino acids to establish a growing co-culture. Using an endpoint sample and considering 47 clones, we analyzed the ratio of the two strains by colony PCR. This resulted in a distribution of 83:17 for the ΔARG and ΔLEU strains, respectively. This ratio is significantly higher as compared to the model predictions (67:33, cf. Fig. 3B) and indicates an unbalanced amino acid exchange between the two CoNoS partners with L-leucine as the limiting factor.

To establish more balanced co-cultures, we further engineered all strains toward higher production of the corresponding cross-fed amino acid. To this end, reversal of feedback inhibition in the selected auxotrophs is a straightforward approach with minimal metabolic engineering. For enhancing L-arginine biosynthesis, relieving the feedback inhibition of the *arg*-operon can be realized by deleting its repressor, namely *argR* (cf. Fig. 2C) (Ikeda et al., 2009). In case of L-histidine, the feedback inhibition can be interrupted by introducing a mutation in HisG (A270D) (Kulis-Horn et al., 2015). The regulation of L-tryptophan can be circumvented by mutating the attenuator *trpL* as well as TrpE (S38A) (Matsui et al., 1987). Finally, in L-leucine biosynthesis, the first enzyme, LeuA, is regulated via feedback inhibition. To increase L-leucine biosynthesis, the native *leuA* gene promoter and the leader peptide *leuL* were replaced by the strong promoter of the elongation factor TU (P_{tuf}) as described previously (Vogt et al., 2014).

In the following, the further engineered auxotrophic strains are labeled with the abbreviation of the target product and a plus sign indicating the level of engineering, *e.g.*, ΔARG LEU$^+$ is a first generation L-leucine overproducing strain. These strains were cultivated under equal co-culture conditions as before. In all cases, CoNoS composed of strains optimized for amino acid over production resulted in stably growing co-cultures, confirming the success of the metabolic engineering strategy (Fig. 3C). Nevertheless, all co-cultures grew much slower than the corresponding control strain, still indicating a severe limitation of amino acid exchange.

2.4. Detailed phenotyping and optimization of selected CoNoS

In the following we focused on the further optimization of the ΔARG LEU$^+$ ↔ ΔLEU ARG$^+$ CoNoS. From the ratio estimation of the non-engineered CoNoS we found a primary bottleneck in the performance of the L-leucine producing strain. Assuming that this bottleneck is still not resolved, we further constructed the ΔARG LEU^{++} strain by exchanging the entire native *leuA* gene with the BS018 *leuA^{fbr}* gene sequence, also under control of a P_{tuf} promotor (Vogt et al., 2014). The resulting ΔARG LEU^{++} ↔ ΔLEU ARG$^+$ CoNoS showed greatly improved growth performance, reaching 75% of the final biomass of the mono-culture with the C1* control strain. The specific growth rate of 0.22 ± 0.01 h^{-1} was also significantly improved and now resembled almost 50% of wild-type level (Fig. 3C).

To study the growth behaviour of both engineered auxotrophs in the co-culture in more detail we performed cultivations in a polydimethylsiloxane (PDMS) based microfluidic cultivation device. To enable a direct visual and quantitative discrimination, the two strains ΔARG LEU^{++} and ΔLEU ARG$^+$ were further engineered by integrating the fluorescent proteins crimson or eYFP, respectively, under control of the P_{tac} promoter. Protein expression was induced by the addition of 100 μM of IPTG and did not effect strain growth as shown previously (Baumgart et al., 2013). The growth behaviour of the CoNoS was observed at single cell level over a time period of 46 h (Fig. 4A and Fig. S1). Starting from a nearly balanced inoculation ratio between both CoNoS partners, the ΔARG LEU^{++} strain grew much faster within the first 10 h of cultivation. A maximum ratio of 64:36 was obtained between the ΔARG LEU^{++} and the ΔLEU ARG$^+$ strain, which is close to the optimal ratio predicted by the modeling (67:33, cf. Fig. 3B). Thereafter, the availability of L-arginine became limiting and cell division slowed significantly. After 20 h of cultivation a stable growth of the CoNoS was observed, resulting in a constant distribution of 47:53 between the ΔARG LEU^{++} and the ΔLEU ARG$^+$ strain (Fig. 4A). This ratio is now significantly lower as compared to the model predictions, indicating an unbalanced amino acid exchange between the two CoNoS partners with L-arginine as the limiting factor.

Closer inspection revealed that in certain areas of the microfluidic chamber where one member of the community was not near its partner, growth occurred only at the beginning of cultivation, where the cells likely relied on the remaining amino acid stores (Fig. S1A). In contrast, growth was more pronounced in areas where the two members of the community were close together. Such 'island effect', with non-growing isolated community member, was not observed in the control mono-culture with the WT (Fig. S1B). This finding again supports the hypothesis that amino acid exchange is a major bottleneck of CoNoS, especially at the earliest stage of cultivation when a small number of cells are struggling to increase the concentration of amino acids.

To verify the potential limitation of L-arginine, we performed transient sampling experiments with the ΔLEU ARG$^+$ and the ΔARG LEU^{++} strains, each cultivated as a monoculture in CGXII medium supplemented with 3 mM of either L-leucine or L-arginine. Only the ΔARG LEU^{++} strain showed growth-associated accumulation of L-leucine, clearly indicating a shift toward L-arginine as the limiting amino acid in the specific CoNoS (Fig. 4B).

To resolve the bottleneck in L-arginine supply, we performed additional metabolic engineering by relieving the feedback-inhibition of ArgB via the mutations A26V M31V (cf. Fig. 2C) (Ikeda et al., 2009) resulting in the ΔLEU ARG^{++} strain. Co-cultivation of the doubly engineered auxotrophs still showed a slightly delayed onset of cell population growth, but a further increased final biomass to about 86% of the control strain (Fig. 5A). Moreover, the ΔARG LEU^{++} ↔ ΔLEU ARG^{++} CoNoS showed a highly increased specific growth rate of 0.47 ± 0.01 h^{-1}, which is equivalent to 83% of the wild type. The latter points to a further increased and much more balanced amino acid exchange between the two auxotrophic strains.

However, in a co-culture such as our CoNoS, direct experimental prove is not possible because only the net accumulation of a particular amino acid species can be measured. Therefore, we followed an indirect approach by process modelling employing a segregated, unstructured model approach (Fig. 5B). In short, the model takes explicit account of the (re)action of the CoNoS with its environment via the exchange of amino acids between the two community members. Model formulation and validation was performed in a stepwise manner to allow integration of available experimental data, and to reduce the degree of freedom of unknown parameters in the final CoNoS model.

As a result, the model enables simulation of the individual growth dynamics of both CoNoS members. According to these predictions, the ΔLEU ARG^{++} strain grew a bit faster and to a slightly higher biomass, which would resemble the second growth phase during the microfluidic cultivations (cmp. Figs. 4A and 5A). Furthermore, the predicted maximum ratio of approx. 45:55 between the ΔARG LEU^{++} and the ΔLEU ARG^{++} strain is nearly identical under both conditions. Most importantly, the estimated specific rates underscore the successful engineering of this CoNoS toward higher L-arginine production performance, and the potential switch back to L-leucine as the limiting amino acid (Table 2).

To verify the predicted limitation of L-leucine and accumulation of L-

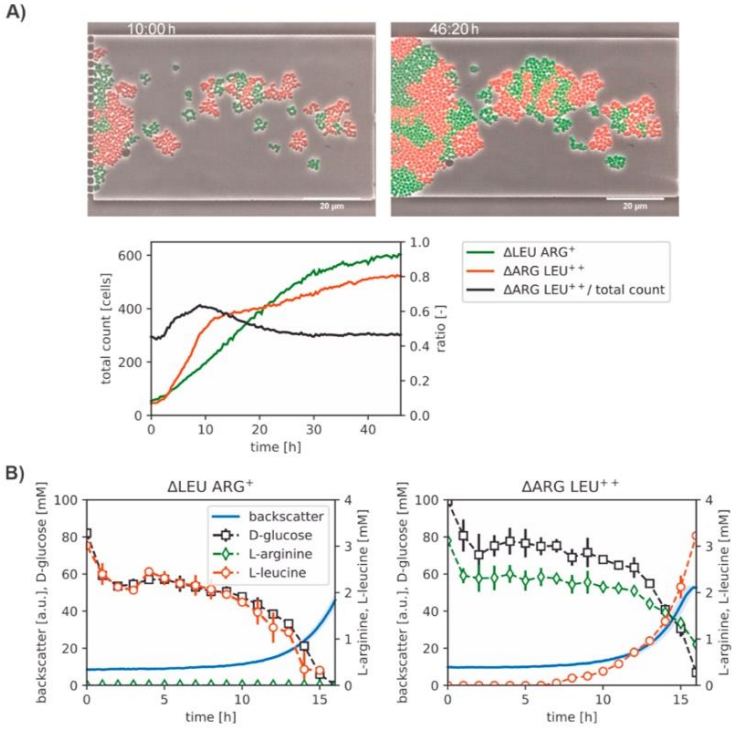

Fig. 4. Detailed phenotyping of selected CoNoS. A) Microfluidic batch cultivation of the ΔARG LEU^{++} (red) ↔ ΔLEU ARG^{+} (green) CoNoS to study co-culture dynamics at single-cell level. Cell count and resulting ratio of the two species as determined by semi-automated image analysis. B) Transient sampling experiments with engineered auxotrophic strains ΔLEU ARG^{+} and ΔARG LEU^{++}. Cultures were performed in triplicate in CGXII medium supplemented with 3 mM of either L-leucine or L-arginine.

arginine, we performed another transient sampling experiment with the best CoNoS (Fig. 6A). Indeed, only enrichment of L-arginine up to 1 mM was found, supporting the expected higher proportion of ΔLEU ARG^{++} cells in the co-culture. From the microfluidic experiments, we hypothesized that initial cell density may be a critical factor in ensuring sufficient amino acid concentration for immediate balanced co-culture growth. Indeed, a fivefold increase in initial biomass resulted in a much faster onset of exponential growth and a further increase in the maximum specific growth rate of CoNoS, which is now even close to that of the wild type (Fig. 6B).

Finally, to test the stability of the CoNoS for long-term cultures we performed a repetitive batch experiments covering ten consecutive batches (Fig. 6C). Application of the fluorescently labeled strains variants allowed online monitoring of the two CoNoS members and showed very stable dynamics of the co-culture composition along the batch series.

3. Discussion

It is widely accepted that cooperation between microorganisms plays a crucial role in the evolution of species and represents a net advantage in terms of efficiency in using the available resources (D'Souza et al., 2014). Furthermore, evolution drives genome reduction to adapt microorganisms to specific ecological niches when the supply of function occurs by a partner organism (Noack and Baumgart, 2019). Now, is it possible to re-create genome-reduced communities that exploit the available resources in a more efficient way? And, most importantly, could these synthetic communities re-direct their carbon and energy toward a more efficient bio-production? Heterogeneous microbial communities, both natural and engineered, potentially manifest higher fitness and productivity opening future perspective for synthetic novel communities that exploit cross-feeding interactions to achieve complex and/or energetically difficult tasks in a stable, robust way (Yang et al., 2020).

In the present work, we succeeded in establishing stable, genome-reduced co-cultures of *C. glutamicum* by generating single community strains carrying broad gene deletions in selected amino acid biosynthesis pathways. Most surprisingly, no fitness advantage was observed when the amino acid auxotrophic strains were cultivated in a mono-culture in supplemented media. Specific growth rate and final biomass yield were carefully analyzed in comparison with the parental non-auxotrophic strain using well-controlled microbioreactor experiments with online monitoring of biomass growth. In another study it was shown, by counting the colony-forming units after 24 h cultivation, that *E. coli*

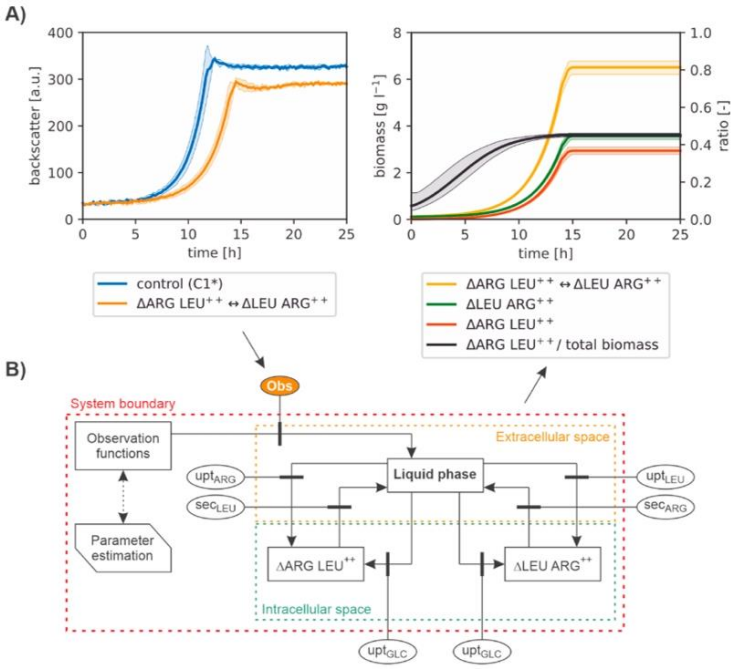

Fig. 5. Optimization and model-based analysis of selected CoNoS. A) Growth performance of multiple engineered ΔARG LEU^{++} ↔ ΔLEU ARG^{++} CoNoS. Cultures were performed in triplicate in non-supplemented CGXII medium with 111 mM D-glucose. B) Segregated, unstructured process modelling to simulate CoNoS dynamics. Based on a pre-parameterization approach, only the backscatter measurements were used as observables for final model validation and prediction of individual species growth dynamics. The confidence bounds for the state variables shown were generated by propagating the error bounds for estimated model parameters.

strains auxotrophic for different amino acids or vitamins, constructed with single-gene deletions, obtained a growth advantage of 13% compared to their parental strain (D'Souza et al., 2014). Instead, in this work, despite the growth rate increase predicted by our model-based analysis, no improved growth performances were detected, possibly due to other limitations occurring such as nutrient uptake or oxygen transfer.

In particular, the ΔHIS and ΔTRP strains not only did not reach the predicted growth benefits (Fig. 2B), but also performed worse than the WT. This indicates effects not taken into account by the model, which could be related to the uptake of the respective amino acid or yet unknown systemic effects of the deleted genes (i.e. *hisE hisG hisH hisA impA hisF hisI hisD hisC hisB* and *hisN* for the ΔHIS strain as well as *trpP trpE trpG trpD trpCF trpB* and *trpA* for the ΔTRP strain). Specifically, the uptake of L-histidine occurs in *C. glutamicum* via the transporter PheP (cg1305) and should not be impaired in the ΔHIS strain. Kulis-Horn and coworkers reported on the growth effect of single deletions of L-histidine biosynthesis genes and no other auxotrophies besides L-histidine are currently known (Kulis-Horn et al., 2014). Also, it was previously speculated about a possible role of HisA in L-tryptophan biosynthesis because in other actinobacteria missing TrpF (i.e. the HisA homologue), HisA plays a bifunctional role in both L-tryptophan and L-histidine biosynthesis (Barona-Gómez and Hodgson, 2003). In our case, however, no L-tryptophan auxotrophy occurred after the deletion of *hisA*. Moreover, L-histidine biosynthesis is linked to the *de novo* purine biosynthetic pathway via the AICAR (5′-phosphoribosyl-4-carboxamide-5-aminoimidazole) cycle, with AICAR being a byproduct of the reaction by HisFH (Alifano et al., 1996). Therefore, deletion of *hisF* and *hisH* and the resulting absence of this AICAR source might impair the *de novo* biosynthesis of AMP (adenosine monophosphate) and GMP (guanosine monophosphate). Nevertheless, the primary precursor PRPP (5-phosphoribosyl 1-pyrophosphate) of the purine pathway can still be synthesized in the ΔHIS strain, so the reasons for the slow growth rate under supplemented conditions remain elusive.

As for the other slow-growing ΔTRP strain, the uptake of L-tryptophan occurs mainly via the general amino acid importer AroP, but is has been hypothesized that there is another import system (Wehrmann et al., 1995). In particular, the *trpP* gene (cg3357) has been suggested to encode an L-tryptophan permease in *C. glutamicum* (Heery et al., 1994), and it was also accordingly annotated after genome sequencing (Kalinowski et al., 2003). Of all the tryptophan operon genes, it is also the only one that can be deleted without causing L-tryptophan auxotrophy (Mormann et al., 2006). Indeed, an L-tryptophan auxotrophic strain still possessing the *trpP* gene grew with a growth rate similar to WT (unpublished data), strongly hinting at a important role of TrpP as a permease for L-tryptophan uptake. Despite the growth limitations of the ΔHIS and ΔTRP strains, we continued to use them for setting up our synthetic communities.

Table 2
Specific uptake and production rates of engineered *C. glutamicum* amino acid producer strains during cultivation in supplemented monocultures and co-cultures, respectively. Rates were derived from model-based analysis by fitting suitable bioprocess models to the time-dependent measurements of replicate cultures in small-scale phenotyping experiments. Asymmetric confidence bounds were estimated by following a parametric bootstrapping approach.

Strain/condition	Monoculture[a]		Coculture[b]		
	ΔARG LEU^{++}	ΔLEU ARG^{+}	ΔARG LEU^{++}	ΔLEU ARG^{++}	ΔARG LEU^{++} ↔ ΔLEU ARG^{++}
Growth rate [h^{-1}]	0.41 [0.405, 0.411]	0.40 [0.397, 0.409]	0.41 [0.410, 0.411]	0.45 [0.437, 0.472]	0.44[c] [0.426, 0.444]
D-glucose uptake rate [mmol g_{CDW}^{-1} h^{-1}]	4.46 [4.428, 4.499]	5.54 [5.321, 5.903]	4.44 [4.441, 4.441]	5.52 [5.521, 5.521]	–
L-leucine uptake rate [mmol g_{CDW}^{-1} h^{-1}]	–	0.32 [0.300, 0.333]	–	0.13 [0.128, 0.138]	–
L-arginine uptake rate [mmol g_{CDW}^{-1} h^{-1}]	0.09 [0.088, 0.102]	–	0.09 [0.093, 0.093]	–	–
L-leucine production rate [mmol g_{CDW}^{-1} h^{-1}]	0.22 [0.210, 0.232]	–	0.17 [0.164, 0.173]	–	0[d] [0, 0]
L-arginine production rate [mmol g_{CDW}^{-1} h^{-1}]	–	0 [0, 0]	–	0.52 [0.305, 0.746]	0.25[e] [0.132, 0.368]

[a] Rates were constant throughout the exponential growth phase, and values represent the mean of maxima across all replicates and time points.
[b] Rates were not constant, and values represent the mean across all replicates at time $t = 12$ h (see Jupyter notebooks for details).
[c] Calculated as: $\mu_{tot} = (\mu_{\Delta ARG} \cdot X_{\Delta ARG} + \mu_{\Delta LEU} \cdot X_{\Delta LEU})/X_{tot}$
[d] Net rate calculated as: $v_{net,LEU} = (v_{syn.\ LEU,\ \Delta ARG} \cdot X_{\Delta ARG} - v_{upt.\ LEU,\ \Delta LEU} \cdot X_{\Delta LEU})/X_{tot}$
[e] Net rate calculated as: $v_{net,ARG} = (v_{syn.\ ARG,\ \Delta LEU} \cdot X_{\Delta LEU} - v_{upt,ARG,\ \Delta ARG} \cdot X_{\Delta ARG})/X_{tot}$

At this point, we established different CoNoS, each combining two different amino acid auxotrophic strains. For all CoNoS tested, growth was observed only in the ΔARG ↔ ΔLEU community. The sufficient biosynthesis and extracellular exchange of the dependent amino acids L-arginine and L-leucine allowed this CoNoS to form a niche that could support the growth of both strains. Noteworthy, it has already been shown that *C. glutamicum* (among other prokaryotic and eukaryotic model organisms) excretes amino acids such as L-arginine as a result of extended overflow metabolism (Paczia et al., 2012). Our results demonstrate that cooperation of *C. glutamicum* strains can indeed arise solely from genome reduction without further engineering, underlining the enormous potential of niche construction through bacterial cross-feeding even in a homogeneous environment (San Roman and Wagner, 2018).

However, we found that amino acid exchange was limiting for the growth of our communities and therefore proceeded with rational metabolic engineering. To strengthen cross-feeding interactions and allow overproduction of amino acids, we first relieved the corresponding end-product feed-back inhibitions, a strategy that has recently been successful in amino acid auxotrophic *E. coli* (Pande et al., 2014) and *S. cerevisiae* (Shou et al., 2007).

This indeed led to a significant increase in growth in all engineered CoNoS (Fig. 3C). However, the growth rates of the co-cultures were still below the level of the wild-type mono-culture. Therefore, we focused on the ΔARG ↔ ΔLEU CoNoS and performed further rational metabolic engineering to gradually and reciprocally debottleneck the amino acid exchange. As expected, the growth limiting bottleneck oscillated from one of the two amino acids to the other at each engineering step. This clearly shows the difficulty of optimally balancing amino acid exchange between two auxotrophic strains in a purely rational manner.

Nevertheless, the final engineered CoNoS ΔARG LEU^{++} ↔ ΔLEU ARG^{++} showed a specific growth rate and biomass titer of approximately 83% and 86% of the control strain, respectively (Fig. 5A). Because the applied metabolic engineering steps in ΔARG LEU^{++} and ΔLEU ARG^{++} were already sufficient to achieve nearly optimal cross-feeding interactions, it is unclear whether a further increase in amino acid production can improve the growth of CoNoS. Nevertheless, further improvements are desirable, since a slightly delayed onset of exponential growth and lower biomass formation occurred in the co-culture, while neither effect occurred in the supplemented monocultures.

At this point, the L-leucine production could be further increased by integrating more copies of the gene encoding the feedback-resistant LeuA into the ΔARG LEU^{++} strain, by deleting *ltbR*, encoding the repressor of *leuBCD*, by increasing D-glucose uptake or by increasing precursor supply as achieved in the currently best L-leucine producer strain MV-Leu F2 (Vogt et al., 2014). Similarly, the L-arginine production could be the target of further metabolic engineering, *e.g.*, by deletion of *farR*, by increasing the NADPH-level and via overexpression of L-arginine biosynthesis genes, especially of the production rate-controlling step encoded by *argGH* (Park et al., 2014). In addition to amino acid biosynthesis, other parameters such as D-glucose uptake, amino acid uptake and amino acid secretion may also be considered. The observed "dilution effect" could indicate a CoNoS limitation due to an insufficient secretion rate of the cross-fed amino acid, as well as difficulties of the strains to take up the corresponding amino acid when present only in low concentrations.

Specifically, L-arginine was shown to be exported via LysE and CgmA (Lubitz et al., 2016), while for L-leucine, BrnFE was identified as an exporter (Kennerknecht et al., 2002). Therefore, overexpression of these export systems could be a valuable option to increase amino acid secretion and thus optimize crossfeeding in the ΔARG ↔ ΔLEU CoNoS. Interestingly, there is currently no known import mechanism for L-arginine in *C. glutamicum*. This might be due to the fact that this amino acid is not metabolizable or even harmful for the cells as shown recently for a corresponding dipeptide supplementation experiment (Lubitz et al., 2016). However, with the L-arginine auxotrophic strain ΔARG growing similar to the WT (Fig. 3A), some L-arginine import must exist. On the other hand, the amino acid import of L-leucine could likely be improved by overexpression of the branched-chain amino acid importer BrnQ (Tauch et al., 1998). Since the K_m value was determined to be 9 μM and the uptake followed conventional Michaelis-Menten kinetics (Ebbighausen et al., 1989), the initial low amino acid concentrations in liquid culture could be considered as the main problem of the CoNoS to overcome.

This factor fits well with an example of a co-culture of two amino acid auxotrophic *E. coli* strains: Evolution of this community in an unstructured environment led to increased formation of spatial structures of multicellular aggregates to enhance metabolite exchange (Preussger et al., 2020). The use of adaptive laboratory evolution (ALE) could indeed be a viable approach to address the bottlenecks in CoNoS development, and the general feasibility of the repetitive batch approach has been successfully demonstrated (see Fig. 6C). Because many targets for optimization, *e.g.*, the mechanism of L-arginine import, are unknown, the ALE approach is particularly useful for identifying novel uptake and production traits (Radek et al., 2017; Tenhaef et al., 2018). Identification and characterization of these traits would provide valuable insights not only into synthetic co-cultures but also into the platform organism *C. glutamicum* in general.

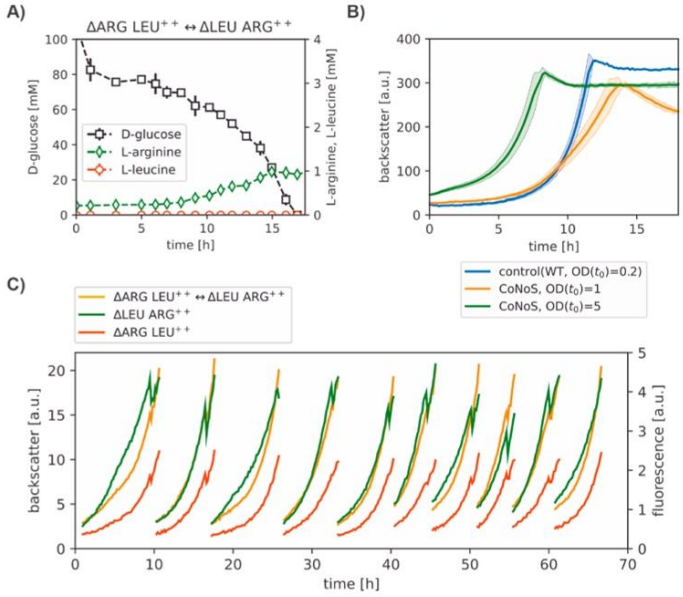

Fig. 6. Detailed phenotyping of improved ΔARG LEU^{++} ↔ ΔLEU ARG^{++} CoNoS and final stability test. A) Transient sampling experiment with the co-culture grown in triplicate in CGXII medium. B) Effect of inoculation density on growth performance. C) Repetetive batch cultivation with online monitoring of total biomass (orange) and fractions of CoNoS partners ΔARG LEU^{++} (red) and ΔLEU ARG^{++} (green), respectively. The fully automated experiment was performed on a Mini Pilot Plant and each batch was started with freshly stored CGXII medium inoculated with 12% v v^{-1} of the previous batch after the predefined backscatter of BS = 15 was reached (for technical details see (Radek et al., 2017)). To investigate a potential effect of the inoculum density, the last 5 batched where inoculated with 24% v v^{-1} of the previous batch.

4. Conclusions

In the present work, following a model-based design, several amino acid-auxotrophic *C. glutamicum* strains were constructed by deleting the entire biosynthetic machinery for the target amino acid. In most cases, the fitness of the newly constructed strains was comparable to that of the control strain when cultured in amino acid-supplemented media, confirming the suitability of the strain in a CoNoS. Releasing feedback inhibition by metabolic engineering proved to be a successful strategy to enhance amino acid exchange and improve the growth performance of new and further engineered CoNoS. The best performing CoNoS ΔARG LEU^{++} ↔ ΔLEU ARG^{++} exhibited a specific growth rate of 83% and a biomass titer of 86% of the control strain, making it the fastest co-culture of two auxotrophic *C. glutamicum* strains to date.

To conclude, synthetic communities can be established using genome-reduced microorganisms that grow with mutual dependency. We have achieved the goal of establishing CoNoS for efficient delivery of biocatalysts for amino acid production. To use CoNoS for production, one needs to take a further step by developing a co-culture/process design that allows enrichment of one of the producer strains and efficiently blocks unwanted consumption of the target amino acid. Here, the implementation of synthetic regulatory growth switches in combination with "edible" inducers is conceivable. This would allow growth of CoNoS to sufficient cell density, enrichment of the targeted production strain, and continuation of the process for efficient amino acid production.

Finally, the presented approach is general and should be applicable to any target product that ensures the necessary interdependence of CoNoS partners for the co-culture to reach sufficient density prior switching to production. In this regard, designs with couplings through native byproducts are also conceivable, which could be particularly interesting for the production of more complex molecules in heterologous pathways.

5. Materials and methods

5.1. Model-based design of CoNoS

For the model-based design and analysis of CoNoS, two different-sized models of the *C. glutamicum* metabolic network were created, namely a genome-scale model (GSM) and a focused model of the central metabolism, respectively. The GSM was derived from the published model iEZ475 (Zelle et al., 2015) and has some minor modifications, which are discussed below. The focused model was created from the GSM by defining the system boundaries around the amino acid biosynthetic pathways and omitting all reactions outside the central metabolism, such as cell wall synthesis. This resulted in a simplified model with 56% fewer reactions and 51% fewer metabolites. In both cases, the transport of amino acids was modeled by assuming free diffusion, and the transport reactions for ARG, GLN, PRO, SER, and TRP that were missing in the original GSM were additionally introduced.

The COnstraint-Based Reconstruction and Analysis (COBRA) toolbox (Heirendt et al., 2019) under MATLAB (Mathworks, R2017b) was applied for cFBA of single amino acid auxotrophic *C. glutamicum* strains. According to the experimental conditions, D-glucose was defined as the sole carbon and energy source, and for quantitative growth rate predictions, the PTS-coupled uptake rate was constrained to the measured rate of 5.6 mmol g_{CDW} h^{-1}. Biomass growth was defined as optimization criteria. Amino acid auxotrophies were mimicked by constraining single essential reactions of the respective amino acid biosynthesis pathway to carry zero flux.

Simulation of different co-cultures based on the CoNoS approach and prediction of the abundance of the underlying auxotrophic strains was performed using the expansion of single-species cFBA (Chan et al.,

2017). In short, SteadyCom seeks to predict the maximum community growth rate of two or more microbial species at community steady-state conditions. The resulting extended linear program is then solved by stepwise optimization of the community growth rate. For the CoNoS simulation, the subnetworks were connected by defining exchange reactions for the corresponding essential amino acids.

5.2. Strain construction

All *C. glutamicum* strains used in this study are listed in Table 1 and are based either on the wild type *C. glutamicum* ATCC 13032 or on its genome reduced variant C1* (Baumgart et al., 2018). For molecular cloning, *Escherichia coli* DH5α (Hanahan, 1983) was used as host. The plasmids used are listed in Table S1 and the oligonucleotides in Table S2. For the construction of deletion strains and for integrating mutations in *C. glutamicum*, the pK19*mobsacB*-system was applied, operating by introducing double crossover events as described previously (Keilhauer et al., 1993; Schafer et al., 1994). The genes deleted for constructing the auxotrophic strains are represented in Fig. 2C. The primer used for the Colony-PCRs to check for mutations or deletions as well as for differentiating between the different auxotrophic strains in the CoNoS are listed in Table S3.

5.3. Bacterial strains and growth conditions

For cultivation of *E. coli* strains, lysogeny broth (LB) agar plates or liquid LB (Bertani, 1951) were used at 37 °C. For strains with plasmids, 50 μg mL^{-1} kanamycin was added. For *C. glutamicum*, either brain heart infusion (BHI) medium (Difco Laboratories, Detroit, USA) or defined CGXII medium (Keilhauer et al., 1993) was used at 30 °C. All cultivations except those for strain construction performed in this study were carried out in biological triplicates. The cultivations were performed in defined CGXII medium consisting of (per litre) 20 g of $(NH_4)_2SO_4$, 5 g of urea, 1 g of KH_2PO_4, 1 g of K_2HPO_4, 0.25 g of $MgSO_4 \cdot 7\ H_2O$, 42 g of 3-morpholinopropanesulfonic acid, 13.25 mg of $CaCl_2$, 10 mg of $FeSO_4 \cdot 7\ H_2O$, 10 mg of $MnSO_4 \cdot H_2O$, 1 mg of $ZnSO_4 \cdot 7\ H_2O$, 0.313 mg of $CuSO_4$, 0.02 mg of $NiCl_2 \cdot 6\ H_2O$, 0.2 mg of biotin (pH 7), 20 g of D-glucose, and 0.03 g of protocatechuic acid (PCA). During medium preparation, some substances were added sterile after autoclaving (D-glucose, PCA, biotin, $MgSO_4 \cdot 7\ H_2O$, $CaCl_2$, $FeSO_4 \cdot 7\ H_2O$, $MnSO_4 \cdot H_2O$, $ZnSO_4 \cdot 7\ H_2O$, $CuSO_4$, $NiCl_2 \cdot 6\ H_2O$) and pH 7.0 was adjusted with 8 M NaOH. In experiments with supplemented CGXII medium, amino acids supplement was added sterile according to the strain requirements. In each mono and co-culture showed in this study, each strain was pre-cultivated in a mono-culture in supplemented CGXII medium inoculated with a single colony from the correspondent strain. After two days of incubation at 30 °C, 250 rpm, the pre-cultures were centrifuged, the pellet was re-suspended in sterile 0.9% (w v^{-1}) NaCl, and used to inoculate the main cultures.

5.4. Microscale cultivations and transient sampling

The main cultures were performed in 48-well FlowerPlates (m2p-labs GmbH, Germany) with dissolved oxygen and pH optodes in a BioLector (m2p-labs GmbH, Germany) at 1400 rpm, 85% humidity and 30 °C. Inoculated FlowerPlates were covered with a sterile gas permeable foil (m2p-labs GmbH, Baesweiler). Mono-cultures were started at an optical density of $OD_{600} \approx 0.2$ and co-cultures were started at an overall optical density of $OD_{600} \approx 1$ by inoculating the correspondent pre-cultures, unless differently specified. The higher CoNoS inoculum density allow an initial medium enrichment with the shared amino acid.

For characterizing the substrate uptake and amino acid production rates of the analyzed strains, automated harvesting of cultures was performed using a Freedom Evo 200 (Tecan, Switzerland) robotic platform which embeds a BioLector cultivation device. The robotic workstation employs a liquid handling arm using eight steel needles, a gripper arm for transport of plates, a Rotanta 460 RSC MTP centrifuge (Hettich) and an Infinite M 200 Pro MTP reader (Tecan). For cultures, 15 ml of supplemented CGXII medium was inoculated with pre-cultivated cells in triplicates as described before. An aliquot of the inoculated media was centrifuged (4500 rpm for 10 min) and the supernatant was stored for HPLC analysis and glucose assays. For each replicate, 800 μL of the inoculated media were distributed in 16 wells of a 48-well FlowerPlate. Inoculated FlowerPlates were covered with a sterile gas permeable foil and the main culture was carried out at 1400 rpm, 85% humidity and 30 °C. For each replicate, one well was harvested and centrifuged (4500 rpm for 10 min) every hour since the beginning of the cultivation using the automated platform. Each supernatant was stored chilled and further processed using the robotic platform in a separated workflow.

At the end of the first automated workflow, the stored cell-free supernatants were filtered through a 96 well filterplate (AcroPrep™ Advance, 1 ml, 0.2 μm Supor® membrane, PES) using the centrifuge and were appropriately diluted with MilliQ water preparing 4 different 96-well micro titer plates (MTP), two MTP were used for amino acid quantification and two for glucose quantification.

5.5. Supernatant analysis

D-glucose quantification was performed with a hexokinase assay (DiaSys) in MTP containing the properly diluted cell-free supernatant. Using the robotic platform described before, 20 μL of diluted cell-free supernatants were mixed with 280 μL assay mastermix and incubated for 6 min at room temperature before absorption measurement at 365 nm in the MTP reader. Results were calibrated against D-glucose serial dilution standards processed in the same way.

For amino acid quantification, 50 mM α-Aminobutyric acid (AABA) was added as an internal standard to MTPs containing the properly diluted cell-free supernatant. Separation of amino acids was performed on a HPLC system (Agilent 1100 Infinity, AgilentTechnologies, Santa Clara, CA). The method used involves a pre-column (Phenomenex, KrudeKatcher Ultra HPLC In-line Filter 0.5 μm Depth Filter x 0.004 in ID) and a reverse phase column (Kinetex 5 μm EVO C18 100 °A, 150 × 4.6 mm) as stationary phase, buffer A (26 mM $NaH_2PO_4 \cdot 2H_2O$, 14.8 mM $Na_2HPO_4 \cdot 2H_2O$, 7.2 pH) + 0.5% tetrahydrofuran and buffer B (50% buffer A, 35% methanol, 15% acetonitrile) with a flow rate of 0.9 mL min^{-1} as mobile phase, a column temperature of 40 °C and an injection volume of 15 μL. Amino acids were separated with the following linear gradient elution conditions (min/B%): 0/20, 7/80, 14/80, 17/100, 23/100, 24/20 and 30/20. Pre-column derivatization with Phthaldialdehyde (OPA) reagent (Sigma-Aldrich, ready-to-use mix) was performed in an automated procedure where 5 μL of OPA, 5 μL of sample and 5 μL of water were mixed in the injection loop 6 times and incubated for 1 min. Detection of amino acids was performed using a fluorescence detector (Agilent 1100 FLD) with excitation wavelength of 230 nm and emission wavelength of 460 nm. Quantification of target amino acids was performed relatively to the internal standard measured in each sample in order to correct variation of signal due to different derivatization conditions within the sample.

5.6. Determination of specific rates

Specific growth rates were determined by processing the raw backscatter data from BioLector experiments using the bletl tool and following the spline-based approximation approach (Osthege et al., 2022). Data visualization was performed using matplotlib (Hunter, 2007).

Specific rates for amino acid uptake and secretion of the ΔLEU ARG^{+}, ΔLEU ARG^{++} and the ΔARG LEU^{++} strain were determined by process modelling. Based on the two monoculture (with three replicates, cf. Fig. 4B) and the final co-culture (with two replicates, cf. Fig. 5A) experiments, three partially dependent models were formulated to

describe the growth and production kinetics of the strains involved. The models are structured by one extracellular compartment for the liquid phase and one intracellular compartment covering either one (i.e. monoculture), or two (i.e. co-culture) engineered strains (cf. Fig. 5B). For model implementation, validation and analysis we used the open-source, python-based modeling tool pyFOOMB (Hemmerich et al., 2020). For all three models the corresponding Jupyter notebooks are provided in GitHub (https://github.com/JuBiotech/Supplement-to-Schito-et-al.-CoNoS-MetabEng-2022) and contain detailed descriptions of all modeling procedures and fitting results.

5.7. Microfluidics

The microfluidic chip fabrication is based on a soft lithography protocol described previously (Grünberger et al., 2013). The PDMS-based microfluidic cultivation device (Kaganovitch et al., 2018) consists of 6 cultivation rows each with several cultivation chambers, each 60 μm × 100 μm x 1 μm (width, length, height) in size. The chamber height enforces the cells to grow in monolayers. Each cultivation chamber is coupled to a medium reservoir resulting in a total cultivation volume of 606 pL in total. The cultivation chamber and the medium reservoir are separated by a thin PDMS double grid structure, which prevent cells from entering the medium reservoir and at the same time ensures diffusive medium exchange between the cultivation chamber and the reservoir. To prevent the evaporation of the low cultivation volumes, the following measures were implemented: an additional water-filled top layer and additional side channels around the cultivation chambers were used and perfused with water during the cultivation. Before inoculating the microfluidic cultivation device the cells were pre-cultivated in mono culture with CGXII medium supplemented with the required amino acid amount as described previously (see Bacterial strains and growth conditions). Cell-free supernatant was resuspended in 0.9% w v^{-1} NaCl and mixed in a ratio 1:1 with the partner strain for establishing a CoNoS. The CoNoS cell suspension was diluted to an OD_{600} of 0.5 and flushed through the medium channels by gently applying pressure to a 1 mL syringe. This flow randomly inoculated single cells of both strains into several chambers. Afterwards fresh media was flushed through the medium channels for 15 min at 200 nl min (nemeSYS syringe pumps, Cetoni GmbH, Germany). By applying pressurized air (600 mbar) at the channel inlet, the residual medium is expelled out of the medium channel, resulting in individual isolated cultivation chambers. Before starting the experiments, the water reservoir and the side channels were filled with deionized water under low pressure (p_{water} reservoir = 40 mbar, p_{side} channel = 90 mbar). To monitor the cultivation a time-lapse microscope setup was used that consists of an inverted fluorescence microscope (Ti Eclipse, Nikon) equipped with a 100× oil immersion objective (Plan Apochromat λ Oil, N.A. 1.45 and a working distance of 170 μm, Nikon Microscopy). Stable temperature conditions were ensured by operating the microscope in an incubation chamber (TempController, 2000-2, PECON, Germany). All cultivations were performed at 30 °C. For time-lapse imaging, phase contrast and fluorescence images were acquired with 100 ms exposure, taking an image every 30 min for the wild type strains and every 20 min for the co-cultures. For *C. glutamicum* WT cultivations, a CMOS camera ANDOR Neo/Zyla (ANDOR, Oxford Instruments, England) was used in combination with the Intensilight (Nikon Microscopy) light source. For the *C. glutamicum* ΔARG LEU^{++}::P_{tac}-crimson ↔ ΔLEU ARG^{++}::P_{tac}-eYFP CoNoS cultivations, a DS-Qi2 camera (Nikon Microscopy) in combination with the sola light engine (Lumencor, USA) was used. For fluorescence measurements, NIKON excitation and fluorescence filter cubes for eYFP (FITC, excitation: 465–495 nm, dichroic mirror: 505 nm, emission: 515–555 nm) and for crimson(excitation: 540–580 nm, dichroic mirror: 593 nm, emission: 600–684 nm) (AHF Analysetechnik, Germany) were used. Acquired time-lapse series were manually pre-processed. This included image alignment, brightness adjustments and cropping the region of interest using the software Fiji (Schindelin et al., 2012).

5.8. Image and data analysis

Time-lapse videos were segmented using Omnipose, a deep neural network approach pre-trained on a comprehensive set of bacterial systems (Cutler et al., 2021), and individual cell contours were computed for every frame. Artifacts were removed by constraining the minimal (0.5 $μm^2$) and maximally (4.5 $μm^2$) allowed cell area and enforcing a maximal length-width ratio (5.5) per cell. The resulting cell contours were used to compute the median red and green fluorescent colors inside the cell body using Gaussian filtered fluorescence images. The extracted colors were normalized per frame, and cells below a fluorescence signal of 35% were discarded. Depending on the dominant fluorescence channel, remaining cells were assigned "green" or "red" labels yielding cell counts and ratio. The results were then manually checked. Due to the large number of cells in the time-lapse (>100k), the contour computation and fluorescence extraction were parallelized to reduce the total computation time to less than 21 min on an AMD Ryzen 7 1800X and an NVIDIA GeForce RTX 2060 GPU. The code and visualizations for the analysis are available in GitHub (https://github.com/JuBiotech/Supplement-to-Schito-et-al.-CoNoS-MetabEng-2022).

Author contributions

Simone Schito: Methodology, Validation, Investigation, Writing - Original Draft, Visualization.

Rico Zuchowski: Methodology, Validation, Investigation, Writing - Original Draft.

Daniel Bergen: Methodology, Formal analysis, Visualization.

Daniel Strohmeier: Methodology, Formal analysis, Data Curation.

Bastian Wollenhaupt: Methodology, Data Curation.

Philipp Menke: Investigation.

Johannes Seiffarth: Software, Formal analysis, Visualization.

Katharina Nöh: Data Curation, Writing - Review & Editing, Supervision.

Dietrich Kohlheyer: Writing - Review & Editing, Supervision, Funding acquisition.

Michael Bott: Resources, Writing - Review & Editing.

Wolfgang Wiechert: Resources, Writing - Review & Editing.

Meike Baumgart: Conceptualization, Methodology, Writing - Review & Editing, Supervision, Funding acquisition.

Stephan Noack: Conceptualization, Methodology, Writing - Review & Editing, Visualization, Supervision, Project administration, Funding acquisition.

Declaration of competing interest

The authors declare that they have no conflict of interest.

Acknowledgements

We thank Niklas Tenhaef and Michael Osthege for programming support on the Mini Pilot Plant. We thank Eric von Lieres and Martin Beyβ for providing computational infrastructure and technical support throughout the project. Christina Mack helped constructing auxotrophic strains. We gratefully acknowledge support and funding from the Deutsche Forschungsgemeinschaft (priority program SPP2170, project no. 427904493 and 428038451). Open Access publication funded by the Deutsche Forschungsgemeinschaft (DFG, German Research Foundation) – 491111487.

Appendix A. Supplementary data

Supplementary data to this article can be found online at https://doi.org/10.1016/j.ymben.2022.06.004.

References

Alifano, P., Fani, R., Liò, P., Lazcano, A., Bazzicalupo, M., Carlomagno, M.S., Bruni, C.B., 1996. Histidine biosynthetic pathway and genes: structure, regulation, and evolution. Microbiol. Rev. 60, 44–69.

Barona-Gómez, F., Hodgson, D.A., 2003. Occurrence of a putative ancient-like isomerase involved in histidine and tryptophan biosynthesis. EMBO Rep. 4, 296–300.

Baumgart, M., Unthan, S., Rückert, C., Sivalingam, J., Grünberger, A., Kalinowski, J., Bott, M., Noack, S., Frunzke, J., 2013. Construction of a prophage-free variant of *Corynebacterium glutamicum* ATCC 13032 for use as a platform strain for basic Research and industrial biotechnology. Appl. Environ. Microbiol. 79, 6006–6015.

Baumgart, M., Unthan, S., Kloß, R., Radek, A., Polen, T., Tenhaef, N., Müller, M.F., Küberl, A., Siebert, D., Brühl, N., Marin, K., Hans, S., Krämer, R., Bott, M., Kalinowski, J., Wiechert, W., Seibold, G., Frunzke, J., Rückert, C., Wendisch, V.F., Noack, S., 2018. *Corynebacterium glutamicum* chassis C1*: building and testing a novel platform host for synthetic biology and industrial biotechnology. ACS Synth. Biol. 7, 132–144.

Bertani, G., 1951. Studies on lysogenesis. I. The mode of phage liberation by lysogenic *Escherichia coli*. J. Bacteriol. 62, 293–300.

Chan, S.H.J., Simons, M.N., Maranas, C.D., 2017. SteadyCom: predicting microbial abundances while ensuring community stability. PLoS Comput. Biol. 13, e1005539.

Cutler, K.J., Stringer, C., Wiggins, P.A., Mougous, J.D., 2021. Omnipose: a High-Precision Morphology-independent Solution for Bacterial Cell Segmentation. bioRxiv.

D'Souza, G., Waschina, S., Pande, S., Bohl, K., Kaleta, C., Kost, C., 2014. Less IS more: selective advantages can explain the prevalent loss of biosynthetic genes in bacteria. Evolution 68, 2559–2570.

Ebbighausen, H., Weil, B., Krämer, R., 1989. Transport of branched-chain amino acids in *Corynebacterium glutamicum*. Arch. Microbiol. 151, 238–244.

Eggeling, L., Bott, M., 2005. Handbook of *Corynebacterium glutamicum*. CRC Press, Boca Raton.

Grünberger, A., Probst, C., Heyer, A., Wiechert, W., Frunzke, J., Kohlheyer, D., 2013. Microfluidic picoliter bioreactor for microbial single-cell analysis: fabrication, system setup, and operation. JoVE 82, e50560.

Hanahan, D., 1983. Studies on transformation of *Escherichia coli* with plasmids. J. Mol. Biol. 166, 557–580.

Heery, D.M., Fitzpatrick, R., Dunican, L.K., 1994. A sequence from a tryptophan-hyperproducing strain of *Corynebacterium glutamicum* encoding resistance to 5-methyltryptophan. Biochem. Biophys. Res. Commun. 201, 1255–1262.

Heirendt, L., Arreckx, S., Pfau, T., Mendoza, S.N., Richelle, A., Heinken, A., Haraldsdóttir, H.S., Wachowiak, J., Keating, S.M., Vlasov, V., 2019. Creation and analysis of biochemical constraint-based models using the COBRA Toolbox v. 3.0. Nat. Protoc. 14, 639–702.

Hemmerich, J., Tenhaef, N., Wiechert, W., Noack, S., 2020. pyFOOMB: Python framework for object oriented modeling of bioprocesses. Eng. Life Sci. 21, 242–257.

Hunter, J.D., 2007. Matplotlib: a 2D graphics environment. Comput. Sci. Eng. 9, 90–95.

Ikeda, M., Mitsuhashi, S., Tanaka, K., Hayashi, M., 2009. Reengineering of a *Corynebacterium glutamicum* L-arginine and L-citrulline producer. Appl. Environ. Microbiol. 75, 1635–1641.

Kaganovitch, E., Steurer, X., Dogan, D., Probst, C., Wiechert, W., Kohlheyer, D., 2018. Microbial single-cell analysis in picoliter-sized batch cultivation chambers. N. Biotech. 47, 50–59.

Kalinowski, J., Bathe, B., Bartels, D., Bischoff, N., Bott, M., Burkovski, A., Dusch, N., Eggeling, L., Eikmanns, B.J., Gaigalat, L., Goesmann, A., Hartmann, M., Huthmacher, K., Krämer, R., Linke, B., McHardy, A.C., Meyer, F., Möckel, B., Pfefferle, W., Pühler, A., Rey, D.A., Rückert, C., Rupp, O., Sahm, H., Wendisch, V.F., Wiegräbe, I., Tauch, A., 2003. The complete *Corynebacterium glutamicum* ATCC 13032 genome sequence and its impact on the production of L-aspartate-derived amino acids and vitamins. J. Biotechnol. 104, 5–25.

Keilhauer, C., Eggeling, L., Sahm, H., 1993. Isoleucine synthesis in *Corynebacterium glutamicum*: molecular analysis of the *ilvB-ilvN-ilvC* operon. J. Bacteriol. 175, 5595–5603.

Kennerknecht, N., Sahm, H., Yen, M.-R., Pátek, M., Saier, M.H., Eggeling, L., 2002. Export of L-isoleucine from *Corynebacterium glutamicum*: a two-gene-encoded member of a new translocator family. J. Bacteriol. 184, 3947–3956.

Kinoshita, S., Udaka, S., Shimono, M., 1957. Studies on the amino acid fermentation. Part I. Production of L-glutamic acid by various microorganisms. J. Gen. Appl. Microbiol. 3, 193–205.

Kulis-Horn, R.K., Persicke, M., Kalinowski, J., 2014. Histidine biosynthesis, its regulation and biotechnological application in *Corynebacterium glutamicum*. Microb. Biotechnol. 7, 5–25.

Kulis-Horn, R.K., Persicke, M., Kalinowski, J., 2015. *Corynebacterium glutamicum* ATP-phosphoribosyl transferases suitable for L-histidine production–Strategies for the elimination of feedback inhibition. J. Biotechnol. 206, 26–37.

Lubitz, D., Jorge, J.M., Pérez-García, F., Taniguchi, H., Wendisch, V.F., 2016. Roles of export genes *cgmA* and *lysE* for the production of L-arginine and L-citrulline by *Corynebacterium glutamicum*. Appl. Microbiol. Biotechnol. 100, 8465–8474.

Matsui, K., Miwa, K., Sano, K., 1987. Two single-base-pair substitutions causing desensitization to tryptophan feedback inhibition of anthranilate synthase and enhanced expression of tryptophan genes of *Brevibacterium lactofermentum*. J. Bacteriol. 169, 5330–5332.

McCarty, N.S., Ledesma-Amaro, R., 2019. Synthetic biology tools to engineer microbial communities for biotechnology. Trends Biotechnol. 37, 181–197.

Mormann, S., Lömker, A., Rückert, C., Gaigalat, L., Tauch, A., Pühler, A., Kalinowski, J., 2006. Random mutagenesis in *Corynebacterium glutamicum* ATCC 13032 using an IS6100-based transposon vector identified the last unknown gene in the histidine biosynthesis pathway. BMC Genom. 7, 205.

Mundhada, H., Schneider, K., Christensen, H.B., Nielsen, A.T., 2016. Engineering of high yield production of L-serine in *Escherichia coli*. Biotechnol. Bioeng. 113, 807–816.

Noack, S., Baumgart, M., 2019. Communities of niche-optimized strains: small-genome organism consortia in bioproduction. Trends Biotechnol. 37, 126–139.

Noack, S., Voges, R., Gätgens, J., Wiechert, W., 2017. The linkage between nutrient supply, intracellular enzyme abundances and bacterial growth: new evidences from the central carbon metabolism of *Corynebacterium glutamicum*. J. Biotechnol. 258, 13–24.

Osthege, M., Tenhaef, N., Zyla, R., Müller, C., Hemmerich, J., Wiechert, W., Noack, S., Oldiges, M., 2022. bletl-A Python package for integrating BioLector microcultivation devices in the Design-Build-Test-Learn cycle. Eng. Life Sci. 22, 242–259.

O'Brien, E.J., Utrilla, J., Palsson, B.O., 2016. Quantification and classification of *E. coli* proteome utilization and unused protein costs across environments. PLoS Comput. Biol. 12, e1004998.

Paczia, N., Nilgen, A., Lehmann, T., Gätgens, J., Wiechert, W., Noack, S., 2012. Extensive exometabolome analysis reveals extended overflow metabolism in various microorganisms. Microb. Cell Factories 11, 122.

Pande, S., Merker, H., Bohl, K., Reichelt, M., Schuster, S., de Figueiredo, L.F., Kaleta, C., Kost, C., 2014. Fitness and stability of obligate cross-feeding interactions that emerge upon gene loss in bacteria. ISME J. 8, 953–962.

Park, S.H., Kim, H.U., Kim, T.Y., Park, J.S., Kim, S.-S., Lee, S.Y., 2014. Metabolic engineering of *Corynebacterium glutamicum* for L-arginine production. Nat. Commun. 5, 4618.

Peters-Wendisch, P., Stolz, M., Etterich, H., Kennerknecht, N., Sahm, H., Eggeling, L., 2005. Metabolic engineering of *Corynebacterium glutamicum* for L-serine production. Appl. Environ. Microbiol. 71, 7139–7144.

Preussger, D., Giri, S., Muhsal, L.K., Oña, L., Kost, C., 2020. Reciprocal fitness feedbacks promote the evolution of mutualistic cooperation. Curr. Biol. 30, 3580–3590 e7.

Radek, A., Tenhaef, N., Müller, M.F., Brüsseler, C., Wiechert, W., Marienhagen, J., Polen, T., Noack, S., 2017. Miniaturized and automated adaptive laboratory evolution: evolving *Corynebacterium glutamicum* towards an improved D-xylose utilization. Bioresour. Technol. 245, 1377–1385.

San Roman, M., Wagner, A., 2018. An enormous potential for niche construction through bacterial cross-feeding in a homogeneous environment. PLoS Comput. Biol. 14, e1006340.

Schafer, A., Tauch, A., Jager, W., Kalinowski, J., Thierbach, G., Puhler, A., 1994. Small mobilizable multi-purpose cloning vectors derived from the *Escherichia coli* plasmids pK18 and pK19: selection of defined deletions in the chromosome of *Corynebacterium glutamicum*. Gene 145, 69–73.

Schindelin, J., Arganda-Carreras, I., Frise, E., Kaynig, V., Longair, M., Pietzsch, T., Preibisch, S., Rueden, C., Saalfeld, S., Schmid, B., Tinevez, J.Y., White, D.J., Hartenstein, V., Eliceiri, K., Tomancak, P., Cardona, A., 2012. Fiji: an open-source platform for biological-image analysis. Nat. Methods 9, 676–682.

Shou, W., Ram, S., Vilar, J.M.G., 2007. Synthetic cooperation in engineered yeast populations. Proc. Natl. Acad. Sci. 104, 1877.

Tauch, A., Hermann, T., Burkovski, A., Krämer, R., Pühler, A., Kalinowski, J., 1998. Isoleucine uptake in *Corynebacterium glutamicum* ATCC 13032 is directed by the *brnQ* gene product. Arch. Microbiol. 169, 303–312.

Tenhaef, N., Brüsseler, C., Radek, A., Hilmes, R., Unrean, P., Marienhagen, J., Noack, S., 1957. Production of D-xylonic acid using a non-recombinant Corynebacterium glutamicum strain. Bioresour. Technol. 268, 332–339.

Unthan, S., Baumgart, M., Radek, A., Herbst, M., Siebert, D., Brühl, N., Bartsch, A., Bott, M., Wiechert, W., Marin, K., Hans, S., Krämer, R., Seibold, G., Frunzke, J., Kalinowski, J., Rückert, C., Wendisch, V.F., Noack, S., 2015. Chassis organism from *Corynebacterium glutamicum*–a top-down approach to identify and delete irrelevant gene clusters. Biotechnol. J. 10, 290–301.

Vidal, L., Pinsach, J., Striedner, G., Caminal, G., Ferrer, P., 2008. Development of an antibiotic-free plasmid selection system based on glycine auxotrophy for recombinant protein overproduction in *Escherichia coli*. J. Biotechnol. 134, 127–136.

Voges, R., Corsten, S., Wiechert, W., Noack, S., 2015. Absolute quantification of *Corynebacterium glutamicum* glycolytic and anaplerotic enzymes by QconCAT. J. Proteomics 113, 366–377.

Vogt, M., Haas, S., Klaffl, S., Polen, T., Eggeling, L., van Ooyen, J., Bott, M., 2014. Pushing product formation to its limit: metabolic engineering of *Corynebacterium glutamicum* for L-leucine overproduction. Metab. Eng. 22, 40–52.

Wehrmann, A., Morakkabati, S., Krämer, R., Sahm, H., Eggeling, L., 1995. Functional analysis of sequences adjacent to *dapE* of *Corynebacterium glutamicum* reveals the presence of *aroP*, which encodes the aromatic amino acid transporter. J. Bacteriol. 177, 5991–5993.

Wynands, B., Otto, M., Runge, N., Preckel, S., Polen, T., Blank, L.M., Wierckx, N., 2019. Streamlined *Pseudomonas taiwanensis* VLB120 chassis strains with improved bioprocess features. ACS Synth. Biol. 8, 2036–2050.

Yang, D.-D., Alexander, A., Kinnersley, M., Cook, E., Caudy, A., Rosebrock, A., Rosenzweig, F., Cann, I., 2020. Fitness and productivity increase with ecotypic diversity among *Escherichia coli* strains that coevolved in a simple, constant environment. Appl. Environ. Microbiol. 86 e00051-20.

Zelle, E., Nöh, K., Wiechert, W., 2015. Growth and production capabilities of *Corynebacterium glutamicum*: interrogating a genome-scale metabolic network model. In: *Corynebacterium glutamicum*: from Systems Biology to Biotechnological Applications. Caister Academic Press, pp. 39–54.

Supplementary information

Communities of Niche-optimized Strains (CoNoS) – Design and creation of stable, genome-reduced co-cultures

Simone Schito[1#], Rico Zuchowski[1#], Daniel Bergen[1], Daniel Strohmeier[1], Bastian Wollenhaupt[1], Philipp Menke[1], Johannes Seiffarth[1], Katharina Nöh[1], Dietrich Kohlheyer[1], Michael Bott[1], Wolfgang Wiechert[1,2], Meike Baumgart[1], Stephan Noack[1,*]

[1]Institut für Bio- und Geowissenschaften, IBG-1: Biotechnologie, Forschungszentrum Jülich, Jülich, Germany

[2]Computational Systems Biotechnology (AVT.CSB), RWTH Aachen University, D-52074 Aachen, Germany

[#]These authors contributed equally to this work

* Corresponding author at: Institute of Bio- and Geosciences, IBG-1: Biotechnology, Forschungszentrum Jülich GmbH, Jülich D-52425, Germany. E-mail address: s.noack@fz-juelich.de

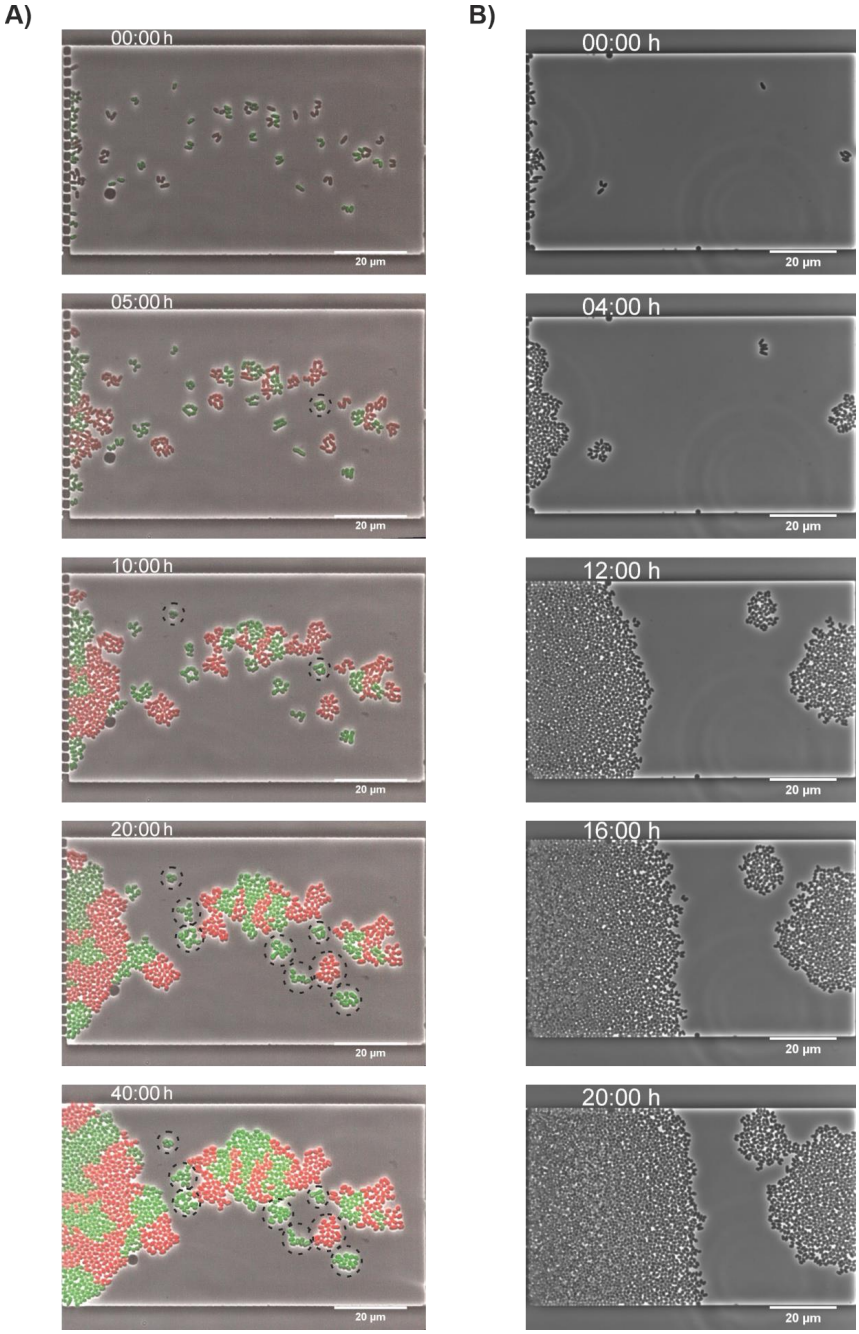
A)
00:00 h
20 µm
05:00 h
20 µm
10:00 h
20 µm
20:00 h
20 µm
40:00 h
20 µm
B)
00:00 h
20 µm
04:00 h
20 µm
12:00 h
20 µm
16:00 h
20 µm
20:00 h
20 µm

Figure S1: Microfluidic batch cultivation of ΔARG LEU^{++}::P$_{tac}$-*crimson* (red cells) ↔ ΔLEU ARG^{+}::P$_{tac}$-*eYFP* (green cells) CoNoS (A) and *C. glutamicum* WT (B) in defined CGXII medium with 111 mM D-glucose. Cluster of cells which stopped growing after a certain cultivation time are marked with dashed circles.

Table S1: List of plasmids used in this study.

Plasmid	Relevant characteristics	Source or reference
pK19*mobsacB*	Kan^r.; plasmid for allelic exchange in *C. glutamicum*; (pK18 oriVE.c., *sacB*, *lac*Zα)	(Schäfer *et al.*, 1994)
pK19*mobsacB* Δ*trp*	Kan^r.; pK19mobsacB derivative for deletion of Δ*trpP* (cg3357) Δ*trpE* (cg3359) Δ*trpG* (cg3360) Δ*trpD* (cg3361) Δ*trpCF* (cg3362) Δ*trpB* (cg3363) Δ*trpA* (cg3364) in *C. glutamicum*	This study
pK19*mobsacB* Δ*serA*	Kan^r.; pK19mobsacB derivative for deletion of *serA* (cg1451) in *C. glutamicum*	This study
pK19*mobsacB* Δ*serC*	Kan^r.; pK19mobsacB derivative for deletion of *serC* (cg0948) in *C. glutamicum*	This study
pK19*mobsacB* Δ*serB*	Kan^r.; pK19mobsacB derivative for deletion of *serB* (cg2779) in *C. glutamicum*	This study
pK19*mobsacB* Δ*leuA*	Kan^r.; pK19mobsacB derivative for deletion of *leuA* (cg0303) in *C. glutamicum*	This study
pK19*mobsacB* Δ*leuCD*	Kan^r.; pK19mobsacB derivative for deletion of *leuC* (cg1487) *leuD* (cg1488) in *C. glutamicum*	This study
pK19*mobsacB* Δ*leuB*	Kan^r.; pK19mobsacB derivative for deletion of *leuB* (cg1453) in *C. glutamicum*	This study
pK19*mobsacB* Δ*nagS*	Kan^r.; pK19mobsacB derivative for deletion of *nagS* (cg3035) in *C. glutamicum*	This study
pK19*mobsacB* Δ*arg*	Kan^r.; pK19mobsacB derivative for deletion of Δ*argC* (cg1580) Δ*argJ* (cg1581) Δ*argB* (cg1582) Δ*argD* (cg1583) Δ*argF* (cg1584) Δ*argR* (cg1585) Δ*argG* (cg1586) Δ*argH* (cg1588) in *C. glutamicum*	This study
pK19*mobsacB* Δ*argR*	Kan^r.; pK19mobsacB derivative for deletion of Δ*argR* (cg1585) in *C. glutamicum*	This study
pK19*mobsacB* Δ*hisEG*	Kan^r.; pK19mobsacB derivative for deletion of Δ*hisE* (cg1699) Δ*hisG* (cg1698) in *C. glutamicum*	This study
pK19*mobsacB* Δ*hisHAFI*	Kan^r.; pK19mobsacB derivative for deletion of Δ*hisH* (cg2300) Δ*hisA* (cg2299) Δ*impA* (cg2298) Δ*hisF* (cg2297) Δ*hisI* (cg2296) in *C. glutamicum*	This study
pK19*mobsacB* Δ*hisBCD*	Kan^r.; pK19mobsacB derivative for deletion of Δ*hisD* (cg2305) Δ*hisC* (cg2304) Δ*hisB* (cg2303) in *C. glutamicum*	This study
pK19*mobsacB* Δ*hisN*	Kan^r.; pK19mobsacB derivative for deletion of Δ*hisN* (cg0910) in *C. glutamicum*	This study
pK19*mobsacB*-P_{tuf} *leuA*_B018_BS	Kan^r.; pK19*mobsacB* derivative containing *leuA* gene from B018 (*Mlu*I/*Spe*I) under control of the *tuf* promoter (*Nde*I/*Mlu*I) flanked by upstream and downstream regions of *leuA*	(Vogt *et al.*, 2014)

Plasmid	Relevant characteristics	Source or reference
pK19*mobsacB*-ArgB$_{A29V\ M31V}$	Kan^r.; pK19*mobsacB* derivative for mutation of ArgB (Cg1582) A29V M31V in *C. glutamicum*	This study
pK19*mobsacB*-HisG$_{A270D}$	Kan^r.; pK19*mobsacB* derivative for mutation of HisG (Cg1698) A270D in *C. glutamicum*	This study
pK19*mobsacB*-TrpL$_{fbr}$ TrpE$_{S38R}$	Kan^r.; pK19*mobsacB* derivative for mutation of *trpL* (TGG->TGA) and TrpE (Cg3359) S38R in *C. glutamicum*	This study
pK18*mobsacB-P$_{tac}$-eYFP*	Kan^r.; pK18*mobsacB* derivative for integration of P$_{tac}$-eYFP fluorescent protein in IGR between cg1121 and 1122	(Baumgart *et al.*, 2013)
pK18*mobsacB-P$_{tac}$-crimson*	pK18*mobsacB* derivative for integration of P$_{tac}$-crimson fluorescent protein in IGR between cg1121 and 1122	(Baumgart *et al.*, 2013)

Table S2: Oligonucleotides used in this study.

Oligonucleotide	Sequence (5' → 3')
Sequencing primers	
B223_M13-fw	CGCCAGGGTTTTCCCAGTCAC
B224_M13-rv	AGCGGATAACAATTTCACACAGGA
Construction of and work with pK19*mobsacB* Δ*trp*	
B453_TRP-D1	AAAACGACGGCCAGTGAATTAATGCCGAGCCATTTGCCAG
B454_TRP-D2	AACAACAACTCTATCCCCACCAATATTCC
B455_TRP-D3	GTGGGGATAGAGTTGTTGTTGCCTTTAAATGTGGCAATGTTTCACG
B456_TRP-D4	CAGGTCGACTCTAGAGGAAGTATTTGGCGCCTTTGCCAAC
B457_TRP-Dfw	TAGAGCGCTTGGGATGCTCC
B458_TRP-Drv	TGGTCCCCCACTTCTTCACTGG
Construction and work with pK19*mobsacB* Δ*cg3035*	
B459_cg3035_D1	AAAACGACGGCCAGTGAATTCCTACCCAGCTTGTTACTGAGG
B460_cg3035_D2	CTAGGCGTCATGCCCGAAAG
B461_cg3035_D3	CTTTCGGGCATGACGCCTAGTTAAAATCCAAAACAGCTAGGGTATAAGTCATGC
B462_cg3035_D4	CAGGTCGACTCTAGAGGACGCGATGTTGAAGTCGCCG
B463_cg3035_Dfw	GCGGAAAGCATGCTTAGAATGTTGCC
B464_cg3035_Drv	CACGTTCTGGTTCGGTGACG
Construction and work with pK19*mobsacB* Δ*arg*	

Oligonucleotide	Sequence (5' → 3')
B465_ARG-D1	AAAACGACGGCCAGTGAATTGCATCACTGGTCGCTTGTGG
B466_ARG-D2	AGTTACACCATACACGTTATGCATGATC
B467_ARG-D3	ATAACGTGTATGGTGTAACTGCATTAGTTTATGGCCTGTGCTGC
B468_ARG-D4	CAGGTCGACTCTAGAGGAACATGTCGGTGATGGTTCCG
B469_ARG-Dfw	AGCTCCCGCTAAGGTAGCTACC
B470_ARG-Drv	TTGGGTTTCATTCAACAACGCGCC
Construction and work with pK19*mobsacB* Δ*serA*	
B471_serA-D1	AAAACGACGGCCAGTGAATTGGGCCGTTCAAAGTGTTGCC
B472_serA-D2	AAGTTACTCCTGGAAAAACTAGGAATGTCC
B473_serA-D3	AGTTTTTCCAGGAGTAACTTTTAGAGATCCATTTGCTTGAACCGCC
B474_serA-D4	CAGGTCGACTCTAGAGGAGGTCGATGGCGCCATCAAAC
B503_ser-Dfw_V2	GTGTGTTTGGTCAGGTTTAGTCGG
B476_serA-Drv	TTAATGTTGAGCATTGCGCCGC
Construction and work with pK19*mobsacB* Δ*serB*	
B477_serB-D1	AAAACGACGGCCAGTGAATTCCTGCTTGGCCTGTCTGTCATTC
B478_serB-D2	GGCAACAATTGTCTCATGTCTGAGCG
B479_serB-D3	GACATGAGACAATTGTTGCCAGATTCGCTTCTCGACGCCC
B480_serB-D4	CAGGTCGACTCTAGAGGATTCCCAGCGTCATCTTCAACG
B481_serB-Dfw	GTCGTTACGCTGACTACCTGG
B482_serB-Drv	TGCTCCACCCACTCAAACGG
Construction and work with pK19*mobsacB* Δ*serC*	
B483_serC-D1	AAAACGACGGCCAGTGAATTCAGCCACCGTAATCAGTAGCC
B484_serC-D2	GTCTTCGGGCAACTTTCTGCG
B485_serC-D3	GCAGAAAGTTGCCCGAAGACTACCCCCACTTTGAAAAACACCCC
B486_serC-D4	CAGGTCGACTCTAGAGGATGGGGTGTGATTGCTTAGCC
B487_serC-Dfw	CGATAAATGCGGTTTAGCCATATCCG
B488_serC-Drv	AACGCCGTTGCAAGAATTTCCC
Construction and work with pK19*mobsacB* Δ*leuA*	
Z1_leuA-D1	AAAACGACGGCCAGTGAATTGATCTTGTGATTCCGAAGTG
Z2_leuA-D2	GCTTTACGACGCCTCCCCCTAGGCTC
Z3_leuA-D3	AGGGGGAGGCGTCGTAAAGCTTTCGACGCCCAGTTCCAG
Z4_leuA-D4	CAGGTCGACTCTAGAGGAAGTACTTTTAGTCGGCGTTG
Z5_leuA-Dfw	GGGTGGATTCCACTTGATTG
Z6_leuA-Drv	GGCTACCCTCCTCACCGTAG

Oligonucleotide	Sequence (5' → 3')
Construction and work with pK19*mobsacB* Δ*leuB*	
Z7_leuB-D1	AAAACGACGGCCAGTGAATTGTTTGTGGCTGCCGCGTTTG
Z8_leuB-D2	TCACTAGTGTAGCTGATTGATC
Z9_leuB-D3	TCAATCAGCTACACTAGTGAGACCCCCTTGCCTTTTATG
Z10_leuB-D4	CAGGTCGACTCTAGAGGAAACGTGCATTACCCGGTGAG
Z11_leuB-Dfw	GGTGCTTAAGGCGGATAAGG
Z12_leuB-Drv	TAAACACCCTCGGTGCTCTG
Construction and work with pK19*mobsacB* Δ*leuCD*	
Z13_leuCD-D1	AAAACGACGGCCAGTGAATTGGAGGTAGGCGGCAAAAACG
Z14_leuCD-D2	ACCCCCACACACAGTGAATCCCTTC
Z15_leuCD-D3	GATTCACTGTGTGTGGGGGTGTTCAGTCTGATAGCGAAAG
Z16_leuCD-D4	CAGGTCGACTCTAGAGGAAAGGTGGCGTGCCGATGATC
Z17_leuCD-Dfw	CCCACGGACTCCGCTAAGC
Z18_leuCD-Drv	TCAAACCCACCGCAATTTACTCG
Construction and work with pK19*mobsacB* Δ*hisEG*	
Z19_hisEG-D1	AAAACGACGGCCAGTGAATTTGATCCATACAGCGTTCCTC
Z20_hisEG-D2	TTTAACTACCCCCGAAAATGTAGTGG
Z21_hisEG-D3	CATTTTCGGGGGTAGTTAAATAATTTCACTCCCCCACCTG
Z22_hisEG-D4	CAGGTCGACTCTAGAGGACGAATCCCTCGTCCCAAATC
Z65_HisEG_fw_neu	GACTGGGACATGTTCACATC
Z66_HisEG_rv_neu	CACGCAGGCATTACATTGAG
Construction and work with pK19*mobsacB* Δ*hisHAFI*	
Z46_hisAHFI-D1_neu	AAAACGACGGCCAGTGAATTGCTCATACTGATTGCTTTTC
Z44_hisAHFI-D2_neu	GGAAGAAATCTTATGAAGCCACGCG
Z45_hisAHFI-D3_neu	GGCTTCATAAGATTTCTTCCATCCACCACACTGGCCTAGC
Z28_hisAHFI-D4	CAGGTCGACTCTAGAGGAGATCTCAGTCTGGTGAGATG
Z29_hisAHFI-Dfw	CCTCGATGGTTACCCAGTTC
Z30_hisAHFI-Drv	GCCCAGAAATCTGTCTAGGC
Construction and work with pK19*mobsacB* Δ*hisBCD*	
Z31_hisBCD-D1	CAGGTCGACTCTAGAGGACGCTGAAGATGTACCCGATG
Z32_hisBCD-D2	CATGAACTCTTCTCCCATCTCTG
Z33_hisBCD-D3	AGATGGGAGAAGAGTTCATGAATGACCACCCCAGATTTAC
Z34_hisBCD-D4	AAAACGACGGCCAGTGAATTCGCTCCAGAATATAGGTCAC

Oligonucleotide	Sequence (5' → 3')
Z35_hisBCD-Dfw	TCAGCCACCAACGCAGATTC
Z36_hisBCD-Drv	ACGAGATCTGCTTGGTCTTG
Construction and work with pK19*mobsacB* Δ*hisN*	
Z37_hisN-D1	AAAACGACGGCCAGTGAATTCTTTTAACTAGACGCGGTTC
Z38_hisN-D2	CCGGGTTTTGCTTGGTTTTC
Z39_hisN-D3	GAAAACCAAGCAAAACCCGGGTTAGTCTAGTGCGCTTAAA
Z40_hisN-D4	CAGGTCGACTCTAGAGGAGATGGCACCTACAACTTCAC
Z41_hisN-Dfw	TTCAGCTCTGCGTTCTTTCC
Z42_hisN-Drv	TTGAAGCGTTGCGGCCTGAG
Construction and work with pK19*mobsacB* Δ*argR*	
Z51_ArgR-D1	AAAACGACGGCCAGTGAATTCTGAAGAAGGCCCAGCAGGC
Z52_ArgR-D2	GTCTTACCTCGGCTGGTTGG
Z53_ArgR-D3	CCAACCAGCCGAGGTAAGACAGCGCCCCTAGTTCAAGGCT
Z54_ArgR-D4	CAGGTCGACTCTAGAGGAAGCCGTGTGCAACGTGGGTA
Z55_ArgR-Dfw	ACTGTGCCGCTGGTGAACTC
Z56_ArgR-Drv	AGTCACGAGCAGGTGCAATG
Construction and work with pK19*mobsacB*-ArgB$_{A29V\ M31V}$	
Z74_ArgB_mut-D1_neu	AAAACGACGGCCAGTGAATTACAATTTGTTCAAGTGCGCA
Z75_ArgB_mut-D2_neu	ACCACGTCGGCAGCAAAAACAGCCTT
Z76_ArgB_mut-D3_neu	GTTTTTGCTGCCGACGTGGTCTTCTTGCGCACCGTGG
Z77_ArgB_mut-D4_neu	CAGGTCGACTCTAGAGGATCCACATTGGTGAGAACCAG
Z78_ArgB_mut-fw_neu	TGTGACCAAGCGCGTTGCTG
Z64_ArgB-mut_rv	GCCGTCAATGACATGAGCAG
Construction and work with pK19*mobsacB*-TrpL$_{fbr}$ TrpE$_{S38R}$	
Z79_TrpE_mut-D1_neu	AAAACGACGGCCAGTGAATTGGCCGTTGAAGGTGGTGAAG
Z80_TrpE_mut-D2_neu	GCTTAGTTAGCGCGTCACCACCACTG
Z81_TrpE_mut-D3_neu	TGGTGACGCGCTAACTAAGCGAGCCTGACACCTCAAGTTG
Z82_TrpE_mut-D4_neu_V3	GGTGATATCAGCGCGTTCCAACAGG
Z83_TrpE_mut-D5_neu	GGAACGCGCTGATATCACCACCAAGAATGGTATTTCTTCC
Z84_TrpE_mut-D6_neu	CAGGTCGACTCTAGAGGACCAGGTCGTTGCGGGCGAGA
Z59_TrpE_mut_fw	GCTGCGGAAACTACGCAAG
Z85_TrpE_mut_rv_neu	CACGGGACACCAAGTGCATC
Z90_TrpE_mut_seq1	GGGCACCTACCGAGGAAATC

Oligonucleotide	Sequence (5' → 3')
Z91_TrpE_mut_seq2	GAGACAAGCTTCCCACTATG
Construction and work with pK19*mobsacB*-HisG$_{A270D}$	
Z86_HisG_A270D-D2	GGCGCTGAAGATATCCTGGC
Z87_HisG_A270D-D3	GCCAGGATATCTTCAGCGCCGAGTCCAGCAAGC
Z88_HisG_A270D-D4	CAGGTCGACTCTAGAGGACGAAAAGCTCGACGGCAAG
Z89_HisG_A270D_rv	GGTTCCTCCACTTTCCGTTAC
Work with pK19*mobsacB*-P$_{tuf}$ *leuA*_B018_BS	
Z92_LeuA_Ptuf_fw	CTGGACTTCGTGGTGGCTAC
Z93_LeuA_Ptuf_seq_rv	TGCCACAGGGTAGCTGGTAG
Z67_PtufLeuA_seq_fw	CTCAGTGGTGTGCTGTTGAC
Z68_PtufLeuA_seq_rv	TCCTTGCCGTTGTGGATGAG
Analysis of fluorescent protein integration	
Z109_Intcg1121 fwd	TTGGCGTGTGGTTGGTTAG
Z110_Intcg1122 rev	CGCATCAAGCAGATCTCTG

References

Baumgart, M., Unthan, S., Rückert, C., Sivalingam, J., Grünberger, A., Kalinowski, J., Bott, M., Noack, S., Frunzke, J., 2013. Construction of a Prophage-Free Variant of *Corynebacterium glutamicum* ATCC 13032 for Use as a Platform Strain for Basic Research and Industrial Biotechnology. Applied and environmental microbiology. 79**,** 6006-6015.

Schäfer, A., Tauch, A., Jäger, W., Kalinowski, J., Thierbach, G., Pühler, A., 1994. Small mobilizable multi-purpose cloning vectors derived from the *Escherichia coli* plasmids pK18 and pK19: selection of defined deletions in the chromosome of *Corynebacterium glutamicum*. Gene. 145**,** 69-73.

Vogt, M., Haas, S., Klaffl, S., Polen, T., Eggeling, L., van Ooyen, J., Bott, M., 2014. Pushing product formation to its limit: metabolic engineering of *Corynebacterium glutamicum* for L-leucine overproduction. Metab Eng. 22**,** 40-52.

2.2 Discovery of novel amino acid production traits by evolution of synthetic co-cultures

Zuchowski, R[*], Schito, S.[*], Neuheuser, F., Menke, P., Berger, D., Hollmann, N., Gujar, S., Sundermeyer, L., Mack, C., Wirtz, A., Weiergräber, O., Polen, T., Bott, M., Wiechert, W., Noack, S., Baumgart, M. (2023). Discovery of novel amino acid production traits by evolution of synthetic co-cultures. *Microbial Cell Factories*, 22:71.

[*] These authors contributed equally to this work.

Author contributions

RZ: Conceptualization, Methodology, Investigation, Data analysis, Writing – Initial Draft, Visualization, Revision & Writing – final manuscript

SS: Conceptualization, Methodology, Investigation, Data analysis, Writing – Initial Draft, Visualization, Revision & Writing – final manuscript

FN: Investigation, Data analysis

PM: Investigation, Data analysis

NH: Investigation, Data analysis, Visualization

SG: Investigation, Data analysis, Writing – Initial Draft

LS: Investigation, Data analysis, Writing – Initial Draft

CM: Investigation, Data analysis

AW: Investigation, Methodology, Data analysis

OW: Supervision, Data analysis, Writing – Initial Draft

TP: Data analysis, Writing – Initial Draft

MBo: Revision & Writing – final manuscript, Funding acquisition

SN: Conceptualization, Supervision, Revision & Writing – final manuscript, Funding acquisition

MBa: Conceptualization, Supervision, Revision & Writing – final manuscript Funding acquisition

Overall contribution: 30%

Zuchowski *et al. Microbial Cell Factories* (2023) 22:71
https://doi.org/10.1186/s12934-023-02078-2

Microbial Cell Factories

RESEARCH

Open Access

Discovery of novel amino acid production traits by evolution of synthetic co-cultures

Rico Zuchowski[1†], Simone Schito[1†], Friederike Neuheuser[1], Philipp Menke[1], Daniel Berger[1], Niels Hollmann[1], Srushti Gujar[1,2,3], Lea Sundermeyer[1], Christina Mack[1], Astrid Wirtz[1], Oliver H. Weiergräber[2], Tino Polen[1], Michael Bott[1], Stephan Noack[1] and Meike Baumgart[1*]

Abstract

Background Amino acid production features of *Corynebacterium glutamicum* were extensively studied in the last two decades. Many metabolic pathways, regulatory and transport principles are known, but purely rational approaches often provide only limited progress in production optimization. We recently generated stable synthetic co-cultures, termed Communities of Niche-optimized Strains (CoNoS), that rely on cross-feeding of amino acids for growth. This setup has the potential to evolve strains with improved production by selection of faster growing communities.

Results Here we performed adaptive laboratory evolution (ALE) with a CoNoS to identify mutations that are relevant for amino acid production both in mono- and co-cultures. During ALE with the CoNoS composed of strains auxotrophic for either L-leucine or L-arginine, we obtained a 23% growth rate increase. Via whole-genome sequencing and reverse engineering, we identified several mutations involved in amino acid transport that are beneficial for CoNoS growth. The L-leucine auxotrophic strain carried an expression-promoting mutation in the promoter region of *brnQ* (cg2537), encoding a branched-chain amino acid transporter in combination with mutations in the genes for the Na^+/H^+-antiporter Mrp1 (cg0326-cg0321). This suggested an unexpected link of Mrp1 to L-leucine transport. The L-arginine auxotrophic partner evolved expression-promoting mutations near the transcriptional start site of the yet uncharacterized operon *argTUV* (cg1504-02). By mutation studies and ITC, we characterized ArgTUV as the only L-arginine uptake system of *C. glutamicum* with an affinity of $K_D = 30$ nM. Finally, deletion of *argTUV* in an L-arginine producer strain resulted in a faster and 24% higher L-arginine production in comparison to the parental strain.

Conclusion Our work demonstrates the power of the CoNoS-approach for evolution-guided identification of non-obvious production traits, which can also advance amino acid production in monocultures. Further rounds of evolution with import-optimized strains can potentially reveal beneficial mutations also in metabolic pathway enzymes. The approach can easily be extended to all kinds of metabolite cross-feeding pairings of different organisms or different strains of the same organism, thereby enabling the identification of relevant transport systems and other favorable mutations.

Keywords Synthetic co-culture, *Corynebacterium glutamicum*, ALE / evolutionary engineering, Arginine import, Metabolic engineering, Arginine production

†Rico Zuchowski and Simone Schito contributed equally to this work

*Correspondence:
Meike Baumgart
m.baumgart@fz-juelich.de
Full list of author information is available at the end of the article

Background

In nature, microorganisms usually live in communities with various other organisms leading to a large number of intraspecies and interspecies interactions. Some organisms are competitors e.g. for nutrients, but at the same time there are numerous cooperations that have beneficial effects for all community members. These kind of syntrophic interactions are a key factor in species evolution and can enable bacteria to use resources more efficiently and grow with a higher productivity [1]. Metabolic auxotrophies can be advantageous for the cells, because uptake of a certain metabolite from the environment is usually cheaper than synthesizing it itself [2]. In this way, whole communities adapt to very specific ecological niches in which the supply with metabolites occurs by co-evolving partners [3].

Based on these observations, we asked the question whether it is possible to generate synthetic communities that can produce a compound of interest more efficiently than a monoculture and developed the concept of Communities of Niche-optimized Strains, in short CoNoS [3]. A CoNoS consists of at least two strains of the same species that are auxotrophic for a certain metabolite and cross-feed each other with the aim to use the available resources more efficiently than a monoculture. In this context, former studies already showed that synthetic communities comprising auxotrophic *Escherichia coli* strains reached a higher biomass and fitness level compared to the monocultures [4, 5]. Furthermore, initial communities with sub-optimal interactions evolved quickly and both partners improved their metabolite production to benefit their corresponding partner [6].

Corynebacterium glutamicum is one of the most important workhorses of industrial biotechnology for the production of amino acids and various other metabolites [7, 8]. Many metabolic pathways as well as regulatory and transport principles are known, but further improvements of amino acid production strains by rational approaches became less and less in the last years. Thus, we decided to use *C. glutamicum* as model organism for our CoNoS approach [9]. We established a fast and stable growing community of an L-arginine and an L-leucine auxotrophic strain, both rationally engineered for higher production of the amino acid required by their partner strain. This CoNoS reached a growth rate equivalent to 83% of the wild type, suggesting some remaining bottlenecks in their cross-feeding relationship [9]. These bottlenecks are most likely related either to amino acid production, which is well studied in *C. glutamicum*, or to transport processes. Amino acid export [10] and import (Additional file 1: Table S1) is known to some extent in *C. glutamicum*, but there are still several gaps, e.g. it is unclear how L-arginine is taken up by the cell. This makes rational approaches rather difficult. One important alternative is the untargeted approach of Adaptive Laboratory Evolution (ALE), which exploits the natural principle of evolutionary adaptation of cells to changing environmental conditions. Many different strategies and technologies have been established to perform ALE experiments [11, 12] and in particular the repetitive batch approach has gained popularity due to its low operating costs, simple experimental implementation, and easy extensibility [13]. In combination with liquid handling robotics, automated ALE experiments can be performed, leading to standardized and robust procedures and thus increasing the chances of successful evolution with identification of new strain features relevant for production [14, 15].

In this study, we performed automated ALE with a CoNoS to identify mutations beneficial for amino acid production and transport both in synthetic communities and monocultures. We isolated single strains from faster growing CoNoS and identified several mutations e.g. in promoters of amino acid transport systems. Among others, we identified and characterized ArgTUV as an L-arginine import system. Finally, deletion of this transporter increased the L-arginine titer by 24% for an L-arginine producing monoculture.

Results

ALE with a CoNoS comprising two amino acid-auxotrophic strains

We recently demonstrated that synthetic CoNoS composed of two complementary amino acid-auxotrophic strains are able to grow based on mutual dependency [9]. To improve amino acid exchange and thus growth of the CoNoS, the strains were metabolically engineered addressing known targets for increased amino acid production [9]. In this work, we exploit ALE to improve the fitness of microbial communities (Fig. 1A) with the aim to identify and investigate new growth-related targets such as transporters that increase amino acid exchange. As starting point, we chose the L-arginine-auxotrophic strain ΔARG LEU^{++} and the L-leucine-auxotrophic strain ΔLEU ARG^{+}. ΔARG LEU^{++} is derived from the *C. glutamicum* wild type lacking all biosynthetic enzymes for L-arginine and carrying a feedback resistant LeuA variant under control of the strong P_{tuf} promoter, which leads to a slight overproduction of L-leucine. ΔLEU ARG+ is derived from the genome-reduced strain C1* with an in frame deletion of *argR* (cg1585) and produces a sufficient amount of L-arginine for co-culture growth. A CoNoS composed of these two strains has a growth rate resembling almost half of the WT level, leaving potential for improvement by selecting for faster growing cultures [9].

For the ALE, we used the Mini Pilot Plant that consists of a microbioreactor combined with a liquid handling robotic system [15, 16]. The CoNoS was grown in CGXII medium with 2% (w/v) (corresponding to 111 mM) D-glucose until a backscatter (BS) threshold (BS = 17) triggered automated transfer of 10% (v/v) of the cell suspension into an empty well that was filled with fresh chill-stored CGXII medium. In this manner, we performed 16 repetitive batches in triplicates. Next to online biomass, the time of each transfer was monitored for each single batch, enabling model-based growth rate estimation (Fig. 1B). Both growth rate and transfer time indicated that in all three replicates the fitness of the CoNoS improved across the batches. Specifically, the transfer time decreased by 23% and the growth rate increased by 23% from batch two to batch 16 in all three replicates. At this point, it was not obvious whether the improved fitness was caused by mutations occurring in only one or in both community members and thus the single evolved strains were isolated for further analysis. Cell suspension of the last batch of each replicate was spread onto CGXII agar plates with 2% (w/v) glucose supplemented either with 3 mM L-leucine or 3 mM L-arginine to select only one community member on each plate (six plates in total). Six colonies from each plate were selected and combined in a CoNoS with the corresponding non-evolved partner to test whether the single evolved strains are able to improve growth of a community (Additional file 1: Fig. S1). Interestingly, not all clones from one ALE affected growth of the CoNoS similarly, which means that even after 16 batches there is obvious heterogeneity in the cultures (Additional file 1: Fig. S1). The best performing clone from each plate was selected for further characterization and named ΔLEU ARG^{+} evo1, ΔLEU ARG^{+} evo2, ΔARG LEU^{++} evo1, ΔARG LEU^{++} evo2, and ΔARG LEU^{++} evo3. Here the numbers indicate the origin of the ALE replicate. All CoNoS composed of a single evolved member and the corresponding non-evolved partner grew with a growth rate at least 7% higher compared to the starting CoNoS (Fig. 1C, D). The growth of ΔLEU ARG^{+} evo3 was not reproducible and this strain was thus excluded from further analysis.

In this experiment, we successfully evolved a CoNoS toward faster growth in three independent setups. The growth rate increase measured for the CoNoS with only one evolved member was lower compared to the final growth rate of the evolution experiment. This suggests that both community members carry mutations that improved growth of the community in an additive manner.

Identification of mutations in the evolved ΔLEU ARG^{+} strain

The CoNoS ALE yielded five strains in total that presumably carried mutations beneficial for CoNoS growth. To identify and analyze these mutations in detail, we isolated genomic DNA from all five strains and sequenced it. Sequencing of the two evolved ΔLEU ARG^{+} strains yielded two mutations per strain (Table 1). Both strains carried the mutation MetC/P_{brnQ}^{*} and an additional mutation in different subunits of the Mrp1 transporter.

The mutation MetC/P_{brnQ}^{*} is located within the coding sequence of *metC* (cg2536), encoding the cystathionine β-lyase MetC [17]. This mutation was present in both strains but not in the parental strain as confirmed by sequencing of the non-evolved strain. *metC* is the first gene of a putative operon formed by *metC*, *brnQ* (cg2537), and cg2538 [18]. *brnQ* and cg2538 are proposed to form a sub-operon with a separate transcriptional start site (TSS), which is located within the coding sequence of *metC* (Additional file 1: Fig. S2) [18]. BrnQ is a Na^{+}-coupled uptake system for branched chain amino acids [19, 20]. Cg2538 encodes an uncharacterized protein annotated as putative FMN-linked alkanal monooxygenase α chain with 43.8% identity to a luciferase-like monooxygenase of *E. coli*. The mutation in *metC* caused an amino acid exchange from serine to phenylalanine at position 332. MetC S332 is moderately conserved in closely related *Corynebacterium* species and not conserved in other homologous aminotransferases of *Actinomycetales* species (Additional file 1: Fig. S3). To analyze the impact of the mutation on protein structure, we compared the best-ranked AlphaFold2 predictions for both

(See figure on next page.)

Fig. 1 ALE of a CoNoS comprising two amino-acid auxotrophic strains. **A** ALE of the CoNoS composed of *C. glutamicum* ΔARG LEU^{++} ↔ ΔLEU ARG+. To start the ALE, both strains were cultivated in shake flask monocultures in CGXII medium with 2% (w/v) glucose and 3 mM of the required amino acid. After 2 days at 30 °C, the cells were washed and used in a 1:1 ratio based on OD_{600} measurements to inoculate the first batch. 16 repetitive batches were cultivated in CGXII medium with 2% (w/v) glucose and 100 µM IPTG in microtiter plates (MTPs) at 30 °C, 1400 rpm. Displayed is the on-line backscatter signal of batches 2–16. A backscatter threshold (dashed grey line) triggered cell suspension transfer to inoculate the following batch. One representative of three independent replicates is shown. **B** Specific growth rate calculation for the ALE shown in (**A**). **C**, **D** Each evolved strain (evo1, evo2, and evo3) was isolated from one independent replicate of the ALE and cultivated in biological triplicates with the corresponding non-evolved partner. WT monoculture and the CoNoS comprising the non-evolved strains are shown as reference cultivations. The CoNoS were cultivated in CGXII medium with 2% (w/v) glucose and incubated in MTPs at 30 °C, 1400 rpm. Mean values and standard deviations are shown as lines and shaded areas, respectively

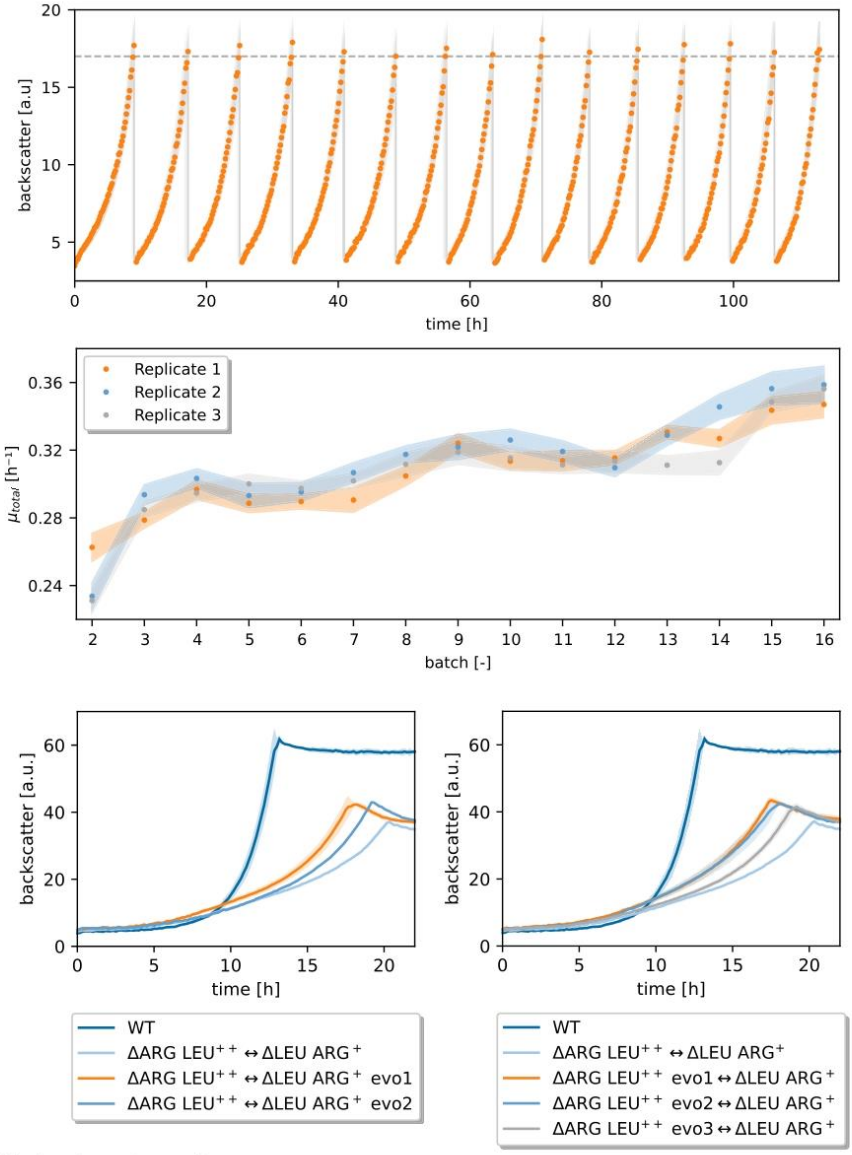

Fig. 1 (See legend on previous page.)

Table 1 Mutations identified by genome sequencing in evolved CoNoS strains

Strain	Position & mutation on DNA level[a]	Locus tag	Mutation	Mutation designation
ΔLEU ARG$^+$ evo1	SNV C281573T	cg0325	$Mrp1C_{G29D}$	$Mrp1C_{G29D}$
	SNV C2044002T	cg2536/P_{cg2537}	$MetC_{S322F}/P_{brnQ}$*	$MetC/P_{brnQ}$*
ΔLEU ARG$^+$ evo2	SNV T283546G	cg0326	$Mrp1A_{H335P}$	$Mrp1A_{H335P}$
	SNV C2044002T	cg2536/P_{cg2537}	$MetC_{S322F}/P_{brnQ}$*	$MetC/P_{brnQ}$*
ΔARG LEU^{++} evo1	SNV T1399043C	P_{cg1504}	P_{cg1504}*[1], mutation of -35 region: ttaagg ➜ ttgagg	P_{argT}*[1]
	SNV G1767718A	cg1874	$Cg1874_{G93D}$	$Cg1874_{G93D}$
	SNV G2712428C	cg2850	$Cg2850_{G30R}$	$Cg2850_{G30R}$
ΔARG LEU^{++} evo2	DEL 1399026–1401854	P_{cg1504}, cg1505, cg1506	deletion of 2829 bp upstream of cg1504[b]	P_{argT}*[2]
	SNV G1767718A	cg1874	$Cg1874_{G93D}$	$Cg1874_{G93D}$
ΔARG LEU^{++} evo3	SNV C1399000T	cg1504	cg1504*, 3rd codon GAG ➜ GAA, synonymous mutation	*argT**
	SNV G1767718A	cg1874	$Cg1874_{G93D}$	$Cg1874_{G93D}$
	SNV G2712428C	cg2850	$Cg2850_{G30R}$	$Cg2850_{G30R}$

[a] Reads were mapped using GenBank accession number CP017995 (for ΔLEU ARG$^+$) or BX927147 (for ΔARG LEU^{++}) as reference. Mutations are given for the plus strand. Abbreviations: deletion (DEL); single nucleotide variant (SNV)

[b] Partial deletion of the intergenic region of cg1504-cg1505, deletion of cg1505 & cg1506, partial deletion of cg1507

MetC and the $MetC_{S322F}$ variant. Superimposition of the two models yielded a C-alpha root mean square distance (C^{α} r.m.s.d.) of 0.26 Å (Additional file 1: Table S2). In fact, AlphaFold2 predicted two alternative local conformational changes in $MetC_{S322F}$ with respect to the wildtype, compensating for the larger side chain: in the rank 1 and rank 4 models of $MetC_{S322F}$, backbone shifting was seen, while in the other models an altered side chain torsion (χ_1) was apparent (Additional file 1: Fig. S4A). Analysis of structural changes by Missense3D [21] revealed that S322 is largely buried in MetC, with only 2.3% relative solvent accessibility, while substitution of S322 by phenylalanine leads to enhanced surface exposure of this residue (14.2%). The hydrogen bond between the side chain hydroxyl oxygen of S322 and the carbonyl oxygen of L333 (distance 2.53 Å) is necessarily disrupted due to the S322F mutation (Additional file 1: Fig. S4A), which is accompanied by a slight shift in the polypeptide backbone around residue 333. In accordance with the annotation (see above), DALI analysis [22] of our MetC models revealed structural similarity to a putative pyridoxal-5'-phosphate (PLP)-dependent cystathionine β-lyase of *Corynebacterium diphtheriae* (PDB code 3fdb) with 55% sequence identity. Superimposition of this protein with our MetC and $MetC_{S322F}$ models gave a C^{α} r.m.s.d. of 0.97 Å and 0.94 Å, respectively. Cystathionine β-lyases catalyze cleavage of the S-C^{β} bond in cystathionine using PLP as the cofactor, yielding homocysteine, pyruvate, and ammonia [23]. The S322F mutation occurred in helix 14 in the C-terminal domain of MetC (Additional file 1: Fig. S3). In *E. coli* MetC, the C-terminal domain is proposed to be involved in the positioning of the substrate [24]. Extending the prediction by AlphaFold2, we suspect the bulky and apolar F322 side chain to associate with a nearby hydrophobic cluster linking the C-terminal domain to an adjacent N-terminal segment. The resulting rigidification, together with the disruption of the S322–L333 hydrogen bonding, might significantly alter the conformational dynamics and thus catalytic activity of the enzyme.

Besides causing an amino acid exchange in MetC, the $MetC/P_{brnQ}$* mutation is located 35 bp upstream of the transcriptional start site (TSS) of *brnQ* and may influence transcription of *brnQ* and the following cg2538. For *brnQ*, no specific -35 region for the major sigma factor σ^{70} was annotated [18]. The $MetC/P_{brnQ}$* mutation increased the similarity of the -35 region of *brnQ* with the weakly conserved "ttgnca" motif by changing "tctaaa" to "tttaaa", which may influence the transcription of the following genes.

In addition to the $MetC/P_{brnQ}$* mutation, both strains had a mutation in the multi-subunit Na^+/H^+ antiporter Mrp1, which is important for environmental Na^+ resistance and alkali tolerance [25]. Mrp1 is encoded by the gene cluster *mrp1* (cg0326-cg0321, *mrp1A, mrp1C, mrp1D, mrp1E, mrp1F, mrp1G*). The mutation in ΔLEU ARG$^+$ evo1 resulted in the amino acid exchange G29D in Mrp1C, whilst the mutation in ΔLEU ARG$^+$ evo2 yielded the amino acid exchange H335P in Mrp1A. The mutated positions in these proteins are highly but not fully conserved among different bacteria [25]. Thus, a mutation at these positions likely has a strong impact on

Mrp1 function. Mrp1A H335 is presumably part of the ion channel and the mutation to proline at this position may alter the characteristics of the channel [25]. Mrp1C G29 is located within the first transmembrane helix of Mrp1C. The exchange of G29 to the charged amino acid L-aspartate probably has a major impact on the protein function as it may disrupt membrane insertion of the helix.

Reconstruction of mutations in the ΔLEU ARG$^+$ strain

To confirm that the identified mutations are indeed responsible for the improved growth in the CoNoS setting, all three mutations were first introduced separately into ΔLEU ARG$^+$ and compared with the wild type and the parental strain ΔLEU ARG$^+$ in a supplemented monoculture (Additional file 1: Fig. S5A). ΔLEU ARG+ grew slower and to a slightly lower final backscatter compared to the wild type and none of the single mutations tested improved this growth behavior (Additional file 1: Fig. S5A). This means that either more than one mutation is required to observe a positive effect or that the improved growth is only apparent in a CoNoS setting. To test this, the two double mutation strains ΔLEU ARG$^+$ MetC/P_{brnQ}* Mrp1A_{H335P} and ΔLEU ARG$^+$ MetC/P_{brnQ}* Mrp1C_{G29D} were constructed and tested under the same conditions (Fig. 2A). These two strains grew even slower than ΔLEU ARG$^+$ in the supplemented monoculture, suggesting that the mutations only have a positive effect in the CoNoS setting. Thus, we combined all single and double mutation strains with the non-evolved strain ΔARG LEU^{++} in a co-culture (Fig. 2B and Additional file 1: Fig. S5B). For the CoNoS with the single mutated strains, the growth rate slightly increased between 0.3 and 4% and the final biomass increased by approximately 4% in comparison to the parental CoNoS (Additional file 1: Fig. S5B). For the CoNoS with the double mutated strains, the growth rate and the final biomass both increased by approximately 6% in comparison to the parental CoNoS (Fig. 2B). In summary, we identified and confirmed several mutations that specifically increased growth in the CoNoS setting but not in monocultures.

Growth with low L-leucine concentrations

Interestingly, we observed the positive effects of the MetC/P_{brnQ}* mutation only in the CoNoS setting but not in monoculture, although the affected L-leucine transporter BrnQ should also be relevant during growth in L-leucine supplemented CGXII medium. Maybe the effect is only apparent when the L-leucine levels are lower than the 3 mM we used in the supplemented cultures. In a CoNoS, we expect a low amino acid concentration in the culture medium because there is a constant, moderate overproduction and concomitant consumption by the partner strain. Thus, we tested the performance of

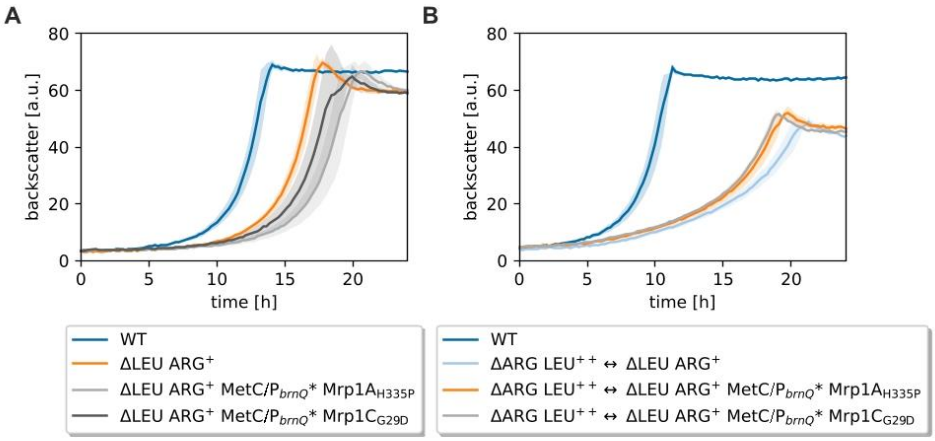

Fig. 2 Growth performance of the reengineered *C. glutamicum* ΔLEU ARG$^+$ strains. The mutations MetC/P_{brnQ}* Mrp1A_{H335P} and MetC/P_{brnQ}* Mrp1C_{G29D} were introduced into ΔLEU ARG$^+$ and the resulting strains tested in supplemented monoculture and in a CoNoS setting. A WT monoculture was used as reference. **A** Monocultures in CGXII medium with 2% (w/v) glucose supplemented with 3 mM L-leucine (WT culture not supplemented). **B** CoNoS composed of parental and reengineered strains in comparison to the WT monoculture cultivated in in CGXII medium with 2% (w/v) glucose. Mean values and standard deviations of biological triplicates are shown as lines and shaded areas, respectively

strain ΔLEU ARG$^+$ MetC/P_{brnQ}* Mrp1C_{G29D} in comparison to the parental strain in monoculture with L-leucine supplementation at concentrations of 100 µM–3 mM. The growth rates of both strains increased in proportion to the amount of L-leucine supplemented. However, we observed no beneficial effect of the mutations under the tested conditions (Additional file 1: Fig. S6A). It is likely that the beneficial effect is only apparent at even lower L-leucine concentrations, but there we did not see any growth in monoculture, presumably because the L-leucine concentration in the supplemented culture is not sufficient to support growth for more than a few generations.

Influence of the MetC/P_{brnQ}* mutation on transcription of *brnQ* and cg2538

After confirming that the evolved mutations are beneficial for CoNoS growth, we wanted to analyze their specific effect with the aim to learn more about factors limiting or promoting CoNoS growth. To test whether the MetC/P_{brnQ}* mutation influences the transcription level of *brnQ* and cg2538, we measured the transcript levels of these two genes by reverse transcriptase quantitative PCR (RT-qPCR) in ΔLEU ARG$^+$ and ΔLEU ARG$^+$ MetC/P_{brnQ}*. The *brnQ* transcript level was increased 2.1 ± 0.07-fold (1.8 ± 0.28-fold in an independent experiment) in ΔLEU ARG$^+$ MetC/P_{brnQ}* compared to the control strain. In contrast, transcription of cg2538 was almost unchanged (1.13 ± 0.04-fold). Thus, it seems that *brnQ* and cg2538 are transcribed independently, which has also been observed in other studies [26, 27], and there might be a separate TSS in front of cg2538. Thus, Cg2538 is most likely not responsible for the effect of the MetC/P_{brnQ}* mutation. In summary, the MetC/P_{brnQ}* mutation increased *brnQ* transcription and presumably the BrnQ content of the cell. As BrnQ activity is regulated based on de novo synthesis [28], we assume that the mutation caused elevated L-leucine uptake of the cell, which then increased growth in the CoNoS setting.

Effects of mutations in Mrp1 during growth with elevated NaCl concentrations

Besides the MetC/P_{brnQ}* mutation, the evolved strains carried mutations in different subunits of Mrp1. To test the effect of Mrp1C_{G29D} on sodium resistance and alkali tolerance without side effects of other mutations, we reconstructed this mutation in the wild type background resulting in strain WT Mrp1C_{G29D}. We analyzed the sodium resistance of this strain in comparison to the wild type in a growth experiment with liquid CGXII medium containing 2% (w/v) glucose as carbon source and either no or 1 M NaCl (Fig. 3A). Without NaCl, growth rate and final backscatter of WT Mrp1C_{G29D} were only slightly decreased compared to the wild type. With 1 M NaCl, the growth rate and the final backscatter were more than 40% decreased for WT Mrp1C_{G29D} in comparison to the wild type. When the two strains were cultivated on CGXII agar plates, both strains grew similarly in the absence of NaCl, while WT Mrp1C_{G29D} grew much worse than the wild type in the presence of 1 M NaCl (Fig. 3C and Additional file 1: Fig. S7). The Mrp1 transporter is especially relevant under alkaline conditions, thus the plate assays were performed both at pH 7 and pH 8, but there was no obvious difference between the two conditions. The results suggested that the G29D mutation strongly impairs, if not completely blocks, the function of Mrp1C.

To test the effects of the Mrp1C_{G29D} and Mrp1A_{H335P} mutations in the auxotrophic strain background, we constructed strains ΔLEU ARG$^+$ Mrp1C_{G29D} and ΔLEU ARG$^+$ Mrp1A_{H335P} as well as the deletion mutant ΔLEU ARG$^+$ Δ*mrp1*, lacking the whole *mrp1* gene cluster. These strains were compared to the parental strain and to the wild type in liquid medium and on agar plates regarding sodium resistance and alkali tolerance. In liquid medium without NaCl addition, all three strains grew like the parental strain ΔLEU ARG$^+$, which is slightly slower than the wild type (Fig. 3B). In liquid medium with 1 M NaCl, ΔLEU ARG$^+$ grew much slower and to a lower final backscatter than the wild type, which means that this strain had already lost some of its ability to cope with NaCl stress (Fig. 3B). Deletion of *mrp1*, as well as mutations Mrp1C_{G29D} and Mrp1A_{H335P}, impaired growth further, which strongly suggested that the mutations led to a loss of function. On solid medium, strain ΔLEU ARG$^+$ already grew much worse than the wild type (Fig. 3C and Additional file 1: Fig. S7). Upon mutation or deletion of *mrp1*, there was no further impact on growth visible, possibly because the effect was masked by the already reduced growth of ΔLEU ARG$^+$. In summary, we observed that both mutations Mrp1C_{G29D} and Mrp1A_{H335} had a similar negative effect in the presence of elevated NaCl concentrations like the entire deletion of *mrp1*. However, we do not know yet why a loss of Mrp1 function is beneficial for CoNoS growth.

Identification of mutations in the evolved ΔARG LEU^{++} strain

Sequencing of the ΔARG LEU^{++} strains isolated in the ALE revealed two or three mutations per strain (Table 1). The mutations occurred in two proteins of unknown function (Cg1874 and Cg2850) and close to the TSS/TLS (translational start site) of cg1504-1502 (named *argTUV* from here onwards), which encode a putative ABC-type amino acid transport system for polar amino acids. Interestingly, identical mutations for cg1874 as well as cg2850 occurred in more than one evolution setup. Sequencing

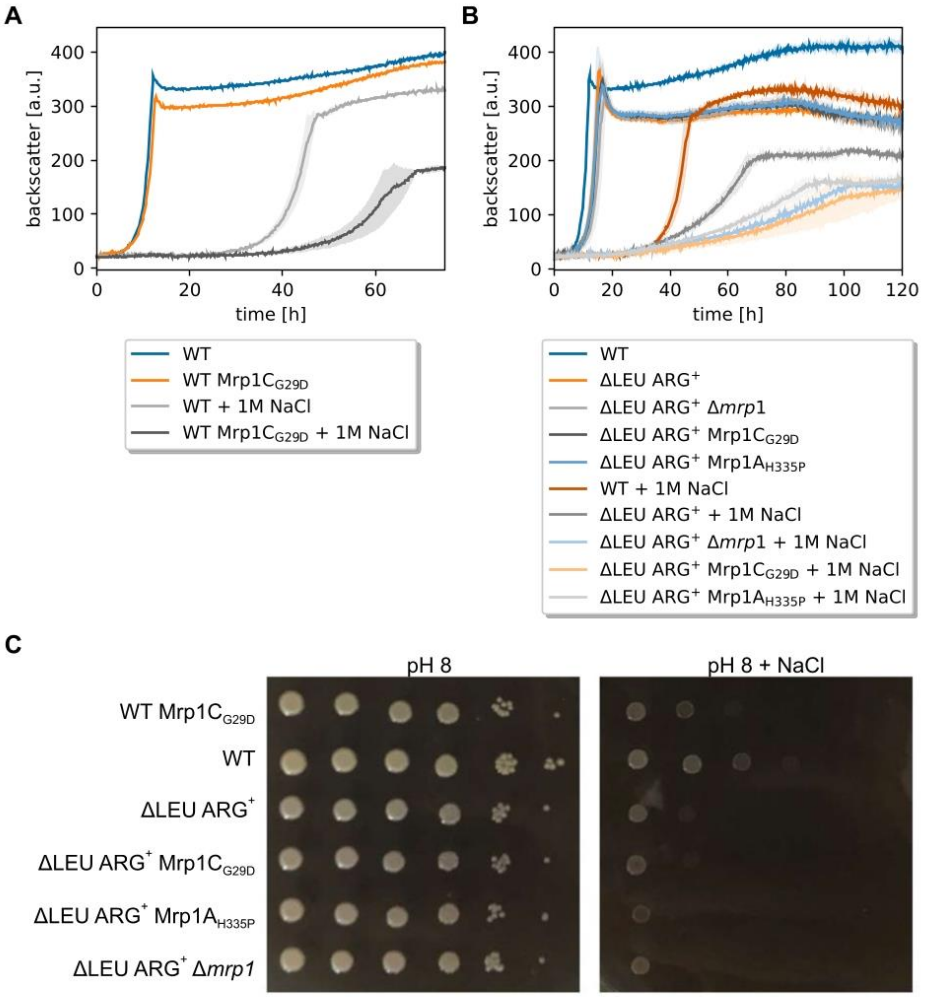

Fig. 3 Growth performance of Mrp1 mutant strains in supplemented monocultures under NaCl stress conditions. **A** Monocultures of WT and WT Mrp1C$_{G29D}$ cultivated with 2% (w/v) glucose. **B** Monocultures of mutated ΔLEU ARG$^+$ strains in comparison to WT, ΔLEU ARG$^+$. For (**A**, **B**) cultures were performed in biological triplicates in CGXII medium with 2% (w/v) glucose, supplemented with 3 mM L-leucine for auxotrophic strains. Mean values and standard deviations are shown as lines and shaded areas, respectively. **C** Tenfold serial dilutions of different *C. glutamicum* Mrp1 mutant strain cultures. Cells were precultivated in test tubes at 30 °C 180 rpm for 8 h in BHI medium. Afterwards, second precultures were prepared in CGXII with 2% (w/v) glucose and 3 mM L-leucine for the auxotrophic strains and cultivated over night at 30 °C 180 rpm. Dilutions were prepared in PBS starting with an OD$_{600}$ of 1 and spotted onto CGXII-agar plates (pH 8.0, 2% (w/v) glucose, 3 mM L-leucine) with different NaCl concentrations (0 M and 0.6 M) and incubated at 30 °C for 48 h, as described elsewhere [25]

of the relevant regions of the non-evolved strains confirmed that these mutations must have appeared independently during evolution.

Cg1874 and Cg2850 are uncharacterized proteins with homologs in closely related species and other *Actinomycetota* genera such as *Arthrobacter* or *Rhodococcus*. To get an idea about their function and the effects of the mutations we performed AlphaFold2 prediction. For Cg2850, superimposition of the top-ranked predicted WT and variant structures resulted in a C^{α} r.m.s.d. of 0.21 Å (residues 1–27 are predicted to be disordered and were excluded from the comparison) (Additional file 1: Table S2). DALI analysis of the Cg2850 models showed high structural similarity (C^{α} r.m.s.d. of 1.89 Å and 1.85 Å for WT and mutant, respectively) and 48% sequence identity with Rv0813c (PDB code 2fwv), a fatty acid binding protein-like protein of *Mycobacterium tuberculosis* [29]. Rv0813c belongs to the calycin superfamily implicated in the transport and storage of small and often hydrophobic molecules. Therefore, it seems conceivable that Cg2850 may participate in shuttling of amino acids or their metabolites, e.g. to/from membrane transporters. In the predicted Cg2850 structure, as observed in Rv0813c, residues 80–229 appear to form an anti-parallel β-barrel which could provide a cavity for non-covalent interactions (binding of ligands), while residues 28–79 constitute a partly helical N-terminal segment that mostly lines the circumference of the barrel on one end and becomes increasingly dynamic toward the N-terminus (Additional file 1: Fig. S4B). This region is relatively conserved between Rv0813c and its orthologs in other *Mycobacteria* and *Corynebacteria* and is proposed to have an important role in mediating protein–protein interactions [29]. The site of mutation (G30), in particular, is conserved across many *Corynebacteria*, *M. tuberculosis, Mycolicibacterium smegmatis,* and *Rhodococcus rhodochrous* (Additional file 1: Fig. S9). Interestingly, the G30R exchange, at the beginning of the N-terminal α-helix, generates a potential salt bridge with E169 on the β-barrel. While the respective atoms are 3.67 Å apart in the model, a favorable hydrogen bonding distance is easily achievable by choosing different rotamers. Concomitantly, a slight decrease in the internal cavity volume (by 43 $Å^3$) was predicted by Missense3D in the $Cg2850_{G30R}$ variant. Formation of the salt bridge at the base of the presumed ligand-binding cavity of $Cg2850_{G30R}$ might therefore affect the overall activity of the protein by restraining the dynamics of the N-terminus. Interestingly, this mutation is about 130 bp upstream of the TSS of cg2849, a putative kinase related to diacylglycerol kinase, and may influence its transcription.

For Cg1874, DALI suggested structural similarity of our AlphaFold2 models to a variety of proteins lacking obvious mutual relationship. These hits are most likely spurious and related to a shared helical bundle topology. While the PDB does not seem to contain entries related to Cg1874, sequence-based analysis using InterPro [30] revealed the presence of a DUF3817 domain in its N-terminal half. This domain of unknown function contains two predicted transmembrane helices and is occasionally found as part of larger membrane proteins such as transporters of the major facilitator superfamily, prokaryotic members of which are involved in nutrient uptake. Given that Cg1874 is a standalone protein, we speculate that it may function as a subunit or modulator of an amino acid transporter in *Corynebacteria*. It has 48% identity to a DUF3817 domain-containing protein from *Arthrobacter gandavensis*, 38% to a membrane protein of *R. rhodochrous* and 36% identity to a membrane protein of *Mycobacterium gallinarium* (Additional file 1: Fig. S8). Despite the mutation from glycine to a charged residue (G93D) and even though the mean pLDDT (predicted local distance difference test) for the mutated variant was higher than for the WT (Additional file 1: Table S2), no prominent structural changes were observed (Additional file 1: Fig. S4C). In fact, the C^{α} r.m.s.d. between WT and mutated structures amounts to only 0.13 Å for this protein. A multiple sequence alignment (MSA) with the sequences of Cg1874 homologs showed a full conservation of G93 (Additional file 1: Fig. S8). In an additional alignment of 980 sequences performed by PredictProtein [31], 20 protein sequences had a D in the position corresponding to G93, which may explain why the G93D exchange did not cause notable disturbance in the predicted structure. We also note that the site of mutation is about 200 bp upstream of the TSS of cg1873, a putative acyl-CoA thioesterase II protein, the expression of which may be affected.

The mutations related to *argTUV* were all close to the TSS/TLS in front of *argT* [18] (Additional file 1: Fig. S10). *argT* is transcribed leaderless, which means that TSS and TLS are identical. The proteins encoded by *argTUV* show high similarity to ABC-type transport systems for polar amino acids. Here, ArgT is a homolog to the secreted component with 46% identity to the glutamine-binding periplasmic protein of *Gordonia paraffinivorans* and 46% identity to the substrate-binding protein of the polar amino acid transport system of *R. triatomae.* It was proposed that the three genes *argTUV* encode an uptake system for polar amino acids such as L-arginine, L-citrulline or L-ornithine, but experimental evidence is missing so far [32, 33].

For mutation $P_{argT}{}^{*1}$, the single nucleotide variant (SNV) 35 bp upstream of the TSS changed the sequence in such a way (ttaagg ➞ ttgagg, Additional file 1: Fig. S10) that the −35 region became more similar to the reported

−35 recognition sequence hexamer "ttgnca" which could lead to an increased transcription of *argTUV* [18]. In the strain with mutation $P_{argT}{}^{*2}$, 2829 bp were deleted upstream of the *argT* TSS. Besides deletion of cg1505 and cg1506 there was also a partial deletion of cg1507 and a partial deletion of the intergenic region between cg1504-cg1505 which led to an altered −35 region that does not really fit to the consensus motif ttgnca (Additional file 1: Fig. S10). Thus, we cannot expect a positive effect on promoter activity here. However, transcription of *argTUV* could be influenced by promoters that are further upstream that read through to *argTUV* due to the deleted region and potentially missing terminators. These promoters are, for example, of cg1507 (phage-type integrase), cg1513 (transposase), cg4005 (putative secreted protein) or of cg1514 (secreted protein). In the strain with mutation *argT**, there is a synonymous mutation of the third ArgT codon from GAG to GAA. Both codons are frequently used in *C. glutamicum* (43.8% and 56.2%, respectively) [34], so we cannot expect a major effect on ArgT translation due to altered codon usage here. As stated above, *argT* is a leaderless transcript and until now it is not fully understood how translation initiation and regulation works for these transcripts [35]. It is known, however, that downstream elements such as CA multimers can improve translation speed in *E. coli* [36], presumably through the provision of a lack of structure, since secondary mRNA structures immediately downstream of the AUG were shown to influence translation efficiency of leaderless mRNA [37]. This structural effect might also account to the *argTUV* mRNA with the G ➞ A mutation, resulting in an increased L-arginine importer level.

Reconstruction of mutations in the ΔARG LEU^{++} strain

To test which of the identified mutations are responsible for improved growth in the CoNoS setting, we first reconstructed the mutation of ΔARG LEU^{++} evo1 in ΔARG LEU^{++} yielding ΔARG LEU^{++} $P_{argT}{}^{*1}$. This strain was compared to the parental strain both in supplemented monoculture and in the CoNoS setting. In monoculture, the mutated strain appeared to start growing a bit earlier, but the growth rate was similar (Fig. 4A). In contrast, the growth rate of the CoNoS containing the strain ΔARG LEU^{++} $P_{argT}{}^{*1}$ was about 13% higher compared to the CoNoS containing the non-mutated parental strain (Fig. 4B). In summary, we did not see any positive effect of the mutation $P_{argT}{}^{*1}$ on growth in monoculture, but we confirmed that it had a positive effect in the CoNoS setting.

To test whether the synonymous mutation of the third *argT* codon has a similar effect, we reconstructed this mutation in ΔARG LEU^{++} yielding ΔARG LEU^{++} *argT**. In monoculture, this strain grew essentially like ΔARG LEU^{++} $P_{argT}{}^{*1}$ (Additional file 1: Fig. S11A), which grew

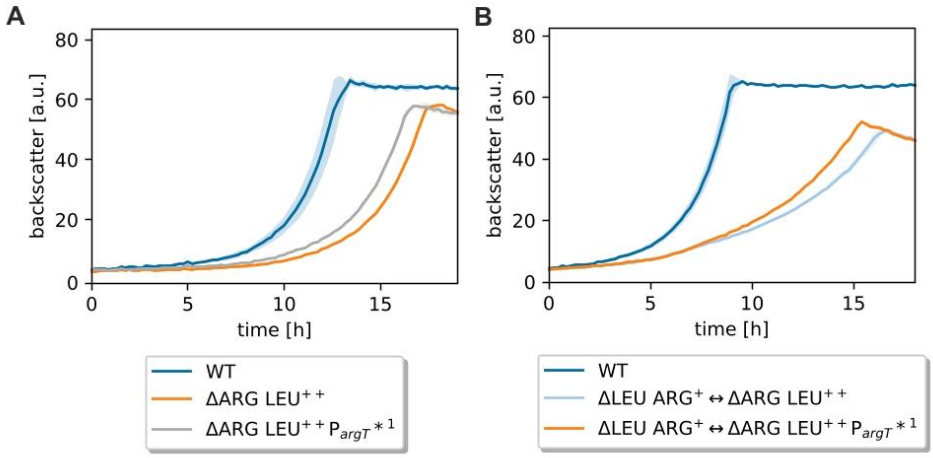

Fig. 4 Growth performance of ΔARG LEU^{++} strains with reengineered mutation $P_{argT}{}^{*1}$ in supplemented monocultures and in the CoNoS setting. **A** Monoculture of mutated strain in comparison to the WT and ΔARG LEU^{++} cultivated in CGXII medium with 2% (w/v) glucose and 3 mM L-arginine. **B** Comparison of WT monoculture, CoNoS consisting of non-evolved strains and CoNoS containing one mutated strain in CGXII medium with 2% (w/v) glucose. Mean values and standard deviations of biological triplicates are shown as lines and shaded areas, respectively

significantly better than the parental strain ΔARG LEU^{++} (Fig. 4A). A CoNoS containing ΔARG LEU^{++} *argT** grew slightly slower than the CoNoS containing ΔARG LEU^{++} $P_{argT}{}^{*1}$ (Additional file 1: Fig. S11B), but presumably better than the parental CoNoS ΔLEU ARG^{+} ⇔ ΔARG LEU^{++} (Fig. 4B). This matches the results from Fig. 1C that the CoNoS including strain ΔARG LEU^{++} evo3 did not grow as good as the CoNoS with the two other evolved strains. As the beneficial effect of the mutation $P_{argT}{}^{*1}$ appeared stronger compared to the effect of *argT**, we decided to only study the first one further.

To investigate the role of $Cg1874_{G93D}$ and $Cg2850_{G30R}$, these mutations were additionally introduced into ΔARG LEU $^{++}$ $P_{argT}{}^{*1}$. The newly constructed strains did not show growth differences compared to their parental strain both in monoculture and in the CoNoS setting (Additional file 1: Fig. S12). Thus, we assume that the two mutations $Cg1874_{G93D}$ and $Cg2850_{G30R}$ play a less important role than the *argT* related mutations for CoNoS growth.

Effects of the *argTUV* related mutations

The mutations $P_{argT}{}^{*1}$ and *argT** both improved the growth in the CoNoS setting. $P_{argT}{}^{*1}$ had a slightly stronger effect than *argT**, thus we decided to study this mutation further. $P_{argT}{}^{*1}$ changed the −35 sequence in such a way that the −35 region became more similar to the reported −35 recognition sequence. We wanted to know whether this mutation has an impact on transcription and analyzed the expression levels of *argT* and *argV* in ΔARG LEU^{++} and ΔARG LEU^{++} $P_{argT}{}^{*1}$ by RT-qPCR. The expression level of *argT* was increased by 8.83 ± 2.97 fold and expression of *argV* was increased by 6.61 ± 2.02 fold in ΔLEU ARG^{+} $P_{argT}{}^{*1}$ compared to the parental strain (Fig. 5A). As expected, the mutation in the −35 region led to an increased transcription of *argTUV*, which is presumably responsible for the improved growth of the strain in the CoNoS setting. To further prove this, we tested whether plasmid-based overexpression of *argTUV* has a similar effect. We compared growth of ΔARG LEU^{++} pPREx2-*argTUV* to ΔARG LEU^{++} pPREx2 in a CoNoS with ΔLEU ARG^{+} pPREx2 in CGXII medium with 2% (w/v) glucose. Even without isopropyl β-D-1-thiogalactopyranoside (IPTG) addition, the CoNoS including strain ARG LEU^{++} pPREx2-*argTUV* had an 18% increased growth rate compared to the control CoNoS containing just the empty plasmid (Fig. 5B). Induction of *argTUV* transcription with 50 or 250 µM IPTG did not have a further positive effect (data not shown).

In the strain with mutation $P_{argT}{}^{*2}$, a larger region upstream of *argT* is deleted including the two genes cg1505 (putative secreted protein) and cg1506 (putative membrane protein). To test whether the deletion of these two genes has an effect on growth, we constructed strain ΔARG LEU^{++} Δcg1505-cg1506. Deletion of those two genes did not affect the growth rate of a supplemented monoculture or of a CoNoS (Additional file 1: Fig. S11C, D).

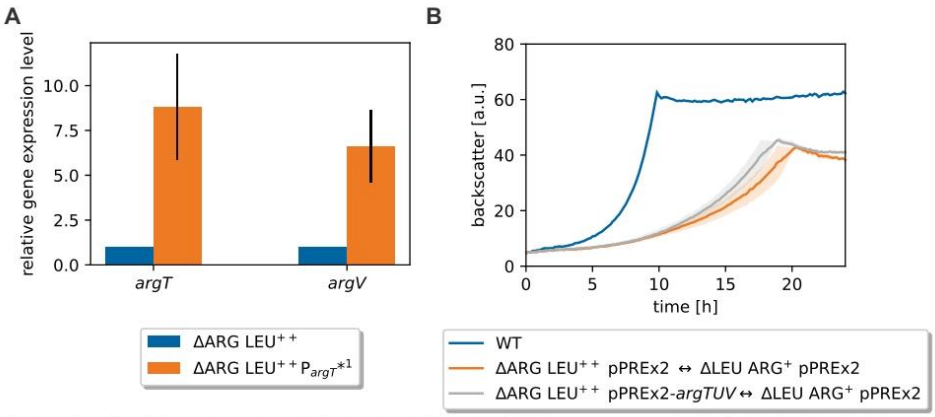

Fig. 5 Analysis of *argTUV* expression levels and their effects in a CoNoS setting. **A** Relative gene expression levels of *argT* and *argV* analyzed via RT-qPCR. **B** Growth performance of CoNoS with strains harboring either empty pPREx2 or pPREx2-*argTUV*. WT monoculture without amino acid supplementation is shown as reference. All strains were pre-cultivated in CGXII medium with 2% (w/v) glucose and 3 mM of the required amino acid. Mean values and standard deviations of three biological replicates are shown as lines and shaded areas, respectively

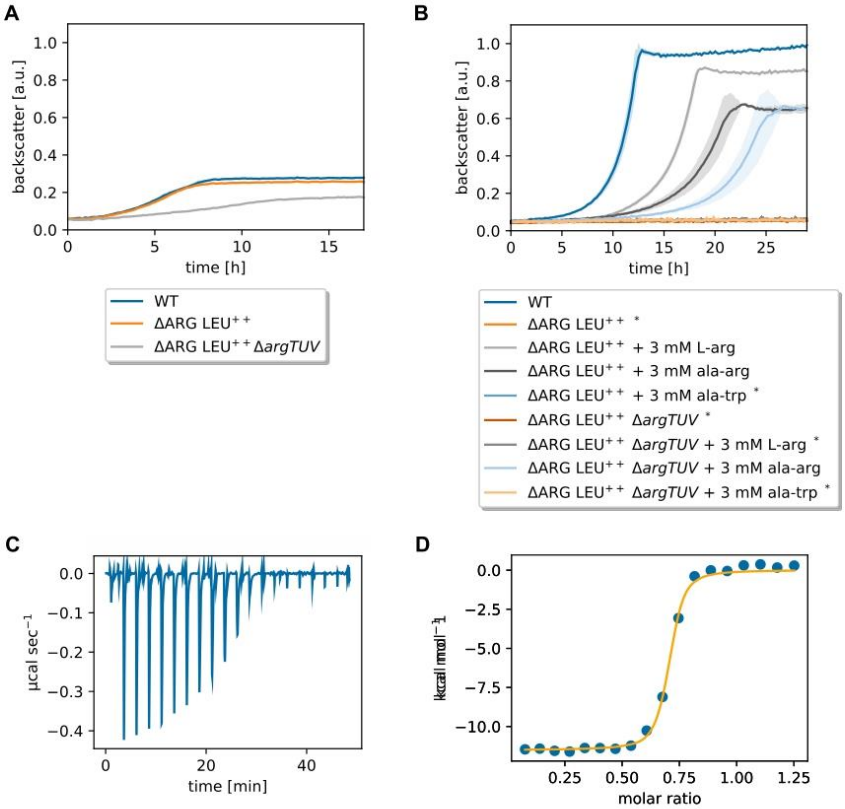

Fig. 6 Characterization of ArgTUV as L-arginine importer. **A** Comparison of ΔARG LEU^{++} Δ*argTUV* to the parental strain and the WT during growth in BHI medium. All strains were precultivated in BHI medium. **B** Comparison of ΔARG LEU^{++} Δ*argTUV* to the parental strain and the WT in CGXII with 2% (w/v) glucose supplemented with L-arginine or dipeptides as indicated. Strains marked with * did not grow. The WT monoculture without amino acid supplementation is shown as reference. ΔARG LEU^{++} Δ*argTUV* was pre-cultivated in BHI, all other strains were pre-cultivated in CGXII medium with 2% (w/v) glucose and 3 mM of the required amino acid. **A**, **B** Backscatter data were normalized by the maximum value recorded for the WT monoculture. Mean values and standard deviations of three biological replicates are shown as lines and shaded areas, respectively. **C** Raw data of an ITC experiment with 200 µM L-arginine and 30 µM His_{10}-ArgT in 40 mM HEPES–NaOH buffer, pH 7.4, with 100 mM NaCl. **D** Corresponding binding isotherm created by plotting the integrated heat peaks against the molar ratio

Subsequently, we tested whether a higher *argTUV* expression enables ΔARG LEU^{++} P_{argT}^{*1} to grow faster than ΔARG LEU^{++} at lower levels of L-arginine in the growth medium. The growth rates of both strains increased in proportion to the amount of L-arginine supplemented. However, no beneficial effect of the mutation was observed (Additional file 1: Fig. S6B).

Characterization of ArgTUV as L-arginine importer

To test whether ArgTUV indeed plays a role in L-arginine uptake, we deleted the respective operon in the L-arginine auxotrophic strain ΔARG LEU^{++}. In BHI medium, the resulting strain ΔARG LEU^{++} Δ*argTUV* grew slower and to a lower final backscatter compared to the parental strain and the WT (Fig. 6A). When the same strains were

cultivated in CGXII medium with 2% (w/v) glucose and 3 mM L-arginine, ΔARG LEU^{++} grew slightly slower and to a lower final backscatter compared to the wild type (Fig. 6B). Strain ΔARG LEU^{++} Δ*argTUV* did not grow (Fig. 6B), which suggested that ArgTUV is indeed an L-arginine importer and obviously the only one active in *C. glutamicum* under the tested conditions. This was further confirmed by the fact that ΔARG LEU^{++} Δ*argTUV* was able to grow when the medium was supplemented with an ala-arg dipeptide, but not with an ala-trp dipeptide (Fig. 6B).

Based on significant sequence homology to other substrate binding proteins such as ArtJ of *Geobacillus stearothermophilus* and hypothetical ancient precursors binding L-arginine as well as further amino acids [38, 39], ArgT was assumed to be the L-arginine binding component of the ABC-transporter ArgTUV. To characterize its ligand binding properties, an ArgT variant with cleavable His-tag and lacking the signal peptide (His_{10}-ArgT) was overproduced in *E. coli* BL21(DE3) pET-TEV-*argT* and purified by Ni–NTA affinity chromatography and size exclusion chromatography (SEC). The purified protein (Additional file 1: Fig. S13) eluted in two peaks from the SEC column (corresponding to monomer and trimer/tetramer) and was used for ligand interaction studies by isothermal titration calorimetry (ITC). Of the tested ligands, only L-arginine and L-citrulline, but not L-histidine, L-glutamate, L-glutamine, L-lysine or L-cysteine were bound by ArgT (Additional file 1: Table S3). Figure 6C shows a representative ITC experiment for His_{10}-ArgT binding L-arginine as a ligand. A representative ITC experiment with L-citrulline is shown in Additional file 1: Fig. S14. From four experiments of two independent His_{10}-ArgT purifications, a mean equilibrium dissociation constant (K_D) of 29.5 ± 4.8 nM was obtained for L-arginine. For L-citrulline, a ten times higher mean K_D of 432 nM (one measurement of one purification) was determined. For both ligands, exothermic binding was measured, for L-arginine with a mean enthalpy change of -12.2 ± 1.1 kcal/mol. These results confirmed that ArgTUV is a high affinity uptake system for L-arginine and may also transport L-citrulline.

Evolution-guided metabolic engineering of CoNoS ΔLEU ARG^{+} ↔ ΔARG LEU^{++}

In the previous sections, we described that single reconstructed strains improved the growth rate of a CoNoS containing either ΔLEU ARG^{+} MetC/P_{brnQ}* Mrp1C_{G29D} or the ΔARG LEU^{++} P_{argT}*^{1} by 6% and 13%, respectively (Figs. 2B, 4B). Hence, we wanted know whether the positive effects are additive and combined these two reconstructed strains in a new CoNoS. This culture reached a growth rate of 0.27 h^{-1}, corresponding to a 21% increase compared to the parental CoNoS (Fig. 7A). Furthermore, the final backscatter value increased by 7% (Fig. 7A). This confirmed that the mutations in both strains increased growth rate of the CoNoS in an additive manner (summarized in Additional file 1: Fig. S15). Finally, the CoNoS with the two reconstructed strains grew with a similar median

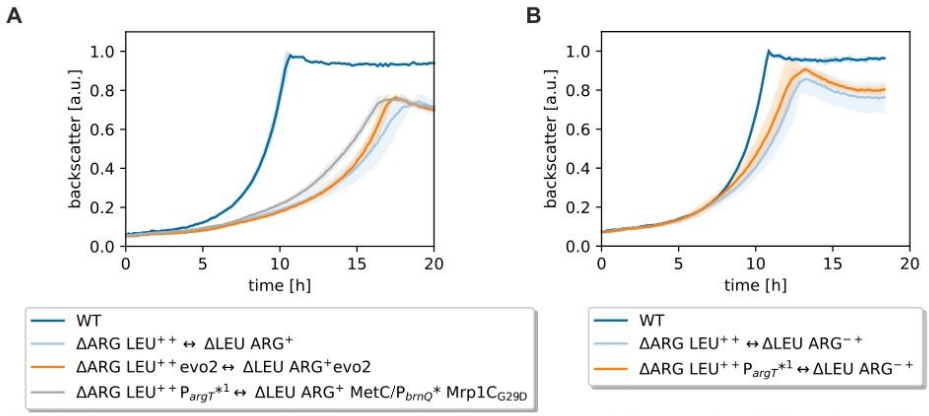

Fig. 7 Growth performance of reengineered CoNoS and effect of beneficial mutation on an a priori better growing CoNoS. **A** Reengineered CoNoS ΔARG LEU^{++} P_{argT}*^{1} with reengineered ΔLEU ARG^{+} MetC/P_{brnQ}* Mrp1C_{G29D} in comparison to the parental CoNoS, to the evolved CoNoS and to a WT monoculture. **B** Rationally optimized CoNoS with the additional P_{argT}*^{1} mutation in comparison to the parental CoNoS and WT monoculture. Mean values and standard deviations of biological triplicates in CGXII medium are shown as lines and shaded areas, respectively

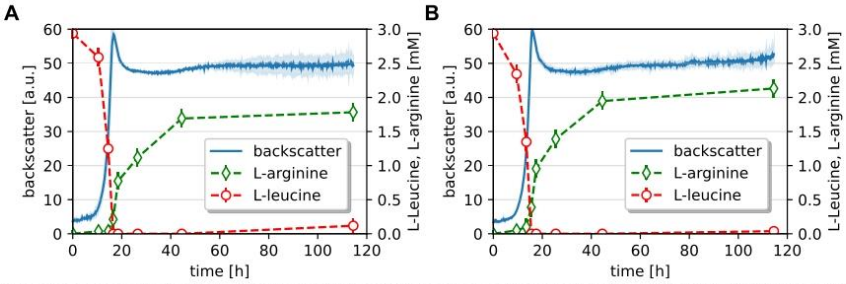

Fig. 8 Characterization of L-arginine production in monocultures of **A** ΔLEU ARG^{++} and **B** ΔLEU ARG^{++} Δ*argTUV* in CGXII with 2% (w/v) D-glucose and 3 mM L-leucine. After precultivation in CGXII defined medium with 111 mM D-glucose and 3 mM L-leucine, the cell suspension of one culture was used to inoculate eight wells of a BioLector Flowerplate. Upon sampling, a full well was harvested for each replicate at a certain time point. L-arginine and L-leucine were quantified in cell-free supernatants via HPLC and mean values are represented including the corresponding standard deviation. Mean values and standard deviations of biological triplicates are shown as lines and shaded areas, respectively

growth rate like the CoNoS consisting of two evolved strains (Fig. 7A), which suggested that we found all relevant major mutations.

For the ALE described in this paper, we chose a CoNoS with limited growth leaving much room for improvement. After confirming the beneficial effect of the single identified mutations on CoNoS growth, we wanted to know whether these mutations further improve a CoNoS so far only optimized by rational engineering. In our previous paper, we described the CoNoS C1*ΔLEU ARG^{++} ↔ WTΔARG LEU^{++} as the best CoNoS available to date [9]. In the meantime, we also tested a CoNoS with strains WTΔLEU ARG−+ (ΔLEU ARG^{-+}) ↔ WTΔARG LEU^{++} where ΔLEU ARG^{-+} only carries the mutations ArgB$_{A26V\ M31V}$ but not the deletion of *argR* (Please note the superscript "−+" to distinguish this strain from the one that only carries the Δ*argR* mutation). This CoNoS performed equally well as the best CoNoS described in [9] and was chosen to test the effect of an additional mutation that we discovered here during this ALE.

We introduced the mutation P_{argT}^{*1} into WTΔARG EU^{++} and co-cultivated this strain with WTΔLEU ARG^{-+}. Here, we indeed observed an increase in growth rate of 7% and an increase in final backscatter of 6% on comparison to the parental CoNoS (Fig. 7B). This demonstrated nicely that the ALE can reveal beneficial mutations for CoNoS growth that are not immediately obvious and that can help to further optimize rationally designed CoNoS.

Effects of *argTUV* deletion on L-arginine production in supplemented monoculture

In some cases, the deletion of specific amino acid importers is beneficial for the production of the transported amino acid. To test whether this is also the case for ArgTUV, the transporter was deleted in ΔLEU ARG^{++} that produces moderate amounts of L-arginine in monoculture. We compared ΔLEU ARG^{++} Δ*argTUV* to the parental strain regarding growth and L-arginine production in a monoculture. The growth of both strains was similar (Fig. 8). Determination of the L-arginine titer in the supernatants by HPLC revealed a significant increase in L-arginine by 24% after around 26 h, and by 20% after 115 h (Fig. 8). Notably, the titer difference was particularly clear in the early cultivation stage (14 h), where the L-arginine accumulation was more than 150% higher in ΔLEU ARG^{++} Δ*argTUV*. However, most of the L-arginine was produced in the late exponential and in the stationary phase.

In summary, we showed that the deletion of *argTUV* had a positive effect on external L-arginine accumulation under the tested conditions. This emphasizes the potential to identify beneficial mutations during ALE of a CoNoS which also have a positive effect on metabolite production with monocultures.

Discussion

Native microbial communities have usually evolved over thousands of years toward an extremely efficient use of the available resources, thereby heavily relying on cooperation and cross-feeding among the community members [1, 3, 5]. Recent advances in evolving synthetic co-cultures of strains of the same species [6, 40] or mixed species communities [41, 42] underlined the potential of increasing product cross-feeding, which could be of high biotechnological value. In this work, we successfully evolved a synthetic community composed of amino acid auxotrophic strains [9], identified the relevant mutations

and used these to increase L-arginine production also in monoculture.

Automated ALE using repetitive batch cultures, which has so far almost exclusively been demonstrated for monocultures [15, 43], proved to be easily applicable for CoNoS to select for faster-growing communities. During the ALE, both the ΔARG and the ΔLEU strains accumulated mutations beneficial for community growth, which was also observed for synthetic co-cultures consisting of L-leucine and L-lysine auxotrophic *E. coli* strains [44]. Several mutations we found increased growth in a co-culture setting, but did not result in better growth of a monoculture supplemented with the required amino acid. This is also in agreement with the *E. coli* approaches, where single evolved community members showed decreased growth in supplemented monocultures [44].

Let's have a closer look on the mutations we found in the evolved CoNoS. These were i) a mutation in the cystathionine β-lyase MetC, ii) mutations in or upstream of amino acid uptake systems, iii) mutations in the multisubunit Na^+/H^+ antiporter Mrp1, and iv) mutations in uncharacterized genes. Based on our MSA and AlphaFold2 data, we proposed the MetC S322F mutation to alter the dynamics of the C-terminal domain, thus modulating substrate binding and/or catalysis. In the context of the ΔLEU ARG^+ strain, the resulting changes to the steady-state levels of homocysteine, cystathionine, and methionine may indirectly influence either L-leucine utilization or L-arginine export. Conflicting results regarding the applicability of AlphaFold2 for predicting the impact of single point mutations in protein structures have been reported [45–48]. In the case of MetC and Cg2850, despite the high similarity of the structures predicted for the WT and the mutated version, small structural changes can be detected in the vicinity of the mutation site. This was not observed for Cg1874. Notably, even if an amino acid exchange does not significantly alter the mean structure, it may nevertheless affect other properties such as protein dynamics, stability, enzymatic activity, or protein–protein and protein–ligand interactions, the investigation of which is beyond the scope of this study.

In our CoNoS with auxotrophic strains, efficient amino acid export and uptake appears to be one of the key factors for community growth. In total, we found four different mutations that presumably increased the amount of available transporters in the cell (Table 1). In this context, we identified and characterized ArgTUV as an L-arginine and L-citrulline importer. Despite ArgT showing significant homology to other secreted substrate-binding proteins such as ArtJ of *G. stearothermophilus* and hypothetical ancient precursors binding also L-histidine, L-lysine, L-cysteine or L-glutamine [38, 39], ArgT bound exclusively to L-arginine and its molecular precursor L-citrulline. When synthetic communities of two *E. coli* strains auxotrophic for histidine or one other metabolite were evolved, several mutations appeared in promoter and regulatory regions that increased e.g. L-histidine and 2-oxoglutarate uptake [40]. Only very few mutations were found in the coding region of transporters, which might alter transporter activity or codon usage or translation by influencing mRNA structure [40]. In a further study, two *E. coli* strains auxotrophic for either L-tryptophan or L-tyrosine were evolved together and the resulting strains produced more of the amino acid required by the partner strain [6]. The evolved strains were not sequenced, thus it is unknown whether also other factors, such as amino acid import, was affected [6]. In another study with a co-culture consisting of two *E. coli* strains auxotrophic for either L-tryptophan or L-tyrosine, mutations were identified in a porin and in the global transcriptional regulator Lrp [49]. The evolution of a lactic acid bacterium, which is naturally auxotrophic for amino acids, together with a *Saccharomyces cerevisiae,* auxotrophic for riboflavin or folate, also revealed several mutations that regulate transcription or are associated with amino acid uptake [41]. Interestingly, most of the mutations influenced transcription or translation of the transporter protein, and only a few the activity of the protein itself, and mutations were almost exclusively associated with uptake systems but not with exporters.

The Mrp1 mutations resulted in severe impairments of the function of the multi-subunit Na^+/H^+ antiporter Mrp1, analogous to gene deletion or other mutations identified in Mrp1 subunits before [25, 50]. The fact that mutations of Mrp1 and the MetC/P_{brnQ}^* mutation evolved together twice in independent experiments suggested a functional link between these two proteins. In most organisms, the L-leucine-import via BrnQ depends on the proton motive force (reviewed in [51]), coupling L-leucine and Na^+-symport across an energy gradient [52]. Mrp1 is the main Na^+/H^+ antiporter in *C. glutamicum* and required to establish the gradient for Na^+-coupled uptake [20, 50]. A defect in Mrp1 presumably leads to a decreased Na^+ gradient and thus a reduced L-leucine import. Therefore, it is not obvious how the Mrp1 mutations are beneficial for the ΔLEU strain.

The fact that the mutations in the uncharacterized proteins Cg1874 and Cg2850 evolved several times independently from each other is a strong hint that they may be somehow beneficial for CoNoS growth. Their specific role is still unclear, as their reconstruction had no obvious effect in monoculture and in a CoNoS setting (Additional file 1: Fig. S12). However, the reconstructed strains were only tested in a CoNoS with the parental ΔLEU ARG^+ strain, so maybe the beneficial

effect is only apparent with a partner carrying mutations $MetC_{S322F}$/P_{brnQ}^{*} and/or mutations in Mrp1.

In summary, these results suggested that the metabolite uptake is often the major bottleneck under the very low metabolite concentrations in a CoNoS as observed before [9]. The identified mutations support the view that transport may be mostly limited by the availability of transporter proteins, because all mutations presumably led to an increased transporter availability. Metabolite production and export appears to be less critical in our setup because we did not find any mutation obviously related to these processes. Nevertheless, rationally increased amino acid production also increased the community growth, suggesting that sufficient amino acid production is still one major bottleneck, leaving room for improvement. For the rational design of synthetic communities, this means that one should concentrate both on metabolite production and on metabolite import to obtain optimal community growths.

At the end of this study, we would like to discuss what kind of mutations we expected to find by evolution of a CoNoS and how this differs from the ALE of monocultures. When selecting for faster growing strains or cultures, the selection pressure is highest on the bottleneck that is limiting growth most strongly. In our case, this was most likely amino acid import, because we found mutations in promoters leading to an increase in L-leucine and L-arginine import. Elevated uptake can not only result from promoter mutations that promote RNA polymerase binding upstream of the importer gene, but also be caused by mutations of regulators, mutations of the transporter start codon to a more favorable one, mutation of the RBS, mutation of the transporter itself increasing binding affinity or transport speed, mutations that lead to more favorable codons and several other mechanisms reviewed elsewhere [53, 54]. Thus, there are numerous potential targets which can mutate to increase import. If export is the limiting factor, the transporter and the corresponding regulatory mechanisms can mutate in a similar way. If transport is no longer limiting, we would also expect mutations in the amino acid biosynthesis pathways themselves. Here, again, regulatory processes can be affected, or the biosynthetic enzymes mutate to release e.g. feedback inhibition or increase reaction speed. Thus, to find mutations in the biosynthetic pathways using ALE, it is necessary to generate a CoNoS that is no longer limited in amino acid import and export.

Conclusions

Even after decades of research, the genome annotations of *C. glutamicum* and other biotechnologically relevant production organisms still contain many uncharacterized segments, harboring potential for not only increasing metabolic understanding but also for increasing metabolite production. The co-culture evolution-guided metabolic engineering approach presented in this study represents one additional tool for exploiting this potential through putting higher selective pressure on communities to grow faster comparable to monoculture approaches. This enabled the identification of amino acid transport systems not identifiable with other evolution approaches so far. Especially the deletion of the identified *argTUV* in existing high-yield L-arginine-producers [55] could therefore be worthwhile. Co-culture evolution-guided metabolic engineering could also easily be extended not only to other CoNoS published before [9] but also to a number of different metabolite cross-feeding pairings, enabling the identification of more transport systems. Additionally, further rounds of evolution with already import-optimized strains with lower levels of production could result in mutations occurring also in metabolic pathway enzymes, since also other co-culture pairings suggested that increasing production via community evolution is possible [6]. Employing the new best CoNoS for future work will enable further progress in improving small molecule production with highly efficient microbial communities [3].

Methods

Bacterial strains and growth conditions

The microbial strains used in this study are listed in Table 2. *C. glutamicum* strains are based either on the wild type *C. glutamicum* ATCC13032 or on its genome reduced variant C1* [56]. Microbial cultivations of *E. coli* and *C. glutamicum* were performed as described [9]. *C. glutamicum* was cultivated at 30 °C in brain heart infusion (BHI) medium (Difco Laboratories, Detroit, USA) or defined CGXII medium [57], notably with 0.03 g L^{-1} of protocatechuic acid (PCA). *E. coli* was cultivated at 37 °C in lysogeny broth (LB) [58] or on LB agar plates, with addition of 50 µg mL^{-1} kanamycin when plasmid bearing strains were used. For analyzing sodium sensitivity, NaCl was added to a concentration of 1 M to CGXII medium after autoclaving it separately [50]. CGXII agar plates were prepared similarly to liquid medium with additional 9 g L^{-1} agar. NaCl was added to a concentration of 0.6 M if appropriate [25].

CoNoS evolution

Adaptive laboratory evolution (ALE) was performed using the Mini Pilot Plant described in previous work [15, 16]. In brief, three wells of a 48-well Flowerplate were used to cultivate the CoNoS of interest in CGXII

Table 2 Bacterial strains used in this study

Strain (abbreviation)	Characteristics	Reference
E. coli		
DH5α	F$^-$Φ80*dlacZ*Δ(*lacZ*)M15 Δ(*lacZYA-argF*) U169 *endA1 recA1 hsdR17* (r_K^- m_K^+) *deoR thi-1 phoA supE44 λ*$^-$ *gyrA96 relA1*; strain used for cloning procedures	[61]
BL21(DE3)	F-*ompT hsdS*$_B$ (r_B-, m_B-) *gal dcm* (DE3); host for protein production	[69]
C. glutamicum		
ATCC13032 (WT)	Biotin-auxotrophic wild type	[70]
WT Mrp1C$_{G29D}$	ATCC13032 with mutation Mrp1C$_{G29D}$ (Cg0325)	This work
C1*	Derivative of ATCC13032 with a genome reduced by 13.4%	[56]
C1*ΔLEU ARG$^+$::P$_{tac}$-*eyfp* (ΔLEU ARG$^+$)	C1*ΔLEU ARG$^+$ with *eyfp* under control of P$_{tac}$ integrated into the IGR between cg1121 and cg1122	[9]
WTΔARG LEU^{++}::P$_{tac}$-*crimson* (ΔARG LEU^{++})	WTΔARG LEU^{++} with *crimson* under control of P$_{tac}$ integrated in the IGR between cg1121 and cg1122	[9]
C1*ΔLEU ARG^{++}	C1* ΔLEU ARG$^+$ with point mutations ArgB$_{A26V\ M31V}$ (Cg1582)	[9]
C1*ΔLEU ARG^{++}::P$_{tac}$-*eyfp* (ΔLEU ARG^{++})	C1*ΔLEU ARG^{++} with *eyfp* under control of P$_{tac}$ integrated into the IGR between cg1121 and cg1122	This work
ΔLEU ARG$^+$ evo1	Derivative of ΔLEU ARG$^+$ isolated after evolution. For details about identified mutations, see Table 1	This work
ΔLEU ARG$^+$ evo2	Derivative of ΔLEU ARG$^+$ isolated after evolution. For details about identified mutations, see Table 1	This work
ΔARG LEU^{++} evo1	Derivative of ΔARG LEU^{++} isolated after evolution. For details about identified mutations, see Table 1	This work
ΔARG LEU^{++} evo2	Derivative of ΔARG LEU^{++} isolated after evolution. For details about identified mutations, see Table 1	This work
ΔARG LEU^{++} evo3	Derivative of ΔARG LEU^{++} isolated after evolution. For details about identified mutations, see Table 1	This work
C1*ΔLEU ARG$^+$::P$_{tac}$-*eyfp* MetC/P$_{brnQ}$* (ΔLEU ARG$^+$ MetC/P$_{brnQ}$*)	C1*ΔLEU ARG$^+$::P$_{tac}$- *eyfp* with mutation MetC$_{S322F}$ (Cg2536), which is also within the promoter region of *brnQ* (cg2537)	This work
C1*ΔLEU ARG$^+$::P$_{tac}$-*eyfp* Mrp1C$_{G29D}$ (ΔLEU ARG$^+$ Mrp1C$_{G29D}$)	C1*ΔLEU ARG$^+$::P$_{tac}$- *eyfp* with mutation Mrp1C$_{G29D}$ (Cg0325)	This work
C1*ΔLEU ARG$^+$ Mrp1A$_{H335P}$ (ΔLEU ARG$^+$ Mrp1A$_{H335P}$)	C1*ΔLEU ARG$^+$::P$_{tac}$- *eyfp* with mutation Mrp1A$_{H335P}$ (Cg0326)	This work
C1*ΔLEU ARG$^+$::P$_{tac}$-*eyfp* MetC/P$_{brnQ}$* Mrp1C$_{G29D}$ (ΔLEU ARG$^+$ MetC/P$_{brnQ}$* Mrp1C$_{G29D}$)	C1*ΔLEU ARG$^+$::P$_{tac}$- *eyfp* MetC/P$_{brnQ}$* with mutation Mrp1C$_{G29D}$ (Cg0325)	This work
C1*ΔLEU ARG$^+$::P$_{tac}$-*eyfp* Δ*mrp1* (ΔLEU ARG$^+$ Δ*mrp1*)	C1*ΔLEU ARG$^+$::P$_{tac}$- *eyfp* with deletion of *mrp1* (cg0321-cg0326) and cg0317-cg0319. The latter encode genes for arsenate/arsenite resistance and were deleted accidentally	This work
WTΔARG LEU^{++}::P$_{tac}$-*crimson* P$_{argT}$*^{1} (ΔARG LEU^{++} P$_{argT}$*^{1})	WTΔARG LEU^{++}::P$_{tac}$-*crimson* with mutation A ➞ G 35 bp upstream of the *argT* (cg1504) TSS/TLS	This work
WTΔARG LEU^{++}::P$_{tac}$-*crimson argT** (ΔARG LEU^{++} *argT**)	WTΔARG LEU^{++}::P$_{tac}$-*crimson* with mutation of the 3rd codon of *argT* (cg1504) GAG ➞ GAA, synonymous mutation	This work
WTΔARG LEU^{++}::P$_{tac}$-*crimson* P$_{argT}$*^{1} Cg1874$_{G93D}$ (ΔARG LEU^{++} P$_{argT}$*^{1} Cg1874$_{G93D}$)	WTΔARG LEU^{++}::P$_{tac}$-*crimson* P$_{argT}$*^{1} with mutation Cg1874$_{G93D}$	This work
WTΔARG LEU^{++}::P$_{tac}$-*crimson* P$_{argT}$*^{1} Cg1874$_{G93D}$ Cg2850$_{G30R}$ (ΔARG LEU^{++} P$_{argT}$*^{1} Cg1874$_{G93D}$ Cg2850$_{G30R}$)	WTΔARG LEU^{++}::P$_{tac}$-*crimson* P$_{argT}$*^{1} Cg1874$_{G93D}$ with mutation Cg2850$_{G30R}$	This work
WTΔARG LEU^{++}::P$_{tac}$-*crimson* Δ*argTUV* (ΔARG LEU^{++} Δ*argTUV*)	WTΔARG LEU^{++}::P$_{tac}$-crimson with in frame deletion of *argTUV* (cg1504-1502)	This work
WTΔARG LEU^{++}::P$_{tac}$-*crimson* Δcg1505-1506 (ΔARG LEU^{++} Δcg1505-cg1506)	WTΔARG LEU^{++}::P$_{tac}$-crimson with deletion of cg1505 and cg1506 including their promoters	This work
WTΔLEU ARG^{-+}::P$_{tac}$-*eYFP* (ΔLEU ARG^{-+})	WT with an in-frame deletion of Δ*leuA* (cg0303), Δ*leuC* (cg1487), Δ*leuD* (cg1488), Δ*leuB* (cg1453), with point mutations ArgB$_{A26V\ M31V}$ (Cg1582) and *eyfp* under control of P$_{tac}$ integrated into the IGR between cg1121 and cg1122	This work

medium in the BioLector. Cell growth was monitored with online backscatter measurement until a backscatter threshold triggered automated cell suspension aliquot transfer to an empty well that was immediately filled with chill-stored CGXII medium for the next batch. In this way, 16 repetitive batches were performed in biological triplicates. Process modelling was performed to estimate specific growth rates for each single batch of the ALE experiment. The model was setup in OpenModelica [59] and validated using the in-house python-based package Estim8 (unpublished). From material of the last batches, single strains were isolated and retested with a non-evolved partner in a CGXII culture in the BioLector.

Microscale cultivation

The fitness of single strains and co-cultures was investigated using a micro bioreactor with online backscatter measurement. All strains were cultivated as described [9]. In brief, each strain was spread from a cryo stock onto BHI plates. Single colonies were used to inoculate a preculture in amino acid-supplemented CGXII medium with 2% (w/v) glucose and cultivated for two days at 30 °C and 250 rpm. Afterwards, the precultures were centrifuged, the pellet was suspended in sterile 0.9% (w/v) NaCl and used to inoculate the main cultures. The main cultures were cultivated in CGXII or CGXII supplemented with amino acids in 48-well Flowerplates (m2p-labs GmbH, Germany) in a BioLector system (m2p-labs GmbH, Germany) at 1400 rpm, 85% humidity and 30 °C. Co-cultures were inoculated in a 1:1 ratio of the two strains. Growth rate evaluation was performed using the Python package Bletl [60] as described [9]. For characterizing the substrate uptake and amino acid production, automated harvesting and processing of cultures was performed using the Mini Pilot Plant and resulting cell-free supernatants were analyzed via HPLC.

Amino acid quantification by HPLC

Amino acids were separated and quantified on an uHPLC system (Agilent 1290 Infinity, Agilent Technologies, Santa Clara, CA). 50 mM α-Aminobutyric acid (AABA) was added as internal standard to the properly diluted cell-free supernatants. A precolumn (Phenomenex, SecurityGuard™ ULTRA C18, sub-2 µm, 2.1 mm internal diameters) and a reverse phase column (Kinetex 2.6 µm EVO C18 100 Å, 100 × 2.1 mm) were used as stationary phase. In the mobile phase, buffer A (10 mM Na_2HPO_4 (anhydr.), 10 mM $Na_2B_4O_7 \times 10\ H_2O$, pH 8.2 with HCl) and buffer B (methanol) with a flow rate of 0.42 mL min^{-1} were used with a column temperature of 40 °C and an injection volume of 1 µL. Precolumn derivatization with ophthaldialdehyde (OPA) reagent (Sigma-Aldrich, ready-to-use mix) was performed in an automated procedure. 2 µL OPA, 1 µL sample and 2 µL water were mixed in the injection loop six times and incubated for 1 min. Amino acids were separated with the following elution conditions (min/B%): 0.0 min/2%; 0.5 min/2% to 20.0 min/57%; 20.1 min/100%; 23.6 min/2%; 25.0 min END. Amino acids were detected using a fluorescence detector (Agilent 1290 FLD) with an excitation wavelength of 340 nm and an emission wavelength of 450 nm. Target amino acids were quantified relatively to amino acid standards of known concentrations measured before and after each run and to the internal standard.

Recombinant DNA work

In this work, *Escherichia coli* DH5α [61] was used as host for molecular cloning. All plasmids used in this study are listed in Additional file 1: Table S4 and all oligonucleotides in Additional file 1: Table S5. Deletions and mutations in *C. glutamicum* were introduced via the pK19*mobsacB*-system as described previously [57, 62].

DNA isolation and sequencing

For DNA isolation, single strains were grown in a CGXII monoculture supplemented with 3 mM of the respective amino acid in the BioLector. From one well per mutant, gDNA was isolated with the DNeasy Blood & Tissue Kit (Qiagen, Hilden, Germany). Resulting gDNA concentration was determined via Qubit 2.0 fluorometer (Thermo Fisher Scientific, Waltham, USA). From the prepared gDNA, 1 µg was used for library preparation employing the NEBNext® Ultra™ II DNA Library Prep Kit (NEB, Frankfurt am Main, Germany). Via qPCR with the KAPA library quantification kit (Peqlab, Erlangen, Germany), the library was evaluated and then normalized via pooling. After in-house sequencing (paired-end sequencing via a MiSeq (Illumina®), read length of 2 × 150 bases), the demultiplexed fastq output files were processed with the CLC Genomic Workbench software (Qiagen, Hilden, Germany). For reads mapping and variants calling, the *C. glutamicum* ATCC 13032 reference genome BX927147 or the genome sequence of *C. glutamicum* C1 (CP017995) were used. Mutations and deletions were assessed manually regarding their specific occurrence between the different samples and their relevance. The data for this study have been deposited in the European Nucleotide Archive (ENA) at EMBL-EBI under accession number PRJEB60176 (https://www.ebi.ac.uk/ena/browser/view/PRJEB60176).

Analysis of gene expression levels

Precultures of 5 mL BHI media in a test tube were inoculated with a single colony from a BHI plate and incubated for seven hours at 30 °C and 170 rpm. The cells

were centrifuged for 5 min at 1700*g* and washed once in PBS (phosphate buffered saline, 137 mM NaCl, 2.7 mM KCl, 10 mM Na_2HPO_4, 1.8 mM KH_2PO_4, pH 7.4 with HCl). Subsequently, the cells were suspended in CGXII medium with 2% (w/v) D-glucose and 3 mM of the appropriate amino acid supplementation and incubated in test tubes at 30 °C and 170 rpm overnight. For the main cultures, 50 ml CGXII media with 2% (w/v) D-glucose and 3 mM of the appropriate amino acid supplementation were inoculated to an OD_{600} of 0.5 in a 500 mL baffled flask and incubated at 30 °C and 130 rpm in a Minitron shaker (Infors HT, Einsbach, Germany) until an OD_{600} of 5 was reached. 25 ml cell suspension was mixed with 25 g ice and centrifuged for 10 min at 3720*g* and 4 °C. The supernatant was removed and the cell pellets were frozen in liquid nitrogen and stored at − 80 °C or used immediately.

For RNA isolation, the RNeasy MiniKit (QIAGEN, Hilden, Germany) was used. The pellets were suspended in 700 µL RLT buffer and transferred into two Precellys® tubes with 250 mg glass beads. The tubes were set into a Precellys®24 tissue homogenizer (Bertin GmbH, Frankfurt, Germany) and the cells were disrupted with two cycles at 6000 rpm, with 20 s per cycle and stored on ice in between runs. The tubes were centrifuged at 21,300 *g* at room temperature for 2 min. The supernatant was transferred to a fresh tube and mixed with 250 µL ethanol (-20 °C). The mixture was added to an RNeasy MiniKit Spin column and centrifuged for 15 s at 12,633*g* and room temperature. Afterwards, the protocol provided by the manufacturer was followed including DNAase on column digest. The purified RNA was diluted 1:10 with ddH2O and the RNA concentration was measured at 260 nm with a Colibri Microvolume Spectrometer (Titertek-Berthold, Germany).

All reverse transcriptase quantitative PCRs (RT-qPCRs) were prepared with the New England Biolabs® Inc. Luna® Universal Probe One-Step RT-qPCR Kit. SYBR®Green was used as probe. For each reaction, the reaction mix with a volume of 20 µL was prepared according to the instructions from the manufacturer. The PCR plate was covered with a foil to prevent evaporation. The plate was centrifuged for 1 min at 665*g* at room temperature. The PCR plate was placed in the PCR cycler qTOWER 2.2 (Analytic Jena, Germany) and incubated with the following program: 55 °C for 10 min, 95 °C for 1 min, 40 times (95 °C for 10 s, 60 °C for 30 s) followed by a melt curve 60–95 °C with 6 s for $\Delta T = 1$ °C. For each qPCR, a standard dilution was prepared for each RNA used in the qPCR. Duplicate 20 µl reactions were prepared containing 500 ng, 50 ng, 5 ng, 0.5 ng or 0.05 ng RNA of the native ΔLEU ARG^+ or ΔARG LEU^{++} strains in nuclease-free water. For all other samples, 300 ng of template RNA were used. As reference gene, meso-diaminopimelate dehydrogenase (*ddh*, cg2900) was used with the oligonucleotides listed in Additional file 1: Table S5, resulting in a 150 bp product. Samples with *ddh* primers were prepared for each RNA used. Primers were designed with Primer3Plus [63]. For all samples, two biological replicates with six technical replicates each were measured. For data analysis, the qPCR software qPCR 3.1 (Analytik Jena, Germany) and the Livak method [64] were used to determine the $2^{\Delta\Delta Ct}$ value.

Prediction of the impact of mutations on protein structures

The MSA-based ab initio prediction of monomeric structures for *C. glutamicum* MetC, Cg1874, and Cg2850 WT proteins as well as of their mutated variants ($MetC_{S322F}$, $Cg1874_{G93D}$, $Cg2850_{G30R}$) was performed using AlphaFold2 via the ColabFold pipeline [65, 66] applying mostly default parameters (use_amber: no, template mode: none, msa_mode: MMSeq2 (UniRef + Environmental), num_recycle: 3). The resulting predicted structures with the highest model confidence (based on pLDDT and predicted aligned error (PAE) confidence measures) for each protein were analyzed for structural changes using ChimeraX [67].

Protein production and purification

His-tagged ArgT was overproduced using *E. coli* BL21(DE3) pET-TEV-*argT*. The strain was cultivated at 37 °C in terrific broth (TB) [68]. After induction of target gene expression with 500 µM IPTG, the cells were cultivated for 18 h at 18 °C. Cells were harvested by centrifugation for 20 min at 5500*g* and suspended in lysis buffer (20 mM Tris–HCl pH 7.9, 500 mM NaCl, 5% (v/v) glycerol, 20 mM imidazole,) containing cOmplete EDTA-free protease inhibitor (Roche, Basel, Switzerland), and disrupted by Multi Shot high-pressure homogenizer (Constant systems Ltd., Daventry, United Kingdom) treatment at 20,000 psi. Soluble protein fractions were obtained by centrifugation (5000*g*, 4 °C, 20 min) and subsequent ultracentrifugation of the supernatant (100,000*g*, 4 °C, 1 h). Supernatants of the ultracentrifugation were loaded onto a HisTrap HP column (GE Healthcare, Chicago, IL, USA) and, after washing, the His-tagged protein was eluted using lysis buffer with increasing imidazole concentrations up to 300 mM. The protein was further purified by size exclusion chromatography on a Superdex 200 10/300 GL column (GE Healthcare, Chicago, IL, USA) equilibrated in HEPES buffer (40 mM HEPES-NaOH, 100 mM NaCl, pH 7.4). Protein concentrations were determined using a Colibri microvolume spectrometer (Berthold Detection Systems GmbH, Pforzheim, Germany) and the molar extinction coefficient was predicted

by the ProtParam tool (http://web.expasy.org/protparam/).

Isothermal titration calorimetry

Purified His_{10}-ArgT was dialyzed overnight in HEPES buffer (40 mM HEPES–NaOH, pH 7.4, 100 mM NaCl). 20 mM stock solutions of the potential ligands were prepared in dialysis buffer, and the pH was adjusted to pH 7.4 using NaOH or HCl. ITC measurements were performed with a MicroCal PEAQ-ITC instrument (Malvern Panalytical, Malvern, United Kingdom) operated at 25 °C. Protein concentrations of 30 µM and ligand concentrations of 50 µM to 2 mM were used. Prior to filling the measuring cell with 300 µL protein solution, the cell was rinsed with dialysis buffer, and the syringe was filled with 75 µL ligand solution. An ITC run was started with an initial injection of 0.4 µL followed by 18 injections of 2 µL each. In addition, control experiments with ligand solution titrated into the dialysis buffer were performed. The data were analyzed using MicroCal ITC analysis software (Malvern Panalytical, Malvern, United Kingdom).

Supplementary Information

The online version contains supplementary material available at https://doi.org/10.1186/s12934-023-02078-2.

Additional file 1. Tables S1–S5, Figures S1–S15.

Acknowledgements

We thank Niklas Tenhaef and Michael Osthege for programming support on the Mini Pilot Plant. We thank Eric von Lieres and Martin Beyß for providing computational infrastructure and technical support throughout the project. We thank Aileen Krüger for support with qRT-PCRs and Dieter Willbold for funding acquisition.

Author contributions

SN and MBa designed the study. RZ, SS, FN, PM, DB, NH, SG, LS, CM and AW performed the research. RZ, SS, FN, SG, LS, OHW, TP, MBa and SN analysed the data. RZ, SS and AW contributed new methods or models. RZ, SS, MBo, SN, SG, LS, OHW, TP and MBa drafted the manuscript. SS, RZ, SN and MBa revised and prepared the final version of the manuscript. All authors read and approved the final manuscript.

Funding

Open Access funding enabled and organized by Projekt DEAL. We gratefully acknowledge support and funding from the Deutsche Forschungsgemeinschaft (priority program SPP2170, project no. 427904493 and 428038451) and by the Heinrich Heine University Düsseldorf within the framework of the Bio24 graduate school.

Availability of data and materials

The genome sequencing data generated during this study has been deposited in the European Nucleotide Archive (ENA) at EMBL-EBI under accession number PRJEB60176 (https://www.ebi.ac.uk/ena/browser/view/PRJEB60176). All other data generated or analysed during this study are included in this published article and its supplementary information files. Strains and plasmids generated during this study are available from the corresponding author upon request.

Declarations

Ethics approval and consent to participate

Not applicable.

Consent for publication

Not applicable.

Competing interests

The authors declare that they have no competing interests.

Author details

[1]Institute of Bio- and Geosciences, IBG-1: Biotechnology, Forschungszentrum Jülich, Jülich, Germany. [2]Institute of Biological Information Processing, IBI-7: Structural Biochemistry, Forschungszentrum Jülich, Jülich, Germany. [3]Institut für Physikalische Biologie, Heinrich-Heine-Universität Düsseldorf, Düsseldorf, Germany.

Received: 12 March 2023 Accepted: 2 April 2023
Published online: 15 April 2023

References

1. Yang DD, Alexander A, Kinnersley M, Cook E, Caudy A, Rosebrock A, et al. Fitness and productivity increase with ecotypic diversity among *Escherichia coli* strains that coevolved in a simple, constant environment. Appl Environ Microbiol. 2020;86(8):e00051–20
2. D'Souza G, Waschina S, Pande S, Bohl K, Kaleta C, Kost C. Less is more: selective advantages can explain the prevalent loss of biosynthetic genes in bacteria. Evolution. 2014;68(9):2559–70.
3. Noack S, Baumgart M. Communities of Niche-Optimized Strains: small-genome organism consortia in bioproduction. Trends Biotechnol. 2019;37(2):126–39.
4. Bernstein HC, Paulson SD, Carlson RP. Synthetic *Escherichia coli* consortia engineered for syntrophy demonstrate enhanced biomass productivity. J Biotechnol. 2012;157(1):159–66.
5. Pande S, Merker H, Bohl K, Reichelt M, Schuster S, de Figueiredo LF, et al. Fitness and stability of obligate cross-feeding interactions that emerge upon gene loss in bacteria. ISME J. 2014;8(5):953–62.
6. Preussger D, Giri S, Muhsal LK, Ona L, Kost C. Reciprocal fitness feedbacks promote the evolution of mutualistic cooperation. Curr Biol. 2020;30(18):3580-90.e7.
7. Eggeling L, Bott M, editors. Handbook of *Corynebacterium glutamicum*. Boca Raton: CRC Press Taylor & Francis Group; 2005.
8. Becker J, Rohles CM, Wittmann C. Metabolically engineered *Corynebacterium glutamicum* for bio-based production of chemicals, fuels, materials, and healthcare products. Metab Eng. 2018;50:122–41.
9. Schito S, Zuchowski R, Bergen D, Strohmeier D, Wollenhaupt B, Menke P, et al. Communities of Niche-optimized Strains (CoNoS)—design and creation of stable, genome-reduced co-cultures. Metab Eng. 2022;73:91–103.
10. Zhang X, Gao Y, Chen Z, Xu G, Zhang X, Li H, et al. High-yield production of L-serine through a novel identified exporter combined with synthetic pathway in *Corynebacterium glutamicum*. Microb Cell Fact. 2020;19(1):115.
11. Mavrommati M, Daskalaki A, Papanikolaou S, Aggelis G. Adaptive laboratory evolution principles and applications in industrial biotechnology. Biotechnol Adv. 2022;54: 107795.
12. Wu Y, Jameel A, Xing XH, Zhang C. Advanced strategies and tools to facilitate and streamline microbial adaptive laboratory evolution. Trends Biotechnol. 2022;40(1):38–59.
13. Stella RG, Gertzen CGW, Smits SHJ, Gatgens C, Polen T, Noack S, et al. Biosensor-based growth-coupling and spatial separation as an evolution strategy to improve small molecule production of *Corynebacterium glutamicum*. Metab Eng. 2021;68:162–73.
14. Bromig L, Weuster-Botz D. Accelerated adaptive laboratory evolution by automated repeated batch processes in parallelized bioreactors. Microorganisms. 2023;11(2):275.

15. Radek A, Tenhaef N, Müller MF, Brüsseler C, Wiechert W, Marienhagen J, et al. Miniaturized and automated adaptive laboratory evolution: Evolving *Corynebacterium glutamicum* towards an improved D-xylose utilization. Bioresour Technol. 2017;245(Pt B):1377–85.
16. Unthan S, Radek A, Wiechert W, Oldiges M, Noack S. Bioprocess automation on a Mini Pilot Plant enables fast quantitative microbial phenotyping. Microb Cell Fact. 2015;14:32.
17. Rückert C, Pühler A, Kalinowski J. Genome-wide analysis of the l-methionine biosynthetic pathway in *Corynebacterium glutamicum* by targeted gene deletion and homologous complementation. J Biotechnol. 2003;104(1–3):213–28.
18. Pfeifer-Sancar K, Mentz A, Rückert C, Kalinowski J. Comprehensive analysis of the *Corynebacterium glutamicum* transcriptome using an improved RNAseq technique. BMC Genomics. 2013;14:888.
19. Tauch A, Hermann T, Burkovski A, Krämer R, Pühler A, Kalinowski J. Isoleucine uptake in *Corynebacterium glutamicum* ATCC 13032 is directed by the *brnQ* gene product. Arch Microbiol. 1998;169:303–12.
20. Ebbighausen H, Weil B, Krämer R. Transport of branched-chain amino acids in *Corynebacterium glutamicum*. Arch Microbiol. 1989;151:238–44.
21. Ittisoponpisan S, Islam SA, Khanna T, Alhuzimi E, David A, Sternberg MJE. Can predicted protein 3D structures provide reliable insights into whether missense variants are disease associated? J Mol Biol. 2019;431(11):2197–212.
22. Holm L. Dali server: structural unification of protein families. Nucleic Acids Res. 2022;50(W1):W210–5.
23. Dwivedi CM, Ragin RC, Uren JR. Cloning, purification, and characterization of β-cystathionase from *Escherichia coli*. Biochemistry. 1982;21(13):3064–9.
24. Clausen T, Huber R, Laber B, Pohlenz HD, Messerschmidt A. Crystal structure of the pyridoxal-5′-phosphate dependent cystathionine β-lyase from *Escherichia coli* at 1.83 Å. J Mol Biol. 1996;262(2):202–24.
25. Xu N, Zheng Y, Wang X, Krulwich TA, Ma Y, Liu J. The lysine 299 residue endows the multisubunit Mrp1 antiporter with dominant roles in Na^+ resistance and pH homeostasis in *Corynebacterium glutamicum*. Appl Environ Microbiol. 2018;84(10):e00110–18
26. Taniguchi H, Wendisch VF. Exploring the role of sigma factor gene expression on production by *Corynebacterium glutamicum*: sigma factor H and FMN as example. Front Microbiol. 2015;6:740.
27. Busche T, Silar R, Picmanova M, Patek M, Kalinowski J. Transcriptional regulation of the operon encoding stress-responsive ECF sigma factor SigH and its anti-sigma factor RshA, and control of its regulatory network in *Corynebacterium glutamicum*. BMC Genomics. 2012;13:445.
28. Boles E, Ebbighausen H, Eikmanns B, Krämer R. Unusual regulation of the uptake system for branched-chain amino-acids in *Corynebacterium glutamicum*. Arch Microbiol. 1993;159(2):147–52.
29. Shepard W, Haouz A, Grana M, Buschiazzo A, Betton JM, Cole ST, et al. The crystal structure of Rv0813c from *Mycobacterium tuberculosis* reveals a new family of fatty acid-binding protein-like proteins in bacteria. J Bacteriol. 2007;189(5):1899–904.
30. Paysan-Lafosse T, Blum M, Chuguransky S, Grego T, Pinto BL, Salazar GA, et al. InterPro in 2022. Nucleic Acids Res. 2023;51(D1):D418–27.
31. Bernhofer M, Dallago C, Karl T, Satagopam V, Heinzinger M, Littmann M, et al. PredictProtein - Predicting protein structure and function for 29 years. Nucleic Acids Res. 2021;49(W1):W535–40.
32. Marin K, Krämer R. Amino acid transport systems in biotechnologically relevant bacteria. Amino acid biosynthesis—pathways regulation and metabolic engineering. Microbiol Monogr. 2007;5:289–325.
33. Mitsuhashi SI. *Method for producing amino acid.* PCT/JP2013/061060 (Patent) 2013.
34. Overbeek R, Larsen N, Walunas T, D'Souza M, Pusch G, Selkov E Jr, et al. The ERGO genome analysis and discovery system. Nucleic Acids Res. 2003;31(1):164–71.
35. Leiva LE, Katz A. Regulation of leaderless mRNA translation in bacteria. Microorganisms. 2022;10(4):723.
36. Martin-Farmer J, Janssen GR. A downstream CA repeat sequence increases translation from leadered and unleadered mRNA in *Escherichia coli*. Mol Microbiol. 1999;31(4):1025–38.
37. Moll I, Grill S, Gualerzi CO, Blasi U. Leaderless mRNAs in bacteria: surprises in ribosomal recruitment and translational control. Mol Microbiol. 2002;43(1):239–46.
38. Clifton BE, Jackson CJ. Ancestral protein reconstruction yields insights into adaptive evolution of binding specificity in solute-binding proteins. Cell Chem Biol. 2016;23(2):236–45.
39. Vahedi-Faridi A, Eckey V, Scheffel F, Alings C, Landmesser H, Schneider E, et al. Crystal structures and mutational analysis of the arginine-, lysine-, histidine-binding protein ArtJ from Geobacillus stearothermophilus. Implications for interactions of ArtJ with its cognate ATP-binding cassette transporter, Art(MP)2. J Mol Biol. 2008;375(2):448–59.
40. Lloyd CJ, King ZA, Sandberg TE, Hefner Y, Olson CA, Phaneuf PV, et al. The genetic basis for adaptation of model-designed syntrophic co-cultures. PLoS Comput Biol. 2019;15(3):e1006213.
41. Konstantinidis D, Pereira F, Geissen EM, Grkovska K, Kafkia E, Jouhten P, et al. Adaptive laboratory evolution of microbial co-cultures for improved metabolite secretion. Mol Syst Biol. 2021;17(8):e10189.
42. Jia N, Ding MZ, Zou Y, Gao F, Yuan YJ. Comparative genomics and metabolomics analyses of the adaptation mechanism in *Ketogulonicigenium vulgare-Bacillus thuringiensis* consortium. Sci Rep. 2017;7:46759.
43. Tenhaef N, Brüsseler C, Radek A, Hilmes R, Unrean P, Marienhagen J, et al. Production of D-xylonic acid using a non-recombinant *Corynebacterium glutamicum* strain. Bioresour Technol. 2018;268:332–9.
44. Zhang X, Reed JL. Adaptive evolution of synthetic cooperating communities improves growth performance. PLoS ONE. 2014;9(10):e108297.
45. Akdel M, Pires DEV, Pardo EP, Janes J, Zalevsky AO, Meszaros B, et al. A structural biology community assessment of AlphaFold2 applications. Nat Struct Mol Biol. 2022;29(11):1056–67.
46. Buel GR, Walters KJ. Can AlphaFold2 predict the impact of missense mutations on structure? Nat Struct Mol Biol. 2022;29(1):1–2.
47. McBride JM, Polev K, Reinharz V, Grzybowski BA, Tlusty T. AlphaFold2 can predict single-mutation effects on structure and phenotype. 2023. BioRxiv.Preprint. https://doi.org/10.1101/2022.04.14.488301.
48. Pak MA, Markhieva KA, Novikova MS, Petrov DS, Vorobyev IS, Maksimova ES, et al. Using AlphaFold to predict the impact of single mutations on protein stability and function. 2021. BioRxiv.Preprint. https://doi.org/10.1101/2021.09.19.460937.
49. Shendure J, Porreca GJ, Reppas NB, Lin X, McCutcheon JP, Rosenbaum AM, et al. Accurate multiplex polony sequencing of an evolved bacterial genome. Science. 2005;309(5741):1728–32.
50. Bartsch AM. Identification and functional characterization of cation/proton antiport systems in *Corynebacterium glutamicum*. Cologne: University of Cologne; 2015.
51. Kaiser JC, Heinrichs DE. Branching out: Alterations in bacterial physiology and virulence due to branched-chain amino acid deprivation. MBio. 2018;9(5):e01188–18
52. Wood JM. Leucine transport in *Escherichia coli*. The resolution of multiple transport systems and their coupling to metabolic energy. J Biol Chem. 1975;250(12):4477–85.
53. Browning DF, Busby SJ. Local and global regulation of transcription initiation in bacteria. Nat Rev Microbiol. 2016;14(10):638–50.
54. Rodnina MV. Translation in prokaryotes. Cold Spring Harb Perspect Biol. 2018;10(9):a032664
55. Park SH, Kim HU, Kim TY, Park JS, Kim SS, Lee SY. Metabolic engineering of *Corynebacterium glutamicum* for L-arginine production. Nat Commun. 2014;5:4618.
56. Baumgart M, Unthan S, Kloß R, Radek A, Polen T, Tenhaef N, et al. *Corynebacterium glutamicum* chassis C1*: building and testing a novel platform host for synthetic biology and industrial biotechnology. ACS Synth Biol. 2018;7(1):132–44.
57. Keilhauer C, Eggeling L, Sahm H. Isoleucine synthesis in *Corynebacterium glutamicum*: molecular analysis of the *ilvB-ilvN-ilvC* operon. J Bacteriol. 1993;175(17):5595–603.
58. Bertani G. Studies on lysogenesis. I. The mode of phage liberation by lysogenic *Escherichia coli*. J Bacteriol. 1951;62(3):293–300.
59. Fritzson P, Pop A, Abdelhak K, Ashgar A, Bachmann B, Braun W, et al. The OpenModelica integrated environment for modeling, simulation, and model-based development. Model Identif Control. 2020;41(4):241–95.
60. Osthege M, Tenhaef N, Zyla R, Muller C, Hemmerich J, Wiechert W, et al. bletl—a Python package for integrating BioLector microcultivation devices in the design-build-test-learn cycle. Eng Life Sci. 2022;22(3–4):242–59.
61. Hanahan D. Studies on transformation of *Escherichia coli* with plasmids. J Mol Biol. 1983;166(4):557–80.

62. Schäfer A, Tauch A, Jäger W, Kalinowski J, Thierbach G, Pühler A. Small mobilizable multi-purpose cloning vectors derived from the *Escherichia coli* plasmids pK18 and pK19: selection of defined deletions in the chromosome of *Corynebacterium glutamicum*. Gene. 1994;145(1):69–73.
63. Untergasser A, Cutcutache I, Koressaar T, Ye J, Faircloth BC, Remm M, et al. Primer3—new capabilities and interfaces. Nucleic Acids Res. 2012;40(15):e115.
64. Livak KJ, Schmittgen TD. Analysis of relative gene expression data using real-time quantitative PCR and the $2^{-\Delta\Delta CT}$ method. Methods. 2001;25(4):402–8.
65. Jumper J, Evans R, Pritzel A, Green T, Figurnov M, Ronneberger O, et al. Highly accurate protein structure prediction with AlphaFold. Nature. 2021;596(7873):583–9.
66. Mirdita M, Schutze K, Moriwaki Y, Heo L, Ovchinnikov S, Steinegger M. ColabFold: making protein folding accessible to all. Nat Methods. 2022;19(6):679–82.
67. Pettersen EF, Goddard TD, Huang CC, Meng EC, Couch GS, Croll TI, et al. UCSF ChimeraX: structure visualization for researchers, educators, and developers. Protein Sci. 2021;30(1):70–82.
68. Lessard JC. Growth media for *E. coli*. Methods Enzymol. 2013;533:181–9.
69. Studier FW, Moffatt BA. Use of bacteriophage T7 RNA polymerase to direct selective high-level expression of cloned genes. J Mol Biol. 1986;189(1):113–30.
70. Kinoshita S, Udaka S, Shimono M. Studies of amino acid fermentation. I. Production of L-glutamic acid by various microorganisms. J Gen Appl Microbiol. 1957;3(3):193–205.

Publisher's Note

Supplement to:

Discovery of novel amino acid production traits by evolution of synthetic co-cultures

Rico Zuchowski[1#], Simone Schito[1#], Friederike Neuheuser[1], Philipp Menke[1], Daniel Berger[1], Niels Hollmann[1], Srushti Gujar[1,2,3], Lea Sundermeyer[1], Christina Mack[1], Astrid Wirtz[1], Oliver H. Weiergräber[2], Tino Polen[1], Michael Bott[1], Stephan Noack[1], Meike Baumgart[1,*]

[1]Institute of Bio- and Geosciences, IBG-1: Biotechnology, Forschungszentrum Jülich, Jülich, Germany

[2]Institute of Biological Information Processing, IBI-7: Structural Biochemistry, Forschungszentrum Jülich, Jülich, Germany

[3]Institut für Physikalische Biologie, Heinrich-Heine-Universität Düsseldorf, Düsseldorf, Germany

[#]These authors contributed equally to this work

*Address correspondence to m.baumgart@fz-juelich.de

Supplemental tables

Table S1: Amino acid importer in *C. glutamicum*

Locus tag(s)	NCgl synonyms	Transporter name	Amino acid substrate	Reference
cg0606-cg0610	NCgl0497-NCgl0501	MetQNI	L-methionine	(Trötschel *et al.*, 2008)
cg1105	NCgl0929	LysI	L-lysine	(Seep-Feldhaus *et al.*, 1991)
cg1167-cg1169	NCgl0985-NCgl0986	MetPS	L-methionine, L-alanine	(Trötschel *et al.*, 2008)
cg1257	NCgl1062	AroP	L-phenylalanine, L-tryptophan, L-tyrosine, L-histidine	(Shang *et al.*, 2013, Wehrmann *et al.*, 1995)
cg1305	NCgl1108	PheP	L-phenylalanine, L-histidine	(Zhao *et al.*, 2011, Kulis-Horn *et al.*, 2014)
cg1314	NCgl1116	PutP	L-proline	(Peter *et al.*, 1997)
cg1502-cg1504	NCgl1276-NCgl1278	ArgTUV	L-arginine	This study
cg2136-cg2139	NCgl1875-NCgl1878	GluABCD	L-glutamate	(Kronemeyer *et al.*, 1995)
cg2537	NCgl2228	BrnQ	L-leucine, L-valine, L-isoleucine	(Ebbighausen *et al.*, 1989, Tauch *et al.*, 1998)
cg2539	NCgl2230	EctP	L-proline	(Peter *et al.*, 1998)
cg2810	NCgl2643	CynT	L-cysteine	(Kondoh and Hirasawa, 2019)
cg3396	NCgl2962	ProP	L-proline	(Peter *et al.*, 1998)

Table S2: Mean pLDDT and C^{α} r.m.s.d. values for WT and mutant structures predicted in this study.

Structures predicted by AlphaFold2 (rank 1)	Mean pLDDT (0–100)	C^{α} r.m.s.d. of WT and mutant
MetC	97.96	0.26 Å
$MetC_{S322F}$	97.84	
Cg1874	94.52	0.13 Å
$Cg1874_{G93D}$	94.69	
Cg2850	89.13	0.21 Å (excluding disordered residues 1–27)
$Cg2850_{G30R}$	89.46	

Table S3: Ligands tested for binding to ArgT via ITC measurements.

Tested amino acids	Binding observed?	Tested concentrations
L-arginine	yes	50 µM - 200 µM
L-citrulline	yes	200 µM, 100 µM
L-cysteine	no	200 µM, 2 mM
L-glutamate	no	200 µM, 2 mM
L-glutamine	no	200 µM, 2 mM
L-histidine	no	200 µM, 2 mM
L-lysine	no	200 µM, 2 mM

Table S4: Plasmids used in this study.

Plasmid	Relevant characteristics	Source or reference
pK19*mobsacB*	Kan^r; plasmid for allelic exchange in *C. glutamicum*; (pK18 ori$V_{E.c.}$, *sacB*, *lacZ*α)	(Schäfer *et al*., 1994)
pK19*mobsacB*-$ArgB_{A29V\ M31V}$	Kan^r; pK19*mobsacB* derivative for mutation of *argB* (cg1582) to yield $ArgB_{A29V\ M31V}$ in *C. glutamicum*	(Schito *et al*., 2022)
pK19*mobsacB*-$MetC_{S322F}$/P_{brnQ}*	Kan^r; pK19*mobsacB* derivative for mutation of MetC (Cg2536) S322F in *C. glutamicum.* This mutation also affects the promoter region of *brnQ* (cg2537).	This study
pK19*mobsacB*-$Mrp1C_{G29D}$	Kan^r; pK19*mobsacB* derivative for mutation of Mrp1C (Cg0325) G29D in *C. glutamicum*	This study
pK19*mobsacB*-$Mrp1A_{H335P}$	Kan^r; pK19*mobsacB* derivative for mutation of Mrp1A (Cg0326) H335P in *C. glutamicum*	This study
pK19*mobsacB*-P_{argT}*[1]	Kan^r; pK19*mobsacB* derivative for the mutation A→G 35 bp upstream of the *argT* (cg1504) TSS/TLS	This study
pK19*mobsacB*-*argT**	Kan^r; pK19*mobsacB* derivative for mutation of the 3rd codon of *argT* (cg1504) GAG→GAA, synonymous mutation	This study
pK19*mobsacB*-Δ*argTUV*	Kan^r; pK19*mobsacB* derivative for in frame deletion of *argTUV* (cg1504-cg1502) in *C. glutamicum*	This study
pK19*mobsacB*-Δcg1505-cg1506	Kan^r; pK19*mobsacB* derivative for in frame deletion of cg1505-cg1506 in *C. glutamicum*	This study
pK19*mobsacB*-Δ*mrp1*	Kan^r; pK19*mobsacB* derivative for deletion of *mrp1* (cg0321-cg0326) and cg0317-cg0319 in *C. glutamicum*. The latter encode genes for arsenate/arsenite resistance and were deleted accidentally.	This study
pPREx2	Kan^r; *E. coli/C. glutamicum* shuttle vector for expression of target genes. Cured pEKEx2-derivative with corrected *lacI*^{q} and without replicative sequences. P_{tacI}; *lacI*^{q}; $ori_{C.g.}$ of pBL1; $ori_{E.c.}$ ColE1 of pUC18.	(Bakkes *et al*., 2020)
pPREx2-*argTUV*	Kan^r; pPREx2 derivative with the *argTUV* genes (cg1504-cg1502) under control of P_{tac} promoter	This study
pET-TEV	Kan^R; pET28b derivative for overexpression of genes in *E. coli*, adding an N-terminal decahistdine tag and a TEV protease cleavage site to the target protein (pBR322 ori$V_{E.c.}$, PT7, lacI)	(Bussmann *et al*., 2010)
pET-TEV-*argT*	Kan^R; pET-TEV derivative coding for the ArgT protein (Cg1504) with an N-terminal decahistdine tag and a TEV protease cleavage site	This study

Table S5: Oligonucleotides used in this study.

Oligonucleotide	Sequence (5' → 3')[1]
Sequencing primers	
B223_M13-fw	CGCCAGGGTTTTCCCAGTCAC
B224_M13-rv	AGCGGATAACAATTTCACACAGGA
Verification of deletion of cg3035	
B463_cg3035_Dfw	GCGGAAAGCATGCTTAGAATGTTGCC
B464_cg3035_Drv	CACGTTCTGGTTCGGTGACG
Work with pK19*mobsacB*-Δ*arg*	
B469_ARG-Dfw	AGCTCCCGCTAAGGTAGCTACC
B470_ARG-Drv	TTGGGTTTCATTCAACAACGCGCC
Verification of deletion of *leuA*	
Z5_leuA-Dfw	GGGTGGATTCCACTTGATTG
Z6_leuA-Drv	GGCTACCCTCCTCACCGTAG
Verification of deletion of *leuB*	
Z11_leuB-Dfw	GGTGCTTAAGGCGGATAAGG
Z12_leuB-Drv	TAAACACCCTCGGTGCTCTG
Verification of deletion of *leuCD*	
Z17_leuCD-Dfw	CCCACGGACTCCGCTAAGC
Z18_leuCD-Drv	TCAAACCCACCGCAATTTACTCG
Verification of deletion of *argR*	
Z55_ArgR-Dfw	ACTGTGCCGCTGGTGAACTC
Z56_ArgR-Drv	AGTCACGAGCAGGTGCAATG
Work with pK19*mobsacB*-ArgB$_{A29V\ M31V}$	
Z78_ArgB_mut-fw_neu	TGTGACCAAGCGCGTTGCTG
Z64_ArgB-mut_rv	GCCGTCAATGACATGAGCAG
Verification of P_{tuf} *leuA*_B018_BS	
Z92_LeuA_Ptuf_fw	CTGGACTTCGTGGTGGCTAC
Z93_LeuA_Ptuf_seq_rv	TGCCACAGGGTAGCTGGTAG
Z67_PtufLeuA_seq_fw	CTCAGTGGTGTGCTGTTGAC
Z68_PtufLeuA_seq_rv	TCCTTGCCGTTGTGGATGAG
Construction and work with pK19*mobsacB*-MetC$_{S322F}$	
n071_cg2536_D1	**AAAACGACGGCCAGTGAATT**GATTCCACGACAACGCC
n072_cg2536_D2	GAGGCGCCTTTTAAAATTCTTCG
n073_cg2536_D3	**GAATTTTAAAAGGCGCCTCT**TCGATCTTG
n074_cg2536_D4	**CAGGTCGACTCTAGAGGA**GCTGACGGTGCGGGATC
n021_cg2536_Dfw	TGCCTGCATACCCTCCTTTC
n022_cg2536_Drv	AACTTGGCTACCGACAACAC
Construction of and work with pK19*mobsacB*-Mrp1C$_{G29D}$	
n023_cg0325_D1	**AAAACGACGGCCAGTGAATT**GCTCCTGTACCTGTCCAA
n024_cg0325_D2	TCAGTGACATGTCGAAGACGATGC

Oligonucleotide	Sequence (5' → 3')[1]
n025_cg0325_D3	**CGTCTTCGACATGTCACTGA**TCGGCCACGCAGCGAACTTG
n026_cg0325_D4	**CAGGTCGACTCTAGAGGA**GGGGATTGCCACGCCACCGACA
n051_cg0325_Dfw	CACCGACGATGGTGGCAAAC
n052_cg0325_Drv	GCGCTATGCTTCTTGAGCTTC
Construction of and work with pK19*mobsacB*-Mrp1A$_{H335P}$	
n027_cg0326_D1	**AAAACGACGGCCAGTGAATT**CGCTGCTTACTGCGGTGGCG
n028_cg0326_D2	CTTAAACAGCGCGGGGCTGAGCGTG
n029_cg0326_D3	**CAGCCCCGCGCTGTTTAAG**TCCTCGTTGTTCATGCTC
n030_cg0326_D4	**CAGGTCGACTCTAGAGGA**GTGGGGTGTTGATGCCGTGCC
n053_cg0326_Dfw	ACCAGCATCGATAGGATGTC
n054_cg0326_Drv	TGTTGATTGCGCGTTCGG
Construction of and work with pK19*mobsacB*-P$_{argT}$*[1]	
n039_cg1504_1399043_D1	**AAAACGACGGCCAGTGAATT**CTTGTGCGGGTGATACTCC
n040_cg1504_1399043_D2	GCAATAACCTCAAGTGAGGC
n041_cg1504_1399043_D3	**CTCACTTGAGGTTATTGC**ACCATGGCAGGTAG
n042_cg1504_1399043_D4	**CAGGTCGACTCTAGAGGA**GTTCTCGCGGCGTTCCTCG
n057_cg1504_Dfw	ACGGACATCGTCGGTCTCTG
n058_cg1504_Drv	CTGCATTTGGATCTGCCTGTTG
Construction of and work with pK19*mobsacB-argT**	
n035_cg1504_1399000_D1	**AAAACGACGGCCAGTGAATT**CCCAACGATCACTTCCACTC
n036_cg1504_1399000_D2	CGGGTGAAACTTTCAATCATGG
n037_cg1504_1399000_D3	**GATTGAAAGTTTCACCCG**ATTGCGAATTTCGCAGACAC
n038_cg1504_1399000_D4	**CAGGTCGACTCTAGAGGA**GGTTTCACGATCAGTTGCCTGC
n057_cg1504_Dfw	ACGGACATCGTCGGTCTCTG
n058_cg1504_Drv	CTGCATTTGGATCTGCCTGTTG
Construction of and work with pK19*mobsacB*-Δ*argTUV*	
n043_cg1502-1504_D1	**AAAACGACGGCCAGTGAATT**CTGCCTCTTCCACTTGTGC
n044_cg1502-1504_D2	**AGCCGATAATGACTCGCA**GCAATAACCTTAAGTGAGGC
n045_cg1502-1504_D3	**CTTAAGGTTATTGC**GCGAGTCATTATCGGCT
n046_cg1502-1504_D4	**CAGGTCGACTCTAGAGGA**GACACGTGAAATAAGGAGG
n059_cg1502-1504_Dfw	AAGAAGTTGCCCGCTTCGGTG
n060_cg1502-1504_Drv	CTGCATTTGGATCTGCCTGTTG
Construction of and work with pK19*mobsacB*-Δcg1505-1506	
n047_cg1505-1506_D1	**AAAACGACGGCCAGTGAATT**GCACCACTACCAGCG
n048_cg1505-1506_D2	**GTTTTATCCGGCATGGG**CCAATTATCTTTCTTTGGCG
n049_cg1505-1506_D3	**CAAAGAAAGATAATTGG**CCCATGCCGGATAAAAC
n050_cg1505-1506_D4	**CAGGTCGACTCTAGAGGA**GCTTGAACCGATGGAAGG
n061_cg1505-1506_Dfw	ACGGACATCGTCGGTCTCTG
n062_cg1505-1506_Drv	TACTCGGCCATGCTGACTCAC
Construction of and work with pK19*mobsacB*-Δ*mrp1*	

Oligonucleotide	Sequence (5' → 3')[1]
n031_cg0322-0326_D1	**AAAACGACGGCCAGTGAATT**CTGTACAACGACAAGACCGCC
n032_cg0322-0326_D2	**CTGCAATAGAATGTGTTC**CTACTTGATGAGTTAGCAAGAGCAC
n033_cg0322-0326_D3	**CTTGCTAACTCATCAAGTAG**GAACACATTCTATTGCAGGG
n034_cg0322-0326_D4	**CAGGTCGACTCTAGAGGA**GCACCTTGTTGAGCGTTG
n055_cg0322-0326_Dfw	ACGTTTCGCAGCAATGCGATAG
n056_cg0322-0326_Drv	TGTTTGCGCAGGTCTTCGG
Primer for gene expression analysis via qPCR	
n083_ddh_qPCR_fw	CCGGAAAGCAAACCCACAAG
n084_ddh_qPCR_rev	CTCGGAGTCGAAGGTTGCTT
n085_cg1502_qPCR_fw	GCAAGTCAATGCCCTTGAGC
n086_cg1502_qPCR_rv	CTGATGCTGAAGGCGCAATC
n087_cg1504_qPCR_fw	ACGAGGTCCATTTCCACACC
n088_cg1504_qPCR_rv	CGTTCCAGATCCTGTACCGG
n089_cg2537_qPCR_fw	AAGGACATGGCTTCTCGTGG
n090_cg2537_qPCR_rv	AACAAGCCCGAATAAAGCGC
Z315_cg2538_qPCR_fw	TCGCCAAATTGTCGACATGC
Z316_cg2538_qPCR_rv	ATATTGCGCGTGGTTGCTTC
Analysis of fluorescent protein integration	
Z109_Intcg1121 fwd	TTGGCGTGTGGTTGGTTAG
Z110_Intcg1122 rev	CGCATCAAGCAGATCTCTG
Construction of and work with pK19*mobsacB*-Cg1874$_{G93D}$	
n003_cg1874_Dfw	TAAATTGCGGGTGCTGTTGG
n004_cg1874_Drv	CTGCAAGCAGCACTGGATCG
n013_cg1874_mutate-D1	**AAAACGACGGCCAGTGAATT**ACTAAAGCTTGGGCAGCGAC
n014_cg1874_mutate-D2	CCGGCAACGAGGTCCTTCTTGTC
n015_cg1874_mutate-D3	**AAGAAGGACCTCGTTGCCGG**CGGATGGCGCTTTTCAGATC
n016_cg1874_mutate-D4	**CAGGTCGACTCTAGAGGA**CTGAGGCAATTCCCCTGGAA

Construction of and work with pK19*mobsacB*-Cg2850$_{G30R}$	
n007_cg2850_Dfw	AACCGCGAACCAACGAGTCC
n008_cg2850_Drv	CCGCTAGTGCGGTATCGAAC
n017_cg2850_mutate-D1	**AAAACGACGGCCAGTGAATT**CTTCCGAATCAACTCCACCA
n018_cg2850_mutate-D2	TGCGTCGGATCGGCTGATGCTTG
n019_cg2850_mutate-D3	**GCATCAGCCGATCCGACGCA**GTAAACCTCGCTGCCGAACA
n020_cg2850_mutate-D4	**CAGGTCGACTCTAGAGGA**AGTTCGTTGGTTGGAAGCAG
Construction of pET-TEV-*argT*	
DB029_pET-TEV_cg1504_AS78_D2	**ACCTGTATTTTCAGGGCCAT**CCCGAAGCTCTGGCTCAGCG
DB030_pET--TEV_cg1504_D3_rev	**AAGCTTGTCGACGGAGCTCG**CTAGTTGAGTGGCTGTTCGTTG

[1] Overhangs for Gibson assembly (Gibson *et al.*, 2009) are marked with bold letters.

Supplemental figures

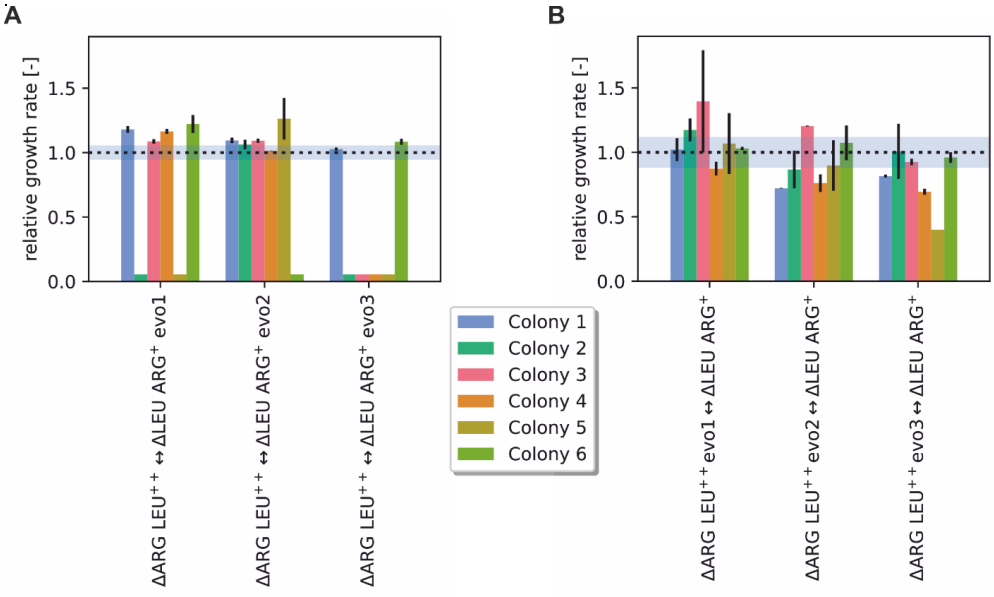

Fig. S1: Growth rates of different CoNoS established using colonies isolated from an ALE experiment. Single auxotrophic CoNoS member were isolated on CGXII plates supplemented with the required amino acid and six colonies from each ALE replicate were tested in combination with the non-evolved partner in a CoNoS setup. The dotted line and the corresponding blue shady background indicate the relative growth rate and the standard deviation of the non-evolved CoNoS as reference cultivation. Control CoNoS were cultivated in biological triplicates, test CoNoS were cultivated in technical duplicates. (A) Test of colonies derived from evolved *C. glutamicum* ΔLEU ARG^{+}. (B) Test of colonies derived from evolved *C. glutamicum* ΔARG LEU^{++}.

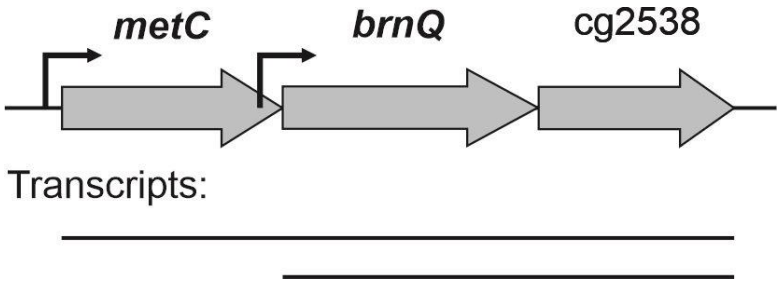

Fig. S2: Genomic organization of the region near *metC* and *brnQ*. Black arrows represent transcriptional start sites. Black lines in the lower part of the figure represent potential operons and sub operons. Transcript and promoter data based on published RNAseq data (Pfeifer-Sancar et al., 2013).

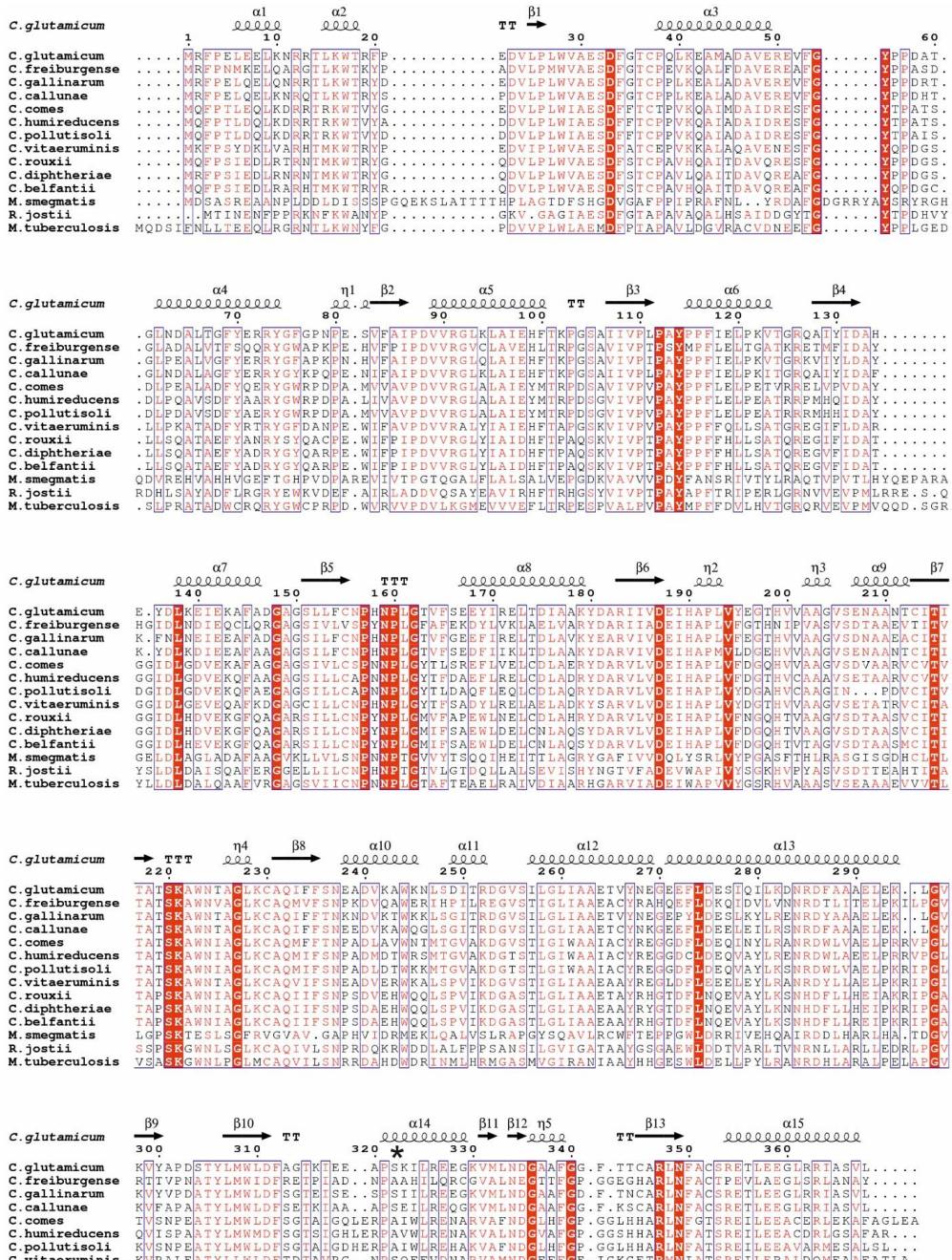

Fig. S3: Multiple sequence alignment of MetC (Cg2536 – Accession number WP_011015029.1) with homologous sequences of *C. freiburgense* (WP_027011762.1), *C. gallinarium* (WP_191732314.1), *C. callunae* (WP_015651815.1), *C. comes*

(WP_156228685.1), *C. humireducens* (WP_040086403.1), *C. pollutisoli* (NLP39668.1), *C. vitaeruminis* (WP_025253321.1), *C. rouxii* (WP_155873664.1), *C. diptheriae* (WP_014310694.1), *C. belfantii* (WP_197691522.1), *Rhodococcus* (*R. jostii* – WP_073366627.1), *Mycolicibacterium* (*M. smegmatis* – WP_233043953.1) and *Mycobacterium* (*M. tuberculosis* – WP_055353591.1) species. Clustal Omega (Sievers *et al.*, 2011) was used to create the alignment. ESPribt 3.0 (Robert and Gouet, 2014) was used to prepare the figure. Similar residues are marked with red colored letters, completely conserved residues with a red background. Structure predictions are given as predicted by AF2 (helices are marked with squiggles, β-strands with arrows and turns with TT letters). An asterisk indicates the position mutated in the evolved strains (S322F).

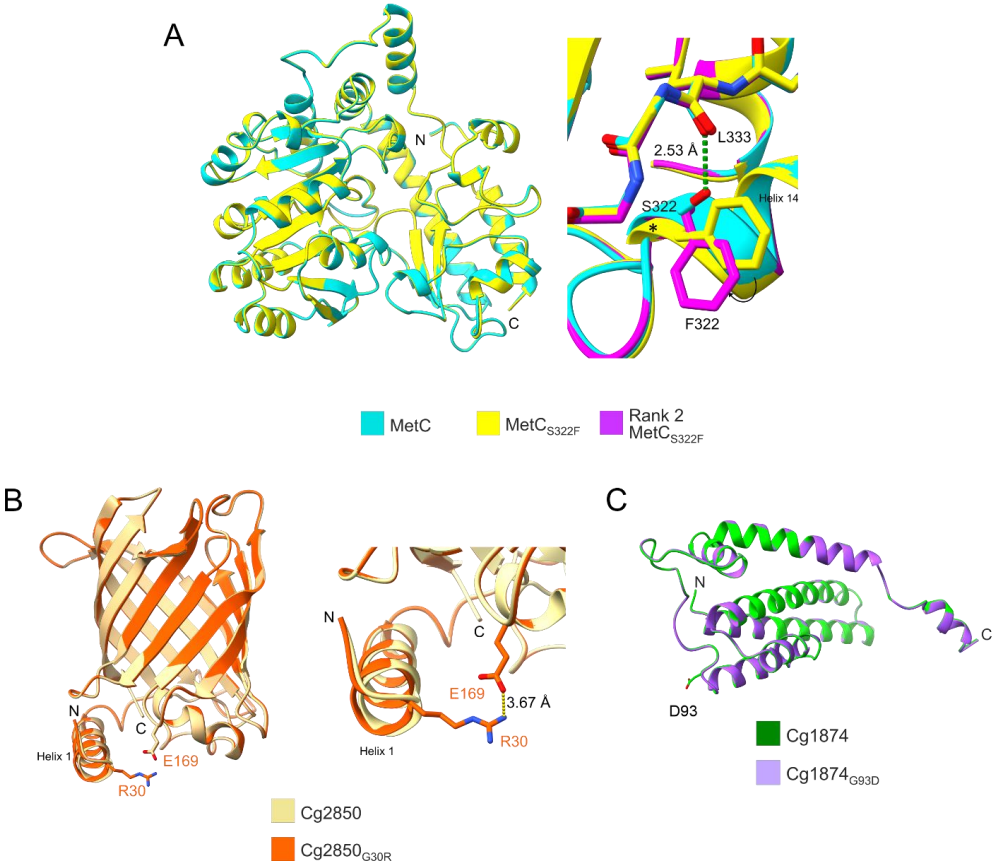

Fig. S4: AlphaFold2 models for proteins mutated during ALE of a CoNoS. (A) Left, superimposition of top-ranked AlphaFold2 predicted structures of MetC (cyan) and MetC$_{S322F}$ (yellow). Right, enlarged view of residues surrounding the site of mutation (S322F); nitrogen: blue, oxygen: red. Here, the second-rank MetC$_{S322F}$ model is included for comparison (violet). Conformational changes predicted by alternative models are indicated: a slight upward shift of the helix around the F322 position (asterisk), leaving the χ1 torsion in res. 322 mostly unaffected, and a re-orientation of the F322 side chain (arrow) without major main chain displacement. The green dashed line represents the hydrogen bond formed in MetC between the S322 gamma oxygen and the L333 carbonyl oxygen. (B) Superimposition of top-ranked AlphaFold2 predicted structures (overview, left, and close-up, right) of Cg2850 (tan) and Cg2850$_{G30R}$ (orange); nitrogen: blue, oxygen: red. The sidechains R30 of the mutant and E169 of WT and mutant are displayed. The yellow dashed line represents the salt bridge between R30 and E169 of Cg2850$_{G30R}$. (C) Superimposition of AlphaFold2 predicted structures of Cg1874 (green) and Cg1874$_{G93D}$ (violet). Figure generation and structure analysis were performed using ChimeraX (Pettersen *et al.*, 2021).

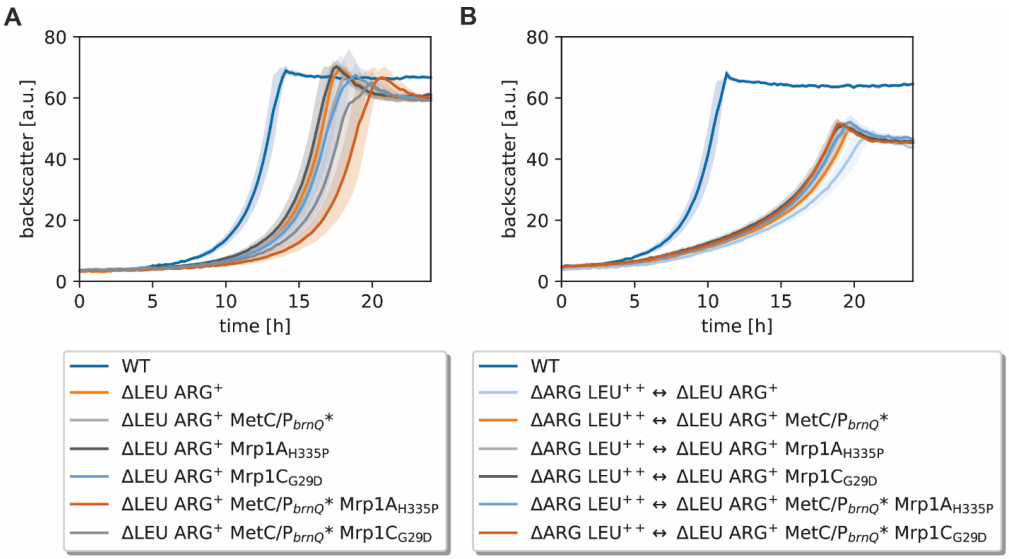

Fig. S5: Growth performance of ΔLEU ARG$^+$ reengineered strains. WT monoculture is shown as reference cultivation. (A) Monocultures of reengineered strains ΔLEU ARG$^+$ with mutations MetC/P$_{brnQ}$*, Mrp1A$_{H335P}$, and Mrp1C$_{G29D}$ as well as ΔLEU ARG$^+$ in CGXII medium with 2 % (w/v) glucose and 3 mM L-leucine. (B) CoNoS comprising one mutated strain and one parental strain in comparison with the native non-evolved CoNoS. Cultures were performed in biological triplicate in CGXII medium with 2 % (w/v) glucose. Mean values and standard deviations are shown as lines and shaded areas, respectively.

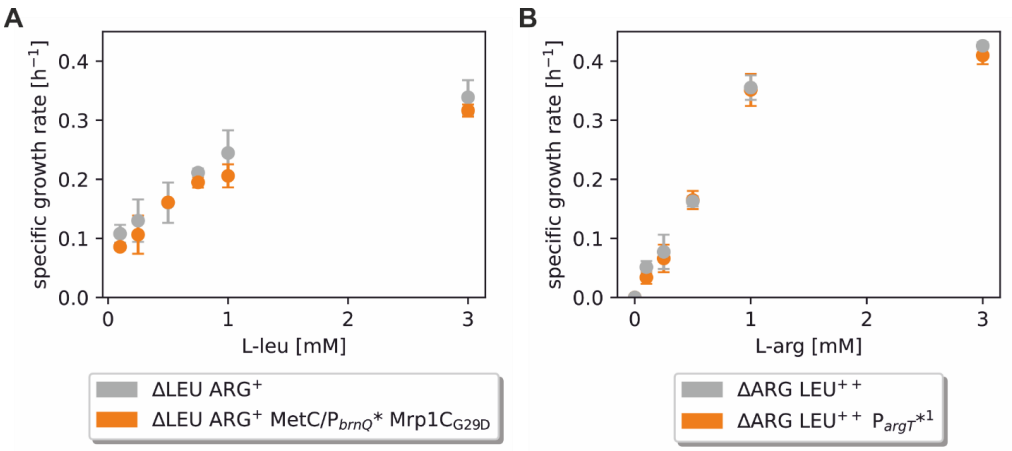

Fig. S6: (A) Growth performance of the reengineered strain ΔLEU ARG^{+} P$_{brnQ}$* Mrp1C$_{G29D}$ and ΔLEU ARG^{+} in monoculture supplemented with different amounts of L-leucine. Cultures were performed in triplicate in CGXII medium. (B) Growth performance of the reengineered strain ΔARG LEU^{++} P$_{argTUV}$* Mrp1C$_{G29D}$ and ΔARG LEU^{+} in monoculture supplemented with different amounts of L-leucine. Cultures were performed in triplicate in CGXII medium. Mean values and standard deviations are shown as points and dashes, respectively.

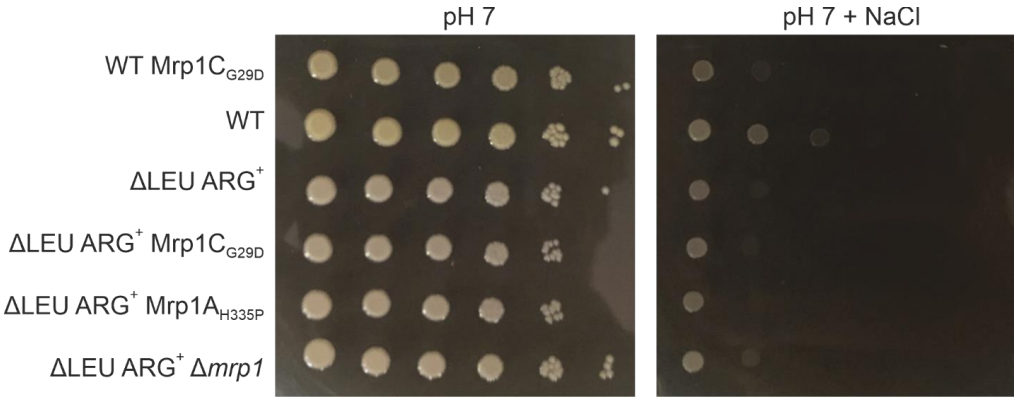

Fig. S7: Effects of Mrp1 point mutations or *mrp1* deletion on *in vivo* NaCl sensitivity of *C. glutamicum*. The given *C. glutamicum* strains were precultivated in liquid cultures first for 8 h in BHI and afterwards overnight in CGXII with 2 % (w/v) glucose and 3 mM L-leucine for auxotrophic strains. Tenfold serial dilutions were spotted onto CGXII-agar plates with 2 % (w/v) glucose, 3 mM L-leucine, pH 7 with different NaCl concentrations (left: 0 M, right 0.6 M) and incubated at 30 °C for 48 h, as performed in (Xu *et al.*, 2018).

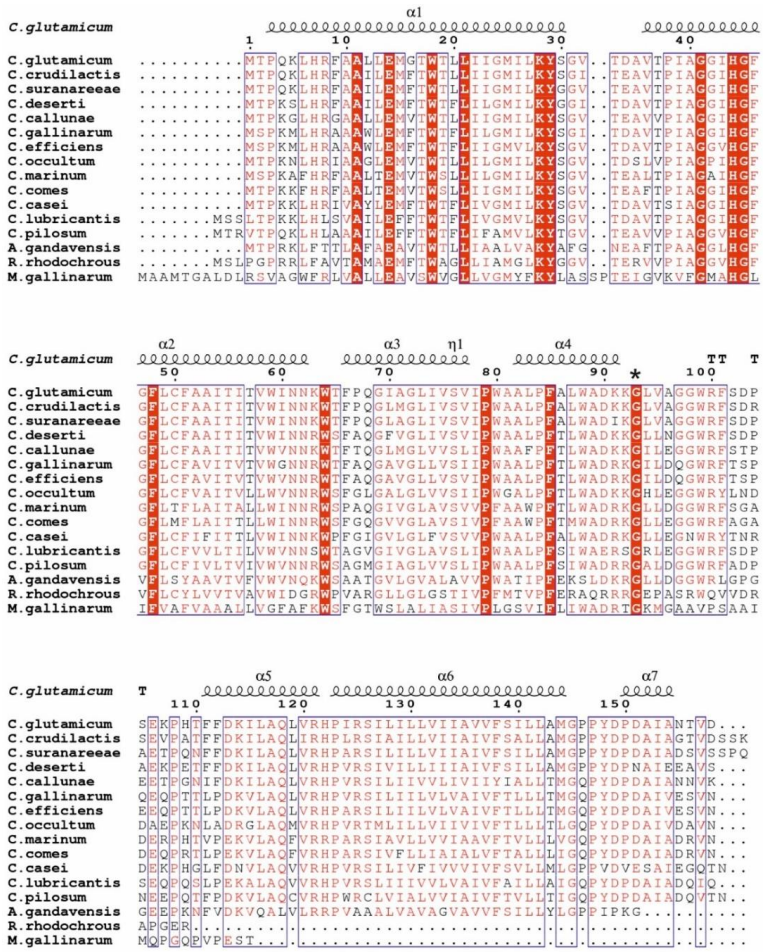

Fig. S8: Multiple sequence alignment of Cg1874 (Accession number WP_011015029.1) with homologous sequences of *C. crudilactis* (WP_066565970.1), *C. suranareeae* (WP_096456201.1), *C. deserti* (WP_053545063.1), *C. calunae* (WP_015651448.1), *C. gallinarum* (WP_191733525.1), *C. efficiens* (WP_035108832.1), *C. occultum* (WP_156231041.1), *C. marinum* (WP_042622591.1), *C. comes* (WP_156229426.1), *C. casei* (WP_006823593.1), *C. lubricantis* (WP_018295645.1), *C. pilosum* (WP_018581290.1), *Arthrobacter* (*A. gandavensis* – WP_194782106.1) *Rhodococcus* (*R. rhodochrous* – OOL31646.1) and *Mycobacterium* (*M. gallinarum* – BBY93031.1) species. Clustal Omega (Sievers *et al.*, 2011) was used to create the alignment. ESPribt 3.0 (Robert and Gouet, 2014) was used to prepare the figure. Similar residues are marked with red colored letters, identical residues with a red background color. Structural data were assigned according to the rank 1 AF2 model (helices are marked with squiggles, β-strands with arrows and turns with TT letters). The position mutated in the evolved strains (G93D) is indicated by an asterisk.

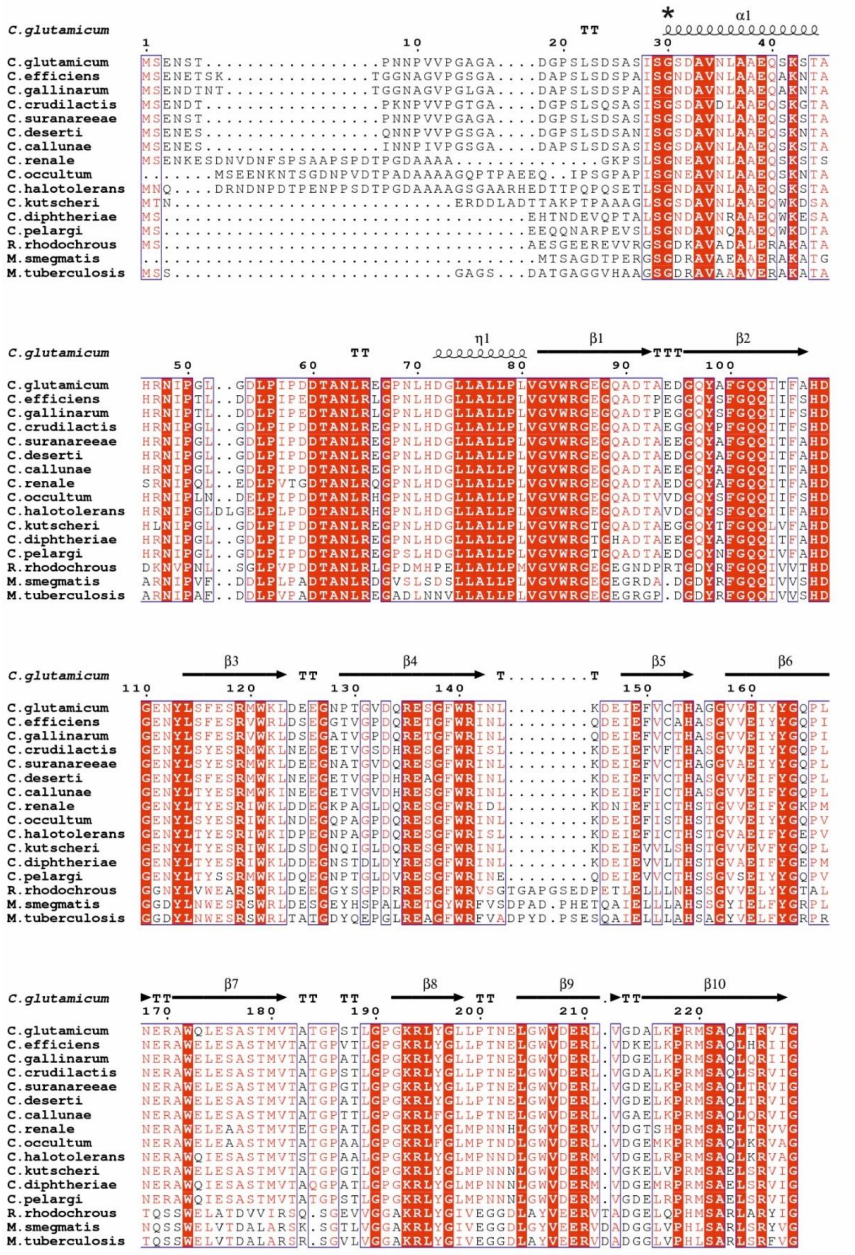

Fig. S9: Multiple sequence alignment of Cg2850 (Accession number WP_011015029.1) with homologous sequences from *C. efficiens* (WP_006769171.1), *C. gallinarum* (WP_191733242.1), *C. crudilactis* (WP_066567847.1), *C. suranareeae* (WP_096458136.1), *C. deserti* (WP_053545607.1), *C. callunae* (WP_247776159.1), *C. renale* (WP_115243769.1), *C. occultum* (WP_156231609.1), *C. halotolerans* (WP_015401779.1), *C. kutscheri* (WP_046438926.1), *C. diphtheriae* (WP_014320394.1), *C. pelargi* (WP_128889270.1),

Rhodococcus (*R. rhodochrous* – OOL29119.1) and *Mycolicibacterium* (*M. smegmatis* – WP_233043311.1) and *Mycobacterium* (*M. tuberculosis* – WP_031701164.1) species. Clustal Omega (Sievers *et al.*, 2011) was used to create the alignment. ESPribt 3.0 (Robert and Gouet, 2014) was used to prepare the figure. Similar residues are marked with red colored letters, identical residues with a red background color. Structure predictions are given as predicted by AF2 rank 1 model (helices are marked with squiggles, β-strands with arrows and turns with TT letters). The position mutated in the evolved strains (G30R) is indicated by an asterisk.

Fig. S10: Promoter regions upstream of *argT* (cg1504) in *C. glutamicum* WT and three evolved ΔARG LEU^{++} strains. -10 site according to (Pfeifer-Sancar et al., 2013), transcriptional start site (red letter and black arrow), and mutated positions/regions in the evolved strains (purple) are given. In Evo2, 2829 bp were deleted starting 18 bp upstream of TSS, which resulted in the given sequence.

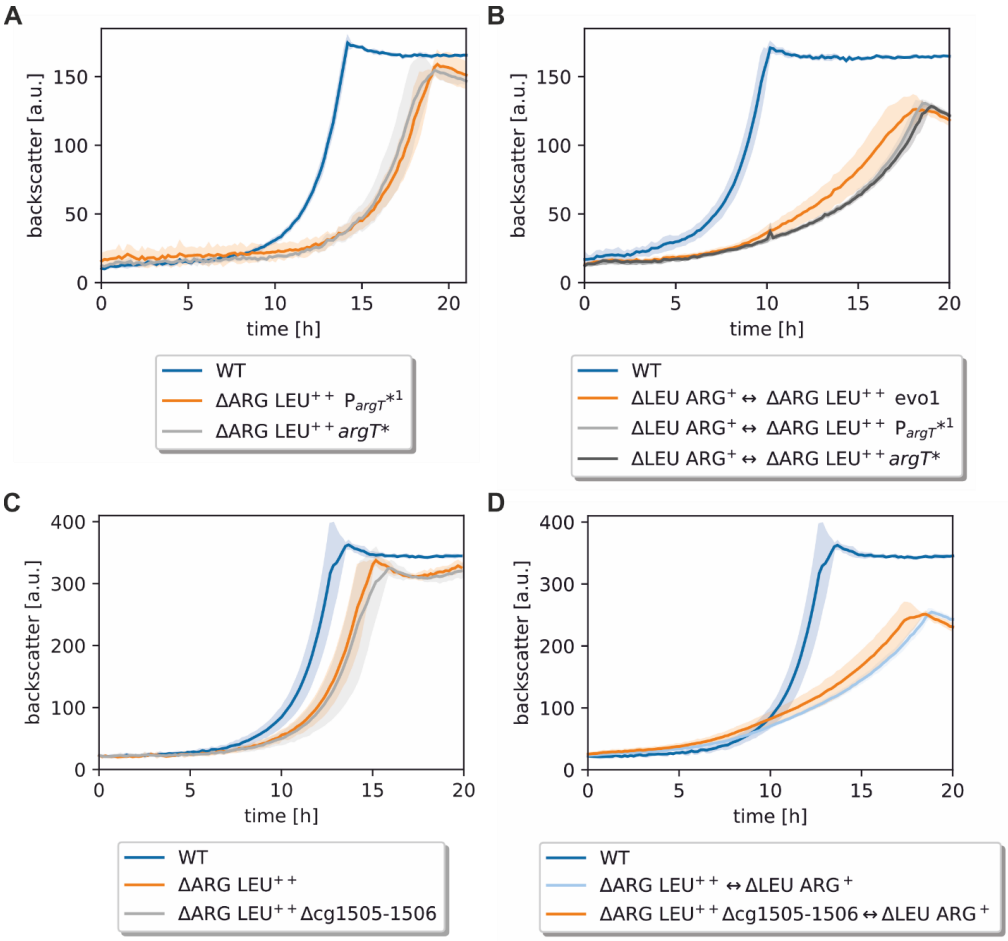

Fig. S11: Growth performance of strains with reengineered mutations in supplemented monocultures and in a CoNoS setting. Mutations were introduced into the promoter (P_{argTUV}*) or into the third codon of the coding region (*argTUV**). In a third strain, cg1505-cg1506 were deleted. (A) Comparison of ΔARG LEU^{++} P_{argT}*^{1} and ΔARG LEU^{++} *argT** in CGXII with 2 % (w/v) glucose and 3 mM L-arginine in comparison to a WT monoculture. For comparison with the non-mutated reference strain ΔARG LEU^{++}, please refer to figure 4A where ΔARG LEU^{++} P_{argT}*^{1} grew better that the reference. (B) Comparison of the above mentioned strains in a CoNoS setup in comparison with a CoNoS containing the evolved strain and a WT monoculture. For comparison with the non-mutated reference strain ΔARG LEU^{++}, please refer to figure 4B where the culture with ΔARG LEU^{++} P_{argT}*^{1} grew better than the reference. (C) Growth of ΔARG LEU^{++} Δcg1505-1506 in comparison to ΔARG LEU^{++} and WT monoculture in CGXII medium with 2 % (w/v) glucose and 3 mM - L-arginine. (D) Growth of ΔARG LEU^{++}Δcg1505-1506 in comparison to ΔARG LEU^{++} in a CoNoS in CGXII medium with 2 % (w/v) glucose. Mean values and standard deviations of biological triplicates are shown as lines and shaded areas, respectively.

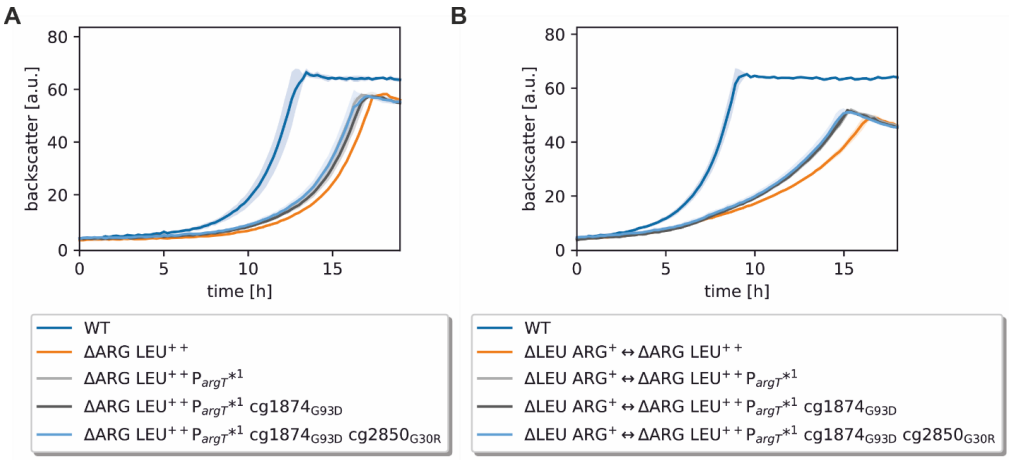

Fig. S12: Growth performance of ΔARG LEU^{++} strains with reengineered mutations. The WT monoculture is shown as reference cultivation. (A) Monocultures in CGXII medium with 2 % (w/v) glucose and 3 mM L-arginine. B) CoNoS cultures in CGXII minimal medium with 2 % (w/v) glucose. Mean values and standard deviations of biological triplicates are shown as lines and shaded areas, respectively.

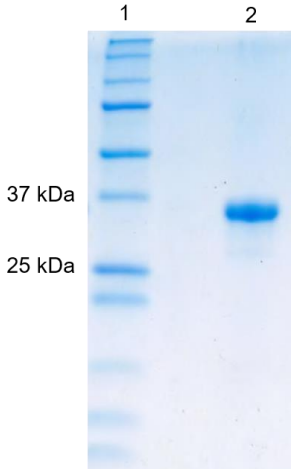

Fig. S13: SDS-PAGE of purified His$_{10}$-ArgT protein. The protein was overproduced in *E. coli* BL21(DE3) using plasmid pET-TEV-*argT* and purified by Ni-NTA affinity chromatography and subsequent size exclusion chromatography. The theoretical molecular weight of ArgT is 33 kDa. The protein sample was mixed with 5x SDS loading buffer and analyzed by SDS-PAGE and Coomassie staining. Lane 1, marker; lane 2, His$_{10}$-ArgT protein.

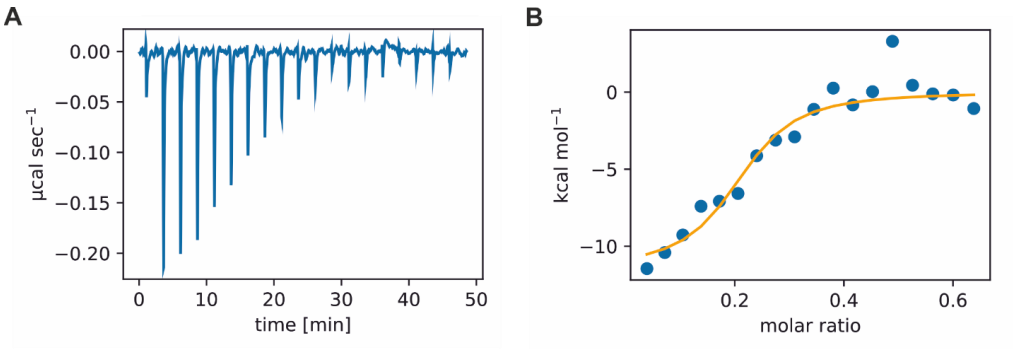

Fig. S14: Representative ITC experiment with His_{10}-ArgT and L-citrulline. (A) Raw data of a titration experiment performed with 100 µM L-citrulline and 30 µM His_{10}-ArgT in 40 mM HEPES-NaOH buffer, pH 7.4, with 100 mM NaCl. (B) Corresponding binding isotherm leading to a K_D value of 432 nM.

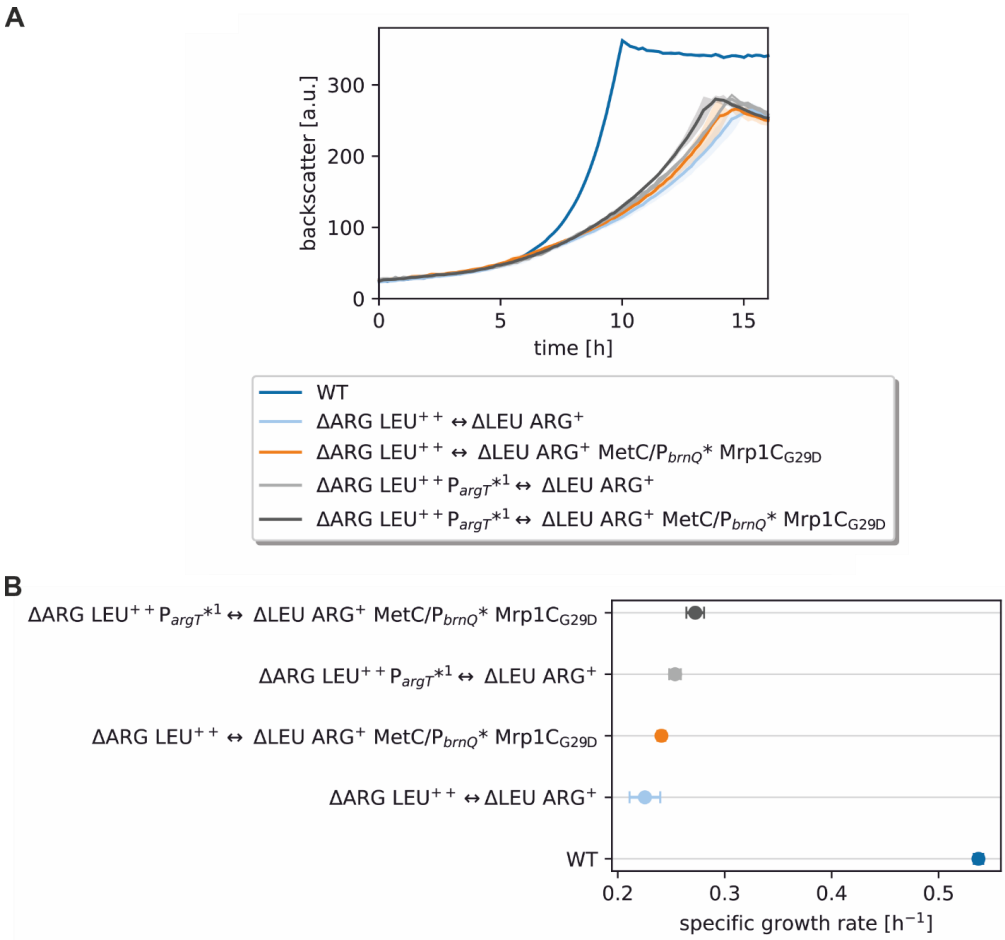

Figure S15: Growth performance of CoNoS comprising ΔLEU ARG^{+} and ΔARG LEU^{++} strains as well as these strains with reengineered mutations. Cultures were performed in biological triplicates in CGXII medium with 2 % (w/v) glucose. (A) The solid line represents the average growth of the replicates, the shady line background represents the standard deviation. WT monoculture is shown as reference cultivation. (B) Average growth rate and standard deviation of the cultures shown in (A).

References

1. Trötschel C, Follmann M, Nettekoven JA, Mohrbach T, Forrest LR, Burkovski A, et al. Methionine uptake in *Corynebacterium glutamicum* by MetQNI and by MetPS, a novel methionine and alanine importer of the NSS neurotransmitter transporter family. *Biochemistry*. 2008;47(48):12698-709.
2. Seep-Feldhaus AH, Kalinowski J, Pühler A. Molecular analysis of the *Corynebacterium glutamicum lysI* gene involved in lysine uptake. *Mol Microbiol*. 1991;5(12):2995-3005.
3. Shang X, Zhang Y, Zhang G, Chai X, Deng A, Liang Y, et al. Characterization and molecular mechanism of AroP as an aromatic amino acid and histidine transporter in *Corynebacterium glutamicum*. *J Bacteriol*. 2013;195(23):5334-42.
4. Wehrmann A, Morakkabati S, Krämer R, Sahm H, Eggeling L. Functional analysis of sequences adjacent to *dapE* of *Corynebacterium glutamicum* reveals the presence of *aroP*, which encodes the aromatic amino acid transporter. *J Bacteriol*. 1995;177(20):5991-3.
5. Zhao Z, Ding JY, Li T, Zhou NY, Liu SJ. The ncgl1108 (PhePCg) gene encodes a new L-Phe transporter in *Corynebacterium glutamicum*. *Appl Microbiol Biotechnol*. 2011;90(6):2005-13.
6. Kulis-Horn RK, Persicke M, Kalinowski J. Histidine biosynthesis, its regulation and biotechnological application in *Corynebacterium glutamicum*. *Microb Biotechnol*. 2014;7(1):5-25.
7. Peter H, Bader A, Burkovski A, Lambert C, Krämer R. Isolation of the putP gene of *Corynebacterium glutamicum* and characterization of a low-affinity uptake system for compatible solutes. *Arch Microbiol*. 1997;168(2):143-51.
8. Kronemeyer W, Peekhaus N, Krämer R, Sahm H, Eggeling L. Structure of the *gluABCD* cluster encoding the glutamate uptake system of *Corynebacterium glutamicum*. *J Bacteriol*. 1995;177(5):1152-8.
9. Ebbighausen H, Weil B, Krämer R. Transport of branched-chain amino acids in *Corynebacterium glutamicum*. *Arch Microbiol*. 1989;151:238-44.
10. Tauch A, Hermann T, Burkovski A, Krämer R, Pühler A, Kalinowski J. Isoleucine uptake in *Corynebacterium glutamicum* ATCC 13032 is directed by the *brnQ* gene product. *Arch Microbiol*. 1998;169:303-12.
11. Peter H, Weil B, Burkovski A, Krämer R, Morbach S. *Corynebacterium glutamicum* is equipped with four secondary carriers for compatible solutes: identification, sequencing, and characterization of the proline/ectoine uptake system, ProP, and the ectoine/proline/glycine betaine carrier, EctP. *J Bacteriol*. 1998;180(22):6005-12.
12. Kondoh M, Hirasawa T. L-Cysteine production by metabolically engineered *Corynebacterium glutamicum*. *Appl Microbiol Biotechnol*. 2019;103(6):2609-19.
13. Schäfer A, Tauch A, Jäger W, Kalinowski J, Thierbach G, Pühler A. Small mobilizable multi-purpose cloning vectors derived from the *Escherichia coli* plasmids pK18 and pK19: Selection of defined deletions in the chromosome of *Corynebacterium glutamicum*. *Gene.* 1994;145(1):69-73.
14. Schito S, Zuchowski R, Bergen D, Strohmeier D, Wollenhaupt B, Menke P, et al. Communities of Niche-optimized Strains (CoNoS) - Design and creation of stable, genome-reduced co-cultures. *Metab Eng*. 2022;73:91-103.
15. Bakkes PJ, Ramp P, Bida A, Dohmen-Olma D, Bott M, Freudl R. Improved pEKEx2-derived expression vectors for tightly controlled production of recombinant proteins in *Corynebacterium glutamicum*. *Plasmid*. 2020;112:102540.
16. Bussmann M, Baumgart M, Bott M. RosR (Cg1324), a hydrogen peroxide-sensitive MarR-type transcriptional regulator of *Corynebacterium glutamicum*. *J Biol Chem*. 2010;285(38):29305-18.

17. Gibson DG, Young L, Chuang RY, Venter JC, Hutchison CA, 3rd, Smith HO. Enzymatic assembly of DNA molecules up to several hundred kilobases. *Nat Methods*. 2009;6(5):343-5.
18. Pfeifer-Sancar K, Mentz A, Rückert C, Kalinowski J. Comprehensive analysis of the Corynebacterium glutamicum transcriptome using an improved RNAseq technique. *BMC Genomics.* 2013;14:888.
19. Sievers F, Wilm A, Dineen D, Gibson TJ, Karplus K, Li W, et al. Fast, scalable generation of high-quality protein multiple sequence alignments using Clustal Omega. *Mol Syst Biol.* 2011;7:539.
20. Robert X, Gouet P. Deciphering key features in protein structures with the new ENDscript server. *Nucleic Acids Res*. 2014;42(Web Server issue):W320-4.
21. Pettersen EF, Goddard TD, Huang CC, Meng EC, Couch GS, Croll TI, et al. UCSF ChimeraX: Structure visualization for researchers, educators, and developers. *Protein Sci*. 2021;30(1):70-82.
22. Xu N, Zheng Y, Wang X, Krulwich TA, Ma Y, Liu J. The lysine 299 residue endows the multisubunit Mrp1 antiporter with dominant roles in Na+ resistance and pH homeostasis in *Corynebacterium glutamicum*. *Appl Environ Microbiol*. 2018;84(10).

3. Discussion

3.1 Development of cooperation and bacterial coevolution

Genome reduction is a frequent consequence of adaptation in nature, and mutual or commensal cooperation via cross-feeding interactions can stabilize species after severe gene loss (see chapter 1.2). Synthetic communities of genome-reduced strains were so far mainly constructed with *E. coli* or *S. cerevisiae* (Shou *et al.*, 2007, Pande *et al.*, 2014). In this thesis, we showed that synthetic communities of *C. glutamicum* strains with different amino acid auxotrophies could be generated. Metabolic dependency is sufficient for microbial cooperation to arise, but engineering of the strains for overproduction of the amino acid fed to the partner strain is required for robust growth (Schito *et al.*, 2022). This is absolutely in line with the finding that obligate dependencies in a spatially isolated, cheater-free environment are one ideal prerequisite for cooperation, as this is from an experimental and also from a mathematical modeling perspective a viable pathway for the emergence of cooperation (Nowak and May, 1992, Hol *et al.*, 2013). Starting with different amino acid auxotrophic strains, only a small number of pairings were able to grow, and their growth was extremely slow, requiring several days to increase the OD two-fold. These pairs constituted our 1st generation CoNoS. There are two possible explanations for the minimal growth of these co-cultures. The first one is that growth was based on the small amount of leakage including the required amino acids (Wendering and Nikoloski, 2022) or exported "extended" overflow metabolites produced by the cells (Paczia *et al.*, 2012), initially supported by the tiny amount of essential amino acids remaining from the pre-cultivation. This is in line with models for community development (Wendering and Nikoloski, 2022) and with the CoNoS growth later being strongly improved by metabolic engineering to increase the production of the amino acid to be fed to the partner strain. One alternative explanation would be adaptations of the strain that result in both strains overproducing the essential metabolite for the partner strain. This was observed before in a co-culture of two *E. coli* strains, having either an L-leucine or an L-isoleucine auxotrophy, in which a global activation of the anabolic metabolism was observed via a transcriptome analysis (Hosoda *et al.*, 2011). Such coexistence and transcriptomic responses between closely related *Salinibacter ruber* strains isolated from their natural habitats were also shown before (Gonzalez-Torres *et al.*, 2015). The mathematical description of the viability of those artificial communities is the rule $S_1S_2 > C_1C_2$ with S_i ($i = 1, 2$) being the amount of the cross-fed metabolite being supplied by each strain and C_i the required metabolite consumption necessary for growth (Momeni *et al.*, 2011), accurately describing also the growing CoNoS.

Several auxotrophic strain pairs were improved to yield a number of viable, engineered 2nd generation CoNoS by increased cross-feeding due to relieved feedback inhibition of key enzymes of the relevant amino acid biosynthesis pathways, similar to approaches for other communities (Pande *et al.*, 2014). These metabolically engineered CoNoS grew significantly faster. The growth rates were further increased by additional mutations, suggesting that community growth depended directly on the concentration of the cross-fed amino acids each partner produced (Schito *et al.*, 2022). The best growing CoNoS at this stage, a ΔHIS LEU^{++}↔ ΔLEU HIS^{+} community, reached 88 % and 97 % of the WT growth rate of and final backscatter, respectively, with the CoNoS notably not being limited to the slower growth rate of the two individual monocultures supplemented with the missing amino acids (see Figure 5.1 in Appendix). Based on that result, it does seem possible to set up a further optimized *C. glutamicum* based CoNoS that can compete with the WT, as it was shown for *E. coli* before (Pande *et al.*, 2014).

One interesting question in the field of microbial communities is how microbes react to other organisms in their surroundings and how symbiosis develops. In our studies, the cooperation between the two strains was determined mainly as a measure of community growth rate (calculated from growth in the BioLector systems), supported by data about the amino acid production (measured via HPLC, allowing only for snapshots of the respective concentrations at certain time points). Metabolic and transcriptomic changes in the strains, however, could prove to be highly interesting for studying and understanding the used CoNoS. Similar approaches with genetically-engineered auxotrophic strains of *E. coli* strongly suggested such transcriptomic changes upon one strain encountering the other (Hosoda *et al.*, 2011). In this study, for example, they found a global activation of the anabolic metabolism, which included pathways for the specific cross-fed metabolites, instead of only activating specific biosynthetic pathways and transporters (Hosoda *et al.*, 2011). Improved RNAseq methods also enable differential expression analysis between mono- and co-culture, as demonstrated elsewhere, e.g., for a mixed culture of *Phascolarctobacterium faecium* and *Bacteroides thetaiotaomicron* (Ikeyama *et al.*, 2020) and for *Bacillus subtilis* natto and *Bifidobacterium animalis* subsp. *lactis* (Wang *et al.*, 2015). This might also be used to elucidate the transcriptional responses of the *C. glutamicum* CoNoS partner strains but would require a further step of separation of the two strains, based, for example, on fluorescence via a FACS (Hullet *et al.*, 1969) or would require single cell isolation (Gross *et al.*, 2015) and single-cell RNAseq (Tang *et al.*, 2009, Olsen and Baryawno, 2018). This could answer questions regarding the origin and the persistence of symbiosis, factors in its ecology, and symbiotic partner adaptations, which are interesting to be

studied in an artificial community with reduced complexity and good controllability as a model for natural systems (Momeni *et al.*, 2011). The general advantages of laboratory-based microbial model systems to answer such questions unattainable via field observation and field experiments have been pointed out before (Jessup *et al.*, 2004).

When synthetic co-cultures are designed, initial metabolite exchange is most likely not optimal. Evolution, together with the identification of evolved changes, is a powerful tool to improve community growth and to identify bottlenecks. Similar to obligate cross-feeding communities of *E. coli* (Lloyd *et al.*, 2019, Preussger *et al.*, 2020) or lactic acid bacteria in mixed cultures with *S. cerevisiae* (Konstantinidis *et al.*, 2021), coevolution of the ΔARG LEU^{++} ↔ ΔLEU ARG^{+} CoNoS with stable, beneficial mutations occurred over time (Neuheuser, 2022, Zuchowski *et al.*, 2023). Mutations with a beneficial effect on community growth accumulated in both partner strains, which is not uncommon (Hillesland and Stahl, 2010, Lloyd *et al.*, 2019, Preussger *et al.*, 2020). Our finding that genomic changes are primarily related to amino acid import matches with the findings in the mentioned evolved *E. coli* and lactic acid bacteria, in which mainly mutations or duplications in different amino acid uptake systems and transcriptional regulators were found (Lloyd *et al.*, 2019, Konstantinidis *et al.*, 2021). In other examples of sequenced communities, mutations in a porin and a global regulator were found in an evolved *E. coli* strain auxotrophic for L-tryptophan (Shendure *et al.*, 2005), and mutations in a gene for lipopolysaccharide biosynthesis resulted in improved adherence to the (exploited) partner in *P. putida* (Hansen *et al.*, 2007). For sequenced evolved consortia so far, this suggests that the metabolite uptake is often the bottleneck and – if this is relieved – that genomic changes resulting in improved production rather affect transcriptional regulators than the genes for the cross-fed metabolite synthesis pathways.

One potential selective pressure on co-cultures over the long run are culture heterogeneity and cheater-cells, which can often arise in spatially unstructured environments during evolution of *E. coli* and *C. glutamicum* (Hol *et al.*, 2013, Stella *et al.*, 2021). As cross-fed amino acids are a costly public good, cheating by losing the ability to overproduce the amino acid while still benefitting from those produced by others is a valid, selectively favored strategy (West *et al.*, 2007). In case of the ΔARG LEU^{++} ↔ ΔLEU ARG^{+} CoNoS, mutations in the genes encoding the feedback-resistant ArgB and LeuA that yield feedback-sensitive variants again could result in faster individual cell growth, and was presumably also observed in this work, in which some isolated cells of the last batch failed to grow with an unevolved partner strain (see Figure S1, (Zuchowski *et al.*, 2023)). This underlines the importance of testing at least several clones after an ALE. Also, as long as the selective pressure lies on faster growth,

strains with mutations resulting in improved production but slower growth are not favored during the ALE (Dragosits and Mattanovich, 2013). Mutations with relation to transport, however, which give an advantage only to the individual cell, are proof to those cheaters in the long run. Still, valuable novel production traits could be identified by the coevolution of the CoNoS (Zuchowski *et al.*, 2023), exemplifying why the evolution of communities is an interesting new approach for evolution-guided metabolic engineering.

3.2 The CoNoS approach as a new strategy for evolution-guided metabolic engineering

Evolution-guided metabolic engineering harbors the potential to use the power of evolution to improve strain performance via novel ways not considered by rational strain design. This strategy, however, is only effective under specific conditions, and therefore, novel approaches such as the CoNoS concept are a valuable addition. Of main importance for the success of the evolution-guided approach is to link the phenotype of the desired mutation that improves small-molecule production to something easily identifiable such as fitness or fluorescence, which has repeatedly been applied to *C. glutamicum*, as reviewed elsewhere (Stella *et al.*, 2019). ALE experiments to select for increased small molecule production were reported that depended on linking the productivity to growth or product tolerance, as observed for putrescine (Li *et al.*, 2018b), L-ornithine (Jiang *et al.*, 2018) and fatty acids (Takeno *et al.*, 2013). For example, in the case of putrescine, high product concentrations impeded strain growth (Schneider and Wendisch, 2010), which was presumably improved via the ALE, resulting in increased growth rate and production at the same time (Li *et al.*, 2018b). A further possibility is the screening for evolved strains with higher production via coupling production of a small molecule, such as L-valine, to fluorescence in a biosensor-coupled approach (Mahr *et al.*, 2015). Nevertheless, the toolbox for identifying novel production traits not related to improved growth or fitness in *C. glutamicum* as well as in other organisms is limited. Therefore, recent successes in evolving communities that rely on cross-feeding interactions, such as a CoNoS, are promising for evolution-guided metabolic engineering for improved small molecule production (Harcombe, 2010, Preussger *et al.*, 2020, Konstantinidis *et al.*, 2021, Zuchowski *et al.*, 2023). It was proposed that the rate of mutations, i.e., molecular evolution, increases in coevolution approaches, leading to accelerated evolution (Paterson *et al.*, 2010, Schulte *et al.*, 2010), which makes community evolution attractive. It is a matter of debate, though, if this applies mainly to antagonistic behavior or also to mutual cross-feeding interactions (Bergstrom and Lachmann, 2003). The fact that the examples from other working groups were often either not sequenced or that the identified mutations were not reintroduced in the parental strain limits the knowledge

available in that field. However, our success in identifying a yet unknown transporter for L-arginine as a novel production trait proves the high potential of the CoNoS approach. Notably, also the evolution-guided engineering of poorly growing monocultures, such as the ΔTRP strain, was successful in identifying a novel L-tryptophan production trait (see Appendix chapter 5.2), suggesting that this procedure can be a relevant first step for certain CoNoS.

Due to the variety of microorganisms that successfully evolved in communities before, we assume that the CoNoS approach is easily transferrable to other organisms or co-culture setups. However, this concept is limited by the effort and resources of the evolution experiment, especially if the growth rate of the community is high: We failed to evolve a further engineered faster growing ΔARG LEU^{++} ↔ ΔLEU ARG^{++} CoNoS in comparison to the one we successfully evolved with the same 16 repetitive-batches ALE approach (Zuchowski *et al.*, 2023). In a laboratory approach for *E. coli* to gain the capacity to metabolize citrate, this took 31,500 generations in an evolution experiment taking 20 years (Blount *et al.*, 2008), suggesting that significantly longer robotic ALEs might be needed if no "easy" mutations are available such as the inactivation of a repressor. Changing our ALE approach (Radek *et al.*, 2017, Tenhaef *et al.*, 2018, Zuchowski *et al.*, 2023) by choosing to evolve fewer replicates and thereby enabling more transfers per replicate might be one suitable solution, especially since the number of possible paths for proteins to evolve can be very limited (Weinreich *et al.*, 2006). On the other hand, screening not for faster growth but for higher community member fluorescence – either increased eYFP or Crimson signal since both strains harbor a different fluorescent protein – could be a complementary approach, employing a different selection regime for improved small-molecule production similar to biosensor approaches (Dragosits and Mattanovich, 2013, Mahr *et al.*, 2015, Preussger *et al.*, 2020). The problem of identifying mainly false positives with mutations in the fluorophore gene can partly be circumvented, as those mutations would only increase the amount of one signal, while mutations increasing cross-feeding would benefit both strains, yielding two increased signals.

Another considerable challenge of this community evolution concept is that it seems to be hitherto limited to mutations in transporters and transcriptional regulators, as those are the important bottlenecks that can easily be relieved due to mutations (Shendure *et al.*, 2005, Konstantinidis *et al.*, 2021, Zuchowski *et al.*, 2023). Additional approaches therefore need to be developed to reach desired mutations in the biosynthetic machinery, as in the cited approaches, mutations in the biosynthetic machinery were either introduced via metabolic engineering (Zuchowski *et al.*, 2023) or were natural prerequisites by choosing natural producers from a natural isolate collection (Konstantinidis *et al.*, 2021). Based on the mutations

identified in the engineered ΔARG LEU^{++} ↔ ΔLEU ARG^{+} CoNoS, it might be a possible solution to introduce the identified beneficial mutations leading to uptake improvements into the 1st generation CoNoS. In a second ALE experiment, this community with improved transporter capacities could experience a selective pressure that potentially shifted to production improvements. To be noted, in liquid cultures in general, the selective pressure seems to push firmly to improving transport. To circumvent this, an alternative would be using spatially structured environments. In one example, this was previously shown to be a viable way for evolving an *E. coli – Salmonella typhimurium* community (Harcombe, 2010). This approach on minimal medium plates yields increasing local metabolite concentration, improves cell aggregation, and limits cheating (Harcombe, 2010, Stella *et al.*, 2021).

With the community-based evolutionary engineering approach, the identification of further production traits, also for other cross-feeding pairs, should be possible. As long as a mutual dependency is guaranteed, further communities could be set up and evolved, potentially also involving cross-feeding of organic acids, vitamins, and carbohydrates since those are also common (predicted) auxotrophies (Goyal, 2018). Experimentally verified examples of cross-feeding interactions include metabolites such as xylose and acetate (Riviere *et al.*, 2015). However, not all pairings might be possible. As discussed in Appendix chapter 5.1, we were not able to evolve the rapidly growing ΔHIS LEU^{++}↔ ΔLEU HIS^{+} CoNoS with a similar approach as reported (Zuchowski *et al.*, 2023), but instead observed a substantial decrease in growth rate after transfer to the second batch. This points to yet unknown limits of the approach, such as the accumulation of toxic intermediates or the disruption of stable strain ratios. Further refined liquid handling robotic systems that allow for intermediate washing steps or that allow for a flexible, fluorescence-based amount of cells transferred to ensure a minimum cell number of both partner strains could be developed in this regard.

3.3 Studying and improving community dynamics within a CoNoS

Through this work, we studied the growth of synthetic *C. glutamicum* communities in detail. One key parameter for co-culture growth is the ratio between the two partner strains, which was therefore *in silico* modeled with the SteadyCom approach predicting metabolic flux distributions consistent with the steady-state community dynamics (Chan *et al.*, 2017) by our project partners (Bergen, 2021) and compared to our findings via colony PCR, fluorescence signal measurements, and automated cell counting (Schito *et al.*, 2022). The simulated strain distribution takes the different demands of amino acids for the cellular composition into account. Due to the metabolic engineering to relieve growth bottlenecks, the strain ratio for the

differently engineered ΔARG ↔ ΔLEU CoNoS changed with each engineering step (ARG/LEU$^{0/+/+/+}$), also changing which of the two strains is more abundant (Schito *et al.*, 2022). However, the stoichiometry of the fastest growing ΔARG LEU^{++} ↔ ΔLEU ARG^{++} CoNoS is still far from the optimum 67:33 ratio predicted by the model (Schito *et al.*, 2022). The two most critical points of this model might be an incomplete knowledge about the metabolism and the physiology of *C. glutamicum*, as well as that the model does not take the rate and costs of the transport of the cross-fed metabolites into account. Therefore, this ideal ratio can likely not be reached in a biological system (Chan *et al.*, 2017). Further developed gap-filling algorithms that make predictions of metabolic interactions and retrieve fitting biochemical reactions from external databases could be implemented to get better models (Giannari *et al.*, 2021).

To circumvent unbalanced strain ratios, several tools of microbial consortia control were recently developed. These tools would enable us to adjust the strain ratio closer to the modeled or, even better, to an experimentally identified ratio for ideal, efficient cross-feeding rates or, in a different setup, to control the strain ratio for a specific increase in the abundance of the strain used for production purposes. One example are metabolic switches based on the exchange of the promoter of an essential gene with a regulable promoter to tune gene expression by adding specific molecules. For *C. glutamicum*, different examples of nutrient-responsive regulation of single-strain growth via gluconate, vanillin, and *myo*-inositol are known (Baumgart *et al.*, 2016, Siebert *et al.*, 2021). Other examples, such as arabinose- and propionate-inducible plasmid-based expression of secretion or production genes for the cross-fed amino acids, were used to control a synthetic community of L-tyrosine or L-tryptophan auxotrophic *E. coli* strains, allowing for a wide range of strain ratio and overall community growth rate (Kerner *et al.*, 2012, Hol *et al.*, 2014). One regulable synthetic *C. glutamicum* consortium was also already established, comprising an L-lysine auxotrophic strain and an L-lysine producer strain regulated via the inducer IPTG as well as through optogenetic control via photocaged IPTG (Burmeister *et al.*, 2021). However, in those examples, the community did not possess a mutual metabolic dependency, therefore the comparison to a CoNoS is difficult. Optogenetic control was also employed to regulate an *E. coli – S. cerevisiae* community (Lalwani *et al.*, 2021). In monocultures, automated optogenetic control reaches high precision and repeatability in regulating gene expression (Milias-Argeitis *et al.*, 2016). Further potential mechanisms successfully applied in different consortia include quorum-sensing systems based on orthogonal cell-signaling molecules and autoinducers (Chen *et al.*, 2015, Stephens *et al.*, 2019) and peptide-based communication systems (Marchand and Collins, 2013).

To control the strain ratio of a *C. glutamicum* co-culture, a metabolic switch system allowing for efficient regulation of the strain ratio did not exist and had to be developed. In the course of this thesis and a related master thesis, different switches for nutrient-responsive gene regulation to control the ΔARG strain via gluconate, vanillin, and *myo*-inositol were tested (Berger, 2023). The gluconate switch (Baumgart *et al.*, 2016) involving the exchange of the native phosphofructokinase *pfkA* promoter (cg1409) with the promoter of the gluconate kinase *gntK* (cg2732) indeed allowed the regulation of the helper strain growth in relation to the initial gluconate concentration. Due to the gluconate-sensitive promoter in front of the essential *pfkA* gene, expression of *pfkA* was repressed by GntR (gluconate-responsive repressor 1 and 2) after the initially present gluconate was fully metabolized (Frunzke *et al.*, 2008) (see Figure 3.4). The CoNoS growth rates and final backscatter signal were regulable. With this tool, an increased accumulation of L-arginine in the supernatant of the ΔARG LEU^{++} ↔ ΔLEU ARG^{+++} CoNoS was possible, presenting this approach as very interesting for the setup of an L-arginine production process (Figure 3.1).

Another notable insight next to the fluctuations in the strains' ratio was the suggested "island effect", meaning that close physical contact between the cells of the partner strains was required, as shown for growth in the microfluidic chamber, especially during the early stage of cultivation (Schito *et al.*, 2022). A high dilution of the cells and the cross-fed amino acids at low starting ODs also significantly reduced the growth rate (see Figure 5.1B). This became especially relevant when a ΔARG LEU^{++} ↔ ΔLEU ARG^{+++} CoNoS growing with a specific growth rate of μ_{max} = 0.47 ± 0.01 h^{-1} (equivalent to 83% of the WT) in a microscale (800 µL) BioLector experiment was cultivated in a 1 L scale batch experiment (see Figure 5.2). In this initially highly diluted and more heterogeneous environment, a μ_{max} = 0.19 ± 0.01 h^{-1} was observed, equivalent to only 53% of WT growth.

One frequent adaptation in nature as well as in synthetic communities are physical aggregation and filaments or tubule formation (Preussger *et al.*, 2020, Ishii *et al.*, 2005, Wanner *et al.*, 2008). Since *C. glutamicum* does not show autoaggregation naturally, engineering the partner strains for physical adherence might be a viable approach for improving community growth. In general, multiple different principles for increased cell interaction in nature were already described, such as the formation of biofilms, pili, or the presentation of either an antibody-antigen pair or other specific interacting proteins on the cell surface (Proft and Baker, 2009, Flemming *et al.*, 2016, Trunk *et al.*, 2018, Nwoko and Okeke, 2021).

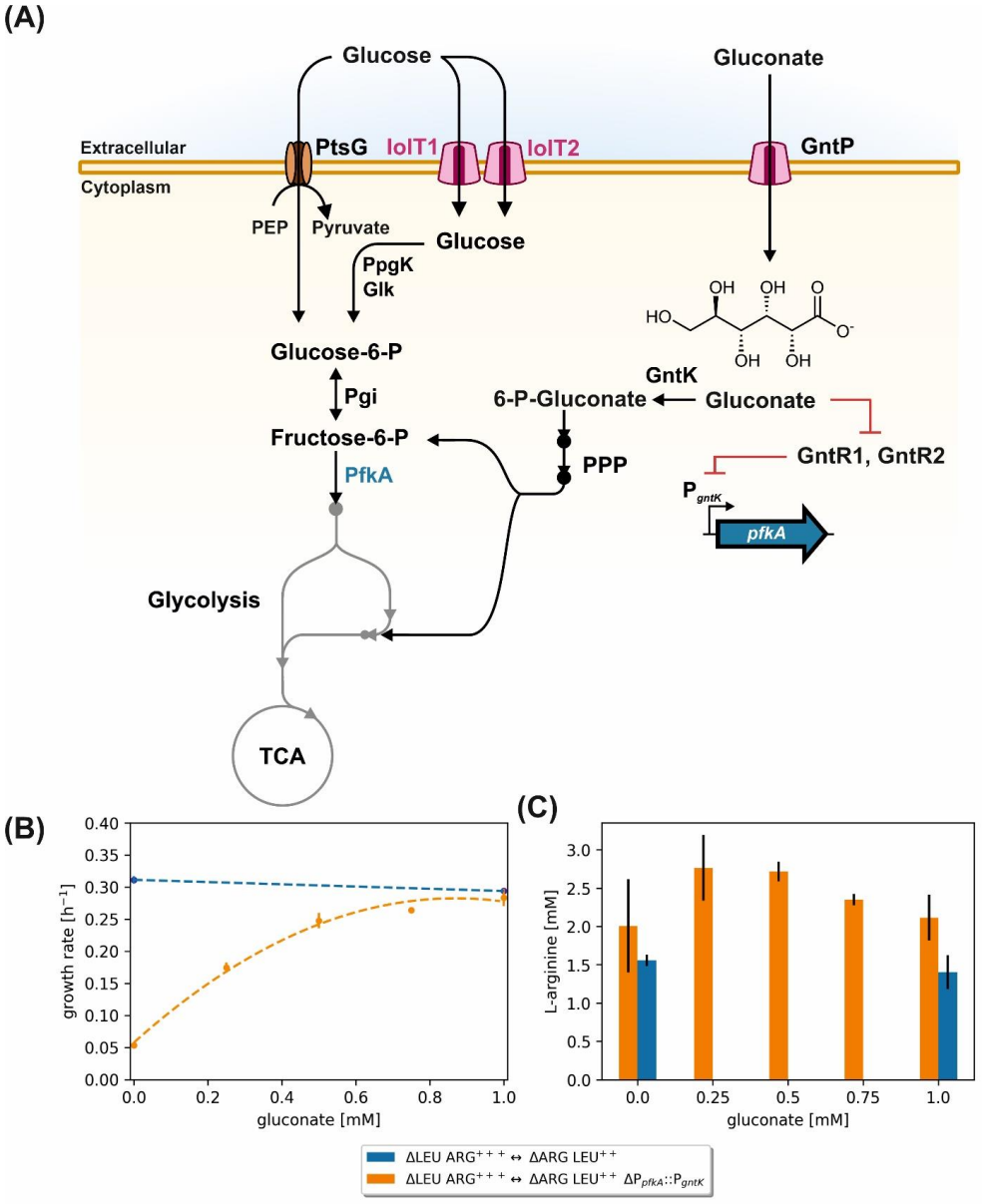

Figure 3.1: Gluconate-dependent regulation of CoNoS growth and L-arginine production **(A)** Primary carbon metabolism of *C. glutamicum* with D-glucose as carbon source. Gluconate is taken up separately from D-glucose and enters the central metabolism via the pentose phosphate pathway (PPP). The native *pfkA* promoter was exchanged with the gluconate-sensitive promoter P_{gntK}, which is repressed by GntR1 and GntR2 in the absence of gluconate, resulting in an interruption of central metabolism. Adapted from (Frunzke *et al.*, 2008, Zelle *et al.*, 2015, Ramp, 2022). **(B)** Characterization of the growth rate of the CoNoS ΔLEU $ARG^{+++} \leftrightarrow$ ΔARG LEU^{++} $\Delta P_{pfkA}::P_{gntK}$ in relation to different initial gluconate concentrations (dashed orange line). The growth rates of this CoNoS are compared to the parental CoNoS ΔLEU $ARG^{+++} \leftrightarrow$ ΔARG LEU^{++} with and without 1 mM gluconate (dashed blue line) **(C)** End-

point determination of L-arginine accumulation in the CoNoS ΔLEU ARG^{+++} ↔ ΔARG LEU^{++} ΔP_{pfkA}::P_{gntK} (orange bars). The L -arginine titer is compared to the parental CoNoS ΔLEU ARG^{+++} ↔ ΔARG LEU^{++} with and without 1 mM gluconate (blue bars). All cultures were performed in triplicate in CGXII medium with 111 mM D-glucose in 800 µL at 30°C and 1400 rpm. CoNoS were inoculated in a 1:1 ratio to OD_{600} = 1. Based on the maximum value recorded for each WT in the respective experiment, the backscatter data were normalized. The mean values are shown as points/bars, and standard deviations as vertical lines. Adapted from (Berger, 2023). Abbreviations: GntK (gluconate kinase), GntP (gluconate permease), GntR1 (gluconate-responsive repressor 1), GntR2 (gluconate-responsive repressor 2), IolT1 (*myo*-Inositol transporter 1), IolT2 (*myo*-Inositol transporter 2), PEP (2-phosphoenolpyruvate), PfkA (6-phosphofructokinase), Pgi (glucose-6-phosphate isomerase), PpgK (polyphosphate glucokinase), PPP (pentose phosphate pathway), PtsG (glucose phosphotransferase system), TCA (tricarboxylic acid cycle).

For stirred tank bioreactors, especially autoaggregation mediated by self-recognizing surface structures such as exopolysaccharides or proteins might be favorable. Examples for *C. glutamicum* are yet lacking, but in *E. coli*, heterologous expression and surface display of YadA of *Yersinia enterocolitica*, for example, resulted in cell aggregation (Trunk *et al.*, 2018). Furthermore, multicellular self-assembly in various patterns could also be conferred to *E. coli* via outer membrane-displayed nanobodies and antigens (Glass and Riedel-Kruse, 2018). Proteins like this could be displayed on the surface of *C. glutamicum* on anchor proteins such as PgsA of *Bacillus subtilis* (Tateno *et al.*, 2007), and several further homologous and heterologous anchor proteins are known (Lee and Kim, 2018). Successful aggregation between the partner strains could then increase the exchange of the cross-fed amino acids, relieving the transport as a bottleneck and thereby improving community growth in large-scale fermentations. Eventually, this could also shift the selective pressure in an ALE experiment from amino acid transport toward a different bottleneck related to production.

3.4 Setting up a production process with a CoNoS

None of the auxotrophic strains had shown a higher growth rate or maximum backscatter as predicted by the *in silico* analyses (Schito *et al.*, 2022) and shown for *E. coli* auxotrophs (D'Souza *et al.*, 2014) before. The additional carbon supply and the energy savings due to the deletion of the highly abundant amino acid synthesis enzymes may still result in a production advantage. For *C. glutamicum* grown on D-glucose as energy and carbon source, the synthesis of 1 mol L-arginine is highly demanding and requires 2 mol ATP and 3 mol NADPH. Providing sufficient cofactors for high L-arginine titers therefore is a metabolic challenge, and metabolic stress could be relieved by the cells not being required to produce those metabolites (Noack and Baumgart, 2019). We analyzed the L-arginine titer of a CoNoS comprising ΔLEU ARG^{+++} as a

producer strain and ΔARG LEU^{++} ΔP_{pfkA}::P_{gntK} as a regulable partner strain to set up a production process in 1 L scale. In addition to previously known targets for metabolic engineering, the genes encoding the L-arginine importer ArgTUV were deleted in the producer strain to prevent the reuptake of the exported product (Zuchowski *et al.*, 2023). Growth and L-arginine production were compared to a WT ARG^{+++} strain, harboring the same modifications for improved L-arginine production without having the auxotrophy for L-leucine (Figure 3.2, see also Appendix 5.1.3).

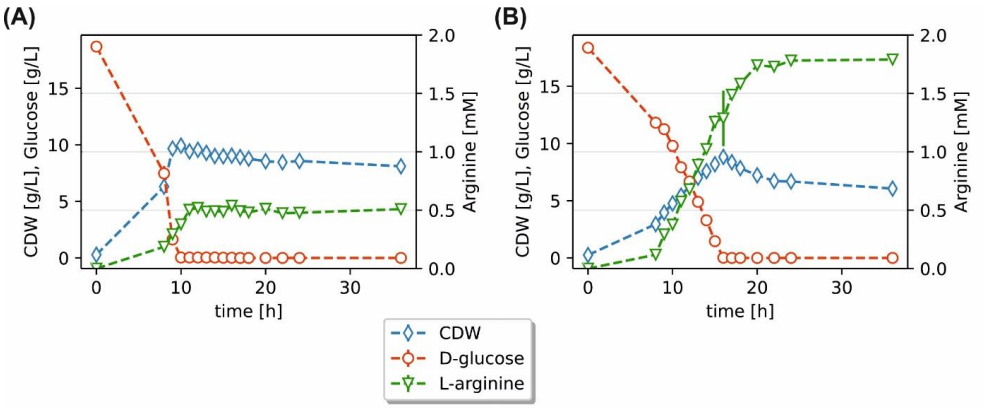

Figure 3.2 Comparison of L-arginine production in 1 L batch cultivation in a CoNoS setup and a WT ARG^{+++} monoculture. The strain WT ARG^{+++} **(A)** and the CoNoS ΔLEU ARG^{+++} ↔ ΔARG LEU^{++} ΔP_{pfkA}::P_{gntK} **(B)** were cultivated in duplicates in CGXII medium with 111 mM D-glucose in a DASGIP 1 L fermentation system. The cultivation was started with an OD_{600} = 1 (i.e., 0.5 per strain in co-culture), and 0.5 mM gluconate was added to the CoNoS. The mean values are shown as diamonds (cell dry weight g/L), circles (D-glucose g/L) and triangles (L-arginine mM), and standard deviations as lines. For further details, see Appendix chapter 5.1.

Astonishingly, a clear increase in L-arginine titer in the CoNoS was observed compared to the reference monoculture, both in a 1 L batch reactor as well as a 1 L fed-batch experiment (see Appendix Figure 5.3). In smaller scales, this result was observed as well (Berger, 2023). This result could indeed implicate that the higher efficiency of communities regarding carbon and energy usage described before (Bernstein *et al.*, 2012, Pande *et al.*, 2014, Yang *et al.*, 2020) can result in improved production, despite the doubts regarding the CoNoS concept (described in chapter 1.3.1). Effects on the production titer could also be attributed to cell lysis effects in the CoNoS, as observable in the CDW development over time. To our knowledge, this is the first time that an increased titer upon introducing selected auxotrophies relieved by cross-feeding interaction in a synthetic co-culture was reported (Noack and Baumgart, 2019).

Previous examples of improved production with natural or synthetic communities exist but are rare (Sabra *et al.*, 2010, Rosero-Chasoy *et al.*, 2021) and can often be related to other factors, such as in the case of increased poly-(3-hydroxybutyrate) (PHB) production to substrates being consumed entirely only in the co-culture (Mohanakrishnan *et al.*, 2020). Other examples, e.g., for improved organic acid production, heavily rely on beneficial synthesis pathway separation on two strains (Li *et al.*, 2018a, Guo *et al.*, 2020) or on spatially separated synergistic fungi (Hölker *et al.*, 2004), which is also not the case for the shown CoNoS, suggesting the discovery of a different way for improving small molecule production utilizing communities.

From these results alone, it cannot be precisely determined what factor is causing this improved L-arginine production. One important hint about the source of the improved production is the observed increase in L-arginine titer related to the L-leucine auxotrophy in a shake flask experiment comparing WT ARG^{+++} and ΔLEU ARG^{+++} (see Appendix chapter 5.1, Figure 5.5). In this experiment, the monoculture ΔLEU ARG^{+++} (supplemented with L-leucine) produced 300% more L-arginine than the strain WT ARG^{+++}. This auxotrophic monoculture also produced 11 % more L-arginine than the CoNoS ΔLEU ARG^{+++} ↔ ΔARG LEU^{++} ΔP_{pfkA}::P_{gntK}. Considering the determined ratio of about 80:20 between the two partner strains (see Appendix Figure 5.3), it seems likely that the carbon and energy loss toward the helper strain caused the lower L-arginine titer compared to the supplemented monoculture. The advantage due to the auxotrophy is in line with the prediction of the CoNoS hypothesis about auxotrophies in production strains. Auxotrophies, including for amino acids, are not uncommon for microbial production strains, as, for example, in an L-tyrosine-auxotrophic L-phenylalanine producing *E. coli* strain (Konstantinov *et al.*, 1991) and an L-methionine and L-isoleucine auxotrophic L-leucine producing *C. glutamicum* strain (Tsuchida and Momose, 1975). The currently best L-arginine producer is auxotrophic for the vitamins biotin and thiamine, and potentially for further metabolites, as the genome of the strain is not published and corn steep liquor, containing vitamins and amino acids, is fed to the strain (Park *et al.*, 2014). For our producer strain ΔLEU ARG^{+++}, it seems likely that the increased production measured in the fermentations is either due to increased efficiency due to the better flow of carbon and energy, which could be related to less concurring side reactions, due to cell lysis effects, or due to specific changes in the transcriptome and proteome due to the auxotrophy. To study this, one crucial first step would be a transcriptomic and proteomic comparison between monocultures of ΔLEU ARG^{+++} and WT ARG^{+++}. Ruling out the possibility that general adaptions to the auxotrophy are at play that result in a generally higher synthesis of other amino acids would be one important step toward nailing down the reason for the increased production with

auxotrophic strains, a prerequisite for a CoNoS. Additionally, it needs to be ruled out that the increases in L-arginine titer result only from increased cell lysis due to the auxotrophy. Both for CoNoS and auxotrophic monocultures in the BioLector (see, e.g., Figure 3 and Figure 6 in (Schito *et al.*, 2022) and Figure 8 in (Zuchowski *et al.*, 2023)), in shake flasks (Appendix Figure 5.5) as well as in the 1 L bioreactor (Figure 3.2), backscatter, OD_{600}, and the CDW development suggested losses in biomass. To sum this up, from these results, it cannot be determined why the introduced L-leucine auxotrophy is resulting in this improved L-arginine production. This proof-of-principle could nevertheless be used as a basis for strains producing on an industrial scale, i.e., producing higher titers and growing in scales far beyond 1 L.

The titer of the process could likely be improved since several other targets for rational metabolic engineering are known (see chapter 1.3.4). In addition, further evolution-guided metabolic engineering could be performed, evolving either the current best CoNoS or a slower-growing CoNoS with improved amino acid uptake to identify further targets. Autoaggregation of the CoNoS strains for improved cross-feeding interactions could also benefit the production process (see chapter 3.3). One critical point is the metabolic switch used to control the CoNoS. From the three switches tried, the switch coupling CoNoS growth to the presence of the inducer molecule gluconate worked best (Berger, 2023). However, other switches might prove to be better. One potential downside of using the gluconate-based switch is the effect of gluconate on other genes in the producer strain. An inactive GntK, for example, was shown to be beneficial for L-ornithine production, a precursor in L-arginine production (Hwang and Cho, 2012). The corresponding gene *gntK*, however, is strongly upregulated in presence of gluconate (Frunzke *et al.*, 2008). Testing further methods of CoNoS regulation, e.g., via an optogenetic approach (see chapter 3.3), could prove to be more beneficial for production, even if those approaches are limited, e.g., by their upscaling capacity.

We currently see numerous options to develop the CoNoS concept further. One CoNoS approach could employ the combination of the producer strain with a “mother strain”. Instead of introducing only one auxotrophy for a central metabolite in the producer strain, several further auxotrophies, e.g., for different amino acids, could still be feasible and increase efficiency. This should not be a metabolic problem since the median of the number of auxotrophies was found in one study to be in the range of 2, and examples of free-living organisms with more than 20 different auxotrophies are known (D'Souza *et al.*, 2014). Since only a surprisingly small fraction of bacteria was found to synthesize the amino acids L-tyrosine, L-phenylalanine, L-histidine, and L-lysine (Mee *et al.*, 2014), those could be ideal further targets for genome reduction. The mother strain, slightly overproducing the respective metabolites,

would provide the producer strain with the relevant metabolites. Synthetic communities with more than two members are also feasible but more difficult to regulate and stabilize (Mee *et al.*, 2014).

3.5 Conclusion

The studies summarized in this thesis describe the design and setup of a synthetic, genome-reduced microbial community according to the CoNoS concept for establishing an L-arginine production process with *C. glutamicum* (Figure 3.3). Mutual dependencies were identified as a sole prerequisite for stable cooperation via cross-feeding to arise, which opened up a lot of possibilities for constructing more stable communities of two or even more *C. glutamicum* strains with different auxotrophies in the future. Based on the constructed auxotrophic strains, both the mono- and co-culture evolution-guided metabolic engineering approach enabled the identification of relevant novel amino acid production traits, such as the L-arginine-importer ArgTUV. Furthermore, unexpected links between the yet uncharacterized *trpP* gene and the function of the *suf* operon and L-tryptophan production were identified in this way. Combining different pairs and following the presented evolution approach, further genes of interest could be identified and characterized. This can also contribute to the identification of the function of yet uncharacterized genes of the biotechnological workhorse *C. glutamicum*.

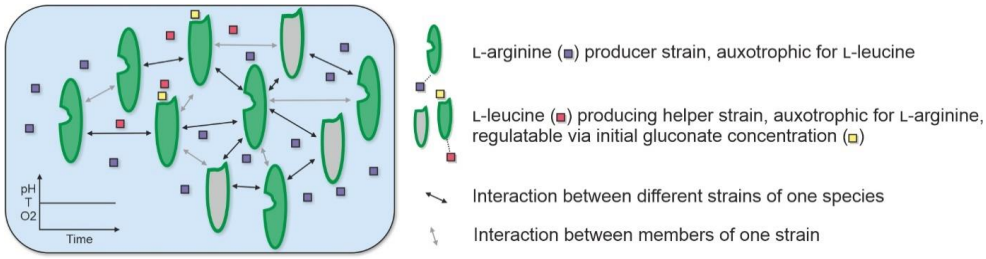

Figure 3.3: Community of Niche-optimized Strains (CoNoS) for L-arginine production. Two *C. glutamicum* strains, a producer strain – harboring an L-leucine auxotrophy and mutations for increased L-arginine production – and a helper strain – harboring an L-arginine auxotrophy and mutations for increased L-leucine production as well as a gluconate dependent metabolic switch – are used to set up a synthetic community. Only by cross-feeding interaction of common goods relieving the specific auxotrophies growth is possible. Growth of the helper strain is controlled via the gluconate concentration (indicated by green color in the presence of gluconate and by grey color without sufficient gluconate). The synthetic community will grow in a bioreactor, enabling tight control of the environmental conditions, e.g., regarding pH, temperature, and O_2 availability. Using a suitable initial gluconate concentration, growth of the helper strain is limited, resulting in a shift in strain ratio towards the L-arginine producer strain, which results in improved L-arginine accumulation. Adapted from (Noack and Baumgart, 2019).

We could show that the L-arginine titer of a CoNoS-based production process consisting of an L-leucine auxotrophic L-arginine producer and a gluconate-regulable L-arginine auxotrophic L-leucine producer can outcompete a fermentation based on pure cultures. We hypothesized that this might be due to energy and carbon savings from the auxotrophy, but critical experiments to prove this are yet missing. Demonstrating a higher carbon flux into the desired product instead of, e.g., biosynthetic enzymes via ^{13}C metabolic flux analysis (MFA) that can discriminate between the different strains could provide important evidence (Weitzel *et al.*, 2013, Gebreselassie and Antoniewicz, 2015). Nevertheless, the reported results are an important step toward even better high-yield production processes, as the introduction of the L-leucine-auxotrophy clearly improved the L-arginine titer. If, for the final process, supplementation of L-leucine or usage of a helper strain in a CoNoS setup is the economically better choice, remains an open question. In general, the increased efficiency of a genome-reduced community presents the CoNoS approach as a relevant concept for bioprocesses, potentially improving the production of L-arginine and further value-added compounds in a sustainable bioeconomy in the future.

4. References

Abe, S., Takayama, K. I. & Kinoshita, S. 1967. Taxonomical studies on glutamic acid producing bacteria. *The Journal of General Applied Microbiology,* 13**,** 279-301.

Aguilar, A., Twardowski, T. & Wohlgemuth, R. 2019. Bioeconomy for Sustainable Development. *Biotechnol J,* 14**,** e1800638.

Alvares, T. S., Meirelles, C. M., Bhambhani, Y. N., Paschoalin, V. M. F. & Gomes, P. S. C. 2011. L-Arginine as a Potential Ergogenic Aid in Healthy Subjects. *Sports Med,* 41**,** 233-248.

Antoniou, E., Fodelianakis, S., Korkakaki, E. & Kalogerakis, N. 2015. Biosurfactant production from marine hydrocarbon-degrading consortia and pure bacterial strains using crude oil as carbon source. *Front Microbiol,* 6**,** 274.

Bailey, J. E. 1991. Towards a science of metabolic engineering. *Science,* 252**,** 1668-1675.

Bakkes, P. J., Ramp, P., Bida, A., Dohmen-Olma, D., Bott, M. & Freudl, R. 2020. Improved pEKEx2-derived expression vectors for tightly controlled production of recombinant proteins in *Corynebacterium glutamicum*. *Plasmid,* 112**,** 102540.

Baumgart, M. & Bott, M. 2011. Biochemical characterisation of aconitase from *Corynebacterium glutamicum*. *J Biotechnol,* 154**,** 163-70.

Baumgart, M., Schubert, K., Bramkamp, M. & Frunzke, J. 2016. Impact of LytR-CpsA-Psr Proteins on Cell Wall Biosynthesis in *Corynebacterium glutamicum*. *J Bacteriol,* 198**,** 3045-3059.

Baumgart, M., Unthan, S., Kloss, R., Radek, A., Polen, T., Tenhaef, N., Muller, M. F., Kuberl, A., Siebert, D., Bruhl, N., Marin, K., Hans, S., Kramer, R., Bott, M., Kalinowski, J., Wiechert, W., Seibold, G., Frunzke, J., Ruckert, C., Wendisch, V. F. & Noack, S. 2017. *Corynebacterium glutamicum* Chassis C1*: Building and Testing a Novel Platform Host for Synthetic Biology and Industrial Biotechnology. *ACS Synth Biol,* 7**,** 132-144.

Baumgart, M., Unthan, S., Rückert, C., Sivalingam, J., Grünberger, A., Kalinowski, J., Bott, M., Noack, S. & Frunzke, J. 2013. Construction of a Prophage-Free Variant of *Corynebacterium glutamicum* ATCC 13032 for Use as a Platform Strain for Basic Research and Industrial Biotechnology. *Applied and Environmental Microbiology,* 79**,** 6006-6015.

Bayan, N., Houssin, C., Chami, M. & Leblon, G. 2003. Mycomembrane and S-layer: two important structures of *Corynebacterium glutamicum* cell envelope with promising biotechnology applications. *J Biotechnol,* 104**,** 55-67.

Becker, J., Rohles, C. M. & Wittmann, C. 2018. Metabolically engineered *Corynebacterium glutamicum* for bio-based production of chemicals, fuels, materials, and healthcare products. *Metab Eng,* 50**,** 122-141.

Beckers, G., Nolden, L. & Burkovski, A. 2001. Glutamate synthase of *Corynebacterium glutamicum* is not essential for glutamate synthesis and is regulated by the nitrogen status. *Microbiology,* 147**,** 2961–2970.

Bergen, D. 2021. *Model-Based Simulation and Analysis of Synthetic Co-Cultures of Corynebacterium glutamicum.* Master thesis, Bielefeld University.

Berger, D. 2023. *Biotechnological production of L-arginine using a Community of Niche-optimized Strains (CoNoS) - Identification and characterization of novel amino acids production traits.* Master thesis, Leibniz University Hanover.

Bergstrom, C. T. & Lachmann, M. 2003. The Red King effect: When the slowest runner wins the coevolutionary race. *Proc Natl Acad Sci U S A,* 100**,** 593-598.

Bernstein, H. C., Paulson, S. D. & Carlson, R. P. 2012. Synthetic *Escherichia coli* consortia engineered for syntrophy demonstrate enhanced biomass productivity. *J Biotechnol,* 157**,** 159-66.

Biebl, H. & Pfennig, N. 1978. Growth Yields of Green Sulfur Bacteria in Mixed Cultures with Sulfur and Sulfate Reducing Bacteria. *Arch Microbiol,* 117**,** 9-16

Binder, S., Schendzielorz, G., Stabler, N., Krumbach, K., Hoffmann, K., Bott, M. & Eggeling, L. 2012. A high-throughput approach to identify genomic variants of bacterial metabolite producers at the single-cell level. *Genome Biol,* 13**,** R40.

Binder, S., Siedler, S., Marienhagen, J., Bott, M. & Eggeling, L. 2013. Recombineering in *Corynebacterium glutamicum* combined with optical nanosensors: a general strategy for fast producer strain generation. *Nucleic Acids Res,* 41**,** 6360-9.

Blount, Z. D., Borland, C. Z. & Lenski, R. E. 2008. Historical contingency and the evolution of a key innovation in an experimental population of *Escherichia coli*. *Proc Natl Acad Sci U S A,* 105**,** 7899–7906.

Bott, M. & Niebisch, A. 2003. The respiratory chain of *Corynebacterium glutamicum*. *J Biotechnol,* 104**,** 129-53.

Brenner, K., You, L. & Arnold, F. H. 2008. Engineering microbial consortia: a new frontier in synthetic biology. *Trends Biotechnol,* 26**,** 483-9.

Brune, I., Jochmann, N., Brinkrolf, K., Hüser, A. T., Gerstmeir, R., Eikmanns, B. J., Kalinowski, J., Pühler, A. & Tauch, A. 2007. The IclR-type transcriptional repressor LtbR regulates the expression of leucine and tryptophan biosynthesis genes in the amino acid producer *Corynebacterium glutamicum*. *J Bacteriol,* 189**,** 2720-2733.

Burmeister, A., Akhtar, Q., Hollmann, L., Tenhaef, N., Hilgers, F., Hogenkamp, F., Sokolowsky, S., Marienhagen, J., Noack, S., Kohlheyer, D. & Grunberger, A. 2021. (Optochemical) Control of Synthetic Microbial Coculture Interactions on a Microcolony Level. *ACS Synth Biol,* 10**,** 1308-1319.

Burmeister, A., Hilgers, F., Langner, A., Westerwalbesloh, C., Kerkhoff, Y., Tenhaef, N., Drepper, T., Kohlheyer, D., Von Lieres, E., Noack, S. & Grunberger, A. 2019. A microfluidic co-cultivation platform to investigate microbial interactions at defined microenvironments. *Lab Chip,* 19**,** 98-110.

Bussmann, M., Baumgart, M. & Bott, M. 2010. RosR (Cg1324), a hydrogen peroxide-sensitive MarR-type transcriptional regulator of *Corynebacterium glutamicum*. *J Biol Chem,* 285**,** 29305-18.

Camacho-Zaragoza, J. M., Hernandez-Chavez, G., Moreno-Avitia, F., Ramirez-Iniguez, R., Martinez, A., Bolivar, F. & Gosset, G. 2016. Engineering of a microbial coculture of *Escherichia coli* strains for the biosynthesis of resveratrol. *Microb Cell Fact,* 15**,** 163.

Chan, S. H. J., Simons, M. N. & Maranas, C. D. 2017. SteadyCom: Predicting microbial abundances while ensuring community stability. *PLoS Comput Biol,* 13**,** e1005539.

Chance, R. E., Kroeff, E. P., Hoffmann, J. A. & Frank, B. H. 1981. Chemical, Physical, and Biologic Properties of Biosynthetic Human Insulin. *Diabetes Care,* 4**,** 147-154.

Chen, Y., Kim, J. K., Hirning, A. J., Josić, K. & Bennett, M. R. 2015. Emergent genetic oscillations in a synthetic microbial consortium. *Science,* 349**,** 986-989.

Choe, D., Cho, S., Kim, S. C. & Cho, B. K. 2016. Minimal genome: Worthwhile or worthless efforts toward being smaller? *Biotechnol J,* 11**,** 199-211.

Cleto, S., Jensen, J. V., Wendisch, V. F. & Lu, T. K. 2016. *Corynebacterium glutamicum* Metabolic Engineering with CRISPR Interference (CRISPRi). *ACS Synth Biol,* 5**,** 375-85.

D'souza, G., Waschina, S., Pande, S., Bohl, K., Kaleta, C. & Kost, C. 2014. Less is more: selective advantages can explain the prevalent loss of biosynthetic genes in bacteria. *Evolution,* 68**,** 2559-70.

Demain, A. L. 2010. History of Industrial Biotechnology. *In:* SOETAERT, W. & VANDAMME, E. J. (eds.) *Industrial Biotechnology: Microorganisms.* . WILEY-VCH Verlag GmbH & Co. KGaA.

Dragosits, M. & Mattanovich, D. 2013. Adaptive laboratory evolution – principles and applications for biotechnology. *Microbial Cell Factories,* 12**,** 1-17.

Ebbighausen, H., Weil, B. & Krämer, R. 1989. Transport of branched-chain amino acids in *Corynebacterium glutamicum*. *Arch. Microbiol.,* 151**,** 238-244.

Eggeling, L. & Bott, M. 2005. *Handbook of Corynebacterium glutamicum*, CRC Press, Boca Raton, USA.

Eggeling, L. & Sahm, H. 2001. The Cell Wall Barrier of *Corynebacterium glutamicum* and Amino Acid Efflux. *JOURNAL OF BIOSCIENCE AND BIOENGINEERING,* 92**,** 201-213.

Elisakova, V., Patek, M., Holatko, J., Nesvera, J., Leyval, D., Goergen, J. L. & Delaunay, S. 2005. Feedback-resistant acetohydroxy acid synthase increases valine production in *Corynebacterium glutamicum*. *Appl Environ Microbiol,* 71**,** 207-13.

Ellermeier, C. D., Hobbs, E. C., Gonzalez-Pastor, J. E. & Losick, R. 2006. A three-protein signaling pathway governing immunity to a bacterial cannibalism toxin. *Cell,* 124**,** 549-59.

Ertan, H. 1992. Some properties of glutamate dehydrogenase, glutamine synthetase and glutamate synthase from *Corynebacterium callunae*. *Arch Microbiol,* 158**,** 35-41.

European-Commission 2012. Innovating for Sustainable Growth -A Bioeconomy for Europe. *In:* INNOVATION, D.-G. F. R. A. (ed.). Luxemburg.

Feng, L. Y., Xu, J. Z. & Zhang, W. G. 2018. Improved L-Leucine Production in *Corynebacterium glutamicum* by Optimizing the Aminotransferases. *Molecules,* 23.

Flavell, R. A., Sabo, D. L., Bandle, E. F. & Weissmann, C. 1975. Site-Directed Mutagenesis: Effect of an Extracistronic Mutation on the In Vitro Propagation of Bacteriophage Qß RNA. *Proc Natl Acad Sci U S A,* 72**,** 367-371.

Fleming, A. 1929. On the antibacterial action of cultures of a penicillium, with special reference to their use in the isolation of *B. influenzae*. *The british Journal of exp. Path.,* 10**,** 226-236.

Flemming, H. C., Wingender, J., Szewzyk, U., Steinberg, P., Rice, S. A. & Kjelleberg, S. 2016. Biofilms: an emergent form of bacterial life. *Nat Rev Microbiol,* 14**,** 563-75.

Frunzke, J., Engels, V., Hasenbein, S., Gatgens, C. & Bott, M. 2008. Co-ordinated regulation of gluconate catabolism and glucose uptake in *Corynebacterium glutamicum* by two functionally equivalent transcriptional regulators, GntR1 and GntR2. *Mol Microbiol,* 67**,** 305-22.

Gebreselassie, N. A. & Antoniewicz, M. R. 2015. ^{13}C-metabolic flux analysis of co-cultures: A novel approach. *Metab Eng,* 31**,** 132-9.

Giannari, D., Ho, C. H. & Mahadevan, R. 2021. A gap-filling algorithm for prediction of metabolic interactions in microbial communities. *PLoS Comput Biol,* 17**,** 26.

Gibson, D. G., Young, L., Chuang, R. Y., Venter, J. C., Hutchison, C. A., 3rd & Smith, H. O. 2009. Enzymatic assembly of DNA molecules up to several hundred kilobases. *Nat Methods,* 6**,** 343-5.

Glass, D. S. & Riedel-Kruse, I. H. 2018. A Synthetic Bacterial Cell-Cell Adhesion Toolbox for Programming Multicellular Morphologies and Patterns. *Cell,* 174**,** 649-658 e16.

Gonzalez-Pastor, J. E., Hobbs, E. C. & Losick, R. 2003. Cannibalism by Sporulating Bacteria. *Science,* 301**,** 510-513.

Gonzalez-Torres, P., Pryszcz, L. P., Santos, F., Martinez-Garcia, M., Gabaldon, T. & Anton, J. 2015. Interactions between closely related bacterial strains are revealed by deep transcriptome sequencing. *Appl Environ Microbiol,* 81**,** 8445-56.

Goyal, A. 2018. Metabolic adaptations underlying genome flexibility in prokaryotes. *PLoS Genet,* 14**,** e1007763.

Grandviewresearch 2023. Amino Acids Market Size, Share & Trends Analysis Report By Raw Material (Plant-based, Animal-based), By Product, By Application, By Livestock In

Animal Feed, By Region, And Segment Forecasts, 2023 - 2030. *In:* RESEARCH, G. V. (ed.). https://www.grandviewresearch.com/industry-analysis/amino-acids-market, accessed 20.01.2023.

Gross, A., Schoendube, J., Zimmermann, S., Steeb, M., Zengerle, R. & Koltay, P. 2015. Technologies for Single-Cell Isolation. *Int J Mol Sci,* 16**,** 16897-919.

Grund, T. N., Kabashima, Y., Kusumoto, T., Wu, D., Welsch, S., Sakamoto, J., Michel, H. & Safarian, S. 2022. The cryoEM structure of cytochrome bd from *C. glutamicum* provides novel insights into structural properties of actinobacterial terminal oxidases. *Front Chem,* 10**,** 1085463.

Guerrero, R., Pedros-Alio, C., Esteve, I., Mas, J., Chase, D. & Margulis, L. 1986. Predatory prokaryotes: Predation and primary consumption evolved in bacteria. *Proc Natl Acad Sci U S A,* 83**,** 2138-2142.

Guo, X., Wang, X., Chen, T., Lu, Y. & Zhang, H. 2020. Comparing *E. coli* mono-cultures and co-cultures for biosynthesis of protocatechuic acid and hydroquinone. *Biochemical Engineering Journal,* 156.

Hallgren, J., Tsirigos, K. D., Pedersen, M. D., Almagro Armenteros, J. J., Marcatili, P., Nielsen, H., Krogh, A. & Winther, O. 2022. DeepTMHMM predicts alpha and beta transmembrane proteins using deep neural networks. *bioRxiv*.

Hanahan, D. 1983. Studies on transformation of *Escherichia coli* with plasmids. *J Mol Biol,* 166**,** 557-580.

Hansen, S. K., Rainey, P. B., Haagensen, J. A. & Molin, S. 2007. Evolution of species interactions in a biofilm community. *Nature,* 445**,** 533-6.

Hänßler, E., Müller, T., Jessberger, N., Völzke, A., Plassmeier, J., Kalinowski, J., Krämer, R. & Burkovski, A. 2007. FarR, a putative regulator of amino acid metabolism in *Corynebacterium glutamicum*. *Appl Microbiol Biotechnol,* 76**,** 625-632.

Harcombe, W. 2010. Novel cooperation experimentally evolved between species. *Evolution,* 64**,** 2166-72.

Hashimoto, S. I. 2017. Discovery and History of Amino Acid Fermentation. *Adv Biochem Eng Biotechnol,* 159**,** 15-34.

Hays, S. G., Patrick, W. G., Ziesack, M., Oxman, N. & Silver, P. A. 2015. Better together: engineering and application of microbial symbioses. *Curr Opin Biotechnol,* 36**,** 40-9.

Heery, D. M. & Dunican, L. K. 1993. Cloning of the *trp* Gene Cluster from a Tryptophan-Hyperproducing Strain of *Corynebacterium glutamicum*: Identification of a Mutation in the *trp* Leader Sequence. *APPLIED AND ENVIRONMENTAL MICROBIOLOGY***,** 791-799.

Heery, D. M., Fitzpatrick, R. & Dunican, L. K. 1994. A sequence from a tryptophan-hyperproducing strain of *Corynebacterium glutamicum* encoding resistance to 5-methyltryptophan. *Biochemical and Biophysical Research communication,* 201**,** 1255-1262.

Helling, R. B., Vargas, C. N. & Adams, J. 1987. Evolution of *Escherichia coli* during growth in a constant environment. . *Genetics,* 116**,** 349-358.

Henriksen, N., Hansen, M. F., Kiesewalter, H. T., Russel, J., Nesme, J., Foster, K. R., Svensson, B., Oregaard, G., Herschend, J. & Burmolle, M. 2022. Biofilm cultivation facilitates coexistence and adaptive evolution in an industrial bacterial community. *NPJ Biofilms Microbiomes,* 8**,** 59.

Hermann, T. 2003. Industrial production of amino acids by coryneform bacteria. *J Biotechnol,* 104**,** 155-72.

Hibbing, M. E., Fuqua, C., Parsek, M. R. & Peterson, S. B. 2010. Bacterial competition: surviving and thriving in the microbial jungle. *Nat Rev Microbiol,* 8**,** 15-25.

Hillesland, K. L. & Stahl, D. A. 2010. Rapid evolution of stability and productivity at the origin of a microbial mutualism. *Proc Natl Acad Sci U S A,* 107**,** 2124-9.

Hol, F. J., Galajda, P., Nagy, K., Woolthuis, R. G., Dekker, C. & Keymer, J. E. 2013. Spatial structure facilitates cooperation in a social dilemma: empirical evidence from a bacterial community. *PLoS One,* 8**,** e77042.

Hol, F. J. H., Voges, M. J., Dekker, C. & Keymer, J. E. 2014. Nutrient-responsive regulation determines biodiversity in a colicin-mediated bacterial community. *BMC Biology,* 12**,** 1-14.

Hölker, U., Höfer, M. & Lenz, J. 2004. Biotechnological advantages of laboratory-scale solid-state fermentation with fungi. *Appl Microbiol Biotechnol,* 64**,** 175-86.

Hosoda, K., Suzuki, S., Yamauchi, Y., Shiroguchi, Y., Kashiwagi, A., Ono, N., Mori, K. & Yomo, T. 2011. Cooperative Adaptation to Establishment of a Synthetic Bacterial Mutualism. *PLoS ONE,* 6.

Hullet, H. R., Bonner, W. A., Barrett, J. & Herzenberg, L. A. 1969. Cell Sorting: Automated Separation of Mammalian Cells as a Function of Intracellular Fluorescence. *Science,* 166**,** 747-749.

Hutchison, C. A., 3rd, Chuang, R. Y., Noskov, V. N., Assad-Garcia, N., Deerinck, T. J., Ellisman, M. H., Gill, J., Kannan, K., Karas, B. J., Ma, L., Pelletier, J. F., Qi, Z. Q., Richter, R. A., Strychalski, E. A., Sun, L., Suzuki, Y., Tsvetanova, B., Wise, K. S., Smith, H. O., Glass, J. I., Merryman, C., Gibson, D. G. & Venter, J. C. 2016. Design and synthesis of a minimal bacterial genome. *Science,* 351**,** aad6253.

Hwang, G. H. & Cho, J. Y. 2012. Implication of gluconate kinase activity in L-ornithine biosynthesis in *Corynebacterium glutamicum*. *J Ind Microbiol Biotechnol,* 39**,** 1869-74.

Ikeda, M., Mitsuhashi, S., Tanaka, K. & Hayashi, M. 2009. Reengineering of a *Corynebacterium glutamicum* L-arginine and L-citrulline producer. *Appl Environ Microbiol,* 75**,** 1635-41.

Ikeda, M. & Nakagawa, S. 2003. The *Corynebacterium glutamicum* genome: features and impacts on biotechnological processes. *Appl Microbiol Biotechnol,* 62**,** 99-109.

Ikeyama, N., Murakami, T., Toyoda, A., Mori, H., Iino, T., Ohkuma, M. & Sakamoto, M. 2020. Microbial interaction between the succinate-utilizing bacterium *Phascolarctobacterium faecium* and the gut commensal *Bacteroides thetaiotaomicron*. *Microbiologyopen,* 9**,** e1111.

Ishii, S., Kosaka, T., Hori, K., Hotta, Y. & Watanabe, K. 2005. Coaggregation facilitates interspecies hydrogen transfer between *Pelotomaculum thermopropionicum* and *Methanothermobacter thermautotrophicus*. *Appl Environ Microbiol,* 71**,** 7838-45.

Jackson, D. A., Symons, R. H. & Berg, P. 1972. Biochemical Method for Inserting New Genetic Information into DNA of Simian Virus 40: Circular SV40 DNA Molecules Containing Lambda Phage Genes and the Galactose Operon of Escherichia coli. *Proc Natl Acad Sci U S A,* 69**,** 2904-2909.

Jensen, J. V. & Wendisch, V. F. 2013. Ornithine cyclodeaminase-based proline production by *Corynebacterium glutamicum*. *Microbial Cell Factories,* 12**,** 1-10.

Jessup, C. M., Kassen, R., Forde, S. E., Kerr, B., Buckling, A., Rainey, P. B. & Bohannan, B. J. 2004. Big questions, small worlds: microbial model systems in ecology. *Trends Ecol Evol,* 19**,** 189-97.

Jiang, L. Y., Chen, S. G., Zhang, Y. Y. & Liu, J. Z. 2018. Metabolic evolution of *Corynebacterium glutamicum* for increased production of L-ornithine. *BMC Biotechnology,* 13.

Jiang, Y., Qian, F., Yang, J., Liu, Y., Dong, F., Xu, C., Sun, B., Chen, B., Xu, X., Li, Y., Wang, R. & Yang, S. 2017. CRISPR-Cpf1 assisted genome editing of *Corynebacterium glutamicum*. *Nat Commun,* 8**,** 15179.

Jinek, M., Chylinski, K., Fonfara, I., Hauer, M., Doudna, J. A. & Charpentier, E. 2012. A Programmable Dual-RNA–Guided DNA Endonuclease in Adaptive Bacterial Immunity. *Science,* 337**,** 816-821.

Johnson, I. S. 1983. Human Insulin from Recombinant DNA Technology. *Science,* 219**,** 632-637.

Jurkevitch, E. & Davidov, Y. 2006. Phylogenetic Diversity and Evolution of Predatory Prokaryotes. *In:* JURKEVITCH, E. (ed.) *Predatory Prokaryotes.* Berlin Heidelberg: Springer-Verlag.

Kabus, A., Niebisch, A. & Bott, M. 2007. Role of cytochrome bd oxidase from *Corynebacterium glutamicum* in growth and lysine production. *Appl Environ Microbiol,* 73**,** 861-8.

Kalinowski, J., Bathe, B., Bartels, D., Bischoff, N., Bott, M., Burkovski, A., Dusch, N., Eggeling, L., Eikmanns, B. J., Gaigalat, L., Goesmann, A., Hartmann, M., Huthmacher, K., Krämer, R., Linke, B., Mchardy, A. C., Meyer, F., Möckel, B., Pfefferle, W., Pühler, A., Rey, D. A., Rückert, C., Rupp, O., Sahm, H., Wendisch, V. F., Wiegräbe, I. & Tauch, A. 2003. The complete *Corynebacterium glutamicum* ATCC 13032 genome sequence and its impact on the production of L-aspartate-derived amino acids and vitamins. *Journal of Biotechnology,* 104**,** 5-25.

Keilhauer, C., Eggeling, L. & Sahm, H. 1993. Isoleucine Synthesis in *Corynebacterium glutamicum*: Molecular Analysis of the *ilvB-ilvN-ilvC* Operon. *Journal of Bacteriology,* 175**,** 5595-5603.

Kennerknecht, N., Sahm, H., Yen, M. R., Patek, M., Saier Jr, M. H., Jr. & Eggeling, L. 2002. Export of L-isoleucine from *Corynebacterium glutamicum*: a two-gene-encoded member of a new translocator family. *J Bacteriol,* 184**,** 3947-56.

Kerner, A., Park, J., Williams, A. & Lin, X. N. 2012. A programmable *Escherichia coli* consortium via tunable symbiosis. *PLoS One,* 7**,** e34032.

Kinoshita, S., Udaka, S. & Shimono, M. 1957. Studies on the amino acid fermentation. Part 1. Production of L-glutamic acid by various microorganisms. *Journal of General and Applied Microbiology,* 3**,** 193-205.

Kirchner, O. & Tauch, A. 2003. Tools for genetic engineering in the amino acid-producing bacterium *Corynebacterium glutamicum*. *J Biotechnol,* 104**,** 287-99.

Kondoh, M. & Hirasawa, T. 2019. L-Cysteine production by metabolically engineered *Corynebacterium glutamicum*. *Appl Microbiol Biotechnol,* 103**,** 2609-2619.

Konstantinidis, D., Pereira, F., Geissen, E. M., Grkovska, K., Kafkia, E., Jouhten, P., Kim, Y., Devendran, S., Zimmermann, M. & Patil, K. R. 2021. Adaptive laboratory evolution of microbial co-cultures for improved metabolite secretion. *Mol Syst Biol,* 17**,** e10189.

Konstantinov, K. B., Nishio, N., Seki, T. & Yoshida, T. 1991. Physiologically Motivated Strategies for Control of the Fed-Batch Cultivation of Recombinant *Escherichia coli* for Phenylalanine Production. *Journal of Fermentation and Bioengineering,* 71**,** 350-355.

Kraxner, K. J., Polen, T., Baumgart, M. & Bott, M. 2019. The conserved actinobacterial transcriptional regulator FtsR controls expression of *ftsZ* and further target genes and influences growth and cell division in *Corynebacterium glutamicum*. *BMC Microbiol,* 19**,** 179.

Kronemeyer, W., Peekhaus, N., Krämer, R., Sahm, H. & Eggeling, L. 1995. Structure of the *gluABCD* cluster encoding the glutamate uptake system of *Corynebacterium glutamicum*. *J Bacteriol,* 177**,** 1152-8.

Kulis-Horn, R. K., Persicke, M. & Kalinowski, J. 2014. Histidine biosynthesis, its regulation and biotechnological application in *Corynebacterium glutamicum*. *Microb Biotechnol,* 7**,** 5-25.

Kulis-Horn, R. K., Persicke, M. & Kalinowski, J. 2015. *Corynebacterium glutamicum* ATP-phosphoribosyl transferases suitable for L-histidine production--Strategies for the elimination of feedback inhibition. *J Biotechnol,* 206**,** 26-37.

Lalwani, M. A., Kawabe, H., Mays, R. L., Hoffman, S. M. & Avalos, J. L. 2021. Optogenetic Control of Microbial Consortia Populations for Chemical Production. *ACS Synth Biol,* 10**,** 2015-2029.

Lamsa, A., Liu, W. T., Dorrestein, P. C. & Pogliano, K. 2012. The *Bacillus subtilis* cannibalism toxin SDP collapses the proton motive force and induces autolysis. *Mol Microbiol,* 84**,** 486-500.

Lapierre, P. & Gogarten, J. P. 2009. Estimating the size of the bacterial pan-genome. *Trends Genet,* 25**,** 107-10.

Lee, J. H. & Wendisch, V. F. 2017. Production of amino acids - Genetic and metabolic engineering approaches. *Bioresour Technol,* 245**,** 1575-1587.

Lee, M. J. & Kim, P. 2018. Recombinant Protein Expression System in *Corynebacterium glutamicum* and Its Application. *Front Microbiol,* 9**,** 2523.

Lee, S. Y. & Kim, H. U. 2015. Systems strategies for developing industrial microbial strains. *Nat Biotechnol,* 33**,** 1061-72.

Lee, S. Y., Kim, H. U., Chae, T. U., Cho, J. S., Kim, J. W., Shin, J. H., Kim, D. I., Ko, Y.-S., Jang, W. D. & Jang, Y.-S. 2019. A comprehensive metabolic map for production of bio-based chemicals. *Nature Catalysis,* 2**,** 18-33.

Leyval, D., Uy, D., Delaunay, S., Goergen, J. L. & Engasser, J. M. 2003. Characterisation of the enzyme activities involved in the valine biosynthetic pathway in a valine-producing strain of *Corynebacterium glutamicum*. *J Biotechnol,* 104**,** 241-52.

Li, T., Zhou, W., Bi, H., Zhuang, Y., Zhang, T. & Liu, T. 2018a. Production of caffeoylmalic acid from glucose in engineered *Escherichia coli*. *Biotechnol Lett,* 40**,** 1057-1065.

Li, Z., Shen, Y. P., Jiang, X. L., Feng, L. S. & Liu, J. Z. 2018b. Metabolic evolution and a comparative omics analysis of *Corynebacterium glutamicum* for putrescine production. *J Ind Microbiol Biotechnol,* 45**,** 123-139.

Limberg, M. H., Schulte, J., Aryani, T., Mahr, R., Baumgart, M., Bott, M., Wiechert, W. & Oldiges, M. 2016. Metabolic profile of 1,5-diaminopentane producing *Corynebacterium glutamicum* under scale-down conditions: Blueprint for robustness to bioreactor inhomogeneities. *Biotechnol Bioeng,* 114**,** 560-575.

Liu, W. T., Yang, Y. L., Xu, Y., Lamsa, A., Haste, N. M., Yang, J. Y., Ng, J., Gonzalez, D., Ellermeier, C. D., Straight, P. D., Pevzner, P. A., Pogliano, J., Nizet, V., Pogliano, K. & Dorrestein, P. C. 2010. Imaging mass spectrometry of intraspecies metabolic exchange revealed the cannibalistic factors of *Bacillus subtilis*. *Proc Natl Acad Sci U S A,* 107**,** 16286-90.

Lloyd, C. J., King, Z. A., Sandberg, T. E., Hefner, Y., Olson, C. A., Phaneuf, P. V., O'brien, E. J., Sanders, J. G., Salido, R. A., Sanders, K., Brennan, C., Humphrey, G., Knight, R. & Feist, A. M. 2019. The genetic basis for adaptation of model-designed syntrophic co-cultures. *PLoS Comput Biol,* 15**,** e1006213.

Löffler, M., Simen, J. D., Jäger, G., Schäferhoff, K., Freund, A. & Takors, R. 2016. Engineering *E. coli* for large-scale production - Strategies considering ATP expenses and transcriptional responses. *Metab Eng,* 38**,** 73-85.

Lubitz, D., Jorge, J. M., Perez-Garcia, F., Taniguchi, H. & Wendisch, V. F. 2016. Roles of export genes *cgmA* and *lysE* for the production of L-arginine and L-citrulline by *Corynebacterium glutamicum*. *Appl Microbiol Biotechnol,* 100**,** 8465-74.

Mahr, R., Gatgens, C., Gatgens, J., Polen, T., Kalinowski, J. & Frunzke, J. 2015. Biosensor-driven adaptive laboratory evolution of L-valine production in *Corynebacterium glutamicum*. *Metab Eng,* 32**,** 184-194.

Makrides, S. C. 1996. Strategies for Achieving High-Level Expression of Genes in *Escherichia coli*. *Microbiological Reviews,* 60**,** 512-538.

Marchand, N. & Collins, C. H. 2013. Peptide-based communication system enables *Escherichia coli* to *Bacillus megaterium* interspecies signaling. *Biotechnol Bioeng,* 110**,** 3003-12.

Martinez-Garcia, E., Nikel, P. I., Chavarria, M. & De Lorenzo, V. 2014. The metabolic cost of flagellar motion in *Pseudomonas putida* KT2440. *Environ Microbiol,* 16**,** 291-303.

Matsui, K., Miwa, K. & Sano, K. 1987. Two Single-Base-Pair Substitutions Causing Desensitization to Tryptophan Feedback Inhibition of Anthranilate Synthase and Enhanced Expression of Tryptophan Genes of *Brevibacterium lactofermentum*. *Journal of Bacteriology,* 169**,** 5330-5332.

Mccarty, N. S. & Ledesma-Amaro, R. 2019. Synthetic Biology Tools to Engineer Microbial Communities for Biotechnology. *Trends Biotechnol,* 37**,** 181-197.

Mcnally, A., Oren, Y., Kelly, D., Pascoe, B., Dunn, S., Sreecharan, T., Vehkala, M., Valimaki, N., Prentice, M. B., Ashour, A., Avram, O., Pupko, T., Dobrindt, U., Literak, I., Guenther, S., Schaufler, K., Wieler, L. H., Zhiyong, Z., Sheppard, S. K., Mcinerney, J. O. & Corander, J. 2016. Combined Analysis of Variation in Core, Accessory and Regulatory Genome Regions Provides a Super-Resolution View into the Evolution of Bacterial Populations. *PLoS Genet,* 12**,** e1006280.

Mcnally, C. P. & Borenstein, E. 2018. Metabolic model-based analysis of the emergence of bacterial cross-feeding via extensive gene loss. *BMC Syst Biol,* 12**,** 69.

Mee, M. T., Collins, J. J., Church, G. M. & Wang, H. H. 2014. Syntrophic exchange in synthetic microbial communities. *Proc Natl Acad Sci U S A,* 111**,** E2149-56.

Mee, M. T. & Wang, H. H. 2012. Engineering ecosystems and synthetic ecologies. *Mol Biosyst,* 8**,** 2470-83.

Mentz, A., Neshat, A., Pfeifer-Sancar, K., Pühler, A., Rückert, C. & Kalinowski, J. 2013. Comprehensive discovery and characterization of small RNAs in *Corynebacterium glutamicum* ATCC 13032. *BMC Genomics,* 14**,** 1-16.

Mertz, J. E. & Davis, R. W. 1972. Cleavage of DNA by RI Restriction Endonuclease Generates Cohesive Ends. *Proc Natl Acad Sci U S A,* 69**,** 3370-3374.

Milias-Argeitis, A., Rullan, M., Aoki, S. K., Buchmann, P. & Khammash, M. 2016. Automated optogenetic feedback control for precise and robust regulation of gene expression and cell growth. *Nat Commun,* 7**,** 12546.

Minty, J. J., Singer, M. E., Scholz, S. A., Bae, C. H., Ahn, J. H., Foster, C. E., Liao, J. C. & Lin, X. N. 2013. Design and characterization of synthetic fungal-bacterial consortia for direct production of isobutanol from cellulosic biomass. *Proc Natl Acad Sci U S A,* 110**,** 14592-7.

Mohanakrishnan, A. S., Easwaran, S. N., Ravi, D. P. & Mahadevan, S. 2020. Understanding the biocalorimetric and respirometric behaviour of co-culture (*R. eutropha*, *P. putida* and *A. vinelandii*) in poly (3-hydroxybutyrate) batch production. *Biochemical Engineering Journal,* 155.

Momeni, B., Chen, C. C., Hillesland, K. L., Waite, A. & Shou, W. 2011. Using artificial systems to explore the ecology and evolution of symbioses. *Cell Mol Life Sci,* 68**,** 1353-68.

Mormann, S., Lomker, A., Ruckert, C., Gaigalat, L., Tauch, A., Puhler, A. & Kalinowski, J. 2006. Random mutagenesis in *Corynebacterium glutamicum* ATCC 13032 using an IS6100-based transposon vector identified the last unknown gene in the histidine biosynthesis pathway. *BMC Genomics,* 7**,** 205.

Morris, J. J. 2015. Black Queen evolution: the role of leakiness in structuring microbial communities. *Trends Genet,* 31**,** 475-82.

Morris, J. J., Johnson, Z. I., Szul, M. J., Keller, M. & Zinser, E. R. 2011. Dependence of the Cyanobacterium *Prochlorococcus* on hydrogen peroxide scavenging microbes for growth at the ocean's surface. *PLoS One,* 6**,** e16805.

Morris, J. J., Lenski, R. E. & Zinser, E. R. 2012. The Black Queen Hypothesis: evolution of dependencies through adaptive gene loss. *mBio,* 3.

Müller, W., Weber, H., Meyer, F. & Weissmann, C. 1978. Site-directed Mutagenesis in DNA: Generation of Point Mutations in Cloned β Globin Complementary DNA at the Positions Corresponding to Amino Acids 121 to 123. *J. Mol. Biol.,* 124**,** 343-358.

Nakamura, J., Hirano, S., Ito, H. & Wachi, M. 2007. Mutations of the *Corynebacterium glutamicum* NCgl1221 gene, encoding a mechanosensitive channel homolog, induce L-glutamic acid production. *Appl Environ Microbiol,* 73**,** 4491-8.

Netzer, R., Peters-Wendisch, P., Eggeling, L. & Sahm, H. 2004. Cometabolism of a nongrowth substrate: L-serine utilization by *Corynebacterium glutamicum*. *Appl Environ Microbiol,* 70**,** 7148-55.

Neuenschwander, S. M., Ghai, R., Pernthaler, J. & Salcher, M. M. 2018. Microdiversification in genome-streamlined ubiquitous freshwater Actinobacteria. *ISME J,* 12**,** 185-198.

Neuheuser, F. 2022. *Analysis of mutations identified in an evolved Corynebacterium glutamicum community composed of strains ΔARG and ΔLEU.* Master thesis, RWTH Aachen.

Nielsen, J. & Keasling, J. D. 2016. Engineering Cellular Metabolism. *Cell,* 164**,** 1185-1197.

Nishimura, T., Teramoto, H., Vertes, A. A., Inui, M. & Yukawa, H. 2008. ArnR, a novel transcriptional regulator, represses expression of the *narKGHJI* operon in *Corynebacterium glutamicum*. *J Bacteriol,* 190**,** 3264-73.

Noack, S. & Baumgart, M. 2019. Communities of Niche-Optimized Strains: Small-Genome Organism Consortia in Bioproduction. *Trends Biotechnol,* 37**,** 126-139.

Noack, S., Voges, R., Gätgens, J. & Wiechert, W. 2017. The linkage between nutrient supply, intracellular enzyme abundances and bacterial growth: New evidences from the central carbon metabolism of *Corynebacterium glutamicum*. *J Biotechnol,* 258**,** 13-24.

Nowak, M. & May, R. M. 1992. Evolutionary games and spatial chaos. *Nature,* 359**,** 826-829.

Nwoko, E. Q. A. & Okeke, I. N. 2021. Bacteria autoaggregation: how and why bacteria stick together. *Biochem Soc Trans,* 49**,** 1147-1157.

O'brien, E. J., Utrilla, J. & Palsson, B. O. 2016. Quantification and Classification of *E. coli* Proteome Utilization and Unused Protein Costs across Environments. *PLoS Comput Biol,* 12**,** e1004998.

Olsen, T. K. & Baryawno, N. 2018. Introduction to Single-Cell RNA Sequencing. *Curr Protoc Mol Biol,* 122**,** e57.

Paczia, N., Nilgen, A., Lehmann, T., Gätgens, J., Wiechert, W. & Noack, S. 2012. Extensive exometabolome analysis reveals extended overflow metabolism in various microorganisms. *Microbial Cell Factories,* 11.

Pande, S., Merker, H., Bohl, K., Reichelt, M., Schuster, S., De Figueiredo, L. F., Kaleta, C. & Kost, C. 2014. Fitness and stability of obligate cross-feeding interactions that emerge upon gene loss in bacteria. *ISME J,* 8**,** 953-62.

Parise, M. T. D., Parise, D., Kato, R. B., Pauling, J. K., Tauch, A., Azevedo, V. a. C. & Baumbach, J. 2020. CoryneRegNet 7, the reference database and analysis platform for corynebacterial gene regulatory networks. *Sci Data,* 7**,** 9.

Park, S. H., Kim, H. U., Kim, T. Y., Park, J. S., Kim, S. S. & Lee, S. Y. 2014. Metabolic engineering of *Corynebacterium glutamicum* for L-arginine production. *Nat Commun,* 5**,** 4618.

Patek, M., Hochmannova, J., Jelinkova, M., Nesvera, J. & Eggeling, L. 1998. Analysis of the *leuB* gene from *Corynebacterium glutamicum*. *Appl Microbiol Biotechnol,* 50**,** 42-47.

Patek, M., Krumbach, K., Eggeling, L. & Sahm, H. 1994. Leucine Synthesis in *Corynebacterium glutamicum*: Enzyme Activities, Structure of leuA, and Effect of *leuA* Inactivation on Lysine Synthesis. *APPLIED AND ENVIRONMENTAL MICROBIOLOGY,* 60**,** 133-140.

Paterson, S., Vogwill, T., Buckling, A., Benmayor, R., Spiers, A. J., Thomson, N. R., Quail, M., Smith, F., Walker, D., Libberton, B., Fenton, A., Hall, N. & Brockhurst, M. A. 2010. Antagonistic coevolution accelerates molecular evolution. *Nature,* 464**,** 275-8.

Paysan-Lafosse, T., Blum, M., Chuguransky, S., Grego, T., Pinto, B. L., Salazar, G. A., Bileschi, M. L., Bork, P., Bridge, A., Colwell, L., Gough, J., Haft, D. H., Letunic, I., Marchler-Bauer, A., Mi, H., Natale, D. A., Orengo, C. A., Pandurangan, A. P., Rivoire, C., Sigrist, C. J. A., Sillitoe, I., Thanki, N., Thomas, P. D., Tosatto, S. C. E., Wu, C. H. & Bateman, A. 2023. InterPro in 2022. *Nucleic Acids Res,* 51**,** D418-D427.

Perez Morales, T. G., Ho, T. D., Liu, W. T., Dorrestein, P. C. & Ellermeier, C. D. 2013. Production of the cannibalism toxin SDP is a multistep process that requires SdpA and SdpB. *J Bacteriol,* 195**,** 3244-51.

Peter, H., Bader, A., Burkovski, A., Lambert, C. & Krämer, R. 1997. Isolation of the *putP* gene of *Corynebacterium glutamicum* and characterization of a low-affinity uptake system for compatible solutes. *Arch Microbiol,* 168**,** 143-51.

Peter, H., Weil, B., Burkovski, A., Krämer, R. & Morbach, S. 1998. *Corynebacterium glutamicum* is equipped with four secondary carriers for compatible solutes: identification, sequencing, and characterization of the proline/ectoine uptake system, ProP, and the ectoine/proline/glycine betaine carrier, EctP. *J Bacteriol,* 180**,** 6005-12.

Petri, K., Walter, F., Persicke, M., Rückert, C. & Kalinowski, J. 2013. A novel type of N-acetylglutamate synthase is involved in the first step of arginine biosynthesis in *Corynebacterium glutamicum*. *BMC Genomics,* 14**,** 1-15.

Pettersen, E. F., Goddard, T. D., Huang, C. C., Meng, E. C., Couch, G. S., Croll, T. I., Morris, J. H. & Ferrin, T. E. 2021. UCSF ChimeraX: Structure visualization for researchers, educators, and developers. *Protein Sci,* 30**,** 70-82.

Pfeifer-Sancar, K., Mentz, A., Rückert, C. & Kalinowski, J. 2013. Comprehensive analysis of the *Corynebacterium glutamicum* transcriptome using an improved RNAseq technique. *BMC Genomics* 14**,** 1-23.

Pocheville, A. 2015. The Ecological Niche: History and Recent Controversies. *Handbook of Evolutionary Thinking in the Sciences.*

Povolotsky, T. L., Orlova, E., Tamang, D. G. & Saier, M. H., Jr. 2010. Defense against cannibalism: the SdpI family of bacterial immunity/signal transduction proteins. *J Membr Biol,* 235**,** 145-62.

Preussger, D., Giri, S., Muhsal, L. K., Ona, L. & Kost, C. 2020. Reciprocal Fitness Feedbacks Promote the Evolution of Mutualistic Cooperation. *Curr Biol,* 30**,** 3580-3590 e7.

Proft, T. & Baker, E. N. 2009. Pili in Gram-negative and Gram-positive bacteria - structure, assembly and their role in disease. *Cell Mol Life Sci,* 66**,** 613-35.

Radek, A., Tenhaef, N., Muller, M. F., Brusseler, C., Wiechert, W., Marienhagen, J., Polen, T. & Noack, S. 2017. Miniaturized and automated adaptive laboratory evolution: Evolving *Corynebacterium glutamicum* towards an improved d-xylose utilization. *Bioresour Technol,* 245**,** 1377-1385.

Radmacher, E., Vaitsikova, A., Burger, U., Krumbach, K., Sahm, H. & Eggeling, L. 2002. Linking central metabolism with increased pathway flux: L-valine accumulation by *Corynebacterium glutamicum*. *Appl Environ Microbiol,* 68**,** 2246-50.

Ramp, P. 2022. *The complex inositol metabolism of Corynebacterium glutamicum and its application for the production of rare inositols.* PhD.

Riviere, A., Gagnon, M., Weckx, S., Roy, D. & De Vuyst, L. 2015. Mutual Cross-Feeding Interactions between *Bifidobacterium longum* subsp. *longum* NCC2705 and *Eubacterium rectale* ATCC 33656 Explain the Bifidogenic and Butyrogenic Effects of Arabinoxylan Oligosaccharides. *Appl Environ Microbiol,* 81**,** 7767-81.

Robert, X. & Gouet, P. 2014. Deciphering key features in protein structures with the new ENDscript server. *Nucleic Acids Res,* 42**,** W320-4.

Rosenberg, G., Steinberg, N., Oppenheimer-Shaanan, Y., Olender, T., Doron, S., Ben-Ari, J., Sirota-Madi, A., Bloom-Ackermann, Z. & Kolodkin-Gal, I. 2016. Not so simple, not so subtle: the interspecies competition between *Bacillus simplex* and *Bacillus subtilis* and its impact on the evolution of biofilms. *NPJ Biofilms Microbiomes,* 2**,** 15027.

Rosero-Chasoy, G., Rodriguez-Jasso, R. M., Aguilar, C. N., Buitron, G., Chairez, I. & Ruiz, H. A. 2021. Microbial co-culturing strategies for the production high value compounds, a reliable framework towards sustainable biorefinery implementation - an overview. *Bioresour Technol,* 321**,** 124458.

Sabra, W., Dietz, D., Tjahjasari, D. & Zeng, A.-P. 2010. Biosystems analysis and engineering of microbial consortia for industrial biotechnology. *Engineering in Life Sciences,* 10**,** 407-421.

Sakanyan, V., Petrosyan, P., Lecocq, M., Boyen, A., Legrair, C., Demarez, M., Hallet, J. N. & Giansdorff, N. 1996. Genes and enzymes of the acetyl cycle of arginine biosynthesis in *Corynebacterium glutamicum*: enzyme evolution in the early steps of the arginine pathway. *Microbiology,* 142.

Sanghavi, G., Gupta, P., Rajput, M., Oza, T., Trivedi, U. & Singh, N. K. 2020. Microbial Strain Engineering. *In:* SINGH, V., SINGH, A. K., BHARGAVA, P., JOSHI, M. & JOSHI, C. G. (eds.) *Engineering of Microbial Biosynthetic Pathways.* Singapore: Springer Nature Singapore.

Schäfer, A., Tauch, A., Jäger, W., Kalinowski, J., Thierbach, G. & Pühler, A. 1994. Small mobilizable multi-purpose cloning vectors derived from the *Escherichia coli* plasmids pK18 and pK19: selection of defined deletions in the chromosome of *Corynebacterium glutamicum*. *Gene,* 145**,** 69-73.

Schito, S., Zuchowski, R., Bergen, D., Strohmeier, D., Wollenhaupt, B., Menke, P., Seiffarth, J., Nöh, K., Kohlheyer, D., Bott, M., Wiechert, W., Baumgart, M. & Noack, S. 2022. Communities of Niche-optimized Strains (CoNoS) - Design and creation of stable, genome-reduced co-cultures. *Metab Eng,* 73**,** 91-103.

Schneider, J. & Wendisch, V. F. 2010. Putrescine production by engineered *Corynebacterium glutamicum*. *Appl Microbiol Biotechnol,* 88**,** 859-68.

Schulte, R. D., Makus, C., Hasert, B., Michiels, N. K. & Schulenburg, H. 2010. Multiple reciprocal adaptations and rapid genetic change upon experimental coevolution of an animal host and its microbial parasite. *Proc Natl Acad Sci U S A,* 107**,** 7359-64.

Schulz, A. A., Collett, H. J. & Reid, S. J. 2001. Nitrogen and carbon regulation of glutamine synthetase and glutamate synthase in *Corynebacterium glutamicum* ATCC 13032. *FEMS Microbiology Letters,* 205**,** 361-367.

Seep-Feldhaus, A. H., Kalinowski, J. & Pühler, A. 1991. Molecular analysis of the *Corynebacterium glutamicum lysI* gene involved in lysine uptake. *Mol Microbiol,* 5**,** 2995-3005.

Sgobba, E., Stumpf, A. K., Vortmann, M., Jagmann, N., Krehenbrink, M., Dirks-Hofmeister, M. E., Moerschbacher, B., Philipp, B. & Wendisch, V. F. 2018. Synthetic *Escherichia coli-Corynebacterium glutamicum* consortia for L-lysine production from starch and sucrose. *Bioresour Technol,* 260**,** 302-310.

Shang, X., Chai, X., Lu, X., Li, Y., Zhang, Y., Wang, G., Zhang, C., Liu, S., Zhang, Y., Ma, J. & Wen, T. 2018. Native promoters of *Corynebacterium glutamicum* and its application in L-lysine production. *Biotechnol Lett,* 40**,** 383-391.

Shang, X., Zhang, Y., Zhang, G., Chai, X., Deng, A., Liang, Y. & Wen, T. 2013. Characterization and molecular mechanism of AroP as an aromatic amino acid and histidine transporter in *Corynebacterium glutamicum*. *J Bacteriol,* 195**,** 5334-42.

Shendure, J., Porreca, G. J., Reppas, N. B., Lin, X., Mccutcheon, J. P., Rosenbaum, A. M., Wang, M. D., Zhang, K., Mitra, R. D. & Church, G. M. 2005. Accurate multiplex polony sequencing of an evolved bacterial genome. *Science,* 309**,** 1728-32.

Shou, W., Ram, S. & Vilar, J. M. G. 2007. Synthetic cooperation in engineered yeast populations. *PNAS,* 104**,** 1877-1882.

Siani, A., Pagano, E., Iacone, R., Iacoviello, L., Scopacasa, F. & Strazzullo, P. 2000. Blood Pressure and Metabolic Changes During Dietary L-Arginine Supplementation in Humans. *American Journal of Hypertension,* 13**,** 547–551.

Siebert, D., Altenbuchner, J. & Blombach, B. 2021. A Timed Off-Switch for Dynamic Control of Gene Expression in *Corynebacterium glutamicum*. *Front Bioeng Biotechnol,* 9**,** 704681.

Sievers, F., Wilm, A., Dineen, D., Gibson, T. J., Karplus, K., Li, W., Lopez, R., Mcwilliam, H., Remmert, M., Soding, J., Thompson, J. D. & Higgins, D. G. 2011. Fast, scalable generation of high-quality protein multiple sequence alignments using Clustal Omega. *Mol Syst Biol,* 7**,** 539.

Stella, R. G., Gertzen, C. G. W., Smits, S. H. J., Gatgens, C., Polen, T., Noack, S. & Frunzke, J. 2021. Biosensor-based growth-coupling and spatial separation as an evolution strategy to improve small molecule production of *Corynebacterium glutamicum*. *Metab Eng,* 68**,** 162-173.

Stella, R. G., Wiechert, J., Noack, S. & Frunzke, J. 2019. Evolutionary engineering of *Corynebacterium glutamicum*. *Biotechnol J,* 14**,** e1800444.

Stephens, K., Pozo, M., Tsao, C. Y., Hauk, P. & Bentley, W. E. 2019. Bacterial co-culture with cell signaling translator and growth controller modules for autonomously regulated culture composition. *Nat Commun,* 10**,** 4129.

Stoebel, D. M., Dean, A. M. & Dykhuizen, D. E. 2008. The cost of expression of *Escherichia coli lac* operon proteins is in the process, not in the products. *Genetics,* 178**,** 1653-60.

Summers, A. O. 2009. Damage control: regulating defenses against toxic metals and metalloids. *Curr Opin Microbiol,* 12**,** 138-44.

Sundermeyer, L., Bosco, G., Gujar, S., Brocker, M., Baumgart, M., Willbold, D., Weiergräber, O. H., Bellinzoni, M. & Bott, M. 2022. Characteristics of the GlnH and GlnX Signal Transduction Proteins Controlling PknG-Mediated Phosphorylation of OdhI and 2-Oxoglutarate Dehydrogenase Activity in *Corynebacterium glutamicum*. *Microbiology Spectrum,* 10**,** 1-23.

Takeno, S., Takasaki, M., Urabayashi, A., Mimura, A., Muramatsu, T., Mitsuhashi, S. & Ikeda, M. 2013. Development of fatty acid-producing *Corynebacterium glutamicum* strains. *Appl Environ Microbiol,* 79**,** 6776-83.

Takors, R. 2012. Scale-up of microbial processes: impacts, tools and open questions. *J Biotechnol,* 160**,** 3-9.

Tang, F., Barbacioru, C., Wang, Y., Nordman, E., Lee, C., Xu, N., Wang, X., Bodeau, J., Tuch, B. B., Siddiqui, A., Lao, K. & Surani, M. A. 2009. mRNA-Seq whole-transcriptome analysis of a single cell. *Nat Methods,* 6**,** 377-82.

Tang, W. L. & Zhao, H. 2009. Industrial biotechnology: tools and applications. *Biotechnol J,* 4**,** 1725-1739.

Tateno, T., Fukuda, H. & Kondo, A. 2007. Production of L-Lysine from starch by *Corynebacterium glutamicum* displaying α-amylase on its cell surface. *Appl Microbiol Biotechnol,* 74**,** 1213-20.

Tauch, A., Hermann, T., Burkovski, A., Krämer, R., Pühler, A. & Kalinowski, J. 1998. Isoleucine uptake in *Corynebacterium glutamicum* ATCC 13032 is directed by the *brnQ* gene product. *Arch. Microbiol.,* 169**,** 303-312.

Tenhaef, N., Brusseler, C., Radek, A., Hilmes, R., Unrean, P., Marienhagen, J. & Noack, S. 2018. Production of D-xylonic acid using a non-recombinant *Corynebacterium glutamicum* strain. *Bioresour Technol,* 268**,** 332-339.

Teramoto, H., Inui, M. & Yukawa, H. 2012. NdnR is an NAD-responsive transcriptional repressor of the *ndnR* operon involved in NAD *de novo* biosynthesis in *Corynebacterium glutamicum*. *Microbiology (Reading),* 158**,** 975-982.

Teramoto, H., Suda, M., Inui, M. & Yukawa, H. 2010. Regulation of the expression of genes involved in NAD de novo biosynthesis in *Corynebacterium glutamicum*. *Appl Environ Microbiol,* 76**,** 5488-95.

Tesch, M., De Graaf, A. A. & Sahm, H. 1999. In Vivo Fluxes in the Ammonium-Assimilatory Pathways in *Corynebacterium glutamicum* Studied by ^{15}N Nuclear Magnetic Resonance. *Appl Environ Microbiol,* 65**,** 1099-1109.

Tettelin, H., Masignani, V., Cieslewicz, M. J., Donati, C., Medini, D., Ward, N. L., Angiuoli, S. V., Crabtree, J., Jones, A. L., Durkin, A. S., Deboy, R. T., Davidsen, T. M., Mora, M., Scarselli, M., Margarity Y Ros, I., Peterson, J. D., Hauser, C. R., Sundaram, J. P., Nelson, W. C., Madupu, R., Brinkac, L. M., Dodson, R. J., Rosovitz, M. J., Sullivan, S. A., Daugherty, S. C., Haft, D. H., Selengut, J., Gwinn, M. L., Zhou, L., Zafar, N., Khouri, H., Radune, D., Dimitrov, G., Watkins, K., O'connor, K. J., Smith, S., Utterback, T. R., White, O., Rubens, C. E., Grandi, G., Madoff, L. C., Kasper, D. L., Telford, J. L., Wessels, M. R., Rappuoli, R. & Fraser, C. M. 2005. Genome analysis of multiple pathogenic isolates of *Streptococcus agalactiae*: Implications for the microbial ''pan-genome''. *PNAS,* 102**,** 13950–13955

Tettelin, H., Riley, D., Cattuto, C. & Medini, D. 2008. Comparative genomics: the bacterial pan-genome. *Curr Opin Microbiol,* 11**,** 472-7.

Thykaer, J. & Nielsen, J. 2003. Metabolic engineering of β-lactam production. *Metab Eng,* 5**,** 56-69.

Torsvik, V., Sorheim, R. & Goksoyr, J. 1996. Total bacterial diversity in soil and sediment communities a review. *Journal of Industrial Microbiolog,* 17**,** 170-178.

Tripathi, A., Anand, K., Das, M., O'niel, R. A., P, S. S., Thakur, C., R, L. R., Rajmani, R. S., Chandra, N., Laxman, S. & Singh, A. 2022. *Mycobacterium tuberculosis* requires SufT for Fe-S cluster maturation, metabolism, and survival in vivo. *PLoS Pathog,* 18**,** e1010475.

Trötschel, C., Follmann, M., Nettekoven, J. A., Mohrbach, T., Forrest, L. R., Burkovski, A., Marin, K. & Krämer, R. 2008. Methionine uptake in *Corynebacterium glutamicum* by MetQNI and by MetPS, a novel methionine and alanine importer of the NSS neurotransmitter transporter family. *Biochemistry,* 47**,** 12698-709.

Trunk, T., Khalil, H. S. & Leo, J. C. 2018. Bacterial autoaggregation. *AIMS Microbiol,* 4**,** 140-164.

Tsoi, R., Wu, F., Zhang, C., Bewick, S., Karig, D. & You, L. 2018. Metabolic division of labor in microbial systems. *Proc Natl Acad Sci U S A,* 115**,** 2526-2531.

Tsuchida, T. & Momose, H. 1975. Genetic Changes of Regulatory Mechanisms Occured in Leucine and Valine Producing Mutants Derived from *Brevibacterium lactofermentum* 2256. *Agr. Biol. Chem,* 39**,** 2193-2198.

Tyo, K. E., Ajikumar, P. K. & Stephanopoulos, G. 2009. Stabilized gene duplication enables long-term selection-free heterologous pathway expression. *Nat Biotechnol,* 27**,** 760-5.

Unthan, S., Grunberger, A., Van Ooyen, J., Gatgens, J., Heinrich, J., Paczia, N., Wiechert, W., Kohlheyer, D. & Noack, S. 2014. Beyond growth rate 0.6: What drives *Corynebacterium glutamicum* to higher growth rates in defined medium. *Biotechnol Bioeng,* 111**,** 359-71.

Unthan, S., Radek, A., Wiechert, W., Oldiges, M. & Noack, S. 2015. Bioprocess automation on a Mini Pilot Plant enables fast quantitative microbial phenotyping. *Microb Cell Fact,* 14**,** 32.

Voges, R., Corsten, S., Wiechert, W. & Noack, S. 2015. Absolute quantification of *Corynebacterium glutamicum* glycolytic and anaplerotic enzymes by QconCAT. *J Proteomics,* 113**,** 366-77.

Vogt, M., Haas, S., Klaffl, S., Polen, T., Eggeling, L., Van Ooyen, J. & Bott, M. 2014. Pushing product formation to its limit: metabolic engineering of *Corynebacterium glutamicum* for L-leucine overproduction. *Metab Eng,* 22**,** 40-52.

Wang, H. H., Isaacs, F. J., Carr, P. A., Sun, Z. Z., Xu, G., Forest, C. R. & Church, G. M. 2009. Programming cells by multiplex genome engineering and accelerated evolution. *Nature,* 460**,** 894-898.

Wang, H. K., Ng, Y. K., Koh, E., Yao, L., Chien, A. S., Lin, H. X. & Lee, Y. K. 2015. RNA-Seq reveals transcriptomic interactions of *Bacillus subtilis* natto and *Bifidobacterium animalis* subsp. *lactis* in whole soybean solid-state co-fermentation. *Food Microbiol,* 51**,** 25-32.

Wanner, G., Vogl, K. & Overmann, J. 2008. Ultrastructural characterization of the prokaryotic symbiosis in "*Chlorochromatium aggregatum*". *J Bacteriol,* 190**,** 3721-30.

Waterhouse, A., Bertoni, M., Bienert, S., Studer, G., Tauriello, G., Gumienny, R., Heer, F. T., De Beer, T. a. P., Rempfer, C., Bordoli, L., Lepore, R. & Schwede, T. 2018. SWISS-MODEL: homology modelling of protein structures and complexes. *Nucleic Acids Res,* 46**,** W296-W303.

Watve, M. G., Tickoo, R., Jog, M. M. & Bhole, B. D. 2001. How many antibiotics are produced by the genus *Streptomyces*? *Arch Microbiol,* 176**,** 386-90.

Wehrmann, A., Morakkabati, S., Krämer, R., Sahm, H. & Eggeling, L. 1995. Functional Analysis of Sequences Adjacent to *dapE* of *Corynebacterium glutamicum* Reveals the Presence of *aroP*, Which Encodes the Aromatic Amino Acid Transporter. *Journal of Bacteriology,* 177**,** 5991-5993.

Weinreich, D. M., Delaney, N. F., Depristo, M. A. & Hartl, D. L. 2006. Darwinian evolution can follow only very few mutational paths to fitter proteins. *Science,* 312**,** 111-4.

Weitzel, M., Nöh, K., Dalman, T., Niedenführ, S., Stute, B. & Wiechert, W. 2013. 13CFLUX2--high-performance software suite for ^{13}C-metabolic flux analysis. *Bioinformatics,* 29**,** 143-5.

Weizmann, C. & Rosenfeld, B. 1937. THE ACTIVATION OF THE BUTANOL-ACETONE FERMENTATION OF CARBOHYDRATES BY *CLOSTRIDIUM ACETOBUTYLICUM* (WEIZMANN). *Biochem.,* 31**,** 619-639.

Wendering, P. & Nikoloski, Z. 2022. COMMIT: Consideration of metabolite leakage and community composition improves microbial community reconstructions. *PLoS Comput Biol,* 18**,** e1009906.

Wendisch, V. F. 2020. Metabolic engineering advances and prospects for amino acid production. *Metab Eng,* 58**,** 17-34.

West, S. A., Diggle, S. P., Buckling, A., Gardner, A. & Griffin, A. S. 2007. The Social Lives of Microbes. *Annual Review of Ecology, Evolution, and Systematics,* 38**,** 53-77.

Wintermute, E. H. & Silver, P. A. 2010. Emergent cooperation in microbial metabolism. *Mol Syst Biol,* 6**,** 407.

Wolf, N., Bussmann, M., Koch-Koerfges, A., Katcharava, N., Schulte, J., Polen, T., Hartl, J., Vorholt, J. A., Baumgart, M. & Bott, M. 2020. Molecular Basis of Growth Inhibition by Acetate of an Adenylate Cyclase-Deficient Mutant of *Corynebacterium glutamicum*. *Front Microbiol,* 11.

Wolf, S., Becker, J., Tsuge, Y., Kawaguchi, H., Kondo, A., Marienhagen, J., Bott, M., Wendisch, V. F. & Wittmann, C. 2021. Advances in metabolic engineering of *Corynebacterium glutamicum* to produce high-value active ingredients for food, feed, human health, and well-being. *Essays Biochem,* 65**,** 197-212.

Wynands, B., Otto, M., Runge, N., Preckel, S., Polen, T., Blank, L. M. & Wierckx, N. 2019. Streamlined *Pseudomonas taiwanensis* VLB120 Chassis Strains with Improved Bioprocess Features. *ACS Synth Biol,* 8**,** 2036-2050.

Xu, M., Rao, Z., Yang, J., Dou, W. & Xu, Z. 2013. The effect of a LYSE exporter overexpression on L-arginine production in *Corynebacterium crenatum*. *Curr Microbiol,* 67**,** 271-8.

Xu, N., Zheng, Y., Wang, X., Krulwich, T. A., Ma, Y. & Liu, J. 2018. The lysine 299 residue endows the multisubunit Mrp1 antiporter with dominant roles in Na^+ resistance and pH homeostasis in *Corynebacterium glutamicum*. *Appl Environ Microbiol,* 84.

Yang, D. D., Alexander, A., Kinnersley, M., Cook, E., Caudy, A., Rosebrock, A. & Rosenzweig, F. 2020. Fitness and Productivity Increase with Ecotypic Diversity among *Escherichia coli* Strains That Coevolved in a Simple, Constant Environment. *Appl Environ Microbiol,* 86.

Ye, J., Kandegedara, A., Martin, P. & Rosen, B. P. 2005. Crystal structure of the *Staphylococcus aureus* pI258 CadC Cd(II)/Pb(II)/Zn(II)-responsive repressor. *J Bacteriol,* 187**,** 4214-21.

Yim, S. H., Jung, S., Lee, S. K., Cheon, C. I., Song, E., Lee, S. S., Shin, J. & Lee, M. S. 2011. Purification and characterization of an arginine regulatory protein, ArgR, in *Corynebacterium glutamicum*. *J Ind Microbiol Biotechnol,* 38**,** 1911-20.

Zelle, E., Wiechert, W. & Nöh, K. 2015. Growth and production capabilities of *Corynebacterium glutamicum*: interrogating a genome-scale metabolic network model. *In:* BURKOVSKI, A. (ed.) *Corynebacterium glutamicum: from Systems Biology to Biotechnological Applications.* Caister Academic Press.

Zhan, M., Kan, B., Dong, J., Xu, G., Han, R. & Ni, Y. 2019. Metabolic engineering of *Corynebacterium glutamicum* for improved L-arginine synthesis by enhancing NADPH supply. *J Ind Microbiol Biotechnol,* 46**,** 45-54.

Zhang, F., Huo, K., Song, X., Quan, Y., Wang, S., Zhang, Z., Gao, W. & Yang, C. 2020. Engineering of a genome-reduced strain *Bacillus amyloliquefaciens* for enhancing surfactin production. *Microb Cell Fact,* 19**,** 223.

Zhang, H., Li, Y., Wang, C. & Wang, X. 2018. Understanding the high L-valine production in *Corynebacterium glutamicum* VWB-1 using transcriptomics and proteomics. *Sci Rep,* 8**,** 3632.

Zhang, X. & Reed, J. L. 2014. Adaptive Evolution of Synthetic Cooperating Communities Improves Growth Performance. *Plos One,* 9.

Zhao, Z., Ding, J. Y., Li, T., Zhou, N. Y. & Liu, S. J. 2011. The *ncgl1108* (*PhePCg*) gene encodes a new L-Phe transporter in *Corynebacterium glutamicum*. *Appl Microbiol Biotechnol,* 90**,** 2005-13.

Zuchowski, R., Schito, S., Neuheuser, F., Menke, P., Berger, D., Hollmann, N., Gujar, S., Sundermeyer, L., Mack, C., Wirtz, A., Weiergraber, O. H., Polen, T., Bott, M., Noack, S. & Baumgart, M. 2023. Discovery of novel amino acid production traits by evolution of synthetic co-cultures. *Microb Cell Fact,* 22**,** 22.

5. Appendix

5.1 Communities of Niche-optimized strains: Analyzing community cultivation in 1 L scale and alternative pairings

5.1.1 Establishing further Communities of Niche-optimized Strains

In the beginning of the experimental work of this thesis, we aimed on constructing several pairings of auxotrophic strains to set up our CoNoS, to have the option of choosing the best ones later. Therefore, ten different pairings were set up and characterized (Schito *et al.*, 2022). However, no stable growth was observed for most communities, and thus amino acid production was improved by metabolic engineering. Here, we report two further CoNoS, which showed rapid and stable growth afterward (Figure 5.1).

The first is the CoNoS comprising the strains WT ΔLEU HIS^+ ↔ WT ΔHIS LEU^{++} was set up. For WT ΔHIS LEU^{++}, feedback inhibition of L-leucine biosynthesis was relieved via increased expression of the *leuA* variant of BS018 (Vogt *et al.*, 2014). For WT ΔLEU HIS^+, we used the feedback resistant ATP phosphoribosyltransferase variant $HisG_{A270D}$ (Kulis-Horn *et al.*, 2015). The WT ΔLEU HIS^+ ↔ WT ΔHIS LEU^{++} community grew with a growth rate of 0.49 h^{-1} ± 0.02 when cultivated in CGXII medium with 2% (w/v) glucose (Keilhauer *et al.*, 1993). In comparison to a WT cultivated under similar conditions on the same BioLector plate, this was equivalent to 88% of WT growth and 97% of WT backscatter. In comparison, the monocultures of the single strains supplemented with either L-leucine or L-histidine had growth rates of 0.49 h^{-1} ± 0.004 (WT ΔLEU HIS^+) and 0.32 h^{-1} ± 0.01 (WT ΔHIS LEU^{++}). These growth rates suggested that CoNoS growth is not limited by the growth rate of the individual strains, at least not by the slower-growing one. However, it needs to be kept in mind that a comparison of the growth rate of the CoNoS and the single strains is difficult, as the CoNoS was inoculated to a starting OD_{600} of 1 (i..e., 0.5 per strain), the single strains only to an OD_{600} of 0.5. Lower starting ODs than 0.5 per strain in a CoNoS setting proofed to be problematic (Schito *et al.*, 2022). The high community growth rate is an important result and makes this CoNoS another suitable candidate for establishing a production process, which could be pursued in the future.

Similarly, a WT ΔLEU TRP^+ ↔ WT ΔTRP LEU^{++} CoNoS was engineered. The mutations for L-leucine production were identical to the WT ΔHIS LEU^{++} strain. For slight L-tryptophan production, translation attenuation via the leader peptide *trpL* was interrupted via a mutation, and feedback inhibition by L-tryptophan was relieved via mutation of $TrpE_{S38R}$ (Matsui *et al.*, 1987). The CoNoS was characterized in comparison to the WT in CGXII medium with 2% (w/v) glucose (Keilhauer *et al.*, 1993). The engineered CoNoS grew with a growth rate of 0.06 h^{-1} ± 0.01 (starting OD_{600} = 1). However, when using the starting OD_{600} = 5, a growth

rate of 0.23 h^{-1} ± 0.03 was reached. A higher starting inoculum enabled the CoNoS also to grow to a significantly higher final backscatter.

Based on the WT ΔLEU HIS^+ ↔ WT ΔHIS LEU^{++} CoNoS, the pairing WT ΔLEU HIS^+::P_{tac}-*crimson* and WT ΔHIS LEU^{++}:: P_{tac}-*eYFP* harboring fluorescent markers was constructed and given to S. Schito (AG Noack). In order to further optimize this community and to potentially identify novel relevant production traits of C. glutamicum, an ALE experiment was performed as described before (Zuchowski *et al.*, 2023). In the automated ALE experiment, however, only the first batch per replicate grew as before (average growth rate 0.45 h^{-1}). Afterward, the growth rate decreased by almost 70 % to an average growth rate of 0.15 h^{-1} and continued to decline (data not shown). This points to yet unknown limits of the evolution approach, such as the accumulation of toxic intermediates or the disruption of stable strain ratios. The exact mechanism behind this decrease in growth was not further examined.

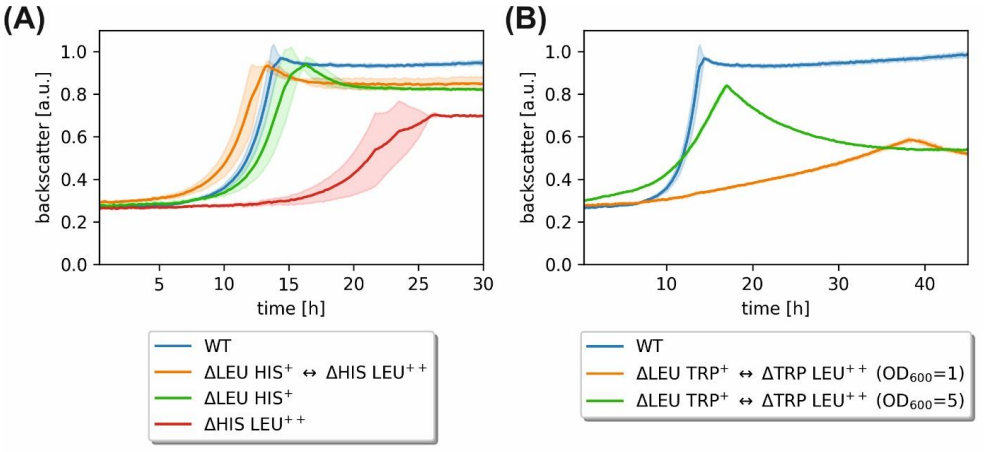

Figure 5.1: Growth characterization of further constructed CoNoS. Cultivation of **(A)** WT ΔLEU HIS^+ ↔ WT ΔHIS LEU^{++} CoNoS and **(B)** WT ΔLEU TRP^+ ↔ WT ΔTRP LEU^{++} CoNoS. All cultures were performed in biological triplicate in CGXII medium with 111 mM D-glucose in 800 µL at 30°C and 1400 rpm with 85% humidity control; 3 mM L-leucine or L-histidine were added for monocultures. Monocultures were inoculated to a starting OD_{600} of 0.5, and CoNoS were inoculated in a 1:1 ratio to OD_{600} = 1 if not stated otherwise. Backscatter data were normalized based on the maximum value recorded for each WT in the respective experiment. Mean values are shown as lines and standard deviations as shaded areas.

5.1.2 First upscaling of CoNoS cultures to 1 L scale

For a first analysis of the growth behavior of a CoNoS in the 1 L scale, the WT ΔARG LEU^{++} ↔ WT ΔLEU ARG^{++} CoNoS was used and compared to the WT (Figure 5.2). On this scale, the WT grew fast with a growth rate of which a μ_{max} = 0.36 ± 0.01 h^{-1}, reaching its

maximum OD_{600} and entire D-glucose consumption after 10 h. Stable CoNoS growth was possible as well. For the CoNoS, the maximum OD_{600} and entire D-glucose consumption was reached after 16 h, which was 6 h later than the WT. A $\mu_{max} = 0.19 \pm 0.01$ h^{-1} was calculated from these growth curves, equivalent to only 53% of WT growth. In comparison to previous cultivations in the BioLector 800 µL scale, in which a $\mu_{max} = 0.47 \pm 0.01$ h^{-1} (equivalent to 83% of the WT) was measured (Schito *et al.*, 2022), this suggested that the gap in growth became more prominent in the highly diluted 1 L scale. An "island effect" was previously observed for a CoNoS in the microfluidic chamber, describing the inability of isolated cells to grow (Schito *et al.*, 2022). Thus, this decrease in CoNoS growth relative to the WT could be attributable to the high dilution.

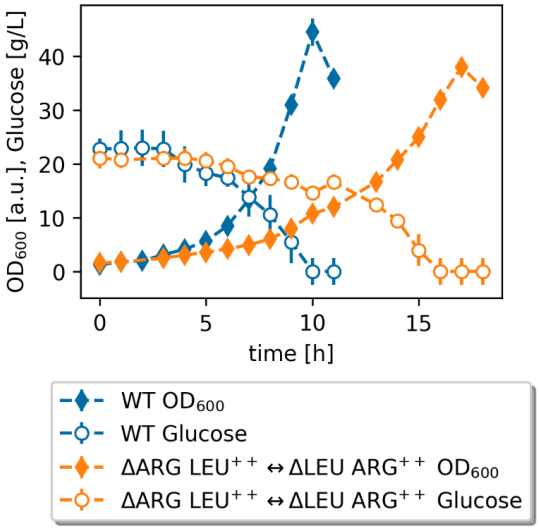

Figure 5.2: Characterization of CoNoS growth in 1 L scale. The CoNoS ΔLEU $ARG^{++} \leftrightarrow$ ΔARG LEU^{++} and the WT were cultivated in duplicates in CGXII medium with 111 mM D-glucose in a DASGIP 1 L fermentation system. The cultivation was started with an $OD_{600} = 1$. The mean OD_{600} values are shown as diamonds, and circles mark the average D-glucose concentrations (g/L), and standard deviations as lines.

5.1.3 Upscaling of CoNoS cultures for L-arginine production

In the course of this thesis, the CoNoS ΔLEU $ARG^{+++} \leftrightarrow$ ΔARG LEU^{++} $\Delta P_{pfkA}::P_{gntK}$ was established, harboring the *gntK* promoter in front of *pfkA*, which resulted in a dependence of strain growth on gluconate concentration. With this metabolic switch, the carbon and energy flow into the helper strain should be limited to the bare minimum, which should result in a higher fraction of the producer strain in the culture and thereby a higher L-arginine titer. This

co-culture was characterized as well and compared to a monoculture of the L-arginine production strain WT ARG^{+++} which harbors identical mutations for increased L-arginine production, however, without harboring a L-leucine auxotrophy (Berger, 2023). The strains were cultivated in a 1 L scale in a batch- (see Figure 3.2) and a fed-batch (Figure 5.3) manner. In both cultivations, the final L-arginine accumulation in the supernatant was significantly increased by at least 70% in the CoNoS.

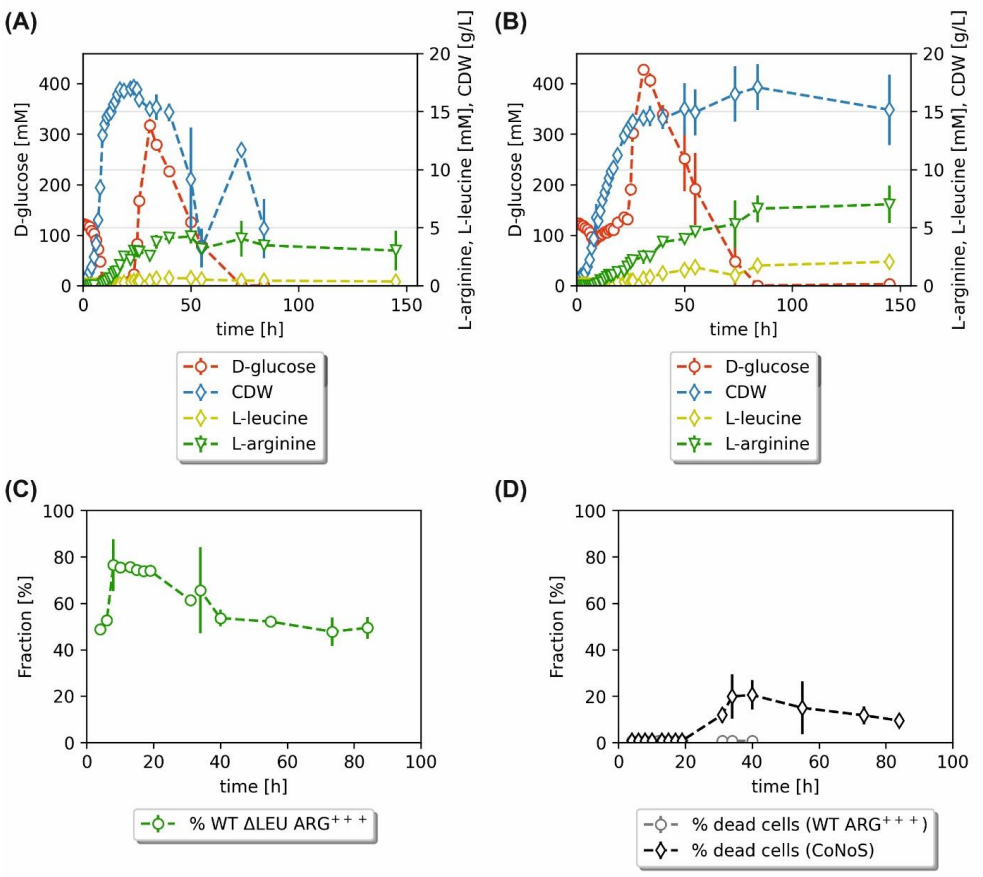

Figure 5.3: Comparison of an L-arginine producer strains in monoculture with a CoNoS in 1 L scale. The WT ARG^{+++} **(A)** and the CoNoS ΔLEU ARG^{+++} ↔ ΔARG LEU^{++} ΔP_{pfkA}::P_{gntK} **(B)** were cultivated in duplicates in CGXII medium with 111 mM D-glucose and 1 mM IPTG in a DASGIP 1 L fermentation system. The cultivation was started with a starting OD_{600} = 1 (i.e., 0.5 per strain in co-culture), and 0.5 mM gluconate was added to the CoNoS. The mean values are shown as diamonds (blue: cell dry weight g/L; yellow: L-leucine mM), circles (D-glucose g/L) and triangles (L-arginine mM), and standard deviations as lines. **(C)** Analysis of the ratio between the two strains in the CoNoS in the bioreactor based on fluorescence signal detection of the different fluorophores in the individual strains and **(D)** of the fraction of dead cells during the cultivation via propidium iodide staining with a MACSQuant (Miltenyi Biotec,

Bergisch Gladbach, Germany). The mean values are shown as green circles (percentage of the amount of ΔLEU ARG^{+++} in the CoNoS), diamonds (percentage of dead cells of the CoNoS), and black circles (percentage of dead cells of the monoculture WT ARG^{+++}), and the standard deviations as lines.

Notably, the number of dead cells identified via propidium iodide staining in the CoNoS measured via MACS (magnetic-activated cell sorting, Miltenyi Biotec, Bergisch Gladbach, Germany) was drastically higher for the CoNoS than for the monoculture, even during early time points of cultivation where D-glucose was still present (Figure 5.3D). Lysis effects could therefore contribute to the improved L-arginine production with the CoNoS. Despite this large amount of dead cells, the depletion in biomass is lower in the CoNoS over time, which can only partly be caused by the overall slower growth and D-glucose consumption. The reason for the drastic loss in biomass, especially in the monoculture WT ARG^{+++}, is unclear.

The MACS analysis also allowed for determining the cell ratio in the CoNoS by discriminating between the eYFP and the Crimson protein fluorescence signals. This ratio shifted quickly from the initial 50:50 ratio to 80:20, favoring the ΔLEU ARG^{+++} strain, which is supposedly due to the helper strain with the gluconate-dependent switch being limited in growth (Figure 5.3C). This ratio, however, decreases during the course of the cultivation, yielding an almost 50:50 ratio after 45h and onwards. These changes in the ratio could be attributed to a higher number of dead ΔLEU ARG^{+++} cells, as the decrease in the ratio coincided with the increase in dead cells. Alternatively or additionally, a suppressor mutation in the metabolic switch of the helper strain could have occurred, resulting in the helper strain increasing in abundance. This hypothesis is backed by the increase in L-leucine titer in the supernatant of the CoNoS after 40h, which results in a significant difference in titer between CoNoS and WT ARG^{+++} monoculture. In the monoculture, this could be attributed to overflow metabolism during times of high D-glucose concentrations (Paczia *et al.*, 2012). However, for the co-culture, this must result from the action of the helper strain.

Overall, further experiments analyzing cell lysis and strain ratio development should be performed before drawing a conclusion regarding the beneficial effect of the community approach on production. Nevertheless, these data suggest that the benefits of L-arginine production with the communities observed on smaller scales (Berger, 2023) are also valid in 1 L scale. Further upscaling experiments could therefore be performed, testing the growth of the CoNoS in larger volumes closer to industrial standards.

5.1.4 By-products of CoNoS-based L-arginine production

During the fed-batch cultivation (Figure 5.3), more than 400 mM D-glucose was present in the medium at specific time points. Despite this amount of carbon source, the determined CDW decreased or only increased further, suggesting that the D-glucose was not fully incorporated to form biomass. Therefore, various metabolites have likely accumulated during the extended overflow metabolism (Paczia *et al.*, 2012). Two 145h samples, one from the CoNoS ΔLEU ARG^{+++} ↔ ΔARG LEU^{++} ΔP_{pfkA}::P_{gntK} and one from the WT ARG^{+++} were submitted for GC-ToF analysis (AG Noack, analysis is pending). The samples were also analyzed regarding further amino acids by HPLC (Figure 5.4). Over 125 mM amino acids were detected in the CoNoS supernatant, including notable concentrations of L-alanine, L-arginine, L-glutamic acid, L-glycine, L-isoleucine, L-leucine, L-lysine, and L-valine. Except for L-glycine, the quantities detected in the CoNoS' supernatant surpassed the amounts accumulated in the monoculture by many-fold. Especially for L-valine, which was present in the monoculture only in small amounts, accumulated in the CoNoS to a concentration of approx. 45 mM.

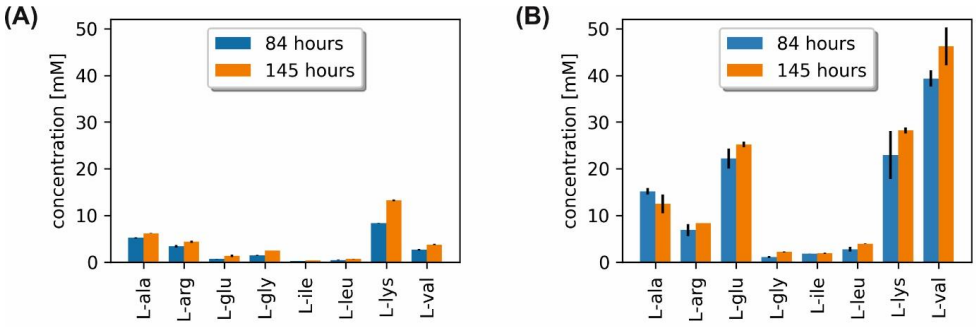

Figure 5.4: Characterization of amino acid accumulation in a CoNoS and the comparable L-arginine producer monoculture. The WT ARG^{+++} **(A)** and the CoNoS ΔLEU ARG^{+++} ↔ ΔARG LEU^{++} ΔP_{pfkA}::P_{gntK} **(B)** were cultivated in duplicates in CGXII medium with 111 mM D-glucose in a DASGIP 1 L fermentation system (see Figure 5.3). The cultivation was started with a starting OD_{600} = 1 (i.e. 0.5 per strain in co-culture), and 0.5 mM gluconate was added to the CoNoS (as inducer molecule for the gluconate-dependent helper strain ΔARG LEU^{++} ΔP_{pfkA}::P_{gntK}). The mean values at two different time points are shown as columns and standard deviations as lines.

This significant difference in accumulated amino acids raised two main questions. i) Is this reproducible, and is this accumulation of amino acids only related to the vast amount of glucose present during the cultivation, resulting in drastic extended overflow metabolism? ii) What is the course of the accumulation over time, especially in comparison to the CoNoS without the metabolic switch, ΔLEU ARG^{+++} ↔ ΔARG LEU^{++}, and to the monoculture of the producer

strain ΔLEU ARG^{+++} supplemented with L-leucine? To answer these questions, a shake flask experiment was performed. (Figure 5.5).

While all strains and communities grew almost equally fast and to a similar final OD_{600}, a significant decrease in OD_{600} was detected for the CoNoSs as well as for the auxotrophic monoculture. This is in accordance with the backscatter development of various previous CoNoS and auxotrophic monocultures in the BioLector (see, e.g., Figure 3 and Figure 6 in (Schito *et al.*, 2022) and Figure 8 in (Zuchowski *et al.*, 2023)) as well as the CDW development in the batch experiment (Figure 3.2).

The four different cultures showed significant differences regarding their amino acid accumulation for most amino acids except for L-glutamic acid, which was accumulated in similar amounts in the supernatant of all cultures. For all other amino acids identified, significant differences between the monoculture of ΔLEU ARG^{+++} supplemented with L-leucine and WT ARG^{+++} were observed. This suggested that the L-leucine auxotrophy caused a drastic increase in the titers of some amino acids, which was most prominent for L-alanine, L-arginine, and L-glycine. While for those amino acids, the titers in the CoNoSs were smaller, this was different for L-isoleucine, L-lysine, and L-valine. This can partly be attributed to the metabolic switch. While both CoNoS' showed similar L-lysine accumulation, the titers L-isoleucine and L-valine were increased in the CoNoS harboring the switch. From this, it can be concluded that three different effects play a role: Firstly, the L-leucine auxotrophy, which potentially caused this drastic increase the amino acid titers. Secondly, growing in a community seems to have an effect, which could be attributed to the helper strain with the L-arginine auxotrophy exporting amino acids as well. Lastly, the metabolic switch influenced the titer. The switch effect resulted in changes in the stoichiometry between the producer and the helper strain, suggesting that for most amino acids, the producer strain contributes more to the formed amino acids.

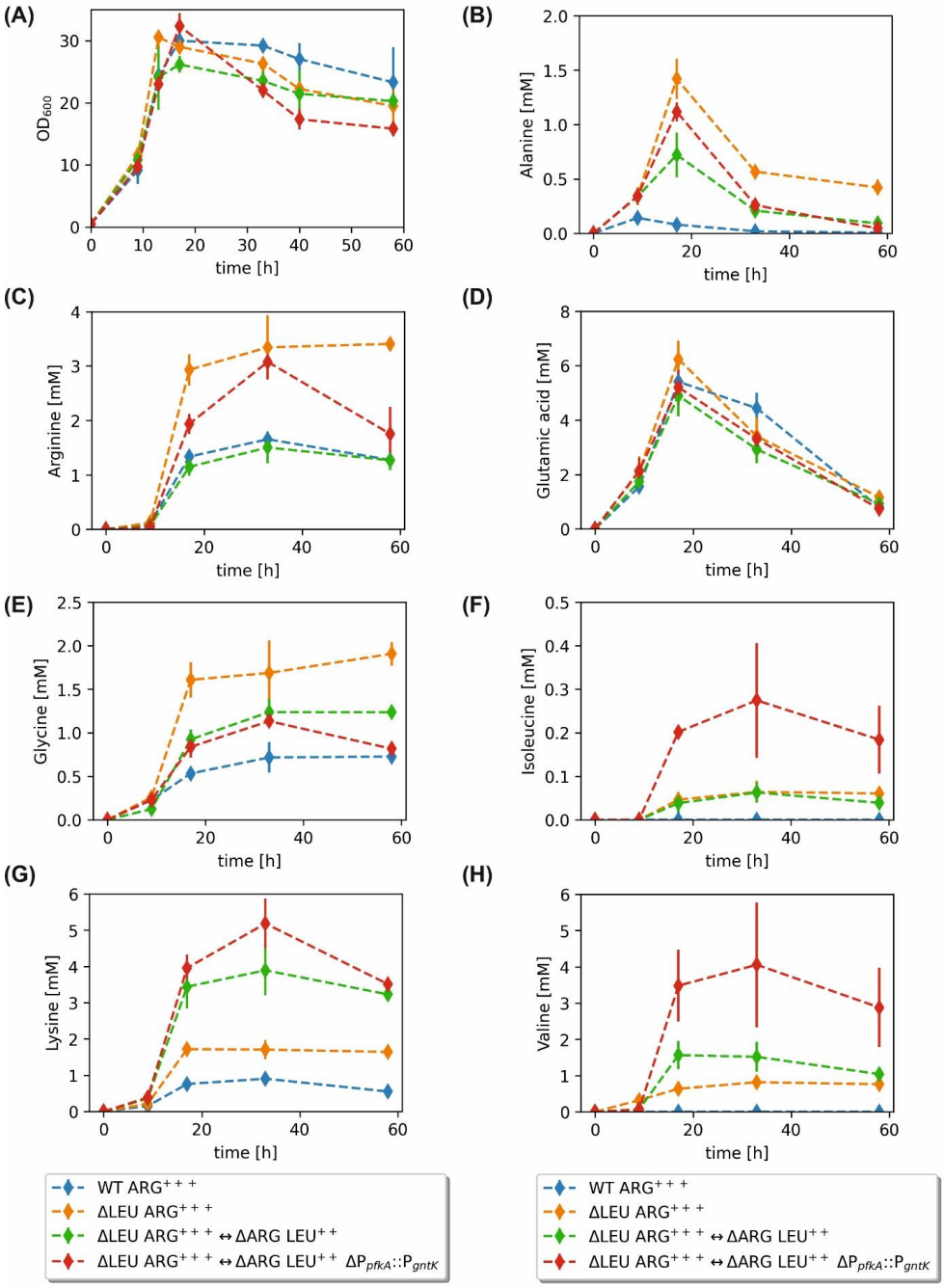

Figure 5.5: Growth and amino acid accumulation in different CoNoS and in comparable L-arginine producer monocultures. The WT ARG^{+++}, the ΔLEU ARG^{+++} producer strain, the CoNoS ΔLEU ARG^{+++} ↔ ΔARG LEU^{++}, and the CoNoS ΔLEU ARG^{+++} ↔ ΔARG LEU^{++} ΔP_{pfkA}::P_{gntK} were cultivated in biological triplicates in CGXII medium with 111 mM D-glucose in 500 ml shake flasks at 30°C, 130 rpm with 85% humidity control. Cultures were inoculated

with a starting OD_{600} = 0.5 per strain (i.e., 0.5 per strain in co-culture), and 0.5 mM gluconate was added to the CoNoS with the metabolic switch. Shown are the development of the optical density **(A)** as well as the accumulation of L-alanine **(B)**, L-arginine **(C)**, L-glutamic acid **(D)**, L-glycine **(E)**, L-isoleucine **(F)**, L-lysine **(G)**, and L-valine **(H)**. The mean values are shown as diamonds and standard deviations as lines.

A beneficial effect of amino acid auxotrophies on the formation of other amino acids has been observed before. For example, an L-isoleucine auxotrophy resulted in increased L-valine formation, supposedly by increased *ilvBNC* expression upon L-isoleucine shortage via an attenuation mechanism and less competing reaction for BCAA formation in *C. glutamicum* (Radmacher *et al.*, 2002). Amino acid auxotrophies are not uncommon in production strains. The L-tyrosine-auxotrophic L-phenylalanine producing *E. coli* (Konstantinov *et al.*, 1991) and the L-methionine and L-isoleucine auxotrophic L-leucine producing *C. glutamicum* (Tsuchida and Momose, 1975) are examples for this. Moreover, the current best L-arginine producer is auxotrophic for the vitamins biotin and thiamine, and potentially for further metabolites, as the genome of the strain is not published and corn steep liquor, containing vitamins and amino acids, is fed to the strain (Park *et al.*, 2014).

Especially for L-arginine, it seems likely that the increased production measured in the fermentations is either caused by increased efficiency due to the better flow of carbon and energy, as proposed by the CoNoS concept (Noack and Baumgart, 2019), which could be related to less concurring side reactions, or due to specific changes in the transcriptome or proteome due to the auxotrophy. To study this, one crucial first step would be a transcriptomic/ proteomic comparison between monocultures of ΔLEU ARG^{+++} and WT ARG^{+++}. Ruling out the possibility that general adaptions to the auxotrophy are at play that result in a generally higher synthesis of other amino acids would be one important step toward nailing down the reason for the increased production with a CoNoS. A further alternative explanation are the above-mentioned lysis effects in auxotrophic strains and in CoNoS. In order to verify that the auxotrophy resulted in energy savings, a drastic effect of cell lysis has to be excluded via further experiments as well.

5.2 Insights into metabolic changes and secondary mutations after *trpP* deletion with relevance for L-tryptophan production in *Corynebacterium glutamicum*

5.2.1 Background

For the setup for the first CoNoS cultures, we generated various strains with auxotrophies for several amino acids. The constructed strains with deletions of the whole biosynthetic machinery for one of the amino acids L-arginine, L-histidine, L-leucine, and L-serine revealed similar

growth behavior when supplemented (Schito *et al.*, 2022). The noteworthy exception was the L-tryptophan auxotrophic strain, with its growth rate also deviating significantly from the previously simulated one (Schito *et al.*, 2022). This piqued our interest in L-tryptophan metabolism in *C. glutamicum*. In this organism, the genes required for L-tryptophan formation from chorismate are organized in one operon, *trpEGDCFBA* (cg3359-3364, see Figure 5.6A). Immediately upstream of this operon, an sRNA potentially involved in regulating TrpE (Mentz *et al.*, 2013) and the divergently located *trpP* is encoded. The gene *trpP* (cg3357) was annotated as an L-tryptophan permease (Kalinowski *et al.*, 2003). Further studies with transposon mutants showed that L-tryptophan auxotrophy is caused when all *trp* genes are hit except for *trpP* (Mormann *et al.*, 2006). The conclusion about TrpP being a permease, however, is solely based on homology data to previously identified transporters in 1994 (Heery *et al.*, 1994). This was supported by the finding that the *trpP* gene product from an L-tryptophan hyper-producer – but not the tested WT sequence, which differed by two point mutations and a potential frameshift-inducing insertion – conferred 5-methyltryptophan (5MT) resistance to *E. coli* (Heery and Dunican, 1993, Heery *et al.*, 1994). With regards to transport of L-tryptophan, the aromatic amino acid transporter AroP (Cg1257) was identified as the main, but, potentially, not the only L-tryptophan importer in *C. glutamicum* (Wehrmann *et al.*, 1995).

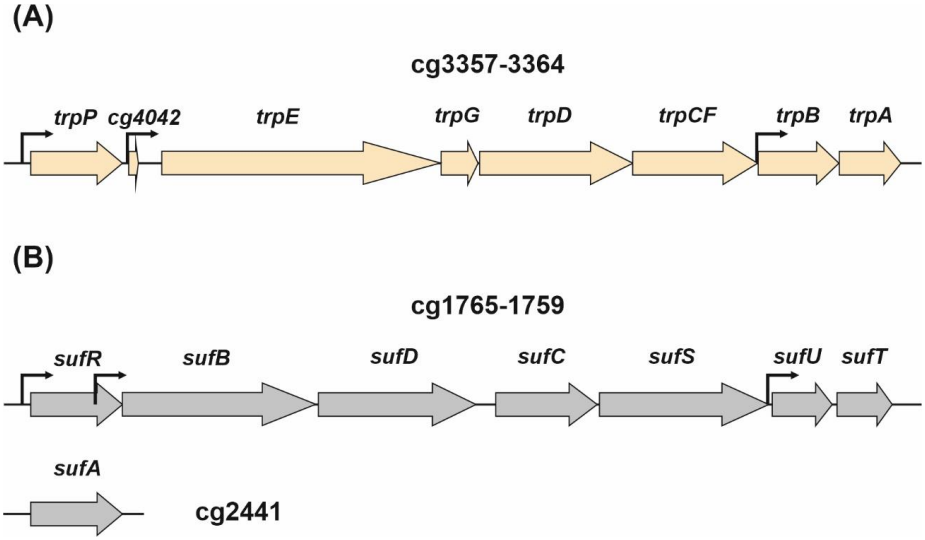

Figure 5.6: Genomic organization of the *trp*-operon (A) and the *suf*-operon (B). TSS are given according to previous studies (Pfeifer-Sancar *et al.*, 2013), sRNAs are given according to (Mentz *et al.*, 2013). The gene cg1759 was assigned *sufT* based on the homology to *sufT* from *M. tuberculosis* (Tripathi *et al.*, 2022).

More recent homology analyses, however, suggested a higher similarity between TrpP (in the study named Cgl1) and the SdpI protein of *Bacillus subtilis* (Povolotsky *et al.*, 2010). Notably, *C. glutamicum* ATCC 13032 TrpP clustered together with proteins of *C. diphteriae* and other *Corynebacteria* but not with proteins of *C. glutamicum* R and *Corynebacterium accolens*, whose SdpI-homologs possess several more transmembrane domains (Povolotsky *et al.*, 2010). *B. subtilis* SdpI is a part of a three-protein signal-transduction system involving SdpI, SdpR, and SpdC, that orchestrates a delay of endospore formation and confers protection against a cannibalistic process induced by SdpC (Ellermeier *et al.*, 2006, Gonzalez-Pastor *et al.*, 2003). The extracellular signaling protein SdpC – after maturation to the 42-residue peptide SDP, harboring one disulfide bridge (Liu *et al.*, 2010), due to the posttranslational action of SdpAB (Perez Morales *et al.*, 2013) – is a toxin involved with intraspecies as well as interspecies defense, as it has, e.g., strong inhibitory effect on *B. simplex* growth (Rosenberg *et al.*, 2016). SDP collapses the proton motive force, which triggers cell autolysis, making it a toxin beneficial in biofilms by inhibiting various neighboring Gram-positive species and releasing their nutrients (Lamsa *et al.*, 2012). SdpC was suggested to interact with the membrane protein SdpI, which changes its conformation upon SdpC binding, resulting in SdpI sequestering the internal autorepressor SdpR – an ArsR family transcription factor – by an unknown mechanism at the membrane and thereby derepressing the *sdpRI* operon, leading to more *sdpI* transcription and thereby to a reaction to the SDP toxin (Ellermeier *et al.*, 2006). When overexpressed, sporulation is delayed, potentially in order to use the nutrients of lysed cells before activating its own starvation response (Gonzalez-Pastor *et al.*, 2003). SdpI protects the cells from the toxin which was proposed to insert itself into the membrane, causing the membrane to become leaky (Ellermeier *et al.*, 2006), resulting in the disruption of the membrane potential and lysis (Lamsa *et al.*, 2012).

C. glutamicum – a non-sporulating bacterium – supposedly does not need a mechanism involved in endospore formation delay and contains no SdpABC homologs. In this study, we aimed to elucidate the role of TrpP in *C. glutamicum* and its potential interaction partner, as well as its role in L-tryptophan metabolism. We identified *trpP* to be a non-essential but highly relevant gene for cell growth, with a surprising linkage to the Fe-S-cluster assembly machinery found via an evolution-guided approach. Moreover, despite TrpP in all likelihood not being the annotated L-tryptophan permease, deletion of *trpP* significantly improved L-tryptophan production, uncovering a relevant new production trait in *C. glutamicum*.

5.2.2 Absence of *trpP* impairs growth of *C. glutamicum*

The deletion of cg3357-cg3364 (i.e., the L-tryptophan auxotrophy used) impaired the growth of *C. glutamicum* ΔTRP even in the presence of external L-tryptophan supplementation (Schito *et al.*, 2022). First, we wanted to examine whether this is a general effect of the L-tryptophan auxotrophy due to, e.g., limited uptake of external L-tryptophan or whether it can be assigned to the deletion of a certain gene. Thus, we constructed strain WT Δcg3359-3364 that lacks the tryptophan biosynthesis genes but still possesses *trpP*. This strain grew almost with WT-level growth rate when supplemented with external L-tryptophan (data not shown). Furthermore, we constructed a deletion mutant lacking only *trpP* (WT Δ*trpP*), which had a similar growth defect as WT Δcg3357-3364 (Figure 5.7A). The observed lower maximum backscatter of WT Δ*trpP* corresponded to a 17% lower OD_{600} after 46h. Analysis of WT Δ*trpP* strain supernatant after 46h revealed no leftover glucose and no noteworthy organic acid formation (data not shown). From this, we concluded that the deletion of the gene *trpP* caused the growth defect observed in the WT ΔTRP strain published (Schito *et al.*, 2022).

To exclude that the observed growth defect is due to any secondary mutation that happened during the deletion process, we performed a complementation experiment. The growth defect of WT Δ*trpP* was relieved through plasmid-based *trpP* expression with pPREx2-*trpP* (Fig. 5.7B), confirming that the observed growth defect was indeed caused by the absence of TrpP. Already low *trpP* expression levels in the absence of IPTG were sufficient to restore strain growth.

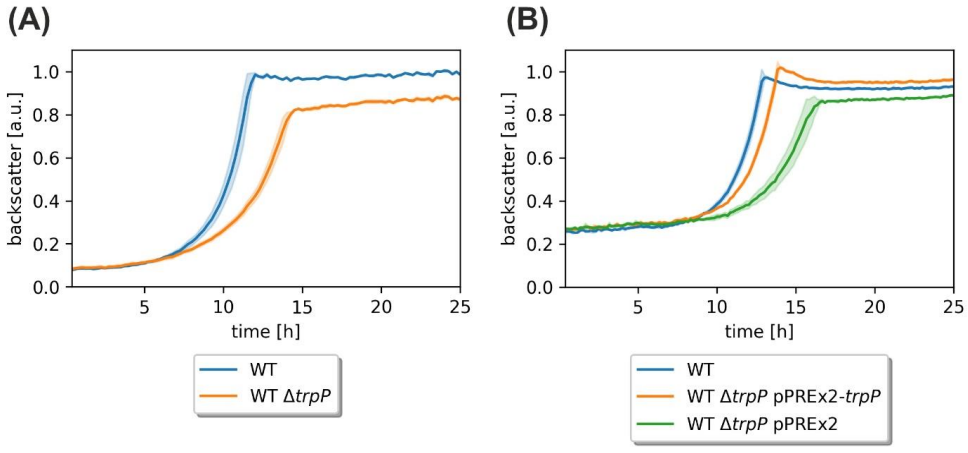

Figure 5.7: Growth characterization and complementation of *trpP* deletion strain. Cultivation of **(A)** WT and WT Δ*trpP* and **(B)** WT and WT Δ*trpP* strains harboring expression plasmids. All cultures were performed in biological triplicates at 30°C, 1400 rpm, and 85% humidity control in non-supplemented CGXII medium with 111 mM D-glucose; 25 µg/ml

kanamycin and no IPTG were added for strains harboring a plasmid. Cultures were inoculated to an OD_{600} of 0.5 with material from a culture first cultivated in BHI medium for 8 h and afterward in CGXII (111 mM D-glucose) medium overnight (25 µg/ml kanamycin was added for strains harboring a plasmid). Based on the maximum value recorded for each WT in the respective experiment, the backscatter data were normalized. The mean values are shown as lines and standard deviations as shaded areas.

The observed growth defect upon *trpP* deletion in *C. glutamicum* appeared to be independent of the L-tryptophan auxotrophy. Nevertheless, a link between *trpP* and L-tryptophan and 5MT has been suggested before (Heery *et al.*, 1994, Heery and Dunican, 1993). Therefore, we analyzed the effect of those two metabolites on growth of WT and WT Δ*trpP* (data not shown). In both strains, adding small amounts of 5MT led to a prolonged lag phase; afterward, growth proceeded for both strains as in medium without 5MT to similar final backscatters with similar growth rates. Moreover, the addition of extracellular L-tryptophan had no negative but, instead, a slightly positive effect on growth rate and maximum backscatter of both strains (data not shown). This suggested that the presence of L-tryptophan and 5MT is not likely to be involved in the observed negative phenotype of the Δ*trpP* strain.

Growth defects caused by deletion of uncharacterized genes often differ depending on the media and the carbon sources used. Therefore, we analyzed the growth of WT and WT Δ*trpP* in different media and with different carbon sources. Under all tested conditions, a clear growth defect of WT Δ*trpP* compared to WT was observed (Figure 5.8). The growth defect of WT Δ*trpP* was the smallest in BHI complex medium, while in CGXII with carbon sources such as gluconate or *myo*-inositol, the lag phase of WT Δ*trpP* was prolonged. Notably, in the case of acetate as the sole carbon source, an initial acetate concentration of 400 mM inhibited the growth of WT Δ*trpP*, while WT could still grow after a prolonged lag phase. The observation suggested a link to the uncoupling activity of acetate on *C. glutamicum* (Wolf *et al.*, 2020). An increased sensitivity of WT Δ*trpP* to the protonophore carbonyl cyanide *m*-chlorophenyl hydrazone (CCCP), however, was not observed (data not shown). Overall, these results suggested that WT Δ*trpP* has severe problems adapting to new environments with different carbon sources.

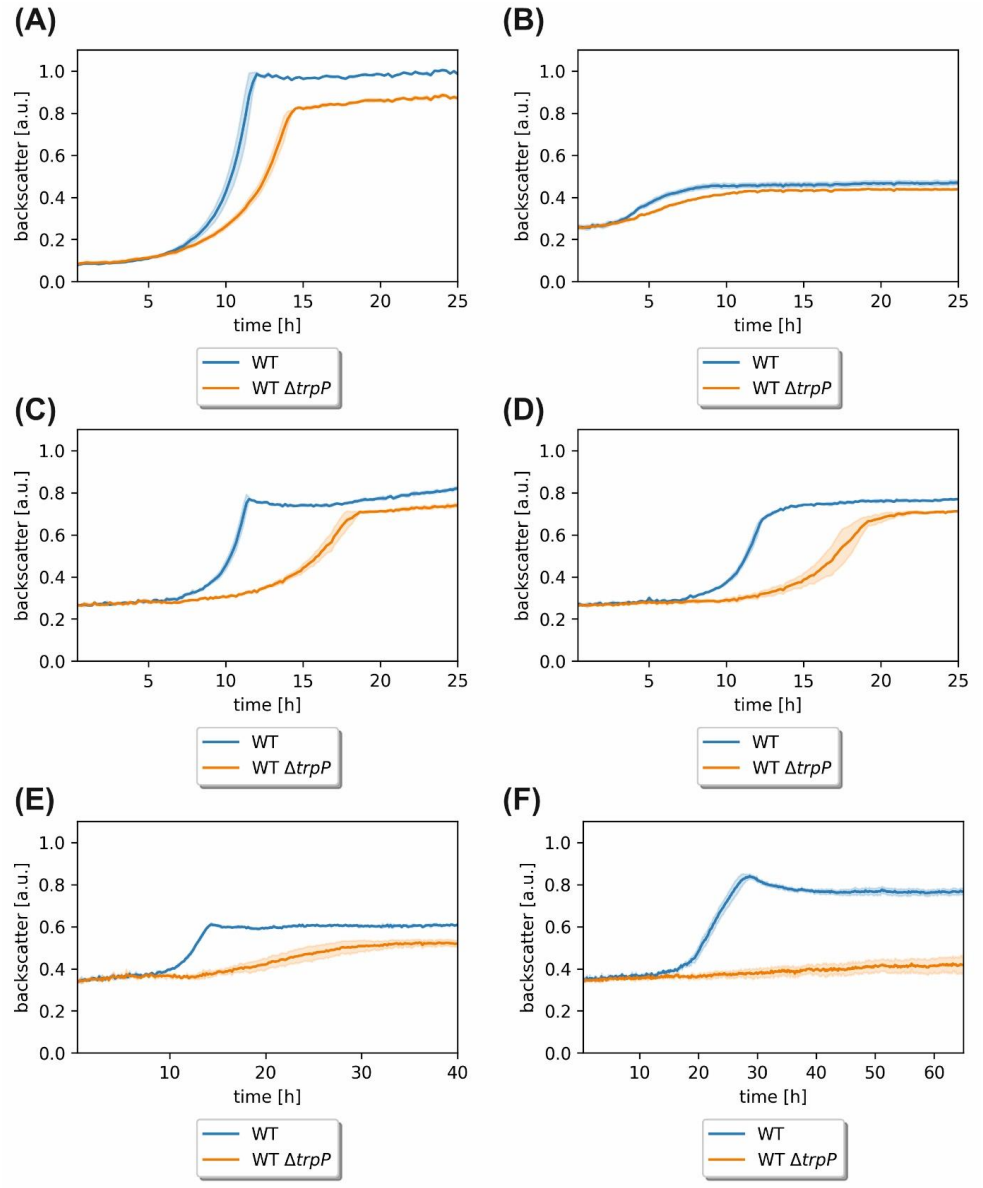

Figure 5.8: Growth characterization of WT and WT Δ*trpP* in different media. Cultivation in **(A)** CGXII medium with 111 mM D-glucose, **(B)** Brain-heart-infusion complex medium (Difco™), **(C)** CGXII medium with 100 mM gluconate, **(D)** CGXII medium with 100 mM *myo*-inositol, **(E)** CGXII medium with 200 mM acetate, and **(F)** CGXII medium with 400 mM acetate at 30°C, 1400 rpm, 85% humidity control. All cultures were performed in biological triplicates. Based on the maximum value recorded for WT in CGXII with D-glucose, the backscatter data were normalized. The mean values are shown as lines and standard deviations as shaded areas.

5.2.3 Evolution-guided WT ΔTRP Δ*trpP* improvement reveals *suf*-cluster upregulation to be beneficial

Since the exact mechanism of why the deletion of *trpP* had impaired WT ΔTRP Δ*trpP* growth was unknown, Adaptive Laboratory Evolution (ALE) was used to identify the bottlenecks of the L-tryptophan auxotrophic strains. Since the C1* ΔTRP Δ*trpP* (constructed before WT ΔTRP Δ*trpP* in (Schito *et al.*, 2022)) possessed a drastically lower growth rate than the WT, there was a high selective pressure on the strain to grow faster, which makes the ALE approach particularly useful for identifying novel uptake and production traits (Radek *et al.*, 2017). For the ALE, the strain C1* ΔTRP Δ*trpP* (i.e., with the deletion cg3357-3364) was used because the isolated effect of the *trpP* deletion on strain growth was not known at that time.

The ALE with the C1* ΔTRP Δ*trpP* was performed in triplicates with a supplemented monoculture. From each replicate, single strains were isolated after 16 independent cultivations and tested afterward regarding growth in comparison to the unevolved C1* ΔTRP Δ*trpP*. Indeed, in all three replicates, the growth rate increased significantly from 0.41 h^{-1} to 0.49 h^{-1} (work from S. Schito, data not part of this thesis). Genomic DNA was prepared and sequenced from those three independent replicates via whole genome sequencing. This revealed one mutation per replicate in the SufR regulatory protein: L25P, R77G, and Q193* (see Table 5.1).

Two mutations were reintroduced in WT ΔTRP Δ*trpP*, yielding WT ΔTRP Δ*trpP* $SufR_{L25P}$ and WT ΔTRP Δ*trpP* $SufR_{Q193*}$. Reengineering of those mutations verified their effect on improving the growth of the L-tryptophan auxotrophic strains (see Figure 5.9A). SufR L25 and R77 positions are highly conserved residues, suggesting that their mutation inhibits protein function (see Figure 5.10).

To test whether deletion of SufR has a similar effect, we constructed WT ΔTRP Δ*trpP* Δ*sufR*. This strain grew indeed better than WT ΔTRP Δ*trpP*, so we assumed that the observed mutation indeed led to loss of SufR function. (see also Figure 5.9A). Similarly, growth of the WT Δ*trpP* strain could be improved due to the effect of the *sufR* deletion, while the *sufR* deletion itself did not improve strain growth (see Figure 5.9B). The WT ΔTRP Δ*trpP* Δ*sufR* strain was subsequently used as a basis for a further evolution experiment to identify additional mutations that improve growth of this strain. However, no further growth improvement was achieved within 16 batches (work from S. Schito, data not part of this thesis).

Table 5.1: Mutations identified in the evolved C1* ΔTRP Δ*trpP* strains

Strain	Position & mutation on DNA level[1]	Locus tag	Mutation
C1* ΔTRP Δ*trpP* evo1	SNV A1481472G	cg1765	$SufR_{L25P}$
C1* ΔTRP Δ*trpP* evo2	SNV T1481317C	cg1765	$SufR_{R77G}$
C1* ΔTRP Δ*trpP* evo3	SNV G1480969A	cg1765	$SufR_{Q193*}$

[1]Genome sequencing was performed with clones isolated from the three independent 16th batches of the ALE experiment. Reads were mapped using accession NZ_CP017995 as the reference genome, single nucleotide variants (SNV) are given for the plus strand.

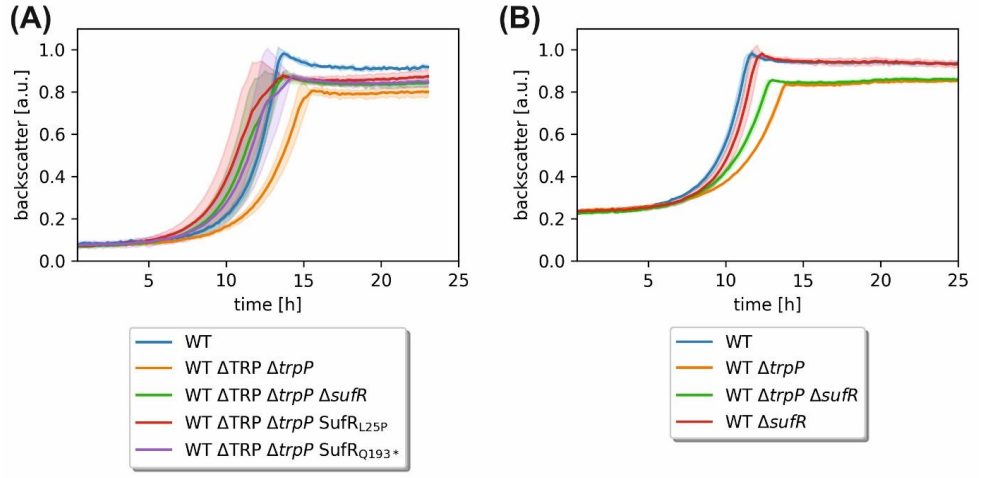

Figure 5.9: Growth of *C. glutamicum* strains with reengineered mutations that appeared during ALE of WT ΔTRP Δ*trpP*. (A) Cultivation of WT ΔTRP based strains. **(B)** Cultivation of WT based strains. All cultures were performed in biological triplicates in CGXII medium with 111 mM D-glucose and 500 µM L-tryptophan for auxotrophic strains at 30°C, 1400 rpm, and 85 % humidity control. Based on the maximum value recorded for each WT in the respective experiment, the backscatter data were normalized. The mean values are shown as lines and standard deviations as shaded areas.

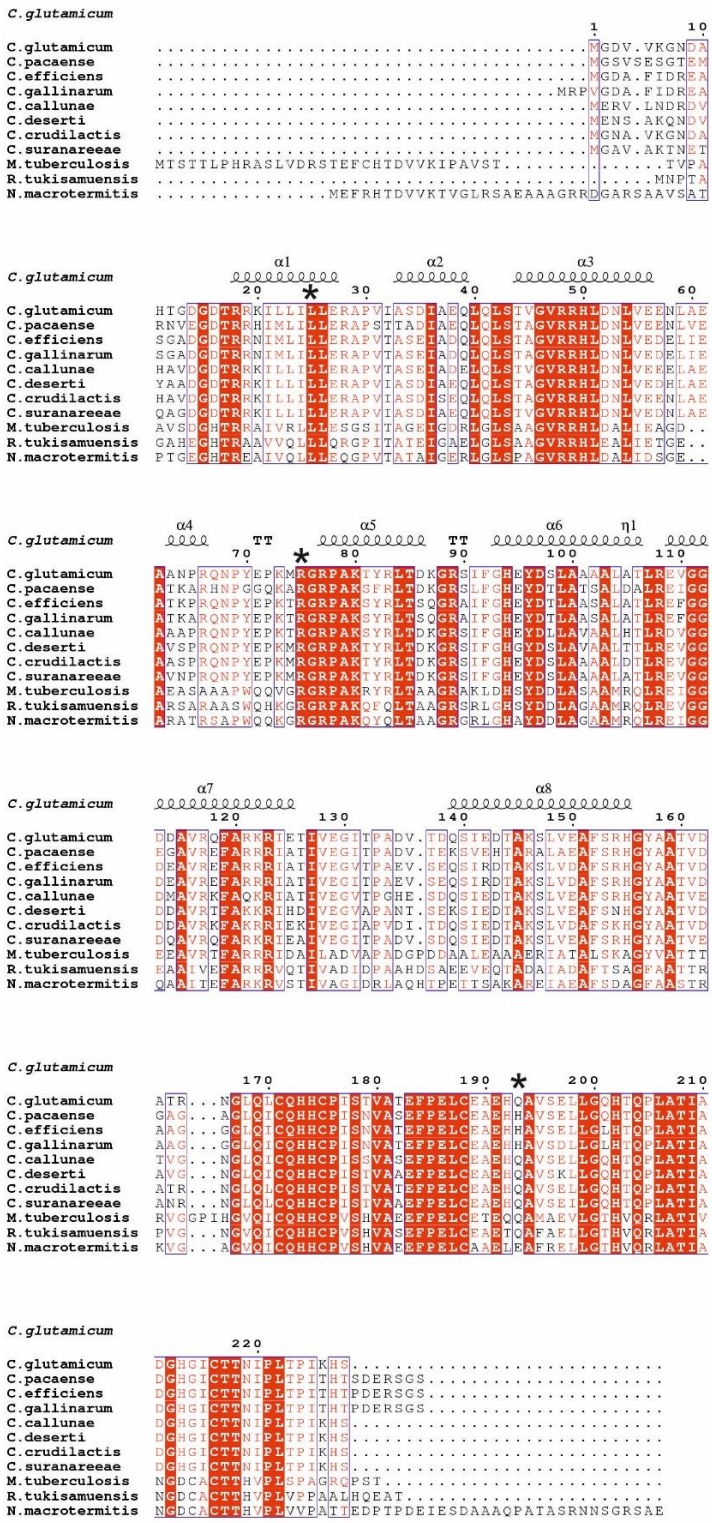
C.glutamicum
C.glutamicum
C.pacaense
C.efficiens
C.gallinarum
C.callunae
C.deserti
C.crudilactis
C.suranareeae
M.tuberculosis
R.tukisamuensis
N.macrotermitis
α1
α2
α3
α4
α5
α6
η1
α7
α8

Figure 5.10: Multiple sequence alignment of SufR sequences of different species. Comparison of SufR of *Corynebacterium* species, *Mycobacterium tuberculosis*, *Nocardia macrotermitis*, *Rhodococcus tukisamuensis*. Clustal Omega was used for the sequence alignment (Sievers *et al.*, 2011). Via Swissmodel, a potential structure of *C. glutamicum* SufR was predicted as a reference (modeled after the crystal structure of RecX PDB 3d5l.1.A) (Waterhouse *et al.*, 2018). The alignment was visualized with ESPribt 3.0 (Robert and Gouet, 2014). The mutation sites identified in the evolved *C. glutamicum* strains are marked with an asterisk.

SufR is a transcriptional regulator with a predicted DNA binding domain located near the N-terminus (Paysan-Lafosse *et al.*, 2023), and the link between iron-sulfur-cluster formation and TrpP is up to now not clear. Only one binding site of SufR in the promoter region of *sufR* itself was predicted according to CoryneRegNet 7 in *C. glutamicum* (Parise *et al.*, 2020). This regulator located upstream of the *suf* operon is transcribed via its own promoter (see Figure 5.6). Since SufR could have yet unknown target genes, we performed microarray experiments to identify genes differentially regulated in the absence of SufR. The results of the transcriptome analysis of WT ΔTRP Δ*trpP* and WT ΔTRP Δ*trpP* Δ*sufR* are shown in Table 5.2.

Table 5.2: Transcriptomic comparison of WT ΔTRP Δ*trpP* Δ*sufR* and WT ΔTRP Δ*trpP*

Locus tag	Gene name	Annotation	N[1]	Average mRNA ratio[2]	p-value
cg1760	*sufU*	cysteine desulfhydrase	3	8.04	0.01
cg1762	*sufC*	Fe-S cluster assembly ATPase	3	6.88	< 0.01
cg1764	*sufB*	Fe-S cluster assembly protein	4	6.70	< 0.01
cg1763	*sufD*	Fe-S cluster assembly membrane protein	4	6.61	< 0.01
cg1765	*sufR*	transcriptional regulator of suf-operon	4	6.32	< 0.01
cg3096	*ald*	aldehyde dehydrogenase	4	4.11	< 0.01
cg2538		alkanal monooxygenase alpha chain	3	2.88	0.01
cg3335	*malE*	malic enzyme	3	2.71	< 0.01
cg2838		putative dithiol-disulfide isomerase	3	2.42	< 0.01
cg2181	*oppA*	ABC-type peptide transport system, secreted component	4	2.39	< 0.01
cg0133	*abgT*	*p*-aminobenzoyl-glutamate transporter	3	2.30	0.011
cg2106		hypothetical protein cg2106	3	2.28	< 0.01
cg2184	*oppD*	ATPase component of peptide ABC-type transport	3	2.14	0.016

Locus tag	Gene name	Annotation	N[1]	Average mRNA ratio[2]	p-value
		system, contains duplicated ATPase domains			
cg2183	*oppC*	ABC-type peptide transport system, permease component	3	2.08	< 0.01
cg1881		putative iron-dependent peroxidase, secreted protein, conserved	4	0.48	< 0.01
cg1883		putative secreted protein	4	0.46	0.017
cg1884		putative copper resistance protein C	4	0.45	< 0.01
cg3140	*tagA1*	probable DNA-3-methyladenine glycosylase I protein	4	0.37	< 0.01
cg3139		hypothetical protein Cg3139	4	0.37	< 0.01
cg1300	*cydB*	cytochrome D terminal oxidase polypeptide subunit	3	0.33	0.035
cg1343	*narH*	dissimilatory nitrate reductase, β-subunit, iron sulfur protein	4	0.33	< 0.01
cg1342	*narJ*	dissimilatory nitrate reductase, δ-subunit, assembly factor	4	0.32	< 0.01
cg1341	*narI*	dissimilatory nitrate reductase, γ-subunit, cytochrome b	4	0.31	< 0.01
cg3138	*ppmA*	putative membrane-bound protease modulator	4	0.31	< 0.01
cg1344	*narG*	dissimilatory nitrate reductase, α-subunit, Mo cofactor-containing	4	0.28	< 0.01
cg1345	*narK*	nitrate/nitrite antiporter	4	0.26	< 0.01

[1] Number of experiments
[2] Results of microarray experiments comparing the gene expression in WT ΔTRP Δ*trpP* Δ*sufR* / WT ΔTRP Δ*trpP*. Shown are all target genes with at least 2-fold change in at least 3 of 4 experiments (p-value < 0.05).

The analysis revealed 11 genes or gene clusters to be ≥ 2 times differently regulated in the WT ΔTRP Δ*trpP* Δ*sufR* strain. Most strongly upregulated is the *suf*-operon. Except for the *suf* operon, none of the other target genes show an obvious relation to SufR, and from the identified genes, only the nitrate reductase contains a Fe-S cluster. This suggested that SufR primarily regulates the *suf*-cluster expression and no other target, which is in line with the data published at CoryneRegNet 7 (Parise *et al.*, 2020). It cannot be excluded, though, that further genes are regulated by SufR since their differential regulation in absence of SufR could be concealed by another regulator.

To verify that higher expression levels of the *suf*-cluster in the strain WT ΔTRP Δ*trpP* are indeed responsible for the improved growth of WT ΔTRP Δ*trpP* Δ*sufR*, the whole *suf*-operon was expressed in WT ΔTRP Δ*trpP*. For this, the pAN6 shuttle vector for regulated gene expression with a P_{tac} promoter in front of the *suf*-operon (Frunzke *et al.*, 2008) was used. The resulting strain WT ΔTRP Δ*trpP* pAN6-*suf*-cluster was characterized in a BioLector experiment with various initial IPTG concentrations (data not shown). However, all tested IPTG concentrations > 0 mM resulted in a growth defect, while the concentration of 0 µM did not change strain growth in comparison to the empty vector control WT ΔTRP Δ*trpP* pAN6. From this result, it could not be concluded if the expression system of the *suf*-cluster is problematic or if the hypothesis about the increased expression of the cluster being responsible for the improved strain growth is wrong. Therefore, in a further experiment, we tested changing the expression levels via promoter exchanges in front of the main promoter of the *suf*-operon, P_{sufB}, to verify that strain growth can be modulated according to the expression level of the *suf*-operon. The native promoter P_{sufB} in the strain WT ΔTRP Δ*trpP* was exchanged with *C. glutamicum* promoters of different strengths (P_{tuf}, P_{dapA}) that have been tested elsewhere before (Shang *et al.*, 2018). The resulting strains were compared regarding their growth in CGXII medium with 2% (w/v) glucose supplemented with L-tryptophan with the WT, their parental strain WT ΔTRP Δ*trpP*, and the improved strain WT ΔTRP Δ*trpP* Δ*sufR* (Figure 5.11). In comparison to the parental WT ΔTRP Δ*trpP* strain, the strain WT Δ*trpP* ΔP_{sufB}::P_{dapA} with the weakly expressed P_{dapA} grew slower, while the WT Δ*trpP* ΔP_{sufB}::P_{tuf} with the strongly expressed P_{tuf} grew faster, reaching a higher final backscatter level. Notably, the latter strain grew with a growth rate 12% higher than WT Δ*trpP* Δ*sufR*. The high differences in growth rates suggested a positive correlation between an increased expression level of the *suf*-cluster and strain growth. This provides evidence that the inactivation of SufR found in the ALE indeed could have improved strain growth by increasing the *suf*-cluster expression. As the expression level of the *suf*-cluster in *C. glutamicum* is comparably high, with those genes belonging to the 15% of genes transcribed the strongest (unpublished data J. Kalinowski, personal communication), this is in line with P_{tuf}, one of the strongest promoters of *C. glutamicum* (Shang et al., 2018), resulting in improved growth.

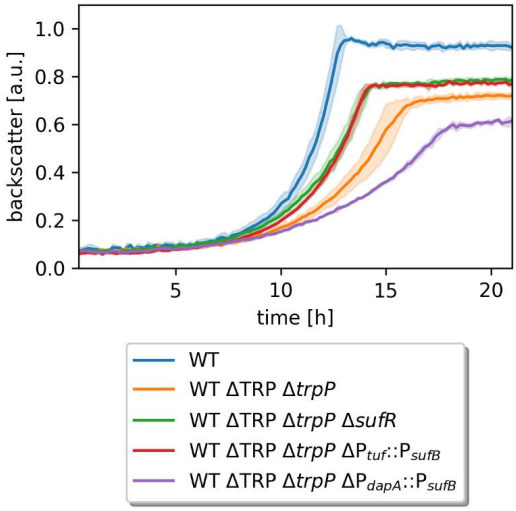

Figure 5.11: Influence of promoter strength in front of *sufB* in WT ΔTRP Δ*trpP* Δ*sufR*. Cultivation in 800 µL CGXII medium 2% (w/v) D-glucose (supplemented with 500 µM l-tryptophan for auxotrophic strains) in biological triplicates at 1400 rpm, 30°C, and 85% humidity control. Based on the maximum value recorded for each WT in the respective experiment, the backscatter data were normalized. The mean values are shown as lines and standard deviations as shaded areas.

5.2.4 Consequences of *trpP* deletion

Further microarray experiments were performed to elucidate the mechanism behind the negative effect on strain growth upon *trpP* deletion. The two differently growing strains, WT ΔTRP Δ*trpP* and WT ΔTRP, were compared to identify genes differentially regulated in the absence of *trpP* (data not shown). Additionally, the transcriptomes of WT Δ*trpP* and WT were analyzed to exclude any potential effects related to the L-tryptophan-auxotrophy (see Table 5.3).

Table 5.3: Transcriptomic comparison of WT Δ*trpP* and WT

Locus tag	Gene name	Annotation	N[1]	Average mRNA ratio[2]	p-value
cg0229	*gltB*	glutamine 2-oxoglutarate aminotransferase large SU	4	4.76	0.017
cg1216	*nadA*	quinolinate synthetase	4	3.99	0.002
cg1628		hydrolase of the alpha/beta superfamily	4	3.99	0.004
cg1218	*ndnR*	transcriptional repressor of NAD *de novo* biosynthesis genes	4	3.79	0.010
cg1626		hypothetical protein cg1626	4	3.71	0.026

Locus tag	Gene name	Annotation	N[1]	Average mRNA ratio[2]	p-value
cg1785	*amt*	high-affinity ammonia permease	4	3.52	0.005
cg0230	*gltD*	glutamine 2-oxoglutarate aminotransferase small SU	4	3.09	0.001
cg1214	*nadS*	cysteine desulfurase-like protein involved in Fe-S cluster assembly	4	2.97	0.001
cg1784	*ocd*	ornithine cyclodeaminase	4	2.91	0.005
cg1299	*cydD*	ABC-type multidrug/protein/lipid transport system, ATPase component	4	2.86	0.005
cg1301	*cydA*	cytochrome D ubiquinol oxidase subunit I	4	2.77	< 0.001
cg1215	*nadC*	quinolinate phosphoribosyltransferase	4	2.70	0.001
cg1300	*cydB*	cytochrome D terminal oxidase polypeptide subunit	4	2.60	0.002
cg1580	*argC*	N-acetyl-gamma-glutamyl-phosphate reductase	4	2.29	0.110
cg2047		putative secreted protein	4	2.20	0.014
cg1298	*cydC*	ABC-type multidrug/protein/lipid transport system, ATPase component	4	2.19	0.008
cg2845	*pstC*	ABC-type phosphate transport system, permease component	4	2.17	0.130
cg2261	*amtB*	low affinity ammonium uptake protein	4	2.16	0.022
cg2843	*pstB*	ABC-type phosphate transport system, ATPase component	4	2.11	0.098
cg0175		secreted protein, signal peptide	4	2.10	0.115
cg2407		hypothetical protein cg2407	4	2.08	0.004
cg1139		allophanate hydrolase subunit 2	4	0.50	0.013
cg1920		hypothetical protein cg1920	4	0.49	0.012
cg1230		hypothetical protein cg1230	4	0.49	0.023
cg1921		hypothetical protein cg1921	4	0.49	0.009
cg1923		hypothetical protein cg1923	4	0.49	0.036
cg1140		allophanate hydrolase subunit 1	4	0.49	0.018
cg2732	*gntV*	putative gluconokinase	4	0.48	0.165
cg1595	*uspA2*	universal stress protein UspA or related nucleotide-binding protein	4	0.48	0.006
cg0922		secreted siderophore-binding lipoprotein	4	0.48	0.012
cg1412		ribose/xylose/arabinose/galac-toside ABC-type transport system, permease component	4	0.48	0.010

Locus tag	Gene name	Annotation	N[1]	Average mRNA ratio[2]	p-value
cg1310	*tfdF*	maleylacetate reductase	4	0.48	0.012
cg0097		hypothetical protein cg0097 |	4	0.48	0.008
cg1922		hypothetical protein cg1922	4	0.48	0.015
cg1919		hypothetical protein cg1919	4	0.47	0.009
cg0202	*iolD*	putative acetolactate synthase protein	4	0.47	0.016
cg3395	*proP*	proline/ectoine carrier	4	0.47	0.005
cg1924		hypothetical protein cg1924	4	0.46	0.014
cg1231	*chaA*	Ca^{2+}/H^{+} antiporter	4	0.45	0.023
cg0201	*iolB*	enzyme involved in inositol metabolism	4	0.45	0.013
cg3385	*catA3*	catechol 1,2-dioxygenase	4	0.45	0.011
cg1226	*pobB*	4-hydroxybenzoate 3-monooxygenase	4	0.44	0.003
cg1225	*benK3*	putative benzoate transport transmembrane protein	4	0.44	0.007
cg1142		Na^{+}/proline, Na^{+}/panthothenate symporter	4	0.44	0.013
cg3047	*ackA*	acetate/propionate kinase	4	0.43	0.011
cg0921		cytoplasmic siderophore-interacting protein	4	0.43	0.016
cg0205	*iolH*	*myo*-inositol catabolism protein	4	0.43	0.003
cg0254		amino acid carrier protein (sodium/alanine symporter)	4	0.42	0.012
cg0347	*hdtZ*	3-hydroxyacyl-thioester dehydratase	4	0.42	0.002
cg3374		putative NADH-dependent flavin oxidoreductase	4	0.42	< 0.001
cg2937		ABC-type dipeptide/oligopeptide/nickel transport system, secreted component	4	0.42	0.010
cg0204	*iolG*	inositol dehydrogenase	4	0.42	0.002
cg2940		ATPase components of ABC-type transport system	4	0.41	0.003
cg1109	*porB*	anion-specific porin precursor	4	0.41	0.003
cg0760	*prpB2*	2-methylisocitrate lyase	4	0.41	0.060
cg2181	*oppA*	ABC-type peptide transport system, secreted component	4	0.41	0.013
cg0344	*fabG1*	3-oxoacyl-(acyl-carrier protein) reductase	4	0.41	0.006
cg3386	*tcbF*	maleylacetate reductase	4	0.41	0.009

Locus tag	Gene name	Annotation	N[1]	Average mRNA ratio[2]	p-value
cg0134		hydrolase, Ama/HipO/HyuC family	4	0.41	0.004
cg0203	*iolE*	2-Keto-*myo*-inositol dehydratase	4	0.40	0.003
cg3127	*tctC*	tricarboxylate-binding protein	4	0.40	0.012
cg0345		metal-dependent hydrolase of the TIM-barrel fold	4	0.40	0.011
cg2628	*pcaC*	γ-carboxymuconolactone decarboxylase	4	0.39	0.004
cg0346	*fadE*	glutaryl-CoA dehydrogenase	4	0.38	0.003
cg2629	*pcaB*	β-carboxy-cis,cis-muconate cycloisomerase	4	0.38	0.003
cg2939		ABC-type dipeptide/oligopeptide/nickel transport system, fused permease and ATPase components	4	0.37	0.012
cg3387	*iolT2*	*myo*-Inositol transporter	4	0.37	0.007
cg0762	*prpC2*	2-methylcitrate synthase	4	0.36	0.055
cg0759	*prpD2*	2-methycitrate dehydratase	4	0.36	0.071
cg0212		phosphate isomerase/epimerase	4	0.36	0.008
cg0637	*betB*	putative betaine aldehyde dehydrogenase (BADH) oxidoreductase	4	0.36	0.002
cg0198		hypothetical protein cg0198	4	0.35	0.009
cg0199	*iolA*	*myo*-Inositol catabolism, aldehyde dehydrogenase	4	0.35	0.009
cg2938		ABC-type dipeptide/oligopeptide/nickel transport system, permease component	4	0.35	0.015
cg0638		HD superfamily hydrolase	4	0.34	0.001
cg2560	*aceA*	isocitrate lyase	4	0.34	< 0.001
cg2559	*aceB*	malate synthase	4	0.34	0.003
cg0211		putative oxidoreductase	4	0.33	0.005
cg0639		ferredoxin reductase	4	0.33	0.002
cg0133	*abgT*	*p*-aminobenzoyl-glutamate transporter	4	0.32	0.005
cg1090	*ggtB*	probable gamma-glutamyltranspeptidase precursor PR	4	0.32	0.001
cg0645	*cytP*	cytochrome P450	4	0.32	0.001
cg2630	*pcaG*	protocatechuate dioxygenase α subunit	4	0.32	0.005

Locus tag	Gene name	Annotation	N[1]	Average mRNA ratio[2]	p-value
cg3126	*tctB*	tricarboxylate transport membrane protein	4	0.32	0.015
cg2636	*catA1*	catechol 1,2-dioxygenase	4	0.31	0.002
cg3125	*tctA*	tricarboxylate transport membrane protein	4	0.31	0.012
cg0088	*citH*	citrate transporter	4	0.31	0.001
cg2631	*pcaH*	protocatechuate dioxygenase beta subunit	4	0.31	0.002
cg2837	*sucC*	succinyl-CoA synthetase subunit beta	4	0.29	0.009
cg0640	*fdxB*	ferredoxin	4	0.28	0.004
cg2966		phenol 2-monooxygenase	4	0.27	0.002
cg0642		hypothetical protein cg0642	4	0.27	0.002
cg0641	*fabG2*	probable short-chain dehydrogenase, secreted	4	0.25	0.001
cg3216	*gntP*	gluconate permease	4	0.24	0.002
cg0223	*iolT1*	*myo*-Inositol transporter	4	0.23	0.002
cg0644		pyruvate phosphate dikinase, PEP/pyruvate binding	4	0.22	0.005
cg2836	*sucD*	succinyl-CoA synthetase alpha subunit	4	0.21	< 0.001
cg1309		3-(3-hydroxyphenyl)propionate hydroxylase	4	0.21	0.002
cg0961		homoserine O-acetyltransferase	4	0.21	0.001
cg2312	*gip*	putative hydroxypyruvate isomerase protein	3	0.20	0.006
cg2616	*vanA*	vanillate demethylase, oxygenase subunit	4	0.16	0.002
cg1612		acetyltransferase	4	0.16	0.002
cg2610		ABC-type dipeptide/oligopeptide/nickel transport system, secreted component	4	0.13	< 0.001
cg3096	*ald*	aldehyde dehydrogenase	4	0.13	0.001
cg3195		flavin-containing monooxygenase (FMO)	4	0.09	< 0.001
cg3107	*adhA*	Zn-dependent alcohol dehydrogenase	4	0.08	< 0.001
cg3357	*trpP*	tryptophan-specific permease	4	0.07	< 0.001

[1] Number of experiments

[2] Results of microarray experiments comparing the gene expression in WT Δ*trpP* / WT. Shown are all target genes with at least 2-fold change in at least 3 of 4 experiments (p-value < 0.05).

Interestingly, a differential expression of the *nadSCAR* gene cluster (cg1214-1218), encoding the machinery for *de novo* NAD biosynthesis, was observed in all experiments, also in the microarray not shown of WT ΔTRP Δ*trpP* and WT ΔTRP. It is known that this cluster is repressed in the presence of NAD via NadR or, vice versa, upregulated when concentration of the corepressor NAD in the cell is low (Teramoto *et al.*, 2012, Teramoto *et al.*, 2010). This suggested that the absence of TrpP could result in a shortage of NAD in WT Δ*trpP*. NadA, the quinolinate synthetase, harbors an Fe-S-cluster, with NadS being responsible for the correct Fe-S-cluster formation of NadA.

The gene cluster that is upregulated the most in WT Δ*trpP* is *gltBD* (cg0229-0230), encoding GOGAT (glutamine 2-oxoglutarate aminotransferase). In the absence of *trpP*, these genes are almost four times higher expressed than in the WT, and, notably, GltD harbors an Fe-S-cluster as well. In *C. glutamicum*, GOGAT together with glutamine synthetase (GS) represents one of the two main pathways for ammonium assimilation, whereby the other way via the glutamate dehydrogenase (GDH) is favored under high ammonium concentrations, and GOGAT is inactive (Tesch *et al.*, 1999). Nitrogen fixation via GOGAT is more expensive than the GDH pathway regarding its ATP and AMP demand (Schulz *et al.*, 2001). GOGAT is only upregulated in the case of nitrogen limitation, and its activity is mainly regulated at the transcription level (Beckers *et al.*, 2001, Schulz *et al.*, 2001). GOGAT activity might also be controlled via product inhibition by NAD^+ and $NADP^+$, as this is the case in *C. callunae* where GOGAT utilizes either NADH or NADPH as coenzymes (Ertan, 1992). In line with the nitrogen limitation, the nitrogen uptake system encoding genes *amt* (cg1785) and *amtB* (cg2261) are more than two-fold upregulated in WT Δ*trpP*. This also accounts for the ornithine cyclodeaminase gene (cg1784), which is almost three-fold upregulated. The ornithine cyclodeaminase with NAD^+ as a cofactor catalyzes the reaction due to which free ammonium is formed, which occurs more often in a medium with a low amount of nitrogen source (Jensen and Wendisch, 2013).

A further operon of interest that was 2.6-fold upregulated in WT Δ*trpP* is the *cydABCD* operon (cg1298-1301), encoding the cytochrome *bd* oxidase. Cytochrome *bd* oxidase of *C. glutamicum* is one of the two terminal oxygen reductases that catalyzes the reduction of molecular oxygen to water and has a pseudosymmetrical heterodimeric architecture formed by the core subunits CydA and CydB (Grund *et al.*, 2022). Both its upregulation and its deletion were shown before to reduce the growth efficiency, i.e., the final OD, and its deletion increased the L-lysine production (Kabus *et al.*, 2007). It is assumed that this comes due to the alternative oxidase, the supercomplex of cytochrome bc_1 complex and cytochrome aa_3, being more

effective in contributing to the generation of the proton motive force by pumping protons after oxidizing menaquinone (Kabus *et al.*, 2007). Cytochrome *bd* oxidase was suggested to be the main terminal oxygen reductase under low oxygen conditions, as it has a higher oxygen affinity, and under copper-deficient conditions (Bott and Niebisch, 2003). Also, in comparison to the cytochrome bc_1 complex, the oxidase does not contain an Fe-S-cluster and could therefore be important under specific conditions where there are less functional Fe-S-cluster. A third pathway for menaquinone oxidation under anaerobic conditions is the nitrate reductase (encoded by *nagGHJI* cg1344-1341), which oxidizes menaquinone to reduce nitrate to nitrite (Bott and Niebisch, 2003, Nishimura *et al.*, 2008). This nitrate reductase contains one Fe-S-cluster, as well, and is downregulated in WT ΔTRP Δ*trpP* Δ*sufR* (Table 5.2), potentially being regulated by SufR.

In contrast to the 21 genes with increased transcription levels, a drastically higher number of genes was downregulated in WT Δ*trpP*. This includes many genes involved in the uptake and metabolism of other carbon sources, such as *myo*-inositol, PCA, citrate, propionate, gluconate, vanillate, and 4-cresol. This result is in line with the observed difficulties of WT Δ*trpP* when grown with different carbon sources (see Figure 5.7). Overall, the impact of the *trpP* deletion in *C. glutamicum* affected the transcription of a large number of genes, from which several could be candidates for being involved in a mechanism that TrpP is part of. Further research is necessary to determine the exact function of TrpP.

5.2.5 The absence of TrpP strongly influenced L-tryptophan and L-valine titer

Initially, a role of TrpP in L-tryptophan metabolism was assumed, especially with the suggestion of TrpP being involved in L-tryptophan transport in literature (Heery and Dunican, 1993, Heery *et al.*, 1994). Therefore, *trpP* and *sufR* were deleted in the moderate L-tryptophan producer strain WT TRP^{+++} in order to study changes in strain performance and L-tryptophan titer. WT TRP^{+++} harbors mutations relieving feedback resistance via TrpE and TrpD, relieving attenuation via *trpL*, as well as a deletion of the main L-tryptophan importer AroP. The growth performance and L-tryptophan accumulation in a shake flask experiment are shown in Figure 5.12. Deletion of *trpP* decreased the growth rate of WT TRP^{+++} and resulted in an 8% lower maximum backscatter. Deletion of *sufR* increased the maximum backscatter of WT TRP^{+++} slightly, while the double deletion grew still worse than WT TRP^{+++} but significantly better than WT TRP^{+++} Δ*trpP*. For the tested induction level with 200 µM IPTG, WT TRP^{+++} pPREx2-*trpP* grew similarly to the empty vector control. Regarding the level of L-tryptophan accumulation, the deletion of *trpP* resulted in an increase of 260% in comparison to WT

TRP^{+++}. The deletion of *sufR* alone did not change the L-tryptophan titer, whereby the double deletion increased the titer by more than 3-fold in comparison to WT TRP^{+++}. The deletion of *trpP*, ideally with the deletion of *sufR*, therefore, marks a novel L-tryptophan production trait. This is true, however, also for the plasmid-based expression of *trpP*, which resulted at the given induction level in an increase in L-tryptophan accumulation by 60%.

Notably, for the amino acid L-valine, drastic changes in production level were observed. While this amino acid appeared as a by-product in the WT TRP^{+++} and WT TRP^{+++} Δ*sufR* strain, the deletion of *trpP* almost completely inhibited the formation of L-valine. In contrast, plasmid-based *trpP* expression increased the L-valine accumulation more than three-fold. It is not clear why *trpP* deletion almost completely abolished the L-valine accumulation. One potential link could be the expression level of the *suf*-cluster: it is known from an L-valine producer strain that its Fe-S cluster assembly proteins are upregulated (Zhang *et al.*, 2018). IlvD, the dihydroxy-acid dehydratase involved in a key step of BCAA biosynthesis (Radmacher *et al.*, 2002), is predicted to possess an iron-sulfur cluster (Paysan-Lafosse *et al.*, 2023). These results strengthen the link between TrpP and the SUF-cluster, suggesting that TrpP is relevant for the full activity of Fe-S-cluster-dependent proteins. The effect of its deletion on L-tryptophan titer, on the other hand, might be related primarily to increased precursor supply and decreased concurring reaction, e.g., because the serine dehydratase SdaA, involved in the degradation of L-serine, an L-tryptophan precursor, potentially contains an Fe-S-cluster (Netzer *et al.*, 2004, Paysan-Lafosse *et al.*, 2023). Another precursor, PEP, could also be available in higher concentrations if metabolic flux into the TCA is slower due to central enzymes such as the aconitase, which also contains an Fe-S cluster (Baumgart and Bott, 2011), which would improve L-tryptophan biosynthesis. However, since a detailed characterization of TrpP is still missing, no concluding evidence for the mechanism of these changed amino acid titers can be given. A further GC-ToF measurement to compare the metabolome of WT TRP^{+++} and WT TRP^{+++} Δ*trpP* is currently pending (AG Noack). With this analysis, further changes in the metabolome, e.g., due to missing activity of Fe-S-cluster enzymes, could be detected.

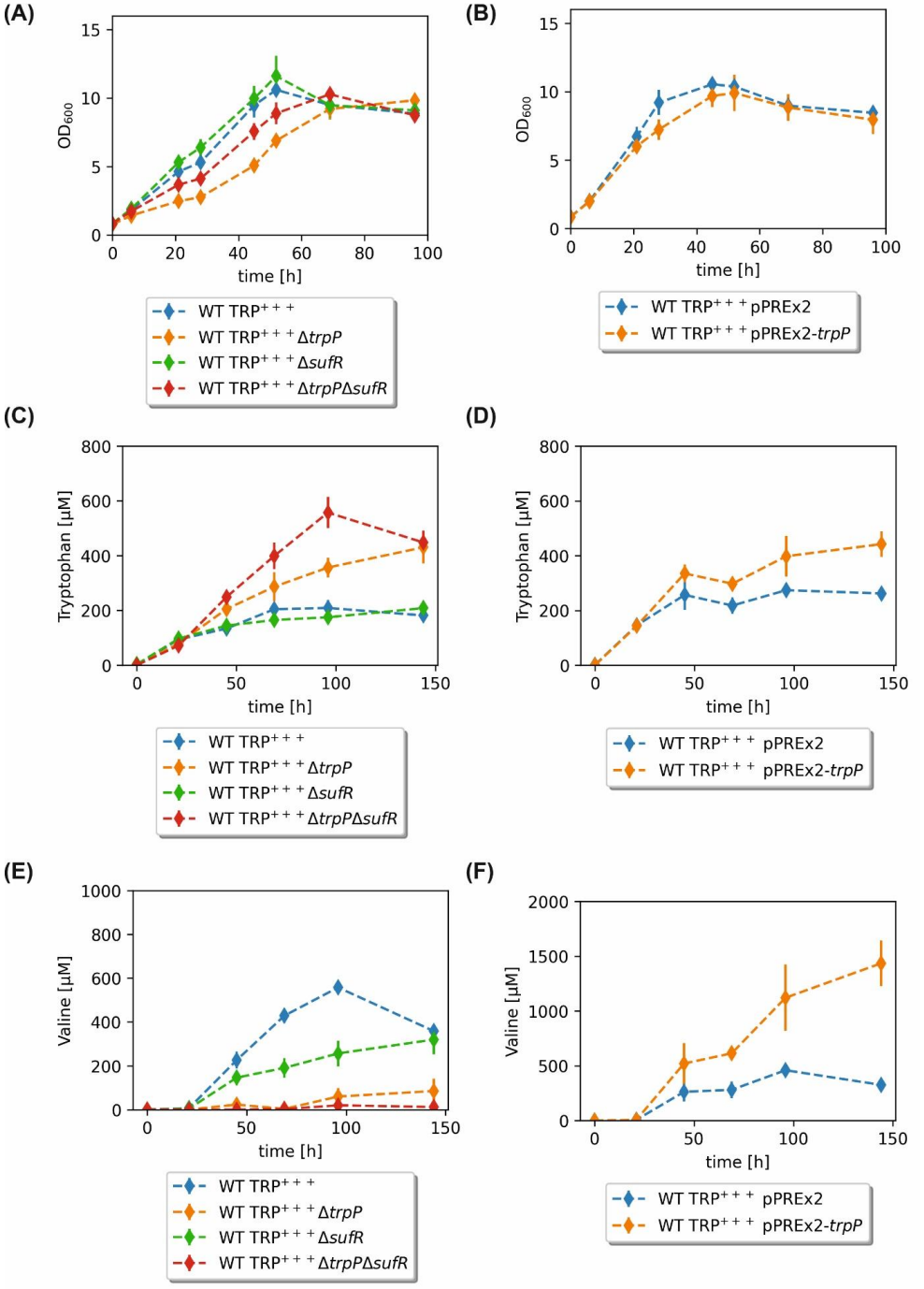

Figure 5.12: Characterization of the influence of *trpP* on amino acid formation in *C. glutamicum*. Cultivation of WT TRP^{+++} derived *trpP* deletion (A, C, E) and plasmid-based expression (B, D, F) strains regarding their growth (A, B), their L-tryptophan accumulation (C, D), and their L-valine accumulation (E, F). The strains were cultivated in biological triplicates

(quadruplicates for the plasmid-harboring strains) in 50 ml CGXII medium with 111 mM D-glucose in 500 ml baffled shake flasks at 30°C, 130 rpm, and 85% humidity control. The cultivation was started with a starting OD_{600} = 0.8, and 200 µM IPTG and 25 µg/ml kanamycin were added to the plasmid-harboring strains. The mean values are shown as diamonds, and standard deviations as lines.

5.2.6 Homology-based analysis of TrpP interaction partner

A previous study suggested TrpP (in this study Cgl1) to be a homolog to the SdpI protein of *B. subtilis* (Povolotsky *et al.*, 2010). Comparing the two sequences via BLAST with standard parameters gave an identity of 26.76 % (E-value 0.022). A sequence alignment suggested a high similarity between the second half of SdpI with the transmembrane domains 4-6, which are involved in the sequestration of the autorepressor SdpR in *B. subtilis*, and the three predicted TMDs of TrpP (Figure 5.13) (Povolotsky *et al.*, 2010). The remaining part of TrpP involving the amino acids 107-170 is predicted to protrude into the cytoplasm with no function predicted via this homology, making additional functions aside from protein sequestration thinkable. The only published residues essential for SdpI-SdpR interaction, Q126 and S156 (Ellermeier *et al.*, 2006), however, are not conserved.

The proteins SdpC, SdpA, and SdpB, responsible for toxin formation in *B. subtilis*, possess no homologs in *C. glutamicum*, and TrpP is missing the SdpC binding domain potentially involved in signal transduction (Povolotsky et al., 2010), suggesting that the function of TrpP in *C. glutamicum* is very different from *B. subtilis*. However, other related *Corynebacteria* were found to have such homologs, and especially SdpA and SdpB appear to be present in different *Corynebacteria*, such as *Corynebacterium propinquum*, *Corynebacterium belfantii*, *C. diphtheriae*, and *Corynebacterium marambiense*. This could mean that similar transduction cascades, not resulting in sporulation but something different, might also occur in *Corynebacteria*.

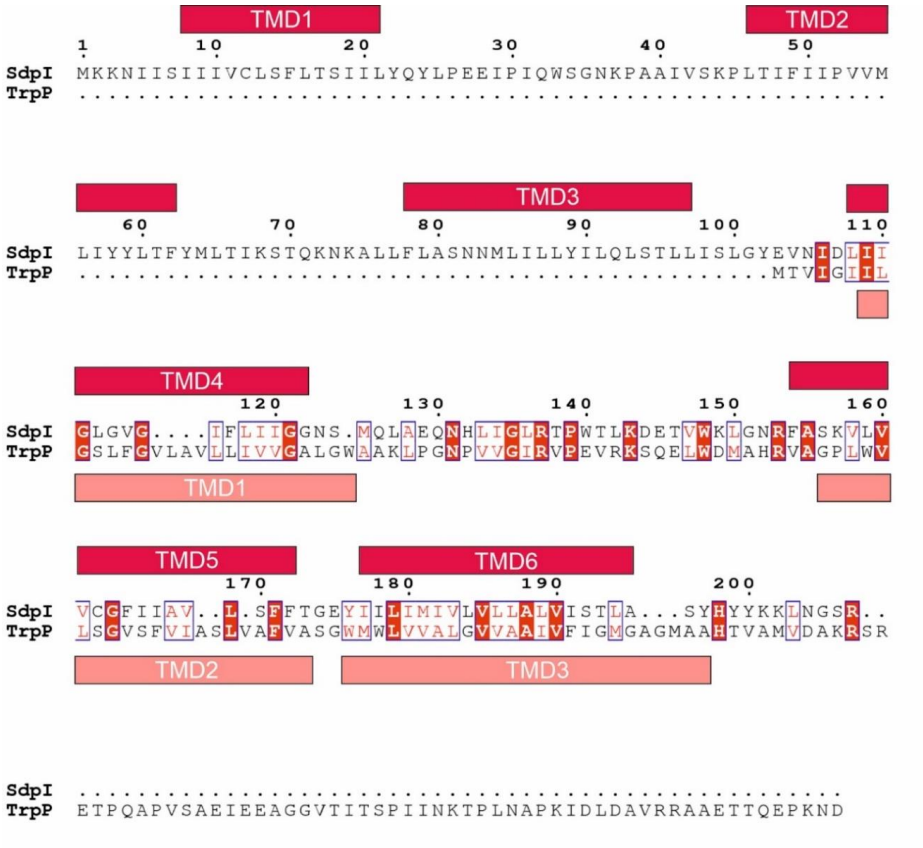

Figure 5.13: Sequence alignment of *B. subtilis* SdpI and *C. glutamicum* TrpP. Alignment prepared with Clustal Omega (Sievers *et al.*, 2011), visualized with ESPribt 3.0 (Robert and Gouet, 2014). Transmembrane domains are given according to DeepTMHMM (Hallgren *et al.*, 2022) for SdpI in red and for TrpP in light red.

For the autorepressor SdpR, homologs were identified via BlastP in *C. glutamicum* ATCC 13032, all – similar to SdpR (Gonzalez-Pastor *et al.*, 2003)– members of the ArsR family of transcription factors. Such transcription factors constitute the largest family of regulators involved in toxic metal defense, acting as homodimers in winged-helix form with helix-turn-helix DNA binding site (Ye *et al.*, 2005, Summers, 2009). Among the ArsR type regulators with homology to SdpR is SufR, the regulator of the *suf*-cluster, which expression level was a decisive factor for growth rate in the absence of TrpP. TrpP might also interact with SufR, changing its capacity to regulate the *suf*-cluster, being a yet unknown member of its regulation cascade.

5.2.7 Summary and outlook

Even after decades of research, important industrial workhorses such as *Corynebacterium glutamicum* contain plenty of uncharacterized genes. When constructing an L-tryptophan auxotrophic strain, we deleted the uncharacterized *trpP* gene (cg3357), which resulted in a severe decrease in strain growth rate and final cell density. The *trpP* deletion resulted in a similar phenotype in *C. glutamicum* WT, and can be complemented by low levels of plasmid-based *trpP* expression. Via evolution-guided metabolic engineering, we identified the inactivation of SufR (Cg1765), annotated as ArsR-type transcriptional repressor of the SUF-cluster (Cg1764-1759), to yield a partial recovery of the respective phenotype. The effect of those secondary inactivation mutations in SufR is related to the increased expression level of the *suf*-operon, which encodes the only system of *C. glutamicum* for the generation and repair of iron-sulfur clusters. The relevance of the expression level was verified via comparative analysis of the transcriptome of the strains as well as a library of different promoters in front of the *suf*-operon. Further transcriptomic analyses revealed several genes to be significantly differentially regulated in a WT Δ*trpP* strain in comparison to the WT, including several operons encoding Fe-S cluster containing proteins such as *nadSCAR*, *gltBD*, and *cydABCD*. Here we suggest, based on homology data between TrpP and SdpI from *B. subtilis*, which has a function in sequestering an ArsR-type transcription factor, that TrpP is involved in a novel signal cascade that is related to the regulation of SufR and the *suf*-operon. Notably, deleting or expressing *trpP* in an L-tryptophan producer strain resulted in significant changes in amino acid level: deletion of *trpP* increased the final L-tryptophan titer and significantly decreased the L-valine titer, an amino acid synthesized involving an enzyme harboring an Fe-S-cluster. Plasmid-based *trpP* expression resulted in a drastic increase in L-valine. This marks the absence of TrpP as a novel interesting amino acid production trait in *C. glutamicum*.

Further experimental work should include the analysis of potential interaction partners of TrpP. Chemical *in vivo* formaldehyde cross-linking of TrpP with interacting proteins followed by co-purification and MALDI-ToF-MS based protein identification (Kraxner *et al.*, 2019) could yield important links about the hypothesized signal cascade. When characterizing the TrpP homolog SdpI and its interaction partner in *B. subtilis*, SdpR, sequestration of SdpR with a fluorescent tag was shown in the presence of SdpI (Ellermeier *et al.*, 2006). Showing this effect would yield proof for a similar transcriptional regulator sequestration model of TrpP in *C. glutamicum*. Further studies regarding the properties of TrpP, e.g., by constructing truncated versions of TrpP to estimate the effect of the C-terminus that is not homologues to SdpI, would be valuable. This could also include the characterization of the membrane topology

of TrpP via fusing the alkaline phosphatase (PhoA) or the β-galactosidase (LacZ) of *E. coli* to different portions of the protein (Sundermeyer *et al.*, 2022).

5.3 Material and Methods Appendix

5.3.1 General methods as described in the previous publications

Strain engineering was performed via the pK19*mobsacB* method (Schäfer *et al.*, 1994) as described elsewhere (Schito *et al.*, 2022). Strain phenotyping, L-arginine quantification via HPLC, bioinformatics protein analysis, and community evolution were performed as described (Zuchowski *et al.*, 2023). The strains listed in Table 5.4 and the oligonucleotides listed in Table 5.5 were used for the experiments.

Table 5.4: Bacterial strains and plasmids used in this study

Strain or plasmid	Relevant characteristics	Source or Reference
E. coli		
DH5α	F^- Φ80*dlac*Δ(*lacZ*)M15 Δ(*lacZYA-argF*) U169 *endA1 recA1 hsdR17* (r_K^- , m_K^+) *deoR thi-1 phoA supE44* λ^- *gyrA96 relA1*; strain used for cloning procedures	(Hanahan, 1983)
C. glutamicum		
ATCC13032 (WT)	Biotin-auxotrophic wild type	(Kinoshita *et al.*, 1957)
WT ΔHIS	WT with an in-frame deletion of Δ*hisE* (cg1699), Δ*hisG* (cg1698), Δ*hisH* (cg2300), Δ*hisA* (cg2299), Δ*impA* (cg2298), Δ*hisF* (cg2297), Δ*hisI* (cg2296), Δ*hisN* (cg0910), Δ*hisD* (cg2305), Δ*hisC* (cg2304), Δ*hisB* (cg2303)	(Schito *et al.*, 2022)
WT ΔLEU	WT with an in-frame deletion of Δ*leuA* (cg0303), Δ*leuC* (cg1487), Δ*leuD* (cg1488), Δ*leuB* (cg1453)	(Schito *et al.*, 2022)
WT ΔTRP LEU^{++}	WT ΔTRP with exchange of *leuA* (cg0303) and 180 bp upstream region to leuA_B018 (B018: L-leucine producing *C. glutamicum* strain created by random mutagenesis) under control of the *tuf* promoter	This study

Strain or plasmid	Relevant characteristics	Source or Reference
WT ΔHIS LEU^{++}	WT ΔHIS with exchange of *leuA* (cg0303) and 180 bp upstream region to leuA_B018 (B018: L-leucine producing *C. glutamicum* strain created by random mutagenesis) under control of the *tuf* promoter	This study
WT ΔHIS LEU^{++} :: P$_{tac}$-*eYFP*	WT ΔHIS LEU++ with eYFP fluorescent protein under control of tac promoter integrated in the IGR between cg1121 and cg1122	This study
WT ΔLEU HIS^{+} :: P$_{tac}$-*crimson*	WT ΔHIS LEU++ with crimson fluorescent protein under control of tac promoter integrated in the IGR between cg1121 and cg1122	This study
WT ΔLEU TRP^{+}	WT ΔLEU with point mutations *trpL*$_{fbr}$ TrpE$_{S38R}$ (Cg3359)	This study
WT ΔARG LEU^{++} :: P$_{tac}$-*crimson*	WT with an in-frame deletion of Δ*argC* (cg1580), Δ*argJ* (cg1581), Δ*argB* (cg1582), Δ*argD* (cg1583), Δ*argF* (cg1584), Δ*argR* (cg1585), Δ*argG* (cg1586), Δ*argH* (cg1588), Δ*nagS* (cg3035), with exchange of *leuA* (cg0303) and 180 bp upstream region to leuA_B018 (B018: L-leucine producing *C. glutamicum* strain created by random mutagenesis) under control of the *tuf* promoter and with crimson fluorescent protein under control of *tac* promoter integrated in the IGR between cg1121 and cg1122	(Schito *et al.*, 2022)
WT ΔLEU ARG^{++} :: P$_{tac}$-*eYFP*	WT ΔLEU with point mutations ArgB$_{A26V\ M31V}$ (Cg1582) and with eYFP fluorescent protein under control of tac promoter integrated in the IGR between cg1121 and cg1122	(Schito *et al.*, 2022)
WT ΔARG LEU^{++} :: P$_{tac}$-*crimson* ΔP$_{pfka}$::P$_{glu}$*c*	WT ΔARG LEU^{++} :: P$_{tac}$-*crimson* with exchange of the native *pfkA* promoter (cg1409) with the promoter of *glnK* (cg2732)	(Berger, 2023)
WT ΔLEU ARG^{+++} :: P$_{tac}$-*eYFP* (WT ΔLEU ARG^{+++})	WT ΔLEU ARG^{++} :: P$_{tac}$-*eYFP* with an in-frame deletion of Δ*argTUV* (cg1502-1504)	(Berger, 2023)
WT ARG^{+++} :: P$_{tac}$-*eYFP* (WT ARG^{+++})	WT with point mutations ArgB$_{A26V\ M31V}$ (Cg1582), with an in-frame deletion of Δ*argTUV* (cg1502-	(Berger, 2023)

Strain or plasmid	Relevant characteristics	Source or Reference
	1504) and with eYFP fluorescent protein under control of *tac* promoter integrated in the IGR between cg1121 and cg1122	
C1*	13.4% genome reduced derivative of ATCC 13032	(Baumgart *et al.*, 2017)
C1* ΔTRP Δ*trpP* (C1* Δcg3357-cg3364)	C1* with an in-frame deletion of Δ*trpP* (cg3357) Δ*trpE* (cg3359) Δ*trpG* (cg3360) Δ*trpD* (cg3361) Δ*trpCF* (cg3362) Δ*trpB* (cg3363) Δ*trpA* (cg3364)	(Schito *et al.*, 2022)
WT ΔTRP Δ*trpP* (WT Δcg3357-cg3364)	WT with an in-frame deletion of Δ*trpP* (cg3357) Δ*trpE* (cg3359) Δ*trpG* (cg3360) Δ*trpD* (cg3361) Δ*trpCF* (cg3362) Δ*trpB* (cg3363) Δ*trpA* (cg3364)	(Schito *et al.*, 2022)
WT Δcg3359-cg3364	WT with an in-frame deletion of Δ*trpE* (cg3359) Δ*trpG* (cg3360) Δ*trpD* (cg3361) Δ*trpCF* (cg3362) Δ*trpB* (cg3363) Δ*trpA* (cg3364)	This study
WT ΔTRP Δ*trpP* Δ*sufR*	WT ΔTRP Δ*trpP* with an partial deletion of sufR (cg1765) until the *sufB* (cg1764) promoter site with an inserted stop codon at the end of *sufR*	This study
WT ΔTRP Δ*trpP* $SufR_{L25P}$	WT ΔTRP Δ*trpP* with point mutation L25P in SufR	This study
WT ΔTRP Δ*trpP* $SufR_{Q193*}$	WT ΔTRP Δ*trpP* with point mutation Q193* in SufR	This study
WT Δ*trpP*	WT with an in-frame deletion of Δ*trpP* (cg3357)	This study
WT ΔTRP Δ*trpP* Δ*sufR*::P_{tuf}	WT ΔTRP Δ*trpP* with an in frame exchange of *sufR* (cg1765) including the native *sufB* promoter sequence with the *tuf* promoter (cg0587)	This study
WT ΔTRP Δ*trpP* Δ*sufR*::P_{dapA}	WT ΔTRP Δ*trpP* with an in frame exchange of *sufR* (cg1765) including the native *sufB* promoter sequence with the *dapA* promoter (cg2161)	This study
WT TRP^{+++}	WT with point mutations $trpL_{fbr}$ $TrpE_{S38R}$ (Cg3359) $TrpD_{A162E}$ (Cg3361) and in-frame deletion of *aroP* (cg1257)	This study
WT TRP^{+++} Δ*sufR*	WT TRP^{++} with an partial deletion of *sufR* (cg1765) until the *sufB* (cg1764) promoter site with an inserted stop codon at the end of *sufR*	This study

Strain or plasmid	Relevant characteristics	Source or Reference
WT TRP^{+++} Δ*trpP*	WT TRP^{++} with an in-frame deletion of Δ*trpP* (cg3357)	This study
WT TRP^{+++} Δ*sufR* Δ*trpP*	WT TRP^{++} Δ*sufR* with an in-frame deletion of Δ*trpP* (cg3357)	This study
Plasmids		
pK19*mobsacB*	Kan^{R}.; plasmid for allelic exchange in *C. glutamicum*; (pK18 *ori*V$_{E.c.}$, *sacB*, *lacZ*α)	(Schäfer *et al.*, 1994)
pK19*mobsacB*-TrpL$_{fbr}$ TrpE$_{S38R}$	Kan^{R}.; pK19*mobsacB* derivative for mutation of *trpL* (TGG->TGA) and TrpE (Cg3359) S38R in *C. glutamicum*	(Schito *et al.*, 2022)
pK19*mobsacB*-P$_{tuf}$ *leuA*_B018_BS	Kan^{r}.; pK19*mobsacB* derivative containing *leuA* gene from B018 (*Mlu*I/*Spe*I) under control of the *tuf* promoter (*Nde*I/*Mlu*I) flanked by upstream and downstream regions of *leuA*	(Vogt *et al.*, 2014)
pK19*mobsacB*-HisG$_{A270D}$	Kan^{r}.; pK19*mobsacB* derivative for mutation of HisG (Cg1698) A270D in *C. glutamicum*	(Schito *et al.*, 2022)
pK19*mobsacB*-ΔP$_{pfkA}$::P$_{gntK}$	Kan^{r}.; pK19*mobsacB* derivative for promoter exchange of *pfkA* (cg1409) with the promoter of *gntK* (cg2732) in *C. glutamicum*	(Berger, 2023)
pK19*mobsacB*-Δ*trpP*	Kan^{R}.; pK19*mobsacB* derivative for in-frame deletion of *trpP* (cg3357) in *C. glutamicum*	This study
pK19*mobsacB*-Δ*aroP*	Kan^{R}.; pK19*mobsacB* derivative for in-frame deletion of *aroP* (cg1257) in *C. glutamicum*	This study
pK19*mobsacB*-Δ*sufR*	Kan^{R}.; pK19*mobsacB* derivative for partial in-frame deletion of *sufR* (cg1765) with an inserted stop codon at the end of *sufR* in *C. glutamicum*	This study
pK19*mobsacB*-SufR$_{L25P}$	Kan^{R}.; pK19*mobsacB* derivative for mutation of SufR (Cg1765) L25P in *C. glutamicum*	This study
pK19*mobsacB*-SufR$_{Q193*}$	Kan^{R}.; pK19*mobsacB* derivative for mutation of SufR (Cg1765) Q193* in *C. glutamicum*	This study

Strain or plasmid	Relevant characteristics	Source or Reference
pK19*mobsacB*-TrpD$_{A162E}$	Kan^R.; pK19*mobsacB* derivative for mutation of TrpE (Cg3361) A162E in *C. glutamicum*	This study
pK19*mobsacB*-Δ*sufR*::P$_{tuf}$*sufB*	Kan^R.; pK19*mobsacB* derivative for deletion of *sufR* (cg1765) with integration of P$_{tuf}$ (cg0587) in *C. glutamicum*	This study
pK19*mobsacB*-Δ*sufR*::P$_{dapA}$*sufB*	Kan^R.; pK19*mobsacB* derivative for deletion of *sufR* (cg1765) with integration of P$_{tuf}$ (cg2161) in *C. glutamicum*	This study
pAN6	Kan^R; *C. glutamicum*/*E. coli* shuttle vector for regulated gene expression using the P$_{tac}$ promoter, derivative of pEKEx2.	(Frunzke *et al.*, 2008)
pAN6-suf-cluster	Kan^R; pAN6 derived *suf*-cluster (cg1764-1759) expression plasmid for *C. glutamicum*	This study
pPREx2	Kan^R; plasmid for expression of target genes	(Bakkes *et al.*, 2020)
pPREx2-TrpP	Kan^R; pPREx2 derived *trpP* (cg3357) expression plasmid under control of P$_{tac}$	This study

Table 5.5: Oligonucleotides used in the Appendix

Oligonucleotide	Sequence (5' → 3') and properties[a]
Sequencing primers	
B223_M13-fw	CGCCAGGGTTTTCCCAGTCAC
B224_M13-rv	AGCGGATAACAATTTCACACAGGA
Work with pK19*mobsacB*-TrpL$_{fbr}$ TrpE$_{S38R}$	
Z59_TrpE_mut_fw	GCTGCGGAAACTACGCAAG
Z85_TrpE_mut_rv_neu	CACGGGACACCAAGTGCATC
Work with pK19*mobsacB*-HisG$_{A270D}$	
Z65_HisEG_fw_neu	GACTGGGACATGTTCACATC
Z89_HisG_A270D_rv	GGTTCCTCCACTTTCCGTTAC
Work with pK19*mobsacB*-P$_{tuf}$*leuA*_B018_BS	
Z92_LeuA_Ptuf_fw	CTGGACTTCGTGGTGGCTAC

Z93_LeuA_Ptuf_seq_rv	TGCCACAGGGTAGCTGGTAG
Z67_PtufLeuA_seq_fw	CTCAGTGGTGTGCTGTTGAC
Z68_PtufLeuA_seq_rv	TCCTTGCCGTTGTGGATGAG
Analysis of fluorescent protein integration	
Z109_Intcg1121 fwd	TTGGCGTGTGGTTGGTTAG
Z110_Intcg1122 rev	CGCATCAAGCAGATCTCTG
Work with pK19*mobsacB*-ArgB$_{fbr}$	
Z64_ArgB_mut_rv	GCCGTCAATGACATGAGCAG
Z78_ArgB_mut-fw	TGTGACCAAGCGCGTTGCTG
Work with pK19*mobsacB*-ArgB$_{fbr}$	
Z208_Pcg2732-PFKA-Dfw	CCTTCTGCGAGTTCGCCATGTG
Z209_Pcg2732-PFKA-Drv	GCGTGCAGAGCAATCCAACC
Construction of deletion plasmid pK19*mobsacB*-Δ*trpP* and PCR-analysis of the resulting mutants	
B453_TRP-D1	**AAAACGACGGCCAGTGAATT**AATGCCGAGCCATTTGCCAG
B454_TRP-D2	AACAACAACTCTATCCCCACCAATATTCC
Z225_TrpP-D3_new	**GTGGGGATAGAGTTGTTGTT**TAATTGAGACAAGCTTCCCAC
Z226_TrpP-D4_new	**CAGGTCGACTCTAGAGGA**GCTGCGTTACCACCGTGTTG
B457_TRP-Dfw	TAGAGCGCTTGGGATGCTCC
Z90_TrpP_Drv	GGGCACCTACCGAGGAAATC
Construction of deletion plasmid pK19*mobsacB*-Δ*aroP* and PCR-analysis of the resulting mutants	
Z136_aroP_D1	**CAGGTCGACTCTAGAGGA**GGTGCCATCTGCCAGGTACG
Z137_aroP_D2	AGGCCGATAGAAATTATTCTGGAC
Z138_aroP_D3	**AGAATAATTTCTATCGGCCT**GTATCAACCGTAAACCCACA
Z139_aroP_D4	**AAAACGACGGCCAGTGAATT**CCGCATGGTCGACTATGTGG
Z140_aroP_dfw	GGTGACGCCAGCGGAAATGC
Z141_aroP_drv	CGTGGTGTGGACAAACAAGG
Construction of deletion plasmid pK19*mobsacB*-ΔsufR and PCR-analysis of the resulting mutants	
Z94_sufR-D1	**CAGGTCGACTCTAGAGGA**GTCGCGTACGACATCCTCGC
Z95_sufR-D2	TAAGCAGTAAGGCAATTTGC
Z96_sufR-D3	**GCAAATTGCCTTACTGCTTA**TGGTGTCACCTCCTGCTTG
Z97_sufR-D4	**AAAACGACGGCCAGTGAATT**GAAAAGCGTTGCCCCTAAAG
Z98_sufR-Dfw	TGAGGCGCTGCTGAAGCATC
Z99_sufR-Drv	GCCATGCAAATCGGCGAATC
Construction of deletion plasmid pK19*mobsacB*-SufR$_{L25P}$ & pK19*mobsacB*-SufR$_{Q193}$ and PCR-analysis of the resulting mutants[b]	
Z100_sufR_SNP_D1	**CAGGTCGACTCTAGAGGA**TTGCCGAAGTCATGATCCGC
Z101_sufR_SNP_D2	ACCCATACGAGCCCAAAATG

Z102_sufR_SNP_D3	CATTTTGGGCTCGTATGGGTTCTGGCGCGGATTTGCCG
Z103_sufR_SNP_D4	**AAAACGACGGCCAGTGAATT**CCTCGCATCAGAGTCTGGTG
Z98_sufR-Dfw	TGAGGCGCTGCTGAAGCATC
Z99_sufR-Drv	GCCATGCAAATCGGCGAATC
Construction of deletion plasmid pK19*mobsacB*- Δ*sufR*::P$_{tuf}$*sufB* and PCR-analysis of the resulting mutants	
Z271_PsufB-D1	**AAAACGACGGCCAGTGAATT**GAAAAGCGTTGCCCCTAAAG
Z272_PsufB-D2	TGGTGTCACCTCCTGCTTG
Z273_PsufB-D3	ATGACTTCGGCAACGACGAACC
Z274_PsufB-D4	**CAGGTCGACTCTAGAGGA**AGATCTCAGGGTGCTCTTTC
Z275_PsufB-Ptuf-D5	**CAAGCAGGAGGTGACACCA**CACAGGGTAGCTGGTAGTTTG
Z276_PsufB-Ptuf-D6	**GTTCGTCGTTGCCGAA***GTCAT*TGTATGTCCTCCTGGACTTC
Z283_PsufB-Ptuf_Dfw	CAACGCCGTTGCCCTTAGGATTC
Z123_sufB_rv	ACTGCGAGTTCCGAGCTGAC
Construction of deletion plasmid pK19*mobsacB*- Δ*sufR*::P$_{dapA}$*sufB* and PCR-analysis of the resulting mutants	
Z271_PsufB-D1	**AAAACGACGGCCAGTGAATT**GAAAAGCGTTGCCCCTAAAG
Z272_PsufB-D2	TGGTGTCACCTCCTGCTTG
Z273_PsufB-D3	ATGACTTCGGCAACGACGAACC
Z274_PsufB-D4	**CAGGTCGACTCTAGAGGA**AGATCTCAGGGTGCTCTTTC
Z277_PsufB-PdapA-D5	**CAAGCAGGAGGTGACACCA**CGCAAAGCTCACACCCACGAG
Z278_PsufB-PdapA-D6	**GTTCGTCGTTGCCGAAGTCAT**AGAGTTCAAGGTTACCTTCT
Z284_PsufB-PdapA_Dfw	CATATAGTTAAGACAACATTTTTGGCTG
Z123_sufB_rv	ACTGCGAGTTCCGAGCTGAC
Construction of expression plasmid pPREx2-*trpP* and PCR-analysis of the resulting mutants	
	GTAAAACGACGGCCAGTGAATTTTAATCATTTTTGGGTTCT
Z257_pPREX2-TrpP_D2	TGCGTAG
Z258_pPREX2-TrpP_D1	**GCAGAAGGAGATATACAT**ATGACGGTGATCGGAATTATTC
Z287_PRP113_pPREx2	CTTCTGGCGTCAGGCAGCCATC
Z288_PRP144	AGACCGCTTCTGCGTTCTG
Construction of deletion plasmid pK19*mobsacB*- TrpD$_{A162E}$ and PCR-analysis of the resulting mutants with AvaI restriction site	
	AAAACGACGGCCAGTGAATTCTCCAGCAACACTGAAAGTT
Z159_TrpD fbr-D1	C
Z160_TrpD fbr-D2	GCGCAATCTCGGGGTTGTACGCA
Z161_TrpD fbr-D3	**ACCCCGAGATTGCGC**ATGTGCAGCCGG
Z162_TrpD fbr-D4	**CAGGTCGACTCTAGAGGA**GGTGCCGTCGGCAAGCAAGG

Z163_TrpD fbr-fw	AACAGCTTCTCGCGAACTAAT
Z164_TrpD fbr-rv	TCGACGATGCTTTCCAACAC
Construction of expression plasmid pAN6-*suf*-cluster and PCR-analysis of the resulting mutants	
Z121_sufR_pan6_fw	**CTGCAGAAGGAGATATAC**ATATGACTTCGGCAACGACGAA
Z122_sufR_pan6_rv	**CTGTGGGTGGGACCAGCT**AGCTAATGTGCGTGCGCAACAG
Z125_pAN6_suf_seq_rv	ATCAGACCGCTTCTGCGTTC
Z132_pAN6_suf_seq_fw_I	TGGTGACCAAGCGCACCAAG
Z133_pAN6_suf_seq_fw_II	CTCCAAGGAACAGGGCAATG
Z134_pAN6_suf_seq_fw_III	AGCCAAGTGGCTAAGCACAG
Z135_pAN6_suf_seq_fw_IV	TGCAGATGGATCCCTCAATG

[a]) Overlaps for Gibson assembly are written in bold letters. Restriction sites are underlined.
[b]) Template: gDNA from the isolated mutant strains. Construct with mutated NdeI restriction site.

5.3.2 Laboratory-scale fermentation

Microbial fermentations on laboratory-scale were performed in technical duplicates using the DASGIP® parallel bioreactor systems (Eppendorf/DASGIP, Jülich, Germany) as described before (Tenhaef *et al.*, 2018). Defined CGXII medium was used in an initial volume of 1 L, containing per liter of deionized water 1 g K_2HPO_4, 1g KH_2PO_4, 5 g urea, 13.25 mg $CaCl_2 \cdot 2\ H_2O$, 0.25 g $MgSO_4 \cdot 7\ H_2O$, 10 mg $FeSO_4 \cdot 7\ H_2O$, 10 mg $MnSO_4 \cdot H_2O$, 0.02 mg $NiCl_2 \cdot 6\ H_2O$, 0.313 mg $CuSO_4 \cdot 5\ H_2O$, 1 mg $ZnSO_4 \cdot 7\ H_2O$, 0.2 mg biotin, 3,4-dihydroxybenzoate (PCA), 0.02% (v v^{-1}) antifoam AF204, 20 g D-glucose, and 1 mM IPTG (Keilhauer *et al.*, 1993). Notably, D-glucose, PCA, trace elements, biotin, $MgSO_4$, $CaCl_2$, IPTG, and AF204 were added sterile after autoclaving. Reactor conditions were tightly controlled. Air flow was set to 0.5 vvm with appropriate stirrer speed (400-1200 rpm) to maintain a dissolved oxygen concentration (DO) of at least 30°%. The temperature was set to 30°C and pH to 7.0. The pH maintenance was achieved by feeding 30% (w/v) H_3PO_4 and 25% (v/v) NH_4OH on demand. DO (Visiferm DO 225, Hamilton, Bonaduz, Switzerland) and pH (405-DPAS-SC-K80/225, Mettler Toledo, Columbus, USA) were controlled via online measurements. Precultivation was performed starting with a preculture in BHI for 8 h, followed by a second preculture overnight in CGXII (111 mM D-glucose) with an additional 1mM IPTG, and main cultures were inoculated to an OD_{600} of 1. For the fed-batch process, a peristaltic pump was used to maintain a constant D-glucose feed. Feeding of a 400 g L^{-1} D-glucose solution in deionized water with a feed rate of 5 mL h^{-1} was started when the first cultures reached the late exponential phase. The feeding rate was increased after 20h to 20 mL h^{-1} for a further 8.5 h.

CDW was determined via a gravimetric method as described (Limberg *et al.*, 2016). Culture supernatants were filtered through a cellulose-acetate syringe filter (0.2 µm, DIA-Nielsen, Düren, Germany) and used for substrate analysis as described (Schito *et al.*, 2022) as well as for amino acid quantification by HPLC as described (Zuchowski *et al.*, 2023)

5.3.3 Flow cytometry analysis

The flow cytometer MACSQuantX (Miltenyi Biotec, Bergisch Gladbach, Germany) was used to analyze the cultures. Cell suspensions were diluted 1:1000 immediately after harvesting with sterile filtered phosphate buffer (58 mM $Na_2HPO_4 \cdot 7\ H_2O$, 42 mM $NaH_2PO_4 \cdot H_2O$). To perform a live/dead assay, a propidium iodide solution (Miltenyi Biotec, Bergisch Gladbach, Germany) was added (1:10 diluted) right before sample analysis. After device calibration according to the protocol (Miltenyi Biotec, Bergisch Gladbach, Germany), samples were measured with a medium flow rate (50 µL min^{-1}). The background signal was determined by measuring cell-free phosphate buffer. Duplet exclusion was performed automatically according to the linear correlation between the height and area of the forward scatter signal. By counting positive events in the B2 channel, dead cells were estimated. The two co-culture strains harbored either eYFP or crimson fluorescent protein which were expressed due to the 1 mM IPTG present during both precultivation and main cultivation. Thus, the ratio of the two strains in the CoNoS was estimated by interpolating the signal of the B1 and the R1 channel.

5.4 References Appendix

All references given in the Appendix are part of the reference list given for the general discussion.

Bakkes, P. J., Ramp, P., Bida, A., Dohmen-Olma, D., Bott, M. & Freudl, R. 2020. Improved pEKEx2-derived expression vectors for tightly controlled production of recombinant proteins in *Corynebacterium glutamicum*. *Plasmid*, 112, 102540.

Baumgart, M. & Bott, M. 2011. Biochemical characterisation of aconitase from *Corynebacterium glutamicum*. *J Biotechnol*, 154, 163-70.

Baumgart, M., Unthan, S., Kloss, R., Radek, A., Polen, T., Tenhaef, N., Muller, M. F., Kuberl, A., Siebert, D., Bruhl, N., Marin, K., Hans, S., Kramer, R., Bott, M., Kalinowski, J., Wiechert, W., Seibold, G., Frunzke, J., Ruckert, C., Wendisch, V. F. & Noack, S. 2017. *Corynebacterium glutamicum* Chassis C1*: Building and Testing a Novel Platform Host for Synthetic Biology and Industrial Biotechnology. *ACS Synth Biol*, 7, 132-144.

Beckers, G., Nolden, L. & Burkovski, A. 2001. Glutamate synthase of *Corynebacterium glutamicum* is not essential for glutamate synthesis and is regulated by the nitrogen status. *Microbiology*, 147, 2961–2970.

Berger, D. 2023. Biotechnological production of L-arginine using a Community of Niche-optimized Strains (CoNoS) - Identification and characterization of novel amino acids production traits. *Master thesis*, Leibnis University Hanover.

Bott, M. & Niebisch, A. 2003. The respiratory chain of *Corynebacterium glutamicum*. *J Biotechnol*, 104, 129-53.

Ellermeier, C. D., Hobbs, E. C., Gonzalez-Pastor, J. E. & Losick, R. 2006. A three-protein signaling pathway governing immunity to a bacterial cannibalism toxin. *Cell*, 124, 549-59.

Ertan, H. 1992. Some properties of glutamate dehydrogenase, glutamine synthetase and glutamate synthase from *Corynebacterium callunae*. *Arch Microbiol*, 158, 35-41.

Frunzke, J., Engels, V., Hasenbein, S., Gatgens, C. & Bott, M. 2008. Co-ordinated regulation of gluconate catabolism and glucose uptake in *Corynebacterium glutamicum* by two functionally equivalent transcriptional regulators, GntR1 and GntR2. *Mol Microbiol*, 67, 305-22.

Gonzalez-Pastor, J. E., Hobbs, E. C. & Losick, R. 2003. Cannibalism by Sporulating Bacteria. *Science*, 301, 510-513.

Grund, T. N., Kabashima, Y., Kusumoto, T., Wu, D., Welsch, S., Sakamoto, J., Michel, H. & Safarian, S. 2022. The cryoEM structure of cytochrome bd from *C. glutamicum* provides novel insights into structural properties of actinobacterial terminal oxidases. *Front Chem*, 10, 1085463.

Hallgren, J., Tsirigos, K. D., Pedersen, M. D., Almagro Armenteros, J. J., Marcatili, P., Nielsen, H., Krogh, A. & Winther, O. 2022. DeepTMHMM predicts alpha and beta transmembrane proteins using deep neural networks. *bioRxiv*.

Hanahan, D. 1983. Studies on transformation of *Escherichia coli* with plasmids. *J Mol Biol*, 166, 557-580.

Heery, D. M. & Dunican, L. K. 1993. Cloning of the *trp* Gene Cluster from a Tryptophan-Hyperproducing Strain of *Corynebacterium glutamicum*: Identification of a Mutation in the *trp* Leader Sequence. *APPLIED AND ENVIRONMENTAL MICROBIOLOGY*, 791-799.

Heery, D. M., Fitzpatrick, R. & Dunican, L. K. 1994. A sequence from a tryptophan-hyperproducing strain of *Corynebacterium glutamicum* encoding resistance to 5-methyltryptophan. *Biochemical and Biophysical Research communication*, 201, 1255-1262.

Jensen, J. V. & Wendisch, V. F. 2013. Ornithine cyclodeaminase-based proline production by *Corynebacterium glutamicum*. *Microbial Cell Factories*, 12, 1-10.

Kabus, A., Niebisch, A. & Bott, M. 2007. Role of cytochrome bd oxidase from *Corynebacterium glutamicum* in growth and lysine production. *Appl Environ Microbiol*, 73, 861-8.

Kalinowski, J., Bathe, B., Bartels, D., Bischoff, N., Bott, M., Burkovski, A., Dusch, N., Eggeling, L., Eikmanns, B. J., Gaigalat, L., Goesmann, A., Hartmann, M., Huthmacher, K., Krämer, R., Linke, B., Mchardy, A. C., Meyer, F., Möckel, B., Pfefferle, W., Pühler, A., Rey, D. A., Rückert, C., Rupp, O., Sahm, H., Wendisch, V. F., Wiegräbe, I. & Tauch, A. 2003. The complete *Corynebacterium glutamicum* ATCC 13032 genome sequence and its impact on the production of L-aspartate-derived amino acids and vitamins. *Journal of Biotechnology*, 104, 5-25.

Keilhauer, C., Eggeling, L. & Sahm, H. 1993. Isoleucine Synthesis in *Corynebacterium glutamicum:* Molecular Analysis of the *ilvB-ilvN-ilvC* Operon. *Journal of Bacteriology*, 175, 5595-5603.

Kinoshita, S., Udaka, S. & Shimono, M. 1957. Studies of amino acid fermentation. I. Production of L-glutamic acid by various microorganisms. *J Gen Appl Microbiol*, 3, 193-205.

Konstantinov, K. B., Nishio, N., Seki, T. & Yoshida, T. 1991. Physiologically Motivated Strategies for Control of the Fed-Batch Cultivation of Recombinant *Escherichia coli* for Phenylalanine Production. *Journal of Fermentation and Bioengineering*, 71, 350-355.

Kraxner, K. J., Polen, T., Baumgart, M. & Bott, M. 2019. The conserved actinobacterial transcriptional regulator FtsR controls expression of ftsZ and further target genes and influences growth and cell division in *Corynebacterium glutamicum*. *BMC Microbiol*, 19, 179.

Kulis-Horn, R. K., Persicke, M. & Kalinowski, J. 2015. *Corynebacterium glutamicum* ATP-phosphoribosyl transferases suitable for L-histidine production – Strategies for the elimination of feedback inhibition. *J Biotechnol*, 206, 26-37.

Lamsa, A., Liu, W. T., Dorrestein, P. C. & Pogliano, K. 2012. The *Bacillus subtilis* cannibalism toxin SDP collapses the proton motive force and induces autolysis. *Mol Microbiol*, 84, 486-500.

Limberg, M. H., Schulte, J., Aryani, T., Mahr, R., Baumgart, M., Bott, M., Wiechert, W. & Oldiges, M. 2016. Metabolic profile of 1,5-diaminopentane producing *Corynebacterium glutamicum* under scale-down conditions: Blueprint for robustness to bioreactor inhomogeneities. *Biotechnol Bioeng*, 114, 560-575.

Liu, W. T., Yang, Y. L., Xu, Y., Lamsa, A., Haste, N. M., Yang, J. Y., Ng, J., Gonzalez, D., Ellermeier, C. D., Straight, P. D., Pevzner, P. A., Pogliano, J., Nizet, V., Pogliano, K. & Dorrestein, P. C. 2010. Imaging mass spectrometry of intraspecies metabolic exchange revealed the cannibalistic factors of *Bacillus subtilis*. *Proc Natl Acad Sci USA*, 107, 16286-90.

Matsui, K., Miwa, K. & Sano, K. 1987. Two Single-Base-Pair Substitutions Causing Desensitization to Tryptophan Feedback Inhibition of Anthranilate Synthase and Enhanced Expression of Tryptophan Genes of *Brevibacterium lactofermentum*. *Journal of Bacteriology,* 169, 5330-5332.

Mentz, A., Neshat, A., Pfeifer-Sancar, K., Pühler, A., Rückert, C. & Kalinowski, J. 2013. Comprehensive discovery and characterization of small RNAs in *Corynebacterium glutamicum* ATCC 13032. *BMC Genomics*, 14, 1-16.

Mormann, S., Lomker, A., Ruckert, C., Gaigalat, L., Tauch, A., Puhler, A. & Kalinowski, J. 2006. Random mutagenesis in *Corynebacterium glutamicum* ATCC 13032 using an IS6100-based transposon vector identified the last unknown gene in the histidine biosynthesis pathway. *BMC Genomics*, 7, 205.

Netzer, R., Peters-Wendisch, P., Eggeling, L. & Sahm, H. 2004. Cometabolism of a nongrowth substrate: L-serine utilization by *Corynebacterium glutamicum*. *Appl Environ Microbiol*, 70, 7148-55.

Nishimura, T., Teramoto, H., Vertes, A. A., Inui, M. & Yukawa, H. 2008. ArnR, a novel transcriptional regulator, represses expression of the *narKGHJI* operon in *Corynebacterium glutamicum*. *J Bacteriol*, 190, 3264-73.

Noack, S. & Baumgart, M. 2019. Communities of Niche-Optimized Strains: Small-Genome Organism Consortia in Bioproduction. *Trends Biotechnol*, 37, 126-139.

Paczia, N., Nilgen, A., Lehmann, T., Gätgens, J., Wiechert, W. & Noack, S. 2012. Extensive exometabolome analysis reveals extended overflow metabolism in various microorganisms. *Microbial Cell Factories*, 11.

Parise, M. T. D., Parise, D., Kato, R. B., Pauling, J. K., Tauch, A., Azevedo, V. a. C. & Baumbach, J. 2020. CoryneRegNet 7, the reference database and analysis platform for corynebacterial gene regulatory networks. *Sci Data*, 7, 9.

Park, S. H., Kim, H. U., Kim, T. Y., Park, J. S., Kim, S. S. & Lee, S. Y. 2014. Metabolic engineering of *Corynebacterium glutamicum* for L-arginine production. *Nat Commun*, 5, 4618.

Paysan-Lafosse, T., Blum, M., Chuguransky, S., Grego, T., Pinto, B. L., Salazar, G. A., Bileschi, M. L., Bork, P., Bridge, A., Colwell, L., Gough, J., Haft, D. H., Letunic, I., Marchler-Bauer, A., Mi, H., Natale, D. A., Orengo, C. A., Pandurangan, A. P., Rivoire, C., Sigrist, C. J. A., Sillitoe, I., Thanki, N., Thomas, P. D., Tosatto, S. C. E., Wu, C. H. & Bateman, A. 2023. InterPro in 2022. *Nucleic Acids Res*, 51, D418-D427.

Perez Morales, T. G., Ho, T. D., Liu, W. T., Dorrestein, P. C. & Ellermeier, C. D. 2013. Production of the cannibalism toxin SDP is a multistep process that requires SdpA and SdpB. *J Bacteriol*, 195, 3244-51.

Pfeifer-Sancar, K., Mentz, A., Rückert, C. & Kalinowski, J. 2013. Comprehensive analysis of the *Corynebacterium glutamicum* transcriptome using an improved RNAseq technique. *BMC Genomics* 14, 1-23.

Povolotsky, T. L., Orlova, E., Tamang, D. G. & Saier, M. H., Jr. 2010. Defense against cannibalism: the SdpI family of bacterial immunity/signal transduction proteins. *J Membr Biol*, 235, 145-62.

Radek, A., Tenhaef, N., Müller, M. F., Brusseler, C., Wiechert, W., Marienhagen, J., Polen, T. & Noack, S. 2017. Miniaturized and automated adaptive laboratory evolution: Evolving *Corynebacterium glutamicum* towards an improved D-xylose utilization. *Bioresour Technol*, 245, 1377-1385.

Radmacher, E., Vaitsikova, A., Burger, U., Krumbach, K., Sahm, H. & Eggeling, L. 2002. Linking central metabolism with increased pathway flux: L-valine accumulation by *Corynebacterium glutamicum*. *Appl Environ Microbiol*, 68, 2246-50.

Robert, X. & Gouet, P. 2014. Deciphering key features in protein structures with the new ENDscript server. *Nucleic Acids Res*, 42, W320-4.

Rosenberg, G., Steinberg, N., Oppenheimer-Shaanan, Y., Olender, T., Doron, S., Ben-Ari, J., Sirota-Madi, A., Bloom-Ackermann, Z. & Kolodkin-Gal, I. 2016. Not so simple, not so subtle: the interspecies competition between *Bacillus simplex* and *Bacillus subtilis* and its impact on the evolution of biofilms. *NPJ Biofilms Microbiomes*, 2, 15027.

Schäfer, A., Tauch, A., Jäger, W., Kalinowski, J., Thierbach, G. & Pühler, A. 1994. Small mobilizable multi-purpose cloning vectors derived from the *Escherichia coli* plasmids pK18 and pK19: selection of defined deletions in the chromosome of *Corynebacterium glutamicum*. *Gene*, 145, 69-73.

Schito, S., Zuchowski, R., Bergen, D., Strohmeier, D., Wollenhaupt, B., Menke, P., Seiffarth, J., Noh, K., Kohlheyer, D., Bott, M., Wiechert, W., Baumgart, M. & Noack, S. 2022. Communities of Niche-optimized Strains (CoNoS) - Design and creation of stable, genome-reduced co-cultures. *Metab Eng*, 73, 91-103.

Schulz, A. A., Collett, H. J. & Reid, S. J. 2001. Nitrogen and carbon regulation of glutamine synthetase and glutamate synthase in *Corynebacterium glutamicum* ATCC 13032. *FEMS Microbiology Letters*, 205, 361-367.

Shang, X., Chai, X., Lu, X., Li, Y., Zhang, Y., Wang, G., Zhang, C., Liu, S., Zhang, Y., Ma, J. & Wen, T. 2018. Native promoters of *Corynebacterium glutamicum* and its application in L-lysine production. *Biotechnol Lett*, 40, 383-391.

Sievers, F., Wilm, A., Dineen, D., Gibson, T. J., Karplus, K., Li, W., Lopez, R., Mcwilliam, H., Remmert, M., Soding, J., Thompson, J. D. & Higgins, D. G. 2011. Fast, scalable generation of high-quality protein multiple sequence alignments using Clustal Omega. *Mol Syst Biol*, 7, 539.

Summers, A. O. 2009. Damage control: regulating defenses against toxic metals and metalloids. *Curr Opin Microbiol*, 12, 138-44.

Sundermeyer, L., Bosco, G., Gujar, S., Brocker, M., Baumgart, M., Willbold, D., Weiergräber, O. H., Bellinzoni, M. & Bott, M. 2022. Characteristics of the GlnH and GlnX Signal Transduction Proteins Controlling PknG-Mediated Phosphorylation of OdhI and 2-

Oxoglutarate Dehydrogenase Activity in *Corynebacterium glutamicum*. *Microbiology Spectrum*, 10, 1-23.

Tenhaef, N., Brusseler, C., Radek, A., Hilmes, R., Unrean, P., Marienhagen, J. & Noack, S. 2018. Production of D-xylonic acid using a non-recombinant *Corynebacterium glutamicum* strain. *Bioresour Technol*, 268, 332-339.

Teramoto, H., Inui, M. & Yukawa, H. 2012. NdnR is an NAD-responsive transcriptional repressor of the *ndnR* operon involved in NAD de novo biosynthesis in *Corynebacterium glutamicum*. *Microbiology (Reading),* 158, 975-982.

Teramoto, H., Suda, M., Inui, M. & Yukawa, H. 2010. Regulation of the expression of genes involved in NAD de novo biosynthesis in *Corynebacterium glutamicum*. *Appl Environ Microbiol*, 76, 5488-95.

Tesch, M., De Graaf, A. A. & Sahm, H. 1999. In Vivo Fluxes in the Ammonium-Assimilatory Pathways in *Corynebacterium glutamicum* Studied by ^{15}N Nuclear Magnetic Resonance. *Appl Environ Microbiol*, 65, 1099-1109.

Tripathi, A., Anand, K., Das, M., O'niel, R. A., P, S. S., Thakur, C., R, L. R., Rajmani, R. S., Chandra, N., Laxman, S. & Singh, A. 2022. *Mycobacterium tuberculosis* requires SufT for Fe-S cluster maturation, metabolism, and survival *in vivo*. *PLoS Pathog*, 18, e1010475.

Tsuchida, T. & Momose, H. 1975. Genetic Changes of Regulatory Mechanisms Occured in Leucine and Valine Producing Mutants Derived from *Brevibacterium lactofermentum* 2256. *Agr. Biol. Chem*, 39, 2193-2198.

Vogt, M., Haas, S., Klaffl, S., Polen, T., Eggeling, L., Van Ooyen, J. & Bott, M. 2014. Pushing product formation to its limit: metabolic engineering of *Corynebacterium glutamicum* for L-leucine overproduction. *Metab Eng*, 22, 40-52.

Waterhouse, A., Bertoni, M., Bienert, S., Studer, G., Tauriello, G., Gumienny, R., Heer, F. T., De Beer, T. a. P., Rempfer, C., Bordoli, L., Lepore, R. & Schwede, T. 2018. SWISS-MODEL: homology modelling of protein structures and complexes. *Nucleic Acids Res*, 46, W296-W303.

Wehrmann, A., Morakkabati, S., Krämer, R., Sahm, H. & Eggeling, L. 1995. Functional Analysis of Sequences Adjacent to *dapE* of *Corynebacterium glutamicum* Reveals the Presence of *aroP*, Which Encodes the Aromatic Amino Acid Transporter. *Journal of Bacteriology*, 177, 5991-5993.

Ye, J., Kandegedara, A., Martin, P. & Rosen, B. P. 2005. Crystal structure of the *Staphylococcus aureus* pI258 CadC Cd(II)/Pb(II)/Zn(II)-responsive repressor. *J Bacteriol*, 187, 4214-21.

Zhang, H., Li, Y., Wang, C. & Wang, X. 2018. Understanding the high L-valine production in *Corynebacterium glutamicum* VWB-1 using transcriptomics and proteomics. *Sci Rep*, 8, 3632.

Zuchowski, R., Schito, S., Neuheuser, F., Menke, P., Berger, D., Hollmann, N., Gujar, S., Sundermeyer, L., Mack, C., Wirtz, A., Weiergraber, O. H., Polen, T., Bott, M., Noack, S. & Baumgart, M. 2023. Discovery of novel amino acid production traits by evolution of synthetic co-cultures. *Microb Cell Fact*, 22, 22.

6. Danksagung

Besonders bedanken möchte ich mich bei Dr. Meike Baumgart: Für die Überlassung des spannenden und wissenschaftlich ergiebigen Themas, für das Interesse an meinen Ergebnissen und für die hilfreichen Diskussionen (in vielen, vielen Zoom-Meetings). Es hat mich gefreut, dein erster Doktorand sein zu dürfen!

Ebenfalls ein großer Dank an Prof. Dr. Michael Bott. Danke für das Interesse an meinem Projekt, den wissenschaftlichen Input und ganz allgemein die fortwährende Unterstützung.

Bei Prof. Dr. Matias Zurbriggen möchte ich mich für die freundliche Übernahme des Zweitgutachtens meiner Arbeit sowie die hilfreichen Diskussionen bedanken.

Mein Dank geht ebenfalls an das gesamte CoNoS-Projektteam. Danke, Dr. Stephan Noack, für deine Hilfe während des gesamten Projektes. Of course, a big thank you to Simone Schito, for all your work in our joined project. Auch dem Rest des CoNoS-Teams, also Daniel, Daniel und Philipp, gilt mein Dank.

Vielen Dank an alle, die mich fachlich und wissenschaftlich bei meinen experimentellen Arbeiten unterstützt haben. Vielen Dank an Tina für die ganzen Klonierungen und Microarrays. Vielen Dank an Astrid Wirtz für die große Hilfe und Geduld mit mir in der Aminosäure-Analytik. Vielen Dank an Dr. Tino Polen und Ulrike Viets für die Arbeit an den Sequenzierungen der evolvierten Stämme. Vielen Dank an Moritz Müller für die Hilfe bei den größeren Fermentationen. Vielen Dank an Dr. Lea Sundermeyer für die tollen ITC-Messungen. Many thanks to Srushti Gujar and Oliver Weiergräber for the help with the AlphaFold protein predictions. Vielen Dank an Bastian Wollenhaupt und das gesamte Mikrofluidikteam für eure Arbeit. Vielen Dank an Aileen Krüger für die Hilfe bei den qPCRs. Vielen Dank an Paul, Karen und Susana für eure Unterstützung, als ihr mich als frischen Doktoranden im Labor angelernt habt.

Ich möchte mich natürlich auch bei Friederike und Daniel bedanken, dass sie mir mit ihren Masterarbeiten enorm geholfen haben, sowie bei Lisa, Laura und Anka, die mich während ihrer Laborpraktika unterstützt haben. Es hat mir viel Spaß gemacht, mit euch zusammenzuarbeiten!

Ein großes Dankeschön geht an alle Mitarbeiter des IBG-1 für die freundliche Arbeitsatmosphäre, die Hilfsbereitschaft und Unterstützung in allen Belangen. Besonders herzlich bedanken möchte ich mich bei allen weiteren Mitgliedern der AG Regulation, mit denen ich in meinen 3,5 Jahren am Institut zusammenarbeiten durfte. Vielen Dank an Alexander, Angela, Astrid, Benita, Brita, Claudia, Jan-Gerrit, Kiki, Lea Zola, Lingfeng, Marielle, Monika und Natalie für die Unterstützung, für die Gespräche, für die gemeinsamen Unternehmungen.

Bei meinen Eltern Andrea und Jürgen, bei meinem Bruder Luca, bei meiner ganzen Familie und meinen Freunden bedanke ich mich für die Unterstützung auf meinem bisherigen Lebensweg, einschließlich während meiner Promotionszeit.

Ein großes Dankeschön an Jan-Eric, weil Du immer für mich da bist, auch und ganz besonders während der stressigeren Phasen dieser Arbeit.

7. Erklärung

Ich versichere an Eides Statt, dass die vorgelegte Dissertation von mir selbständig und ohne unzulässige fremde Hilfe unter Beachtung der „Grundsätze zur Sicherung guter wissenschaftlicher Praxis an der Heinrich-Heine-Universität Düsseldorf“ erstellt worden ist. Die Dissertation wurde in der vorgelegten oder in ähnlicher Form noch bei keiner anderen Institution eingereicht. Ich habe bisher keine erfolglosen Promotionsversuche unternommen.

_____

Düren, den 30.05.2023

Band / Volume 269
The complex inositol metabolism of *Corynebacterium glutamicum* and its application for the production of rare inositols
P. Ramp (2023), VI, 161 pp
ISBN: 978-3-95806-699-1

Band / Volume 270
Spin- and orbital-dependent band structure of unconventional topological semimetals
K. Hagiwara (2023), v, 115 pp
ISBN: 978-3-95806-701-1

Band / Volume 271
Neutron scattering
Experimental Manuals of the JCNS Laboratory Course held at Forschungszentrum Jülich and at the Heinz-Maier-Leibnitz Zentrum Garching edited by T. Brückel, S. Förster, K. Friese, M. Kruteva, M. Zobel and R. Zorn (2023), ca 150 pp
ISBN: 978-3-95806-705-9

Band / Volume 272
Ab-initio investigation of the interplay between the hyperfine interaction and complex magnetism at the nanoscale
S. R. S. Shehada (2023), ix, xi, 119 pp
ISBN: 978-3-95806-718-9

Band / Volume 273
Analysis of the signal transduction cascade tuning the 2-oxoglutarate dehydrogenase activity in *Corynebacterium glutamicum*
L. Sundermeyer (2023), VI, 119 pp
ISBN: 978-3-95806-722-6

Band / Volume 274
Multicellular defense against phage infection in *Streptomyces* – impact of secondary metabolites and mycelial development
L. Kever (2023), iv, 246 pp
ISBN: 978-3-95806-724-0

Band / Volume 275
Investigation of the electronic band structure of 2D transition metal dichalcogenides via angle-resolved photoemission spectroscopy
B. Parashar (2023), xvii, 156 pp
ISBN: 978-3-95806-725-7

Band / Volume 276
Strain- and process engineering for polyketides production with *Pseudomonas taiwanensis* VLB120 in two-phase cultivations
T. P. Schwanemann (2023), 230 pp
ISBN: 978-3-95806-726-4

Band / Volume 277
Quantitative atomic-level investigation of solid materials through multidimensional electron diffraction measurements
H. L. Lalandec-Robert (2024), xxi, 152 pp
ISBN: 978-3-95806-735-6

Band / Volume 278
Studies on the cAMP-responsive regulatory network of *Corynebacterium glutamicum*
N. Wolf (2024), iii, 122 pp
ISBN: 978-3-95806-736-3

Band / Volume 279
Rare-earth atoms on two-dimensional materials: ab initio investigation of magnetic properties
J. P. Carbone (2024), 235 pp
ISBN: 978-3-95806-740-0

Band / Volume 280
Communities of Niche-optimized Strains (CoNoS) – a novel concept for improving biotechnological production
R. Zuchowski (2024), VIII, 168 pp
ISBN: 978-3-95806-743-1

Schlüsseltechnologien / Key Technologies
Band / Volume 280
ISBN 978-3-95806-743-1

Mitglied der Helmholtz-Gemeinschaft

JÜLICH
Forschungszentrum